Федеральное государственное автономное образовательное учреждение
высшего образования «Уральский федеральный университет имени первого Президента России Б. Н. Ельцина»

Уральский энергетический институт
Кафедра «Атомные станции и возобновляемые источники энергии»

**На правах рукописи**

Агьекум Эфраим Бонах

# ИССЛЕДОВАНИЕ ПОТЕНЦИАЛА ВЕТРОВОЙ И СОЛНЕЧНОЙ ЭНЕРГИИ В РЕСПУБЛИКЕ ГАНА И НАУЧНОЕ ОБОСНОВАНИЕ ПЛОЩАДОК ДЛЯ РАЗМЕЩЕНИЯ ВЭУ И СЭС

2.4.5. Энергетические системы и комплексы

ДИССЕРТАЦИЯ
на соискание учёной степени
кандидата технических наук

Научный руководитель:
Доктор технических наук, доцент,
Велькин Владимир Иванович

Екатеринбург – 2022

Federal State Autonomous Educational Institution Higher Education «Ural Federal University named after the first President of Russia B.N. Yeltsin»

Ural Power Engineering Institute

Department of «Nuclear Power Plants and Renewable Energy Sources»

**As a manuscript**

Agyekum Ephraim Bonah

# STUDY OF THE POTENTIAL OF WIND AND SOLAR ENERGY IN THE REPUBLIC OF GHANA AND SCIENTIFIC JUSTIFICATION OF SITES FOR THE INSTALLATION OF WPP AND SPP

**2.4.5. Energy systems and complexes**

DISSERTATION

Degree of Candidate of Technical Sciences

Scientific supervisor:

Doctor of Technical Sciences, Associate Professor,

Velkin Vladimir Ivanovich

Yekaterinburg – 2022

TABLE OF CONTENT

# INTRODUCTION

## General description of work

The availability of energy is the most important strategic raw material for the socio-economic development of every country. Fossil fuels have been the main source of energy generation worldwide for many years, and their impact on the environment is very devastating. The need to protect the environment today and for future generations has intensified the discussion of the need to search for alternative sources of energy generation around the world. The development and use of renewable energy sources (RES) is growing all over the world, as they are "green" and reliable, and their cost is constantly decreasing. Renewable energy helps countries move towards a more environmentally responsible level of energy generation through an environmentally sound approach to energy generation that has a long-term positive impact on climate conditions.

The paper presented evaluates the potential and suitable locations for the installation of large-scale solar and wind power in Ghana. As Ghana is located in the tropics, solar photovoltaic converter (PV) technology will play a key role in sustainable energy issues. However, the PV technology has some disadvantages, such as reduced efficiency with increasing operating temperature and low energy conversion, which negatively affect its operation. Increasing the temperature of the PV panel mainly affects its operating parameters, which ultimately reduces the output of the power plant. Any increase in the ambient temperature by 1 ºC reduces the performance of the solar cell by 0,4 – 0,5%, therefore, in this study, options for cooling the solar cell modules were proposed.

**Relevance of work:** the work is designed to solve problems in the RE sector. Ghana currently has only 0,5% of RE in its energy generation mix. This has been identified as woefully inadequate especially considering the country’s huge RE resources. The Government of Ghana has therefore planned to increase the composition of RE in the country’s energy generation mix to some 10% by 2030. The outcome of this study is intended to assist various stakeholders in the energy sector to resolve some of the challenges confronting the country’s renewable energy sector. These stakeholders

include, investors, government, international donor agencies, local and international research, and development (R&D) institutions, NGOs, and educational institutions. The new method for the identification of appropriate sites for the development of various RE resources can be used anywhere in the world especially in developing countries. Also, the new PV module cooling mechanisms proposed in this work can be used in hot arid countries.

**The degree of elaboration of the research topic:** Research on the use of renewable energy sources for power supply to rural and isolated settlements and the development of power plants based on renewable energy sources were carried out by well-known Russian scientists: Alekseev V.A., Alferov Zh.I., Alekseenko S.V., Strebkov D.S., Bezrukikh P. .P., Elistratov V.V. Kharchenko V.V., Nikolaev V.G., Shcheklein S.E., Solomin E.V., Sheryazov S.K. Among the foreign scientists one could mention the well-known Martin E., Kriegel H., Jorg S. and Xu H. (all from Germany), Saaty T. (USA), Al Garni H. (Canada) and Dorg J. (Mauritius).

**The purpose of the study:** Research on the potential of renewable energy and development of a calculation methodology to determine the optimal solar and wind parks in the Republic of Ghana. To achieve this goal, the following tasks were set:

1. Assessing the renewable energy potential of Ghana to identify solar and wind energy opportunities.
2. Determining the optimal locations for installing wind and solar power plants in Ghana using a combination of the search for the optimal location of renewable energy sources based on DBSCAN clustering and Analytical hierarchical process method.
3. Experimental analysis of various ways to reduce the temperature of the solar PV modules.
4. Development of ways to stabilize the temperature of solar photovoltaic modules in hot weather conditions of equatorial countries to improve the performance of solar PV modules.

5. Assessment of the technical and economic potential of wind and solar energy in Ghana and the development of specific recommendations for the placement of wind turbines and solar power plants in the northern, middle, and southern geographic regions of the country.

**The object of the research:** solar and wind energy, enhancement of PV panel efficiency.

**Research subject:** the efficiency of the PV panels, sites for the installation of large-scale solar and wind power plants in Ghana.

**Research methods:** during the study, different theoretical methods were employed, some of these include density-based clustering method; analytical hierarchy process; machine learning; parametric methods; and methods of statistical processing of experimental results.

**The main provisions of the dissertation submitted for defense:**

1. Assessment of the technical and economic potential, and the results of the selection of suitable sites for large-scale installation of solar and wind power plants in Ghana.
2. Results of using the method of dual surface cooling of a photovoltaic module to improve the efficiency of solar cells.
3. Results of increasing the efficiency of solar panels through the use of discrete aluminum heat sinks and an ultrasonic humidifier for cooling solar cells.
4. Results of the energy, exergy, and economic analysis of the use of a combination of a phase change material (paraffin wax) and aluminum fins for cooling a PV panel.

**Scientific novelty of dissertation research**

1. For the first time, an assessment was made of the potential of solar energy and wind energy in three geographical zones of the territory of the Republic of Ghana: northern, central, and southern.
2. For the first time, based on the use of an integrated methodology of DBSCAN and AHP, suitable sites for the installation of large-scale solar and wind

power plants were determined, taking into account existing electricity transmission and road networks.

3. An efficient dual-surface cooling mechanism for solar cells has been developed and implemented.
4. A method has been developed and implemented that uses a combination of aluminum fins and a phase-change material (paraffin wax) to cool PV panels, which made it possible to increase efficiency in equatorial countries.
5. For the first time, a combination of an ultrasonic humidifier and aluminum fins was proposed and implemented for efficient cooling of the PV panel.

**The theoretical and practical significance of the work is:**

1. Proposed and substantiated suitable sites in Ghana for the development of wind and solar power plants. An important feature of the method used to determine suitable sites for the installation of renewable energy sources is the ability to determine the contours of the clusters.

2. The developed methods for lowering the temperature make it possible to increase the efficiency of modified solar cells up to 5-11% in hot weather.

**Credibility and validity:** The results of this work are in good agreement with the classical methods for calculating renewable energy sources, recognized programs used for calculating RES, such as RETScreen, PVsyst, System Advisor Model (SAM), HOMER, and the results of other authors and scientists.

**Personal contribution:** The author personally participated in:

1. Development and installation of experimental stands and implementation of pilot work on cooling methods for the PV panels.
2. Proposed a combination of the method for finding the optimal location of renewable energy sources based on DBSCAN clustering and the process hierarchy analysis method (AHP).
3. Theoretically and experimentally investigated the effectiveness of the developed methods for increasing the efficiency of solar cells at high ambient temperatures.

4. Completed the processing and analysis of the obtained data, generalization and publication of research results and recommendations on the use of PV panels under the weather conditions of equatorial countries.
5. Developed a map of the territorial zoning of the Republic of Ghana with the definition of the most effective areas for the installation of large-scale wind and solar power plants.

**Approbation of work:** sections of the results in this dissertation were presented and discussed at the following conferences, International Scientific Electric Power Conference ISEPC-2019 23-24th of May 2019, Peter the Great St. Petersburg Polytechnic University; CONECT – International Scientific Conference of Environmental and Climate Technologies, 13th to 15th May 2020, Riga, Latvia; International Conference "Energy, Ecology, Climate 2020 – WCAEE-ICEEC-2020»; XVIII International Conference of Students, Postgraduates and Young Scientists, Tomsk, April 27-30, 2021 V. 1: Physics. — Tomsk, 2021; XVII International Conference “Renewable and Small Energy – 2020. Energy Efficiency. Autonomous energy supply systems of stationary and mobile consumers” Moscow Power Engineering Institute (MPEI), Moscow, Russia, April 23-24, 2020.

**Publications:** 25 articles were published on the topic of the dissertation, including 23 in the international databases Scopus and Web of Science and 2 publications in journals recommended by the Higher Attestation Commission.

**The structure and scope of the thesis:** The dissertation consists of an introduction, 5 chapters, a conclusion, a 245 bibliography and appendices. In total, the dissertation has 224 pages, 114 figures and 37 tables.

# CHAPTER 1. LITERATURE REVIEW

## 1.1. Overview of Ghana's Energy Sector and Renewable Energy Potentials

### 1.1.1. Current State of Ghana's Energy Sector

The Energy Commission of Ghana's 2018 report on the country's energy demand and supply outlook indicates that, the country has a total installed generation capacity of 4310 MW [1]. Fig. 1.1 shows the composition of generation mix.

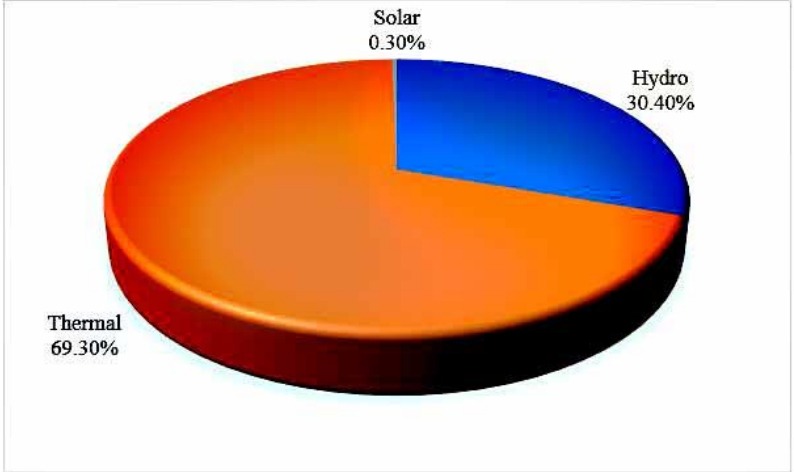


**Fig. 1.1.** Electricity generation mix by close of 2018 in Ghana [1]

Including the two major solar power plants in the country at the distribution level increases the total installed capacity to almost 4398,8 MW. The total grid-electricity was 14069 GWh, this includes embedded generation, which is made up of thermal (59,9%), solar (0,2%) and 39,9% (hydro). Grid at the level of transmission was estimated to be 14309 (±1%) GWh including imports. Electricity demand at peak hours excluding exports stood at 2077 MW, whiles that including exports was 2192 MW in 2017. The country's entire dependable capacity during that same period was estimated to be around 3890 MW which is in excess of about 1700 MW (±3%) [1]. The share of RE including hydropower in Ghana's generation mix is higher compared to neighboring countries such as Togo, Benin and Cote d'Ivoire who depend greatly on thermal power generation. Ghana has about 11,5% of the total identified medium-large-scale renewable energy projects in the

ECOWAS sub-region [2]. The country's largest hydropower plant is located in Akosombo, it has an installed capacity of 1020 MW. Fig. 1.2 shows the Akosombo dam in Ghana. A 6,5 MW solar power plant is also installed in Lawra in the Upper West region of Ghana. Fig. 1.3 illustrate the 6,5 MW solar power plant in Lawra.

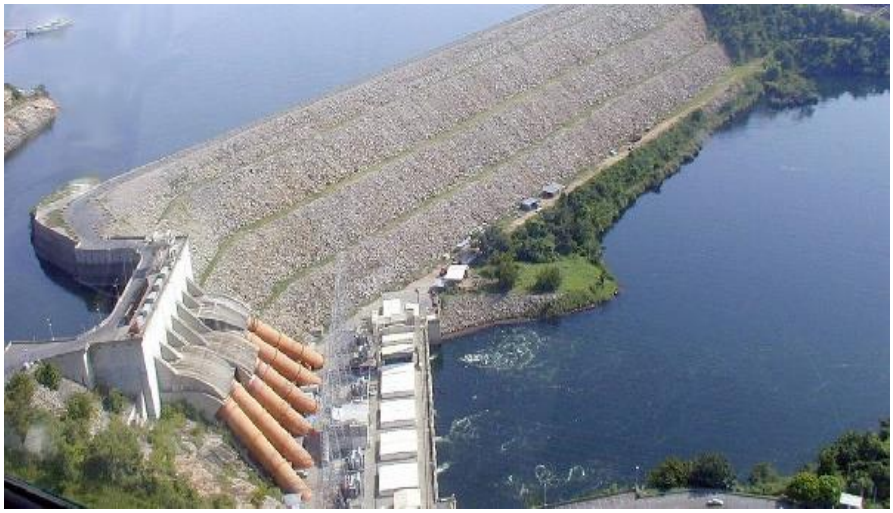

**Fig. 1.2.** The 1020 MW Akosombo hydropower plant [3]

**Fig. 1.3** Lawra solar power plant [4]

### 1.1.2. Ghana's Strategy Towards Universal Access to Electricity and GHG Reduction

The electricity sector in Ghana is faced with several challenges which most nations on the African continent are also confronted with as they try to build inclusive and green

economies. Ghana aims at providing universal access to cheap electricity, promoting economic growth and reducing the susceptibility of its power systems to erratic rainfall patterns and cost or availability of imported fuels [5]. The country is endowed with several renewable energy potentials, resources such as solar, biomass, wind and small to mini hydropower. These, when harnessed, can contribute greatly to the expansion of access to electricity while reducing the recurring energy crises. The government of Ghana has targeted to increase the composition of renewable energy in the total installed electricity generation capacity to 10% by end of 2030 [6]. It has also aimed at reducing GHG emissions by 15% in the country with respect to the business-as-usual scenario by 2030. The government has however, projected an extra 30% reduction in emission should the country get external funding to cover the full cost of executing the mitigation action developed by the government [7].

## 1.2. Ghana's Renewable Energy Resources

Renewable energy is the best option in terms of clean, reliable, and safe electricity generation. RE such as solar, geothermal, wave/tidal, hydro and wind among others are expected to play crucial role in the world's search for sustainable electricity. Ghana's strategic objective is to fast-track the development and utilization of these RE resources. The Energy Ministry has targeted some 500 MW of power from renewables comprising: solar, wind, hydro and biomass which requires a total investment of US$ 640 – 900 million [8].

### 1.2.1. Hydropower potential in Ghana

The country has about 17 medium and 22 mini hydropower potential locations with available capacities ranging from 15 kW to 100 MW. Small hydropower (SHP) is a system used to generate electricity. According to the ECREEE, an SHP is a plant whose installed capacity is less than 30 MW, under Ghana's Renewable Energy Act, hydropower with capacities up to 100 MW meet the requirements for renewable electricity Feed-in Tariff (FiTs) [9]. According to the Ministry of Power in 2015, some initiatives were

launched by the Government to assess the feasibility of some hydropower sites across the country and these are [9]:

- Assessment of six potential hydropower sites on the White and Black Volta rivers has been done with funding from the Swiss Government through SECO under a Hydropower Sustainability Assessment Project (HSAP). These sites consist of Lanka, Koulbi, Ntereso, Kalpawn, Daboya and Jambito with a combined exploitable capacity of about 362 MW.
- The World Bank, VRA and the Agence Françoise de Development also funded a feasibility study on the Juale (90 MW) and the 40 MW Pwalugu sites.
- The Bui Power Authority and the China Water Electric funded a full feasibility study on the 60 MW hydropower project.
- The African Development Bank and the Ministry of Power (under the GEDAP project) are in the course of contracting prefeasibility studies on 10 extra small and medium hydropower sites with a combined exploitable capacity of 248 MW.

### 1.2.2. Wind energy potential in Ghana

Ghana has a lot of potential in terms of wind energy generation, it is estimated that the country has more than 5000 MW energy potential in that sector alone. The country's average wind speed is between 6,4 – 7,5 m/s which corresponds to wind speed class categories of 3 and 4 according to data from IRENA [9]. The mountains along the eastern coastal areas and south-eastern part of the country are the most promising areas for the development of wind power. Research shows that about 200 – 400 MW of onshore power from wind could be established at these locations with 8 m/s wind speed [10].

The government in collaboration with the World Bank and the private sector have commenced some initiatives to develop the country's wind energy resource, these includes the following [11]:

- The Energy Ministry with support from the World Bank has embarked on an assessment of wind resource across the country at 60 m above ground level in about eight locations. This is aimed at obtaining bankable wind data for planning. Results

indicate that Anloga has a moderately high wind speed of 6 m/s as well as 4,5 m/s at Gomoa Fete in the Central region.

- VRA plans to install some 150 MW of wind power by 2020 and also embark on wind resource assessments across the country.
- A site at Ada in the Greater Accra region has been acquired by EleQtra/InfraCo who intend to develop a 30-50 MW wind farm by 2020.

### 1.2.3. Solar energy potential in Ghana

Ghana has a lot of potential in solar energy as a result of its geographical location, solar resources spread across the entire country. Daily solar irradiation in the country ranges between 4 kWh/$m^2$/day to 6 kWh/$m^2$/day with annual sunshine duration ranging between 1800 to 3000 hours which gives it a high potential for grid connection [12]. The intensity of solar irradiation in Ghana can be divided as follows: Upper West, Upper East, North East, Savannah, Oti, Bono, Bono East, Ahafo and some part of the Volta region experiences 4,0 – 6,5 kWh/$m^2$/day, whiles the middle belt of the country consisting the Ashanti, Western North, Central and parts of Volta regions experience solar intensities in the region of 3,1 – 5,8 kWh/$m^2$/day, the coastal belt comprising of the Greater Accra, parts of the Volta, parts of Eastern and Central as well as sections of the Western regions experience 4,0 – 6,0 kWh/$m^2$/day of solar intensities [9].

### 1.2.4. Wave energy potential in Ghana

Ghana has a vast coastline capable of generating wave energy to power the country, but this area of energy generation is now being exploited just like other countries. Wave power is a developing energy sector in the rapidly developing renewable energy space and has the potential of providing a substantial amount of electricity globally. Waves are predictable resource and exist 24/7 all year round. TC's energy, a Ghanaian renewable energy production company has contracted Sea-based company to construct a wave energy plant near Ada, Ghana. The company was contracted to construct a 100 MW park which is one of the largest commercial contracts in the wave energy generation industry

[13,14]. Fig. 1.4 shows the coastal area for West Africa displaying Bathymetry and the location of Wave Rider Buoy.

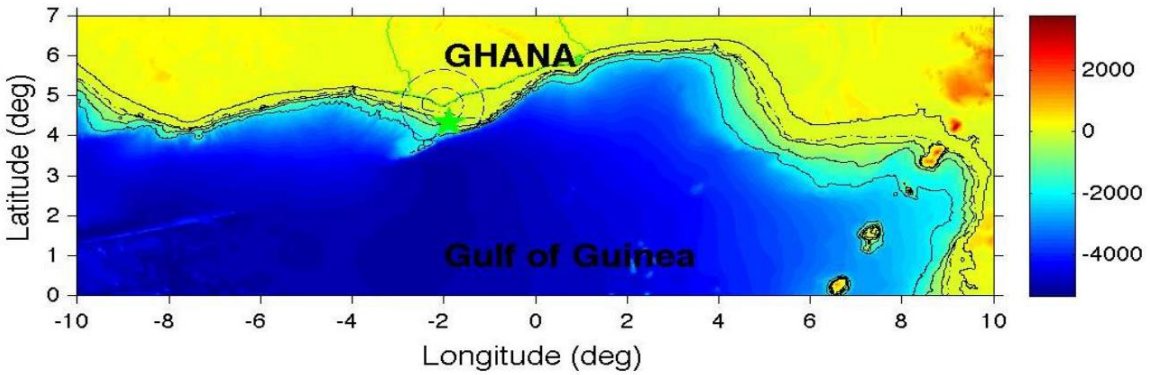


**Fig. 1.4** Coastal area of Ghana displaying Bathymetry and the location of Wave Rider Buoy [15]

### 1.2.5. Biomass Energy potential in Ghana

The total stock of Ghana's dominant energy (i.e., biomass) source is about 832 million tons; this is expected to increase unless there is sharp development in energy efficiency in other forms of energy generation. It is projected to increase from between 38 – 46 million tons to 54 – 66 million tons by 2020 [16]. Logging of timber produces about 1,0 – 1,4-million-meter cubic residue every year. These comprises of offcuts, edging, peeler cores, sawdust, and waste products from the manufacturing of plywood. The Ashanti region has the highest concentration of residues due to the presence of a number of sawmills and plywood manufacturing factories located in that enclave, the Greater Accra region also has large scale furniture mills. Other several such mills are spread across the country. More wood residue may also be obtained from forest skidding trails from timber haulage and road constructions [9].

# CHAPTER 2. SITE LOCATION AND ALLOCATION DECISION FOR ONSHORE WIND FARMS, USING SPATIAL MULTI-CRITERIA ANALYSIS AND DENSITY-BASED CLUSTERING. A TECHNO-ECONOMIC-ENVIRONMENTAL ASSESSMENT, GHANA

## 2.1. State of the art of using geographic information systems (GIS) for evaluating RES potentials

Making a choice between different renewable energy technologies (RETs) to deliver a specified energy service is dependent on the analysis of the appropriate connections between the local RES, the specific characteristics of the energy demand, and the technical aspects of each RET. Such analysis should usually demonstrate that a chosen technical system agrees with socio-economic, market choices and environmental concerns, and is also in compliance with available legislations [17]. In order to generate cleaner energy, we normally consider renewable sources, however, these resources and their energy that they can generate are inherently dependent on the location of the facility. As a result, the optimum way to arrive at maximizing the use of these resources is the use of spatial analysis to improve upon energy generation, transmission, and distribution [18]. The ability to achieve policy objectives set for the RE sector with relatively minimal impact on policy goals outside the domain of RE is limited by a number of geographical forces which relates to resource potential, land suitability/availability, distribution of resources, the local socio-political acceptance and the absorptive capacity of proximal infrastructure [19].

Traditionally, RE mapping exercises mostly concentrate on site-suitability using the top-down approach to locate and quantify the potential of a particular resource [20]. The analytical framework usually starts with the identification of the physical factors which determine the intensity and scale of the RE over a landscape – i.e. the ‘theoretical potential’- after which the factors such as technical and social restrictions from which one can differentiate resources that are accessible and convertible at a bankable cost – i.e., the techno-economic potential [19].

The GIS is a tool that is currently used to evaluate the potential of RE across the world. A number of GIS models are being developed to help in RETs planning to either complement or replace conventional power plants that rely on fossil fuels [21]. Such tools are important for planning commissions, policymakers, environmental and techno-economic researchers as well as utility companies. It is important to note that, the valuation of RES potentials at a particular locality generally results in a systematic reduction of preliminary values of the theoretical potential to give the techno-economic and market potential values as indicated in Fig. 2.1 [21].

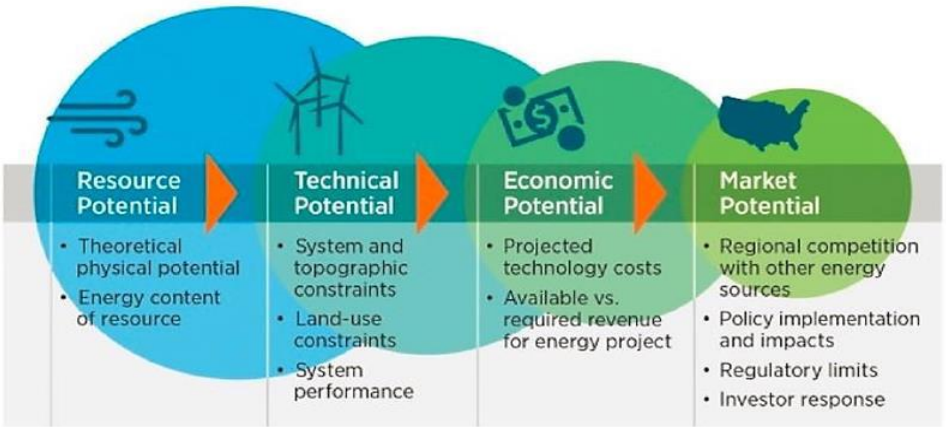


**Fig. 2.1.** Reduction in the initial RES potential at each stage of evaluation, NASA, NREL (2015) [21]

Several renowned researchers in the field have used the multicriteria-decision making (MCDM)-GIS methodology in assessing different RE potentials at different sites globally. Tahri et al. [22], studied the outcome of combining both MCDM and GIS methods to evaluate the suitability of solar power projects in Morocco. They used four different criteria, i.e., orography, location, climate, and land use. The AHP was used in calculating their corresponding weights. The study identified climate as the most important criterion because it has a direct effect on the amount of electricity production for a specific area. Amjad and Shah [23], proposed a methodology that primarily focuses on sites that have a high potential for solar energy using GIS and density-based clustering approach for the identification and grouping of the sites in Pakistan, the limitation of this

study was that it a limited number of criteria for the location decision. Fluri [24], also used the GIS approach to identify suitable areas in South Africa for the development of large-scale CSP power plants. An area according to the study is classified as suitable if it receives enough solar radiation, has low ruggedness, close to transmission lines, it has a suitable land use profile and the vegetation cover in that area is not under threat.

Furthermore, Marques-Perez et al. [25], used the MCDM methodology combined with GIS to create a suitability map that indicates the ranking of areas with high solar energy potential for the Valencian Community in Spain. The locations were identified, evaluated, and ranked using the Preference Ranking Organization Method for Enrichment Evaluations (PROMETHEE) methodology. The position of each criterion as well as sub-criteria was determined using the AHP approach. Merrouni et al. [26], used the GIS-based AHP methodology to evaluate the ability of Morocco's Eastern region to support CSP technologies. They developed a high spatial resolution GIS database using layers from different governmental institutions. Their results indicated that Eastern Morocco can be regarded as a good place for site selection for the development of CSP plants.

Sindhu et al. [27], also employed a combination of fuzzy Techniques for Order Preference by Similarity to Ideal Solution (TOPSIS) and AHP methodology to select suitable sites for solar energy development in India. Their study identified Sonepat as the best place for the development of solar power plants. Mensour et al. [28], similarly used the MCDM method to identify appropriate sites to host PV power plants in southern Morocco. The AHP and GIS process was adopted to construct a high-resolution map that compares the ability of the selected region to support the development of commercial PV projects. Their study found out that, 24.08% of the area studied is suitable as sites for the development of PV power plants. Doljak et al. [29], employed the GIS and the MCDM to evaluate the potential for Serbia to support large-scale PV power development. The study identified that the country's suitable areas for hosting PV systems cover about 12.79 square kilometers. Doorga et al. [30], investigated the spatial suitability for the development of SPPs based on social, legal, environmental, economic, and cultural

perspectives using the GIS and MCDM techniques. Their study was done using six exclusion criteria.

The processes involve in using the GIS approach to arrive at a desired output is represented in Fig. 2.2.

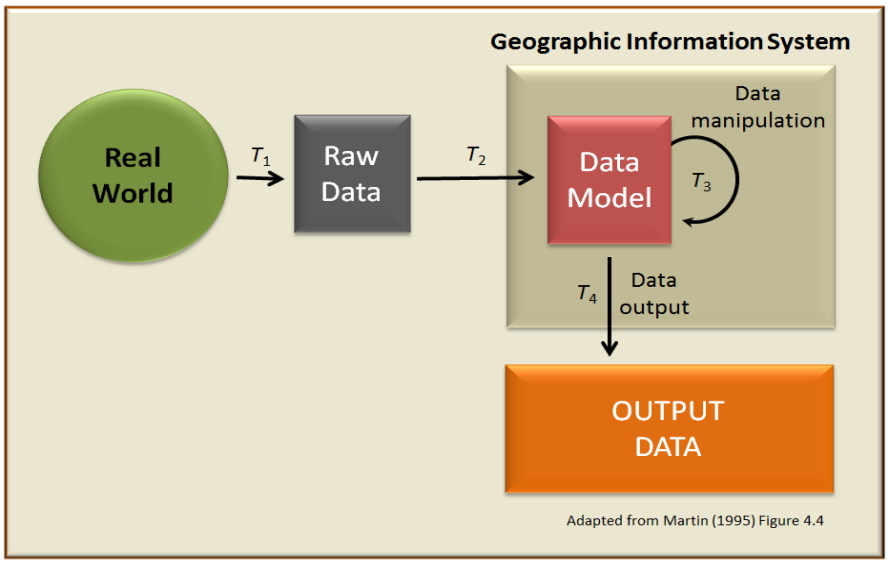


**Fig. 2.2** Processes for the GIS approach [31]

## 2.2. Optimization of sites for wind farms introduction

Wind energy is currently among the world's top exploitable RE resources along with solar and tidal energy, it is leading the global market principally because of its high availability, technological maturity, cost competitiveness, and macro-level data availability [32]. The total cumulative wind power capacity globally increased from 24 GW in 2001 to over 591 GW in 2018, it is projected to exceed 908 GW by 2023. China reached a cumulative installed capacity of 211 GW in 2018 making it the leader in wind energy generation in the world, followed closely by the United States with 96 GW and India with 35 GW [33].

One of the major limitations in the introduction of the RE in developing countries has been the lack of reliable data about various available renewable resources. The international development agencies have partly addressed this limitation by compiling macro-data necessary for resource evaluation and planning. However, comprehensive

resource availability analysis in addition to the optimum location of the resources along with the additional infrastructure requirements to tap these resources are required for investment decisions. This has been one of the reasons why developing countries are slow in developing RE systems on a large commercial scale. Investors rely on such data to evaluate the techno-economic potentials of locations during planning [13].

This chapter would identify wind hotspots in Ghana using a hybrid methodology for site selection of wind power plants using the spatial multi-criteria analysis along with density-based clustering. The GIS-based approach is employed to eliminate the unsuitable locations, followed by the application of the density-based clustering on the remaining candidate sites to exactly pinpoint the top sites of energy available for the development of wind power plants. The proposed methodology has been applied on Ghana for demonstration and validation purposes. It incorporates for the first time the spatial multi-criteria with density-based clustering for final site selection decision for wind power projects anywhere in the world. This makes such analysis easier since it does not require human intervention relative for the identification of the boundary contours of the candidate sites. A detailed techno-economic-environmental analysis of hybrid Wind power plant/Diesel generator/Battery/Converter system for all identified clusters was done to assess the viability of such a project at the identified sites using HOMER Pro software.

## 2.3. Methodology

This chapter proposes a hybrid methodology for the site selection of wind power plants using the spatial multi-criteria analysis in combination with density-based clustering. The application of density-based clustering is aimed at identifying distinctive geographical clusters in the area under analysis. It is also employed to determine the exact size of the identified clusters with their wind potential to compute the theoretical power generation capacity in the analysis. Moreover, any constraint which hampers the development of the wind site can be identified as noise and discarded from the analysis to make the wind potential approximation as close as possible to the actual function. Additionally, the

preference to use density-based clustering instead of conventional clustering approaches is that it identifies clusters of irregular shapes without human supervision for the required numbers of clusters. The main novelty of this study is in its region of interest i.e., Ghana for which no study in this form on the availability of wind resource exists. The other novelty of this study is in the use of SMCA and DBC for the identification and contour optimization of the wind farms. The only study that recently used the DBC used it on solar energy as shown in Ref [23], it only showed the DBC with a smaller number of spatial criteria, i.e. solar irradiance and slope, but did not discuss any final site ranking. This study augmented this study by incorporating multiple spatial criteria suitable for wind farm location selection.

The classical approach for the site selection of wind power plants is aggregated in three basic phases of analysis. The first phase identifies the factors and constraints of the location decision. The classical factors are the energy availability, the distance from the transmission lines, the distance from road and rail network, distance from population centers, and the terrain suitability. These factors are categorized into multiple categories of decreasing order from highly suitable to unsuitable. Similarly, the constraints or the Boolean factors dictate whether the site is suitable or unsuitable, the classical constraints are the protected areas, rivers, lakes, and agricultural land, airports, etc. The second phase of the analysis is assigning the factor weights using multi-criteria decision methodologies and domain expert knowledge, this step varies for different areas of interest, as different countries or areas of interest have different development limitations. The third phase of the analysis uses the input from the first two phases and generates a combined raster output with the corresponding geographical suitability scores. This approach when applied to a regional analysis yields the macro-level understanding of the site suitability. The typical wind farm site selection criteria are given in Table 2.1, which were also confirmed by some consulted experts in Ghana’s Energy Commission as appropriate for Ghana.

**Table 2.1** Wind farms location selection criteria [34]

| Factor | Suitability Ranking | | | |
|---|---|---|---|---|
| | Highly Suitable | Moderately Suitable | Low suitability | Not suitable |
| | 3 | 2 | 1 | 0 |
| Wind speed (m/s) | > 6 | 5 < x ≤ 6 | 4 < x ≤ 5 | < 4 |
| Proximity to roads (km) | 0,5 < x ≤ 2 | 2 < x ≤ 5 | 5 < x ≤ 10 | > 10 |
| Proximity to transmission lines (km) | 0,5 < x ≤ 2 | 2 < x ≤ 5 | 5 < x ≤ 10 | > 10 |
| Land use | Barren grassland | Agricultural land | Short vegetation and shrubs | Public settlements, wetlands, airports, etc. |
| Slope (%) | 0 ≤ x ≤7 | 7 < x ≤ 12 | 12 < x ≤ 15 | > 15 |
| Distance to airports (km) | > 4 | 3,5 < x ≤ 4 | 3 < x ≤ 3,5 | ≤ 3 |
| Distance from residential area (km) | > 3 | 2 < x ≤ 3 | 1< x ≤ 2 | ≤ 1 |

Some limitations of the above analysis are that firstly, it introduces infrastructure proximity biases at the initial phase of the analysis, this biasness can limit the optimal selection of the site. Secondly, it does not provide the flexibility of selecting the sites of the desired minimum size which is an essential requirement of policy planning as the size of the wind power plant is associated with available areas hence impacts the generation capacity of the wind farm. Thirdly the output is not ranked which can cause ambiguity in setting the developmental priorities. These main limitations are addressed in the proposed methodology which is flexible and can accommodate any evaluation criterion depending on the needs of the individual country's development.

The proposed hybrid methodology can be aggregated into four macro steps i.e.,

- data preparation,
- zone localization and evaluation,
- zone clustering,

- zone ranking.

This methodology is shown in Fig 2.3. The first three steps of data preparation, zone localization and evaluation, and zone clustering were carried out in QGIS [35] and R [36]. For conducting the density-based clustering, the FPC package [37] was used, and for the final visualization of the results of density-based clustering, the R package factoextra [38] and ggmap [39] were used.

### 2.3.1. Data sources for the analysis

This segment makes available an overview of the multiple spatial data set used in the analysis. All the datasets are available in the spatial projection WGS 84. The dataset for the road, rail, transmission lines, administrative boundaries, airports, lakes, rivers, elevation data, and land-use was extracted from the national renewable energy laboratory [40], the data set was provided in the vector format. The protected areas' dataset used in the analysis was extracted from [41], the dataset was in vector format for all the national parks, forest reserves, wildlife sanctuaries, and resource reserves. For the corresponding dataset on the spatial distribution of the population densities Ref [42,43] was used, this dataset was in GeoTIFF format at a resolution of 3 arcs (approximately 100 m at the equator). The final data set of average wind speed was extracted from [44] which provides wind resource mapping at 250 m horizontal grid spacing at 10, 50, 100, 150, and 200 m above ground level.

### 2.3.2. Data Preparation

The first step is to prepare the different raster and vector datasets. Multiple rasters of wind speed at the height of 50, 100, 150 and 200 meters are combined into one raster. Wind turbines of different generation capacities require blades of various lengths which dictates the height of the generator from the ground. The effective height limits at which the blades of the wind turbine operate can vary from 50 to 200 meters depending on the height of the generator and its blade length requirements. As our objective is the identification of the most wind intensive areas for the installation of the wind farm, this

is why we have combined the wind speed at multiple heights. Another approach could be to limit the analysis to a specific height, but this approach requires preselection of the wind turbines which is seldom the case in the regional analysis. This combined wind speed raster data is used subsequently in the site selection decision.

The data set for the Boolean factors are rasterized with the consideration of appropriate minimum buffer zones. These minimum buffer zones are based on existing literature on wind farm site selection and are provided in Fig. 2.3. The other factors important in the siting decision of the wind farm are also briefly discussed subsequently.

Wind speed is one of the most important technical criteria considered during planning for the development of wind farms. The higher the wind speed at a locality, the higher the potential output of the wind power plant. It is one of the criteria that usually receive a high score from experts in the sector during such analysis [45,46].

Land-use type is a key factor that is assessed before investment in most energy projects. Experts recommend the selection of barren land for the development of wind energy projects. Areas with shorter vegetation are most suitable than areas with tall vegetation as tall vegetation can affect the wind speed by introducing turbulence to the flow of air [34,47,48]. In this analysis, we have only considered the open wildland or shorter vegetation areas and the arid regions for the installation of the wind farms and excluded the agricultural and the forest regions. Similarly, we excluded protected areas which comprise nature reserves, protected forests, etc. These areas are essential to maintain and protect natural wildlife. Lakes and the rivers were also excluded from the analysis with a minimum buffer of 0.5 km from water bodies.

The cost of construction of a wind farm may likely increase at areas with steeper slopes since such areas will require more earth movements and grading than a gentle slope. Additionally, it may hinder the accessibility of trucks and cranes which will be transporting the wind turbines to the sites. It is the view of experts that wind farms should be sited at areas with a maximum slope threshold which ranges from 10% - 45% [34]. Ghana's terrain is relatively smooth with the highest elevation of 830 meters above sea level but is prone to land-sliding issues due to rainfall and minor earthquake. For this, we

incorporated the data set of land-sliding and have excluded the regions prone to land-sliding [49].

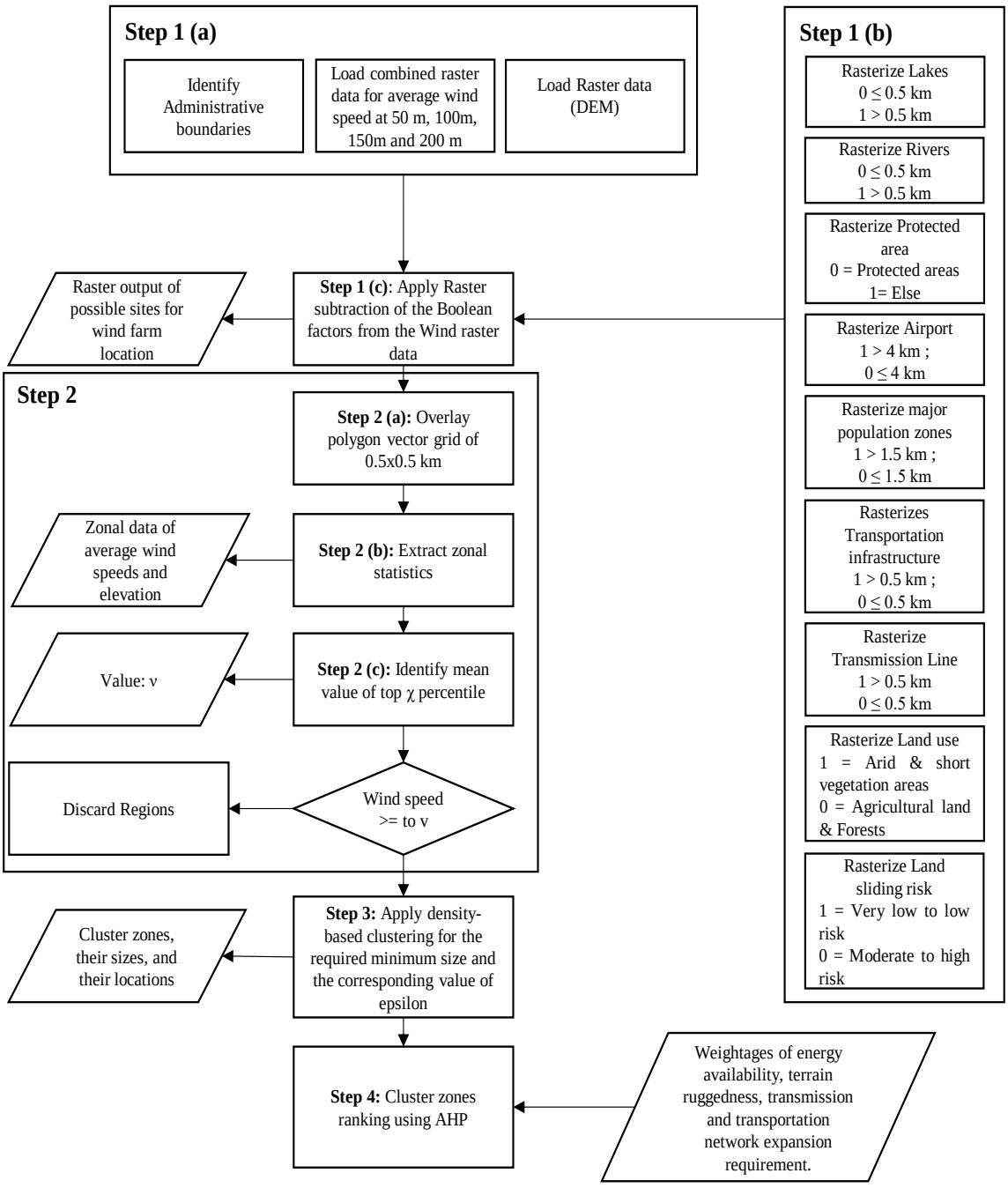


**Fig. 2.3** Process flow diagram of the hybrid model for wind farm location selection

Proximity to infrastructure i.e., either human settlement or transportation and transmission network is important for the siting decision of the wind farm. A buffer between wind farms and residential areas is important because of the potential noise and nuisance it can cause to people in the residential areas, and, similarly, siting wind farms

near airports is discouraged as wind turbines can interfere with signals from the aviation radar [50]. For economic and accessibility reasons, wind farms should be sited close to existing road and transmission networks. Siting such facilities close to the available infrastructure minimize the cost of construction [34], [46]. But in the context of infrastructure expansion planning and developing new renewable energy resources these constraints must be considered later when considering the prioritization of the zone development.

After the preparation of the data, the Boolean factors are subtracted from the corresponding wind speed raster using a raster subtraction feature of the QGIS as shown in Step 1(c) of Fig. 2.3. The output from this step provides all the available areas for the site selection of the wind power plant. The next phase of the analysis will focus on evaluating the output of this step.

### 2.3.3. Zone localization and evaluation

To localize data within the raster layer of wind energy, a vector grid of $0{,}5 * 0{,}5\ km^2$is used (Step 2a). Subsequently, raster statistics on wind speed are collected on the above-mentioned vector grid using the zoning statistics feature of the QGIS (Step 2b). The data set obtained from this step is used in the descriptive statistics on the wind speeds of the area of interest. These descriptive statistics are used to further refine the decision regarding the top wind energy available sites. In the zone evaluation phase of the methodology (Step 2c), several decisions are made. Restrictions on the data are decided. For instance, the application of the restriction to include or exclude wind speed above a certain threshold is decided at this stage. Multiple scenarios can be planned, which is top 5%, 10%, or any other percentile can be decided based on the preferences of the individual country commitments to exploiting their renewable resources. We are only concerned with developing wind farms with the top 10 % of the wind resources of Ghana.

### 2.3.4. Zone clustering

In step 3 this study conducted the density-based clustering using the output of the previous step. The advantages of density-based clustering are that this technique can be used to identify dense clusters of any shape. The other clustering approaches i.e., k-means [51] and k-medoid [52] usually make clusters around central points, concentric clusters are rare in geographical context because of the terrain irregularities. The other advantage is the flexibility of choosing the minimum sized clusters, by adjusting the values of epsilon and minimum size requirements. Fig. 2.4 shows pictorially the procedure of the density-based clustering and how the parameter of epsilon values and the corresponding size of the cluster impact the clustering procedure. As the clustering proceeds, the minimum size required is checked in this case it is 9 and the cluster is formed, the clustering procedure is terminated if the required minimum size required is not satisfied. The output from this step is the formation of clusters of the minimum size which satisfy the constraints defined in the zone evaluation phase.

### 2.3.5. Zone ranking

The final stage of the analysis includes zone ranking (Step 4). For this step, the individual clusters are ranked on multiple criteria using the AHP, this step produces a ranked list of site locations for wind farm development as well as it also serves as a road map for future transmission network development. The criteria considered in this step are the energy availability of the cluster, terrain ruggedness of the sites which is a proxy of the land development requirement, its proximity to transmission lines, and its proximity to transportation networks. As the high energy-dense cluster clusters have already been identified, this proximity to the transportation and the transmission network is the additional infrastructure required for developing these resources.

For economic and accessibility reasons, wind farms should be sited close to existing road networks. Siting such facilities close to roads minimize the cost of construction by allowing easy transportation of equipment for construction and maintenance purposes. These are classical site selection narratives, we are deliberately applying these evaluation

criteria in the last stage of analysis to remove the infrastructure proximity biases, the logic of which is discussed in the initial part in this chapter.

### 2.3.6. Density-based clustering approach (DBCA)

DBCA can be used to recognize or detect clusters of any shape within a data set containing outliers and noise. The fundamental concept behind the DBCA approach is realized from the human intuitive clustering method. Clusters are condensed areas in a data space, which is separated by areas with lower density of points. The main idea in the cluster approach is that given any point of a cluster, the Eps-neighborhood $Ep > 0$ of a given radius must have at least a minimum number of points [53]. In other words, there is a certain threshold that must be exceed by the density in the Eps-neighborhood of points [54].

The DBCA idea can be generally represented into two important ways. Firstly, any notion of neighborhood can be used rather than an Eps-neighborhood provided the description of the neighborhood is premised on a binary predicate that is reflexive and symmetric. Secondly, we can also use other procedures to describe the cardinality of that neighborhood rather than merely counting the objects in the neighborhood. The DBC has several definitions but two of them are presented below, readers may refer to Ref [55] for more:

**Definition 1:** (neighborhood of an object) – Take $NPred$ to be a binary base on $D$ that is symmetric and reflexive, that is, for all $p, q \in D$: $NPred$ $(p, p)$ and, if $NPred(p, q)$ then $NPred(q, p)$. Therefore, the $NPred$ – neighborhood of an object $O \in D$ can be defined as $N_{NPred}(O) = \{O' \in D | NPred(O, O')\}$.

The cluster approach is $N_{Eps}(O) = \{O' \in D || O - O'| \leq Eps\}$ i.e., is limited to the special situation of a distance-based neighborhood (DBN). A DBN is a characteristic idea of an area for point objects, yet on the off chance that grouping spatially expanded objects, for example, a set of polygons to a great extent different sizes, it might be increasingly suitable to utilize neighborhood predicates such as intersects for discovering clusters of

polygons. In spite of the fact that in numerous applications the local predicate is characterized by utilizing just spatial properties of the objects, the formalism is not the slightest bit confined to simply spatial neighborhoods. We can also utilize non spatial traits and consolidate them with spatial properties of objects to determine a local predicate. Another approach to consider the non-spatial properties of objects is as a sort of "weight" while ascertaining the "cardinality" of the area of an item. To keep things as basic as could be expected under the circumstances, let us not present a weight function working on objects, however a weighted cardinality function $wCard$ for sets of objects. The "weight" of a solitary object $O$ would then be able to be communicated by the weighted cardinality of the singleton containing $O$ i.e., $wCard(\{O\})$.

**Definition 2:** ($MinWeight$ of set of objects) – take $wCard$ as a function originating from the powerset of the database $D$ into non-negative real numbers, $wCard: 2^D \rightarrow \Re^{\geq 0}$ and a positive real number be $MinCard$. Then, $MinWeight$ which is the predicate for a set $S$ of objects can be defined as true iff $wCard(S) \geq MinCard$.

The condition $\left|N_{Eps}(O)\right| \geq MinPts$ is generalized by the expression $wCard(S) \geq MinCard$ in the definition of DBC where cardinality is merely a special case of the $wCard$ function.

### 2.3.7. Zone Clustering

There are two types of clustering algorithms such as the hierarchical and partitioning algorithms. Hierarchical decomposition (HD) of $D$ is created by the hierarchical algorithms. The HD is denoted by a dendrogram, which is a tree that iteratively divide $D$ into subsets up until every subset contains of only single object. Every node of the tree denotes a cluster of $D$ in a hierarchy. Readers are referred to Ref [54] for more details. In the case of the partitioning algorithm (PA), there is a construction of a partition of $D$ of $n$ objects to a set of $k$ clusters. PA usually commences with an initial partition of $D$ then an iterative control strategy is used to improve the objective function. Each cluster is denoted by either one of the objects which is located near its center ($k - medoid\ algorithms$)

or by the gravity of the cluster ($k-means\ algorithms$. Therefore, a partition is in the form of a Voronoi diagram and individual cluster is confined in one of the Voronoi polygons [54].

However, the $k-means\ algorithms$ and the $k-medoid\ algorithms$ are appropriate if the dataset is built around a central point. It therefore suggests that the two algorithms mentioned earlier under the PA will not yield appropriate results at dense areas with irregular and longitudinal shapes [23] this is because such algorithms will provide wind strategic zones in an interested area but not exact location.

The DBCA however, does not exhibit same deficiencies, the user does not have to specify the number of clusters that must be generated; it can identify any shape of clusters, i.e., it does not have to be circular; and also, outliers can be identified by the DBCA algorithm. There are two parameters that are required in DBCA, i.e.: the epsilon value which defines the radius of influence or neighborhood and the conditions of minimum points $MinPts$. The minimum number of neighbors in the "epsilon" radius is the $MinPts$. Any point within the data set, whose neighborhood count is greater or equal to $MinPts$ is identified as a core point. If the number of neighbors is less than $MinPts$ then we say $x$ is the border point, however, it is part of the $\epsilon$ – neighborhood of core point $z$. A point is known as an outlier if it is not a core or border point [30].

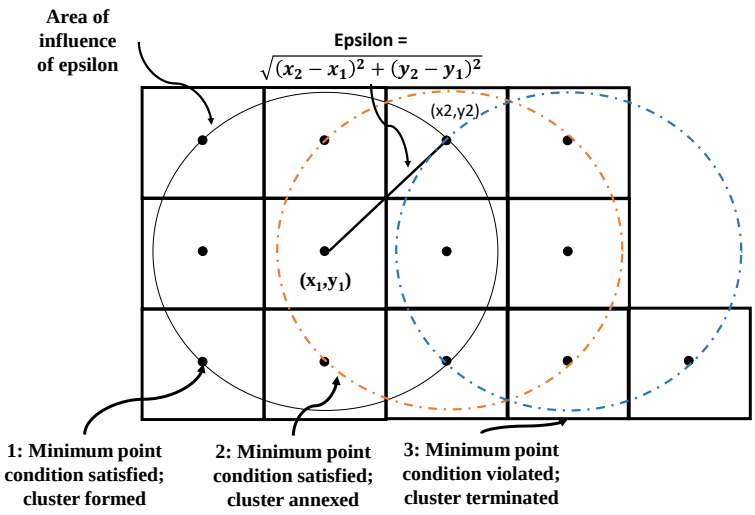


**Fig. 2.4** Density-based clustering procedure, extracted from [23]

### 2.3.8. The analytic hierarchy process (AHP) methodology

The AHP is a mathematical approach first developed by Saaty [56,57]. It can reduce complicated decisions to a series of pairwise comparisons. The AHP approach also checks the consistency of a decision made by an individual and minimizes the biases in the decision-making process [26]. The pairwise comparison matrix $M = [C_{ij}]$ denotes the intensity of an expert's preference between individual criteria or factors under consideration. Eq. (2.1) represents the judgment matrix for $n$ number of criteria in a specific study [58,59]. We calculated each criterion weight using Saaty's fundamental scale, also known as the 9-point scale shown in Table 2.2.

$$M = \begin{vmatrix} c_{11} & c_{12} & \dots & c_{1(n-1)} & c_{1n} \\ c_{21} & c_{22} & \dots & c_{2(n-1)} & c_{2n} \\ \vdots & \vdots & \ddots & \vdots & \vdots \\ c_{n1} & c_{n2} & \dots & c_{n(n-1)} & c_{nn} \end{vmatrix} \quad (2.1)$$

Where $C_{ij}$ represents the comparative importance of the criterion $C_i$ over $C_j$.

Therefore, for $n$ criteria the decision matrix is filled from the pairwise comparisons. To consolidate judgments from the experts, the geometric mean approach was used with the AHP calculator designed by [60]. The priorities, in this case, are denoted by $p_i$ from each expert are evaluated using the row geometric mean method (RGMM). For a pairwise $n \times n$ comparison matrix $M = [C_{ij}]$, the following mathematical relations Eq. (2.2) – (2.4) are used [61,62]:

We evaluate:

$$r_i = exp\left[\frac{1}{N}\sum_{j=1}^{N} \ln(c_{ij})\right] = \left(\prod_{i=1}^{N} c_{ij}\right)^{1/N} \quad (2.2)$$

Then normalize it using Eq (2.3).

$$p_i = \frac{r_i}{\sum_{i=1}^{N} r_i} \quad (2.3)$$

The geometric consistency index (GCI) can be assessed using Eq. (2.4).

$$GCI = \frac{2\sum_{i<j} lnc_{ij} - ln\frac{p_i}{p_j}}{(N-1)(N-2)} \quad (2.4)$$

Twenty-six experts were consulted for their inputs for the AHP analysis in Ghana, mainly through face-to-face interviews and emails. In the end, twenty-three responses were received, out of which three were invalid responses because they were incomplete. A total of twenty were considered valid and used to calculate the various weights used for the analysis.

**Table 2.2** Saaty's 9-point scale of relative importance [59]

| The intensity of the weight | Explanation | Implication |
|---|---|---|
| 1 | Equal significant | Two criteria contribute equally to objectives |
| 3 | Moderately more significant | One criterion slightly favored over another |
| 5 | Strongly more significant | One criterion strongly favored over another |
| 7 | Very strongly more significant | One criterion favored very strongly over another |
| 9 | Enormously more significant | The evidence favoring one criterion over another is of the highest possible order of affirmation |
| 2, 4, 6, 8 | Intermediate values | Employed to represent a compromise between the priorities listed above |
| | Reciprocals | If criteria $i$ has one of the above non-zero numbers assigned to it when compared to criteria $j$, then $j$ has the reciprocal value when compared with criteria $i$ |

## 2.4. Techno-economic analysis

This section assesses the techno-economic potential of wind power plants for the various identified suitable sites in the country. The techno-economic assessment was

conducted using the HOMER Pro software. It is a tool designed for optimizing RETs. It conducts many simulations to identify the optimum possible matching between demand and supply which helps developers during design stages [63]. The HOMER software's flow diagram is as illustrated in Fig. 2.5. Data for the simulations were obtained from the National Aeronautics and Space Administration (NASA). It is a monthly average wind speed of 50 m above the earth's surface for 30 years (January 1984 – Dec 2013).

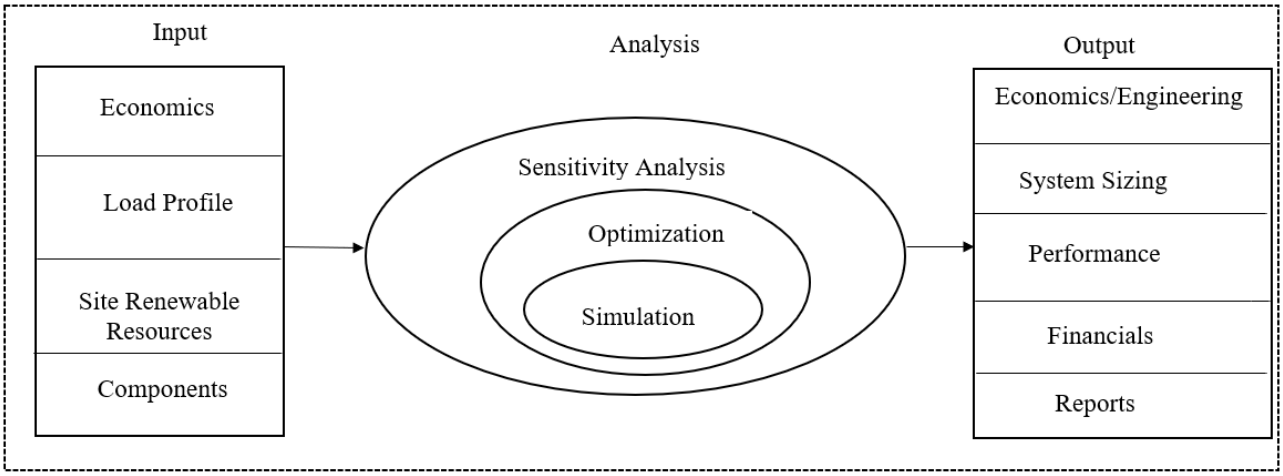


**Fig. 2.5** Flow-diagram for the HOMER software

### 2.4.1. Technical feasibility aspect

For the technical analysis, wind speed distribution is key in evaluating the energy potential in a specific site. The Weibull distribution is identified as a good fit for the estimation of wind speed and potential for candidate sites. The Weibull probability density function (PDF) can be estimated using Eq. (2.5) [63,64]. The Vestas V47 wind turbine was selected for the analysis, this turbine has a hub-height of 50 m and a lifetime of 20 years. The power curve for the vestas wind turbine power plant is presented in Fig. 2.6.

$$f(v) = {}^{k}/_{c} \cdot ({}^{v}/_{c})^{k-1} \cdot exp[-({}^{v}/_{c})^{k}] \quad (2.5)$$

Where, $k$ is the Weibull shape factor, $c$ denotes the Weibull scale parameter, $v$ signifies the wind speed (m/s).

The power curve of a wind turbine signifies the amount of power that is produced by the turbine as a function of the wind speed at a particular height. It must however be noted that the power output for a particular wind turbine is dependent on the wind speed. The turbine's output power can therefore be computed using the quadratic model as indicated in Eq. (2.6) [63,65].

$$P_w(V_v) = \begin{cases} P_n \cdot \dfrac{v_v^2 - v_d^2}{v_n^2 - v_d^2}, & V_d < V_v < V_n \\ P_n, & V_n \leq V_v < V_c \\ 0, & V_v \leq V_d \; et \; V_v \geq V_c \end{cases} \tag{2.6}$$

In this case, the nominal power is denoted by $P_n$, the outpower is denoted by $P_w$, $V_c$ signifies the cut-off speed of the wind, $V_d$ represents the cut-in speed of the wind, and $V_n$ also denote the rated wind speed.

The wind power can be evaluated when the speed of wind at a particular height is known, and thus can be computed using Eq. (2.7) [63].

$$\frac{v(z)}{v(z_a)} = \left(\frac{z}{z_a}\right)^{\alpha} \tag{2.7}$$

Where the mean wind speed at the desired height $z$ is represented by $v(z)$, $\alpha$ is the power index and the wind speed at the anemometer height $z_a$ is denoted by $v(z_a)$.

For the capacity factor (CF), it denotes the time fraction of the operation of the wind turbine over the period of the year on the site. This is estimated using Eq. (2.8) [65].

$$\boldsymbol{C_f = \frac{E_{out}}{E_r}} \tag{2.8}$$

Where $E_{out}$ (Wh) denotes the wind turbine's annual energy generated as expressed in Eq. (2.9), and $E_r$ (Wh) also represent the rated energy as expressed in Eq. (2.10).

$$E_{out} = \Delta T \cdot \int_0^{\infty} P_w \cdot f(v) \cdot dv \tag{2.9}$$

Where all parameters are as defined supra.

$$E_r = 8760 \cdot P_r \tag{2.10}$$

Where the rated power is denoted by $P_r$ (W).

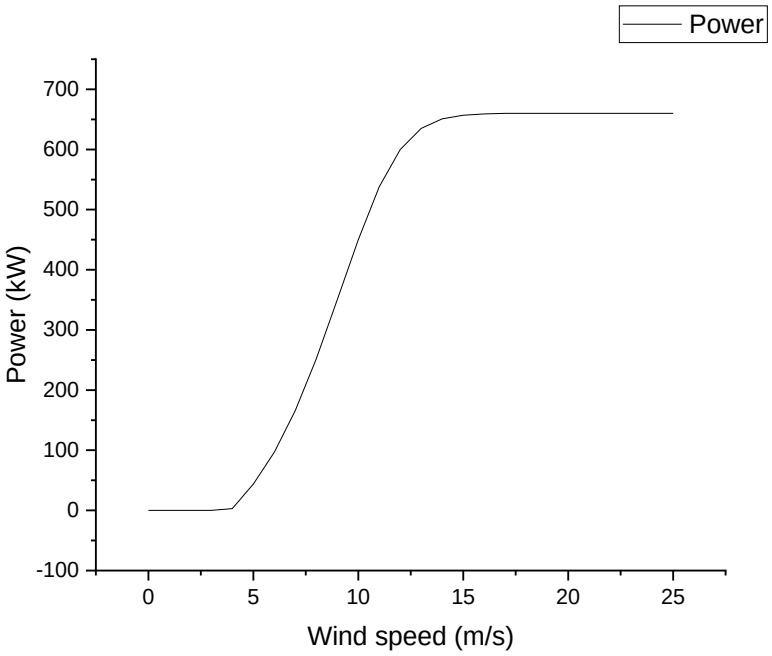


**Fig. 2.6** Power curve for the selected wind turbine (Data obtained from HOMER)

### 2.4.2 Diesel generator

The electrical output power for a diesel generator plant is a function of the fuel's lower heating value (LHV), electrical efficiency, and the mass flow rate of the fuel. The output electricity from the diesel generator can be computed using Eq. (2.11) [66]:

$$P_{DG,e} = m_{fuel} \times LHV_{fuel} \times \eta_{DG,e} \tag{2.11}$$

Where the diesel generator's electrical efficiency is represented by $\eta_{DG,e}$, and the mass flow rate of the fuel is also represented by $m_{fuel}$. The cost of fuel used for the assessment was 0,993 $/L which is the current cost of fuel in Ghana [63].

The heat output of the diesel generator, however, is contingent on the heat recovery ratio ($\eta_{DG,hr}$) as indicated in Eq. (2.12).

$$P_{DG,h} = m_{fuel} \times LHV_{fuel} \times (1 - \eta_{DG,e}) \times \eta_{DG,hr} \quad (2.12)$$

The schematic for the simulated power plant is represented in Fig. 2.7.

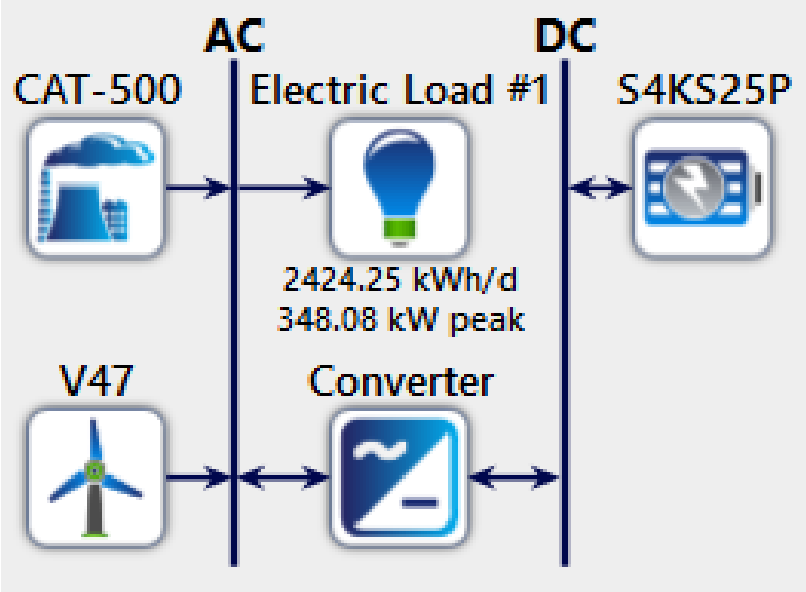


**Fig. 2.7** Schematic of the power plant system (obtained from HOMER)

### 2.4.3. Battery storage

The battery system is integrated into the system to store excess generated electricity from the WPP. This stored power is relied on during deficiency in electricity from the WPP unit [63].

## 2.5. Economic feasibility aspect

Economic viability assessment in the energy sector can be done using several financial indicators or factors, some of these include the levelized cost of electricity (LCOE), net present cost (NPC), equity payback period (EPP), internal rate of return (IRR) and simple payback period (SPP) [64]. This study assessed the bankability of WPP at the various identified sites in the country by finding some of these indicators and comparing them with each other to give both policymakers and other stakeholders a fair idea of the various sites for their viability.

### 2.5.1. Levelized Cost of Electricity

The LCOE is normally employed in the calculation of the unit cost of electricity that is produced and is described as the ratio of the present value of the entire cost incurred during the lifetime of the power plant and the entire energy that is extractable during that period. This is computed using Eq. (2.13) [67].

$$Min_{LCOE}\left(\frac{\$}{kWh}\right) = \frac{NPC_T * CRF(\vartheta, \partial)}{\sum E_{gen}(t)} \tag{2.13}$$

Where the minimum LCOE is represented by $Min_{LCOE}$, the capital recovery factor is also represented by $CRF$, $NPC_T$ denotes the total NPC. The annual discount rate and the life of the plant are represented by $\vartheta$ and $\partial$, respectively. The energy produced by the power plant in the $t$th hour is denoted by $E_{gen}(t)$. The CRF can be used to convert the overall NPC to the yearly capital cost using Eq. (2.14).

$$CRF = \frac{\vartheta(1+\vartheta)\partial}{(1+\vartheta)\partial - 1} \tag{2.14}$$

Also, the NPC is made of the operations and maintenance cost (O&M) and the present value of the initial investment cost ($IIC$). This is expressed mathematically as indicated in Eq. (2.15) [67].

$$NPC_T = IIC + \frac{\sum_{t=1}^{N}(O\&M)_t}{(1+i)^t} \tag{2.15}$$

Where the discount factor is represented by $i$, $(O\&M)_t$ represents the O&M cost for the $t$th year and the $N$ denotes the total number of years.

### 2.5.2. Simple payback period

SPP is commonly determined taking the ratio of the total initial investment costs and the yearly cash flow, this can be expressed mathematically as indicated in Eq. (2.16) [68].

$$SPP = \frac{C - I}{(C_e + C_s) - (C_f + C_{O\&M} + C_c)} \tag{2.16}$$

In this case, grants and incentives are represented by $I$, the annual life cycle savings is also represented by $C_s$, the yearly revenue from the electricity generation is denoted by $C_e$, expenditure for fuel is represented by $C_f$, $C_c$ denote annual debt cost, $C_{O\&M}$ signifies the annual operation and maintenance cost and $C$ is the total initial cost.

### 2.5.3. Internal rate of return

It is a metric employed in the financial analysis to evaluate the bankability of a probable investment. IRR is defined as the discount rate that makes the net present value (NPV) for all cash flows equivalent to zero in a discounted cash flow analysis. It is calculated using Eq. (2.17).

$$\sum_{i=0}^{N} \frac{C_i}{(1 + IRR)^i} \tag{2.17}$$

Where $C_i$ represents the cash flow for $i$ number of years and $N$ denotes the project lifetime and years.

### 2.5.4. Net present value

NPV is present value of the difference amount among the cash inflows and outflows over the lifetime of the power plant and can be estimated using Eq. (2.18) [64].

$$NPV = \sum_{i=0}^{N} \frac{\hat{C}_i}{(1+r)^i} \tag{2.18}$$

Where the discount rate is represented by $r$, the number of years is also represented by $i$, and $\hat{C}_i$ denotes the after-tax cash flow.

A capital cost of 1500 $/kW, replacement cost of 1500 $/kW and O&M cost of 0,03 $/year as used in [63,69] were adopted for the simulations for the WPP. The load profile for the simulation is represented in Fig. 2.8.

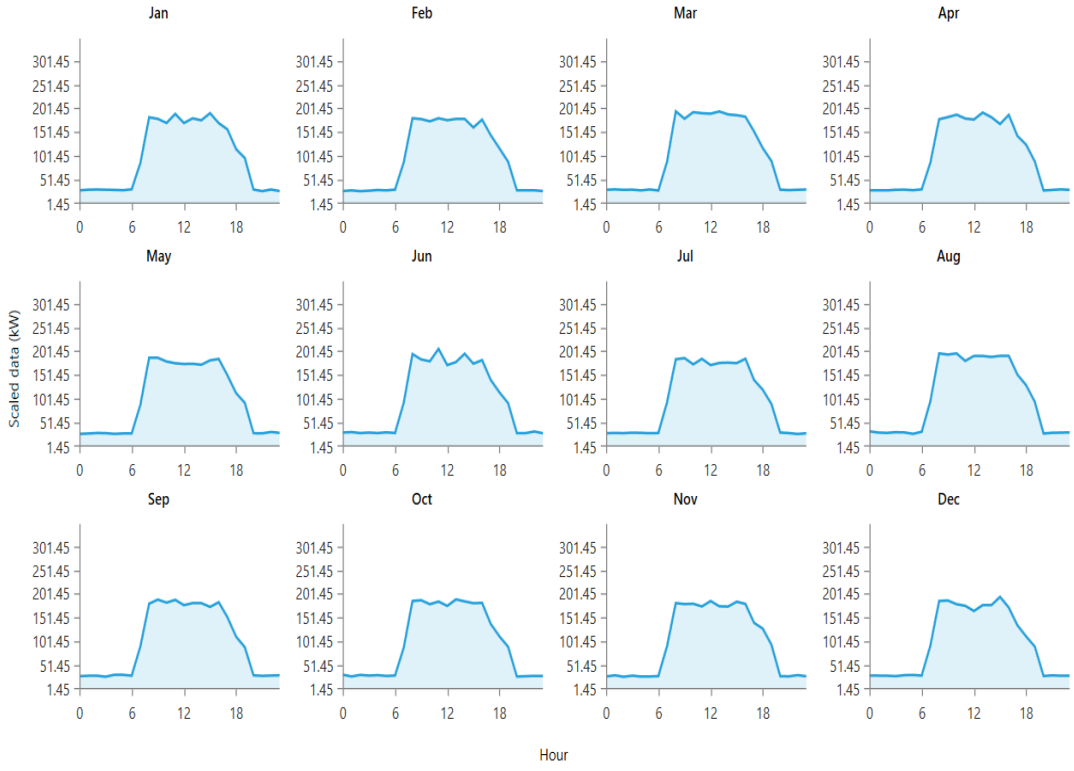


**Fig. 2.8** Monthly load profile used for the study

## 2.6. Results and Discussion

This section presents the results attained by means of the proposed methodology, the results were further discussed to give detail to the areas identified as suitable for the development of wind farms in Ghana. It also includes a techno-economic analysis of potential hybrid energy system i.e., Wind/DG/Battery/Converter for the identified sites.

### 2.6.1. Outcome of the implementation of Density-Based Clustering for wind

The first step of the methodology excludes all the unfavorable locations and provides only those sites that meet the minimum demography, environmental, and infrastructure variables. Fig. A1 in the appendix shows the spatial representation of all these variables. Step 2 evaluates the available sites for their average wind speeds using descriptive statistics, the top 10 percent of the sites available in Ghana have average combined wind speeds of 22,07 m/s. These statistics give the regions which are the most suitable for installing wind farms**.** Fig. 2.9 presents these suitable sites and represents approximately 1936 $km^2$ and provides the macro understanding of the availability of the resources but does not provide dense clusters available for the siting of the wind farm. Most of these sites are concentrated in the south to the central part of the country, with relatively small regions of high wind availability present in the country's northern section.

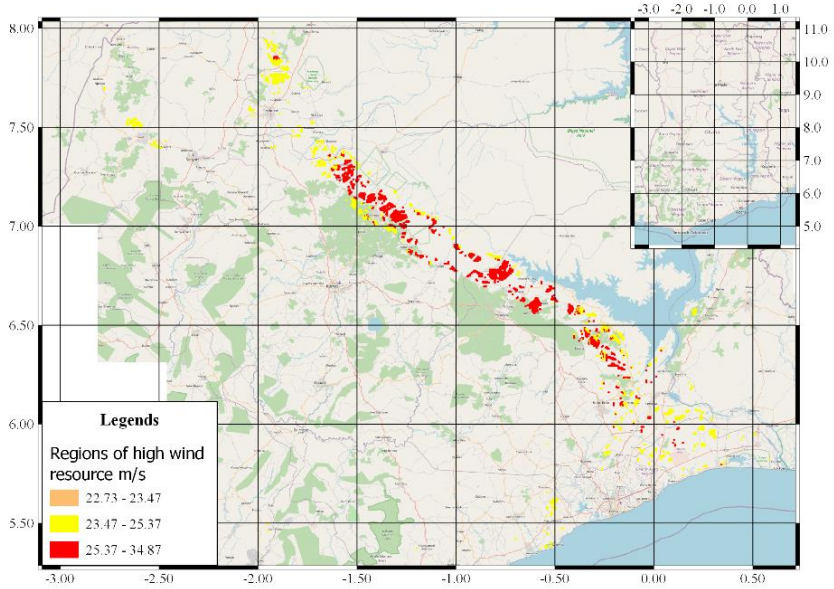


**Fig. 2.9** The top 10 percent of the wind energy sites

Step 3 of the analysis is the application of density-based clustering to detect geographically dense clusters of the required sizes. This requires the selection of an appropriate value of the parameters of the DBC i.e., minimum size of the cluster and the corresponding epsilon values, refer to Fig. 2.4**.** The minimum size of the cluster depends on the rated generation capacity required from the wind farm and is an exogenous policy

decision. In the case of Ghana, we have tested multiple scenarios by varying the minimum size for the required wind farm size ranging from 2,25, 6,25, and 15,25 $km^2$ with the corresponding epsilon values ranging from 0,007072, 0,014144, and 0,021216, respectively. By progressively increasing the parameters of the DBC the larger available dense clusters are identified and localized. The cluster pattern formation analysis reveals that the best contour optimization can be achieved using the DBC parameters of epsilon 0,007072, and the minimum size of 2,25 $km^2$. These parameters of the DBC not only provide the smallest cluster but also identified the largest clusters of complex contours and identified 117 distinct clusters ranging from size 2,25 $km^2$ to the largest cluster of 32 $km^2$. The comparison between the corresponding output of the DBC at a specified location using the different parameters is presented in Fig 2.10. Using the original data after step 2 of the analysis DBC is applied by varying the parameters and progressively larger dense clusters are formed.

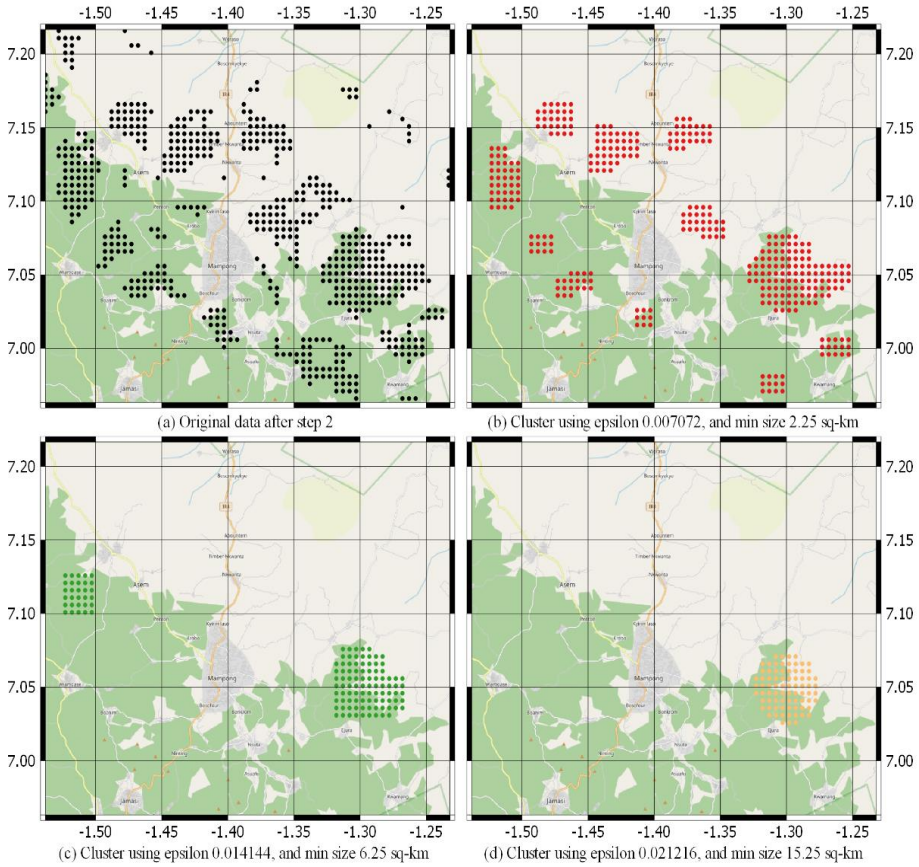


**Fig. 2.10** Cluster contours formation by varying the DBC parameters

The incorporation of DBC provides additional flexibility for policymakers in terms of the rated generation required from the wind farm this also provides the exact location and the theoretical generation capacity expected from the wind farm. It also provides the approximate contours of the wind farm optimizing its generation capacity. These characteristics are not provided by any other methodology used in the spatial multi-criteria analysis; our proposed methodology has this inherent contour optimization which helps in optimizing the generation capacities of the wind farm. This methodology is suitable for power plants in which the area requirement are high i.e., solar and wind power plants. The proposed methodology additionally identifies and optimizes the location selection process from the regional analysis. The other methodologies only provide suitable regions that require an additional survey to identify the optimal contours for the wind farm.

The final phase of the analysis is the final ranking of these identified clusters based on the criteria of energy availability of the cluster, the proximity of the cluster to road network, its terrain ruggedness, and the nearness of the cluster to transmission network. Based on the analysis of the cluster contour optimization analysis, the largest clusters will be ranked for the sake of brevity, and to conform with the main objective of the paper only the largest clusters based on their areas will be ranked for the future development priorities.

### 2.6.2. Ranking of candidate clusters

The application of the AHP on the clusters yields a ranked list of sites for the development of wind farms simultaneously providing policy input for future transmission expansion planning. Based on the analysis for the country of Ghana, 14 dense clusters of high wind energy availability were identified along with their contours for the optimization of the energy output from these clusters. Together these 14 clusters represent areas of approximately 280 $km^2$ which can be utilized for the generation of renewable energy using wind resources of the country. The ranking of the clusters is based on the additional development requirements need to harness these wind resources for the

generation of renewable energy using wind. These development criteria are the additional road development, additional transmission network development, the land ruggedness. Every country has different capabilities in developing these infrastructures and the relative importance of these infrastructures in the case of Ghana has been identified using AHP, the results of which are presented in Tables A1 to A3 in the Appendix section. The consistency ratio obtained for the AHP matrix was found to be acceptable and hence the decision matrix can be used for further analysis.

An important observation is that the largest sites are within relative proximity of the national transmission network and the transportation network. Interestingly the highly ranked sites are not present near the coast but are present in the central part of the country near the cities of Mampong and Techiman. Fig. 2.11 and the corresponding tabular data on the sites are also presented in Table 2.3. The average size of the clusters is around 19 $km^2$ with a maximum size of up to 32 $km^2$.

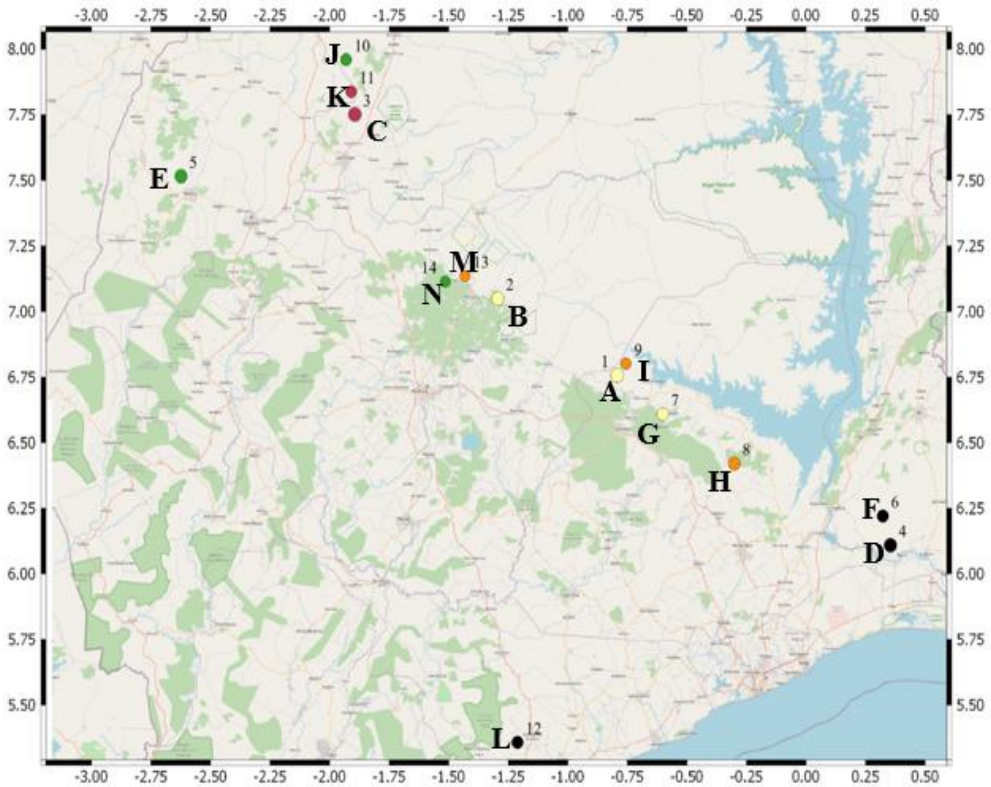


**Fig. 2.11** Sites ranking for development of wind farm, Ghana

**Table 2.3** Ranking and the site characteristics of the wind clusters

| Priority | Size in $km^2$ | Mean TRI | Combined average mean speed (m/s) | Distance from road (km) | Distance from transmission (km) | Average wind speed (m/s) | | | |
|---|---|---|---|---|---|---|---|---|---|
| | | | | | | 50 m | 100 m | 150 m | 200 m |
| 1 | 31,75 | 1,62 | 31,66 | 4,70 | 10,00 | 6,40 | 7,63 | 8,59 | 9,04 |
| 2 | 28,5 | 1,68 | 29,56 | 4,00 | 4,50 | 6,10 | 7,30 | 7,96 | 8,19 |
| 3 | 32 | 1,14 | 23,75 | 3,00 | 10,00 | 4,71 | 5,78 | 6,52 | 6,74 |
| 4 | 29 | 0,92 | 22,55 | 5,00 | 13,00 | 4,26 | 5,14 | 6,15 | 7,01 |
| 5 | 26,25 | 1,59 | 23,38 | 3,50 | 13,50 | 4,62 | 5,55 | 6,33 | 6,88 |
| 6 | 17,25 | 0,96 | 22,52 | 4,00 | 5,70 | 4,29 | 5,17 | 6,11 | 6,95 |
| 7 | 18,5 | 2,05 | 29,09 | 4,00 | 4,00 | 6,08 | 7,24 | 7,80 | 7,95 |
| 8 | 21,25 | 2,14 | 25,88 | 3,20 | 5,00 | 5,33 | 6,43 | 7,02 | 7,10 |
| 9 | 10 | 0,47 | 28,09 | 7,00 | 11,00 | 5,59 | 6,71 | 7,59 | 8,22 |
| 10 | 14,5 | 1,38 | 22,88 | 2,50 | 9,00 | 4,44 | 5,46 | 6,29 | 6,69 |
| 11 | 13 | 1,07 | 24,91 | 3,90 | 13,50 | 5,11 | 6,12 | 6,73 | 6,94 |
| 12 | 17 | 1,97 | 22,69 | 3,00 | 7,00 | 4,43 | 5,31 | 6,17 | 6,78 |
| 13 | 10,25 | 1,57 | 28,40 | 2,00 | 9,50 | 5,78 | 6,86 | 7,61 | 8,14 |
| 14 | 10 | 2,39 | 23,68 | 2,30 | 16,00 | 4,66 | 5,61 | 6,40 | 7,01 |

For identification purposes, the various clusters as presented in Table 2.4 are also assigned identification letters to make it easier for reference.

**Table 2.4** Specific site locations for the various identified clusters

| Identification | Clusters | x-centroid | y-centroid |
|---|---|---|---|
| A | 127 | -0,792 | 6,757 |
| B | 114 | -1,294 | 7,050 |
| C | 128 | -1,893 | 7,752 |
| D | 116 | 0,355 | 6,109 |
| E | 105 | -2,624 | 7,516 |
| F | 69 | 0,322 | 6,221 |
| G | 74 | -0,601 | 6,609 |
| H | 85 | -0,301 | 6,421 |
| I | 40 | -0,756 | 6,801 |
| J | 58 | -1,931 | 7,961 |
| K | 52 | -1,909 | 7,839 |
| L | 68 | -1,211 | 5,357 |
| M | 41 | -1,432 | 7,136 |
| N | 40 | -1,514 | 7,115 |

The exact sizes of the various clusters in square kilometers have already been calculated and presented in Table 2.3. Fig. 2.12 shows the monthly average wind speed characteristics for the various sites.

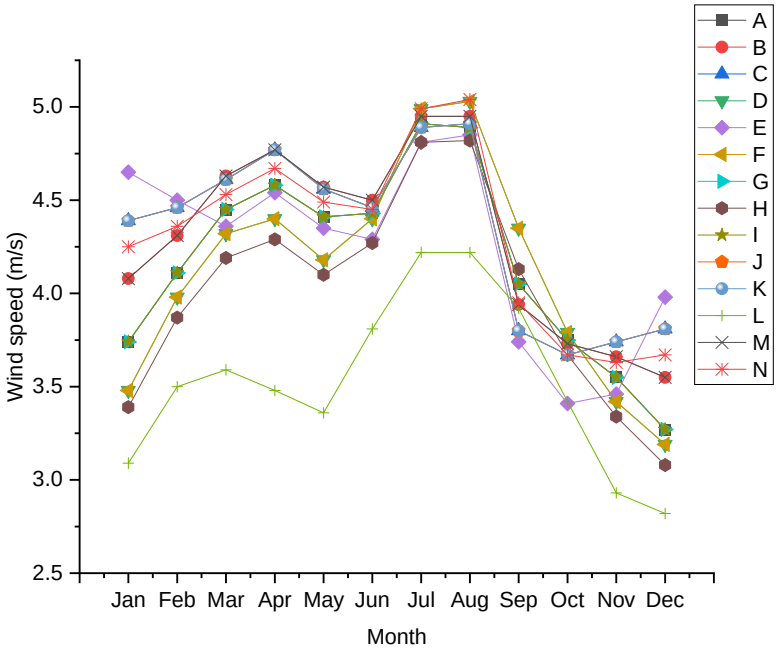


**Fig. 2.12** Wind speed characteristics at the various clusters at 50 m (data obtained from NASA)

### 2.7. Sensitivity analysis

In order to understand the possible effect of different views from experts in the sector, a sensitivity analysis was conducted on the AHP to assesses the effect of different weighting options on the ranking. Such analysis helps stakeholders to appreciate the impact of other factors on the final site selection. Three sensitivity scenarios are developed to check the consistency of the cluster ranking. The current AHP scenarios give a weight of 0,570 to energy availability (i.e., technical parameter) and 0,429 to economic factors. We developed two more scenarios; in the first scenario, we assigned equal weights to the technical and economic factors, i.e., 50 percent technical and 50 percent economic. We reversed the current AHP weights by giving 0,43 to technical and 0,570 to economic factors in the second scenario, as shown in Table 2.5. Under these two additional scenarios, we checked the change in the ranking of the identified clusters.

**Table 2.5** Sensitivity analysis for different scenarios

| | Technical | Economic | | |
|---|---|---|---|---|
| Sensitivity scenario | Energy availability (i.e., wind speed) | Transmission proximity | Terrain ruggedness | Transportation proximity |
| Current AHP weights | 0,570 | 0,110 | 0,254 | 0,065 |
| Equal weights | 0,500 | 0,166 | 0,166 | 0,166 |
| Higher economic weights | 0,429 | 0,190 | 0,190 | 0,190 |

According to the results, as indicated in Fig. 2.13**,** the effect of the two other scenarios had a significant effect on the final rankings of the various sites. For instance, clusters A, B, C, D remained unchanged under equal weights scenario.

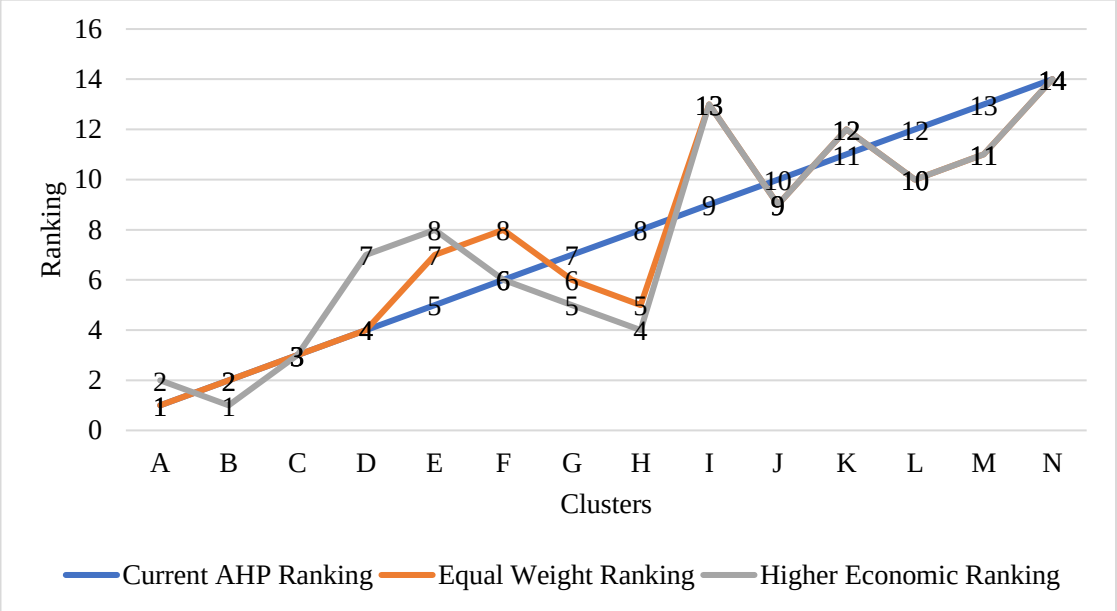


**Fig. 2.13** Sensitivity analysis on the AHP

However, the same cannot be observed about the higher economic weights scenario because all the priority areas had their positions changed under that scenario. For example, under the base case scenario where experts gave more prominence to technical parameters, the priority is cluster A, which is 31,75 km$^2$ with a distance to road and transmission of 4,7 km and 10 km. However, under the case where economic factors are given higher importance, the priority area will be cluster B, a total area of 28,5 km$^2$ with

a distance to road and transmission network of 4 km and 4,5 km. Thus, the results from the various scenarios have shown the significant effect of both technical and economic factors on the final site selection.

### 2.8. Techno-economic analysis

The results of the technical analysis for the various WPP at the various sites are presented in this section. The HOMER software was employed to evaluate different scenarios of WPP relative to their techno-economic potentials. The results as presented include a detailed analysis of both technical and economic indicators.

#### 2.8.1. Technical analysis

The economics of a power plant is greatly affected by its capacity factor and the annual electricity generation, this is because these factors are vital input variables for assessing the economics of the system. Results from the simulations as indicated in Table 2.6 have shown that cluster C located around the Techiman enclave has the highest electricity generation from the WPP. The least electricity output for the WPP plant was recorded at cluster L which is an area around Abura Asebu Kwamankese in the Central region. It therefore suggests that the diesel generator operated longer hours in cluster L which has implications not only on the economics of the power plant but also on the level of emissions from the plant into the environment. The hours of operation for the diesel generator and the CF at the various cluster sites are represented in Fig. 2.14. It is clear from the results that the higher the CF of the WPP, the lesser the operational hours of the diesel generator. It, therefore, suggests that increasing the wind speed at a particular site could lead to a reduction in the consumed fuel. Therefore, the hub height of the turbine can be increased from the current 50 m used for the analysis to experience higher wind speeds since as indicated supra, the wind speed is higher at higher heights. The highest electricity output for the WPP occurs in July and August with the least occurring in the last three months of the year for all sites.

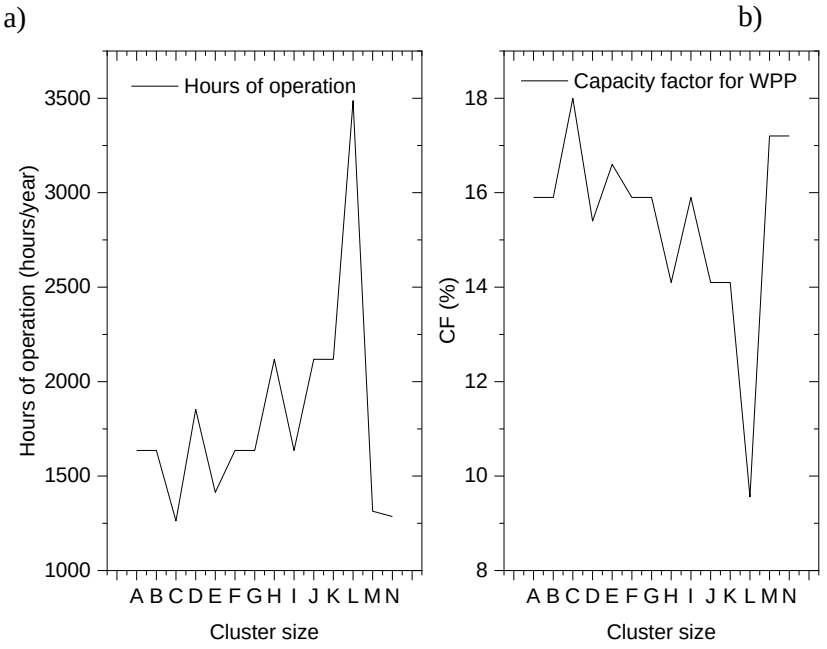


**Fig. 2.14** Operation hours (a) for diesel generator and CF (b) for WPP using HOMER

**Table 2.6** Electrical output and fuel consumption for the various sites

| Cluster | Generator output, kWh/year | WPP output, kWh/year | Excess electricity, kWh/year | Renewable fraction, % | Total fuel consumed, L |
|---|---|---|---|---|---|
| A | 209970 | 917672 | 141297 | 76,3 | 62501 |
| B | 209970 | 917672 | 141297 | 76,3 | 62501 |
| C | 165927 | 1 038105 | 212944 | 81,2 | 49435 |
| D | 237686 | 890589 | 146854 | 73,1 | 70761 |
| E | 185467 | 957020 | 153754 | 79,0 | 54938 |
| F | 209970 | 917672 | 141297 | 76,3 | 62501 |
| G | 209970 | 917672 | 141297 | 76,3 | 62501 |
| H | 274353 | 812408 | 108687 | 69,0 | 81496 |
| I | 209970 | 917672 | 141297 | 76,3 | 62501 |
| J | 274353 | 812408 | 108687 | 69,0 | 81496 |
| K | 274353 | 812408 | 108687 | 69,0 | 81496 |
| L | 451174 | 552444 | 48145 | 49,0 | 134055 |
| M | 170198 | 992261 | 172611 | 80,2 | 50558 |
| N | 166376 | 994646 | 170724 | 81,2 | 49435 |

### 2.8.2. Economic analysis

The financial viability of any project is part of the essential parameters that any investor will want to look at before making an investment decision. The economic analysis was done by identifying certain key financial indicators such as the LCOE, IRR, NPC, OC, SPP, and ROI. A comparative data for the various identified candidate sites are presented in Table 2.7, it is found out that the LCOE of all sites fundamentally falls within a range of 0,20 – 0,30 $/kWh. The LCOE for a standalone WPP without the diesel generator as indicated in Table 2.7 shows a reduced LCOE compared to the hybrid DG/WPP/Battery/Converter system. The reduction in LCOEs can be attributed to the fact that there was no cost of fuel in that system. The current cost of electricity in Ghana ranges between 12 – 17 ¢/kWh for the residential sector, 15 – 25 ¢/kWh for the non-residential sector, and 16 – 22 ¢/kWh for the industrial sector (i.e., special load tariff system for industrial energy use purposes; supply voltages HV-High Voltage (33000 V); MV- Medium Voltage (11000 V); and LV–Low Voltage [70]. The DG/WPP/Battery/Converter system will be too expensive for the residential sector if implemented in its current form without any subsidies to the customer or incentives to the investor from the government. It will, however, fall within the tariff structure for the non-residential and industrial sectors if implemented under the conditions used for the study. However, the WPP recorded LCOEs fall below that of the DG/WPP/Battery system, which if implemented under the conditions used for the current study will present an affordable tariff structure for all consumers. The tariffs for the non-residential and industrial sectors can be reduced by almost 50% if the upper limit of the current range of tariff structure is taken into consideration.

Other very important economic indicators during the analysis of such projects are IRR and the return on investment (ROI). ROI is a traditional tool that is employed mostly in the private sector to assess and compare investments and projects. Most simply, it is defined as the ratio of the net earnings accrued from a particular project and the project costs. Currently, it is also used in the public sector for several evaluations [71].

**Table 2.7** Economic results for the various sites

| Site | NPC, $ | LCOE, $/kWh (DG/WPP/Battery system) | OC, $ | LCOE, $/kWh (WPP, only) |
|---|---|---|---|---|
| A | 2 084902 | 0,22 | 76385,66 | 0,11 |
| B | 2 084902 | 0,22 | 76385,66 | 0,11 |
| C | 1 983466 | 0,21 | 63528,74 | 0,10 |
| D | 2 153978 | 0,23 | 84335,23 | 0,11 |
| E | 2 023936 | 0,21 | 69099,23 | 0,11 |
| F | 2 084902 | 0,22 | 76385,66 | 0,11 |
| G | 1 964796 | 0,22 | 76385,66 | 0,11 |
| H | 2 268500 | 0,24 | 95025,09 | 0,13 |
| I | 2 084902 | 0,22 | 76385,66 | 0,11 |
| J | 2 268500 | 0,24 | 95025,09 | 0,13 |
| K | 2 268500 | 0,24 | 95025,09 | 0,13 |
| L | 2 753957 | 0,29 | 146254,50 | 0,18 |
| M | 1 967386 | 0,21 | 64618,32 | 0,10 |
| N | 1 964796 | 0,21 | 63633,19 | 0,10 |

ROI gives information on the level at which the amount of money invested in a particular project returns as profit or loss. In other words, it allows for the assessment of efficiency [72]. The payback period for projects is also one of the many ways that can be employed to evaluate the profitability of projects such as the one considered in this study. The economic indicators for the various sites are presented in Table 2.8. An economically viable project must have its IRR to be more than the discount rate [64]. Considering the 10% discount rate used for the analysis in this study and comparing same to the various IRR for all clusters sites suggests that all sites are economically viable for the studied project. Data from the table also suggests that the site with cluster M comes as the optimum site since the least SPP of 4,30 years and highest IRR 22,8% were obtained for the power plants at that site.

**Table 2.8** Economic indicators for the DG/WPP/Battery system for all sites

| Site | Present worth, $ | Annual worth, $/year | ROI, % | IRR, % | SPP, years | Discounted payback, % |
|---|---|---|---|---|---|---|
| A | 1 653340 | 152813 | 17,4 | 22,0 | 4,45 | 5,69 |
| B | 1 653340 | 152813 | 17,4 | 22,0 | 4,45 | 5,69 |
| C | 1 754775 | 162188 | 17,7 | 22,4 | 4,37 | 5,57 |
| D | 1 584263 | 146428 | 17,0 | 21,6 | 4,52 | 5,80 |
| E | 1 714306 | 158448 | 17,6 | 22,3 | 4,39 | 5,60 |
| F | 1 653340 | 152813 | 17,4 | 22,0 | 4,45 | 5,69 |
| G | 1 653340 | 152813 | 17,4 | 22,0 | 4,45 | 5,69 |
| H | 1 469742 | 135844 | 16,2 | 20,7 | 4,70 | 6,09 |
| I | 1 653340 | 152813 | 17,4 | 22,0 | 4,45 | 5,69 |
| J | 1 469742 | 135844 | 16,2 | 20,7 | 4,70 | 6,09 |
| K | 1 469742 | 135844 | 16,2 | 20,7 | 4,70 | 6,09 |
| L | 984284 | 90974 | 13,0 | 17,2 | 5,53 | 7,54 |
| M | 1 770855 | 163674 | 18,1 | 22,8 | 4,30 | 5,46 |
| N | 1 773445 | 163914 | 18,1 | 22,7 | 4,31 | 5,48 |

### 2.8.3. Environmental impact assessment

One major challenge globally is the impact of emissions from traditional power plants that rely on fossil fuels for electricity generation, this is more important because of the many health issues and hazards they are associated with. It is for this reason that protocols and standards have been set to help minimize and mitigate greenhouse gas emissions [73]. As indicated in Fig. 2.15, the higher the output or CF of the RE system, the lesser the emissions of GHG from the power plant. This is obviously due to the fewer operational hours of the diesel generator; thus, the environmental GHG emissions reduction potential will be higher.

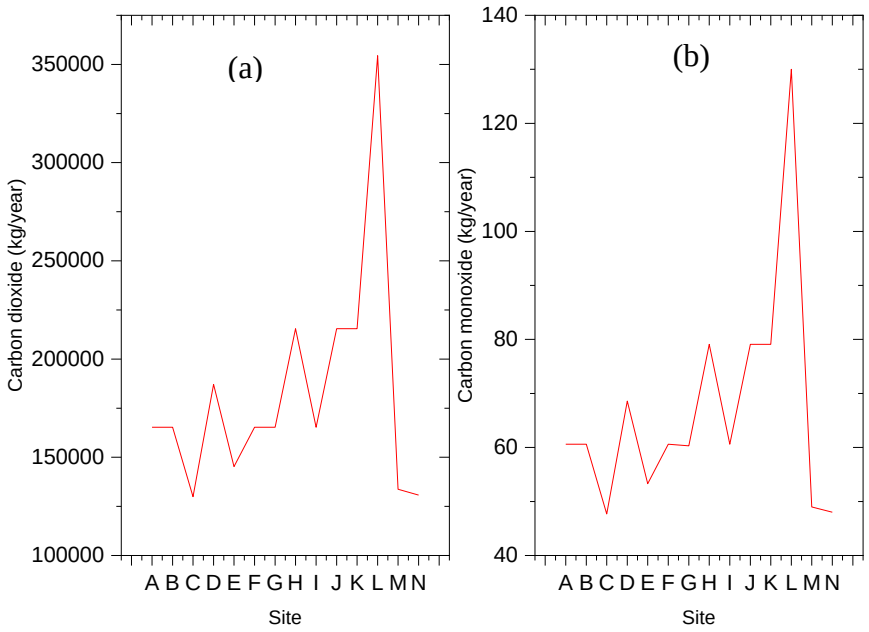


**Fig. 2.15** Carbon dioxide (a) and Carbon monoxide (b) emissions for each site using HOMER

The environmental analysis puts sites C, M, and N in a better position than the other sites, this can be ascribed to the higher CF values of the WPP recorded at those sites due to the high wind speed. Site L was identified as the worst site for WPP installation. A carbon dioxide and carbon monoxide of 354,474 kg/year and 130 kg/year, respectively, were emitted at that site.

## 2.9. Conclusions and policy implications for chapter 2

The selection of an appropriate site for the development of wind farms is one of the significant implementation steps for such projects. This paper proposed a new approach for selecting the optimal sites for developing wind farms in emerging economies, different from the existing approach, which is generally biased towards the availability of existing infrastructure. The existing methodologies are mainly favorable to developed economies with well-structured and advanced infrastructural facilities spread evenly, which is not the same for most developing countries. The spatial multi-criteria analysis

and density-based clustering approach implemented was used for the first time to identify sites with high wind speed in Ghana.

The results provide policy input for future transmission network expansion planning. A total of 14 clusters were identified from the analysis. The average size of the clusters is around 19 $km^{2,}$ with a maximum area of up to 32 $km^2$. All identified geographical clusters are in relative proximity to both transmission and transportation networks. These clusters represent the most wind energy-rich regions of Ghana. The methodology that we have proposed does not suffer from infrastructure bias. This methodology applied spatial multi-criteria analysis to eliminate problematic areas, density-based clustering to identify the dense cluster and their complexity contours. The combination of the spatial multi-criteria and the density-based clustering is helpful for other location decisions of other renewable resources, which require large areas for extracting and converting renewable energy resources, i.e., solar, and tidal.

The techno-economic and environmental analysis conducted identified the least LCOE of 0,21 $/kWh at sites C, E, M, and N. The results also suggest that cluster M has the least SPP of 4,30 years, and the highest IRR 22,8% were obtained for the power plant at that site. The environmental analysis puts sites C, M, and N better than the other sites, attributed to the higher CF values of the WPP recorded at those sites due to the high wind speed.

With the obtained results, the Ghanaian government can develop a master plan for developing the country's wind energy sector by concentrating on the top 10 percent sites identified in this study. The proposed methodology can be used in any case study to identify optimal locations for developing wind energy farms anywhere worldwide, particularly in developing countries with less-developed electricity transmission networks. A combined wind and solar power plant sites are presented in Fig. 2.16.

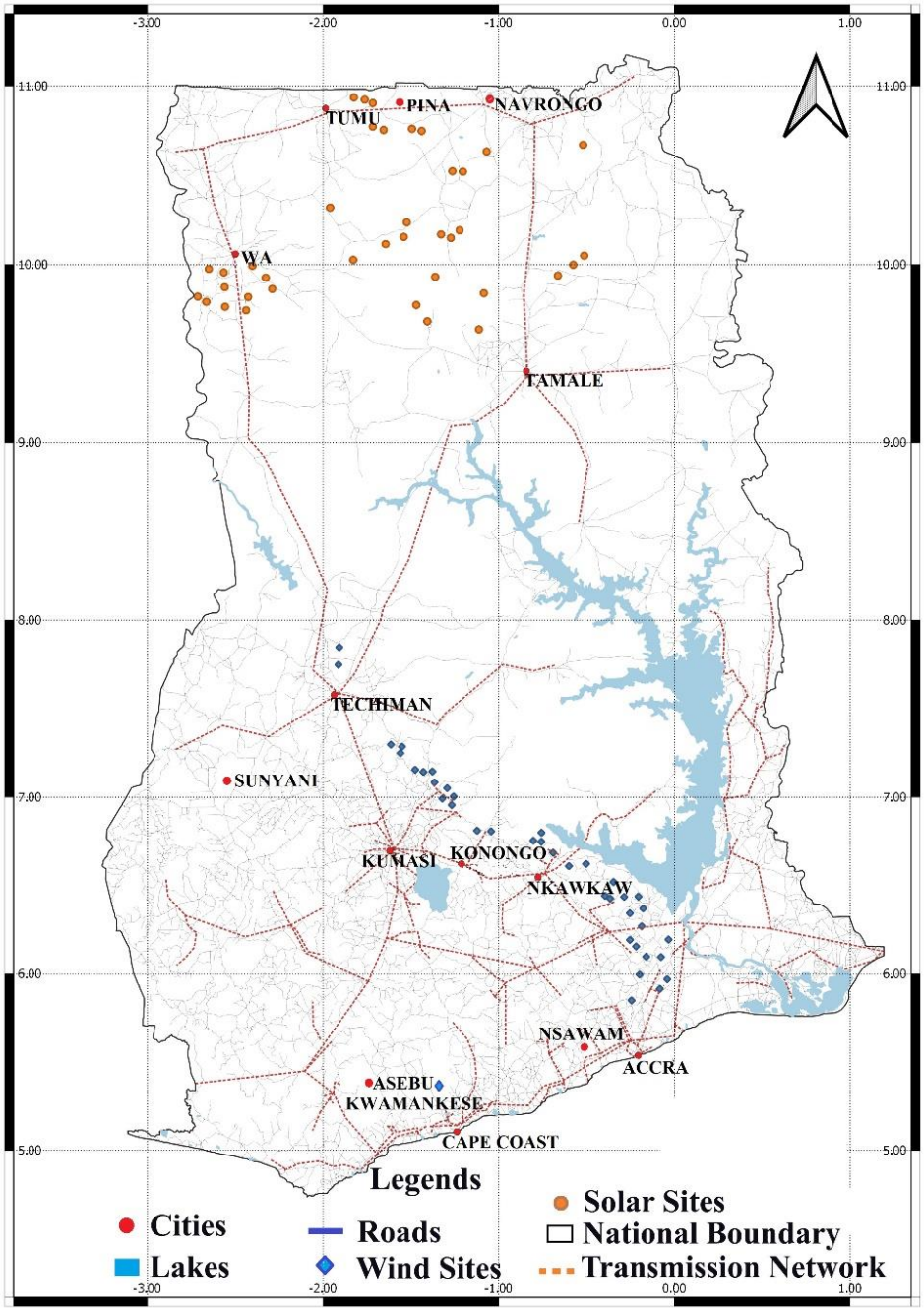


**Fig. 2.16** Combined wind and solar power plant sites in Ghana

# CHAPTER 3. OPTIMIZING PHOTOVOLTAIC POWER PLANT SITE SELECTION USING ANALYTICAL HIERARCHY PROCESS AND DENSITY-BASED CLUSTERING – POLICY IMPLICATIONS FOR TRANSMISSION NETWORK EXPANSION, GHANA

## 3.1. Optimizing photovoltaic power plant sites for Ghana

This study uses a combination of DBSCAN, AHP and the GIS as presented in chapter 2 for the identification of the appropriate site for the installation of solar power plants (SPP). This methodology incorporates local capabilities to generate a final ranking of solar sites for development. This study will serve as reference material for policy and decision-makers during planning for the development of solar PV systems in developing countries.

## 3.2. Land requirements for solar power plant installations

SPP, either on the ground or rooftops, requires considerable space for installation. Although SPP has some significant sustainability advantages over conventional thermal power plants (i.e., natural gas or coal-based), a critical drawback of SPP is the large area required to generate a relatively less energy capacity. For instance, research shows that a thermal power plant with 100 MW capacity requires less than 10% of the total land area required for an equivalent capacity SPP [74]. The National Renewable Energy Laboratory (NREL) conducted a study to assess the land requirements for installing various SPP technologies in the US. The results of their study are in Table 3.1. A pictorial description of the study area is presented in Fig 3.1.

**Table 3.1** Land-Use Requirements for PV and CSP Projects [75]

| Technology | Direct Area | | Total Area | |
|---|---|---|---|---|
| | Capacity-weighted average land use (acres/MWac) | Generation-weighted average land use (acres/GWh/year) | Capacity-weighted average land use (acres/MWac) | Generation-weighted average land use (acres/GWh/year) |
| Large scale PV (>20 MW) | 7,2 | 3,1 | 7,9 | 3,4 |
| Fixed | 5,8 | 2,8 | 7,5 | 3,7 |
| Single-axis | 9,0 | 3,5 | 8,3 | 3,3 |
| Double-axis CPV | 6,1 | 2,0 | 8,1 | 2,8 |
| Small PV (>1 MW, < 20 MW) | 5,9 | 3,1 | 8,3 | 4,1 |
| Fixed | 5,5 | 3,2 | 7,6 | 4,4 |
| Single-axis | 6,3 | 2,9 | 8,7 | 3,8 |
| Double-axis flat panel | 9,4 | 4,1 | 13 | 5,5 |
| Double-axis CPV | 6,9 | 2,3 | 9,1 | 3,1 |
| CSP | 7,7 | 2,7 | 10 | 3,5 |
| Tower | 8,9 | 2,8 | 10 | 3,2 |
| Parabolic trough | 6,2 | 2,5 | 9,5 | 3,9 |
| Linear Fresnel | 2,0 | 1,7 | 4,7 | 4,0 |
| Dish Stirling | 2,8 | 1,5 | 10 | 5,3 |

**Note:** the capacity-based land-use intensity is expressed in MWac or GWac to maintain consistency, this is because CSP systems are expressed as such. Readers are referred to Ref [75] for the conversion factor between ac-rating and dc-rating since that is beyond the scope of this study.

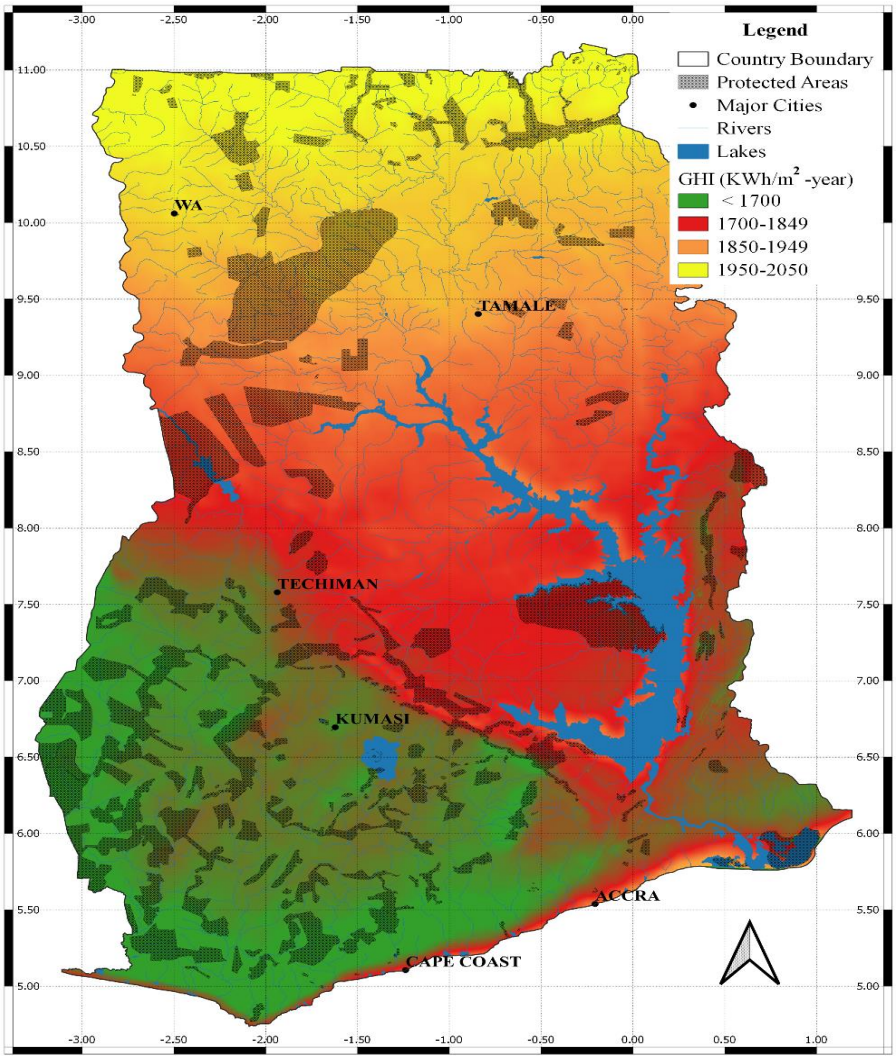


**Fig. 3.1** Study area map

### 3.3. Materials and Methodology

The methodology utilized in the identification of the top sites for Ghana has three macro phases of analysis. The first phase of the analysis is data preparation, the main objective of this phase of analysis is the elimination of the unsuitable areas from further considerations. The second phase of the analysis is clustering identification with an objective of identifying the most suitable sites with solar irradiance and then applying density-based clustering for the minimum desired site sizes. The third phase of the analysis cluster ranking considers the local infrastructure development capabilities and ranks the site clusters using AHP.

In data preparation, the data set on the evaluation criteria is rasterized using QGIS [35], the constraints used in the rasterization process are discussed in the section on evaluation criteria (section 3.4). The evaluation criteria that are considered in the analysis are the minimum solar irradiance required for the economically viable solar project, the land categories, the protected areas, the maximum acceptable slope percentages for the solar power plant, land sliding hazard triggered by earthquakes and rainfall, terrorism events, densely populated areas, flooding hazards, economic sustainability factors, and minimum infrastructure buffer requirement. After identification of the minimum constraints of these factors in the context of the SPP, a raster analysis was applied to obtain the suitable areas. The main objective of this analysis is to eliminate the unsuitable areas from the further SPP site location decision.

In the cluster identification phase of the analysis, several policy-related decision criteria are incorporated, the first is related to the governmental priority of developing the available solar power resources i.e., developing the top 5 percent or top 10 percent available sites in terms of solar irradiance, etc. The second is on the minimum area's requirements i.e., governments execute large-scale renewable projects progressively due to budgetary constraints. In this work, we will be demonstrating the scenario of developing the top 20 percent suitable sites of minimum areas of 432 acres. The generation capacities of the solar farm and the corresponding size requirement are already presented in Table 3.2. After the identification of these decisional constraints, the density-based clustering is applied to the output of the previous phase of analysis. This step identifies the clusters of the required minimum size of any irregular shape. Refer to Fig. 2.4 for a pictorial representation of the density-based clustering.

In the final phase, the analysis ranking of the identified clusters is carried out using AHP. Multiple criteria are used to rank the clusters these criteria are the energy availability, the ruggedness of the terrain, the transmission network expansion requirements from the cluster center, and the transportation network expansion requirement from the cluster center. Each country has its capabilities for developing the infrastructure requirements for the SPP. These capabilities can be surveyed from the

corresponding governmental official. In the case of Ghana, we have surveyed the officials of the Energy Commission to evaluate the relative importance of the above-discussed criteria using the pairwise comparison method AHP, the corresponding weightage of these criteria are presented in Table A2 in the Appendix section. The AHP is used extensively in the multi-criteria evaluation and provides the mechanism to check the consistency of the decision. For a detailed description of AHP readers are referred to [26,47,76].

### 3.3.1. Evaluation Criteria

The selection of a site for the installation of a PV system is affected by multiple factors. These factors can be classified into technical, environmental, social, and financial. These features are contingent on the biophysical attributes, geographical locations, and socio-economical infrastructure in the area under study [77]. After a complete literature review, we have identified the criteria and their corresponding limits which are of importance for the siting decision of the SPP the corresponding dataset used for the analysis are also discussed with the individual criteria. These criteria will help in excluding the unsuitable regions from the final site selection process.

**(a) Solar radiation**: Availability of solar irradiation plays a key role in the construction of solar power plants. For a commercial PV, an annual global horizontal irradiance (GHI) of more than 1700 kWh/m$^2$/year is required for construction [76]. The PV system can function in converting the DNI (Direct nominal irradiation) and the reflected diffuse horizontal irradiation (DHI). The GHI value of a spot is a function of DNI and DHI. The solar-powered power plants for which DNI values are important relies primarily on concentrating the solar irradiance for heating a medium and subsequent energy generation from the medium [78,79], such a power plant also has to incorporate solar tracking technologies to capture the maximum solar irradiance with the movement of the sun. For the power plant which directly converts the solar irradiance to electricity, GHI is more important as this represents

both the direct and indirect irradiance to a unit area, the indirect irradiance is due to the reflectance of direct irradiance by water molecules or aerosols present in the environment. The data for the solar radiation for Ghana was obtained from the Global Solar Atlas [80], Fig. 3.1, this dataset is provided in the WGS 84. The resolution of the solar resource data is in 9 arcsec (nominally 250 meters). The scope of this study is the direct conversion of the solar irradiance to electricity we will consider only GHI value for the location selection.

The energy output of the SPP depends on multiple factors, the GHI which gives the irradiance at a unit area is the most used variable in the siting decision of the fixed PV SPP. As this variable gives irradiance on the unit area ($kWh/m^2$), this study used the yearly average values for the GHI yearly average of solar irradiance in $kWh/m^2$/year. The GHI variable gives both the direct irradiance (DNI) and the indirect irradiance (DHI).

**(b) Natural and social hazards**: Construction of large scale SPP requires a vast flat land, an acceptable maximum land percentage slope which ranges between 3% to 5,2% is acceptable for PV power plants [48]. A higher slope will increase the cost of construction and maintenance as well as increase the chances of landslide due to rainfall and earthquakes. This paper excludes surface areas with more than 5% of slope for the PV installation. This is also important because terrains with high slopes make it difficult for constructors of such power plants to get the right angle for the panels. The data set of the slope is taken from [40,81]. The data on the areas at higher risk to land sliding is taken from [49].

The other natural hazards considered in the is study are the hazards of flooding, both coastal and river flooding. Installing large power plants in the areas prone to flooding can seriously increase the operations and maintenance cost of the projects. As these power plants require significant investment and have a long service life, protecting the investment from such hazards is important. For the coastal flood risk assessment [82,83] was used, and for flood risk [84] was used for the analysis.

The third hazard which is categorized as a social hazard which is considered in this study is the hazards caused by society. Developing nations are prone to social unrest due to the change in social and economic conditions. This change manifests in the form of terrorist acts and social unrest. As the large power project needs to be safeguarded from these social hazards, we have also considered the historical terrorism acts in the final siting. The data set for the social hazards are taken from [85].

**(c) Land use and coverage**: Experts recommend barren land for the installation of such facilities [86], as the environmental impact to the barren lands are minimal when installing SPP. Conversely, forests and large vegetation also negatively affect the SPP, as taller vegetation in the proximity can shade PV collectors and thus require additional maintenance for preventing the shading. In the absence of barren lands, shorter vegetation areas are, therefore preferred [47]. The land-use data of Ghana indicates a relatively fewer barren lands, Fig. 3.2, so in the analysis, the arid land and the open wildlands are considered suitable in the final site selection decision. Although the SPP installation costs for the open wildland will be relatively higher than barren land. Forest and agricultural land are excluded from the location decision, this decision was taken to preserve the ecological and social footprint. The dataset available for the land-use classifies the total area in urban, agricultural, arid, forest, open wildland, and water bodies. For details about the characteristics of these classifications refer to [47].

**(d) Major settlement areas:** Solar power plants require large space for their installation, and as a result installation near urban settlements is discouraged. Site selection of such facilities at already developed areas sometimes lead to huge cost since there will be the need to resettle the people living in such environment, such relocations also comes with resettlement compensations or packages which later affect the cost of the power plant. It is for these reasons that experts advise to site such facilities in areas far from residential areas. Upon a detailed assessment of Ghana’s population distribution, Fig. 3.3, the population is sparsely distributed

outside the major urban centers. To maximize the site selection area and minimize the resettlement of people we have only considered for the SPP site selection the areas which have population densities of less than 10 people per 100x100 meter square grid, the data set from [43] was used for this analysis.

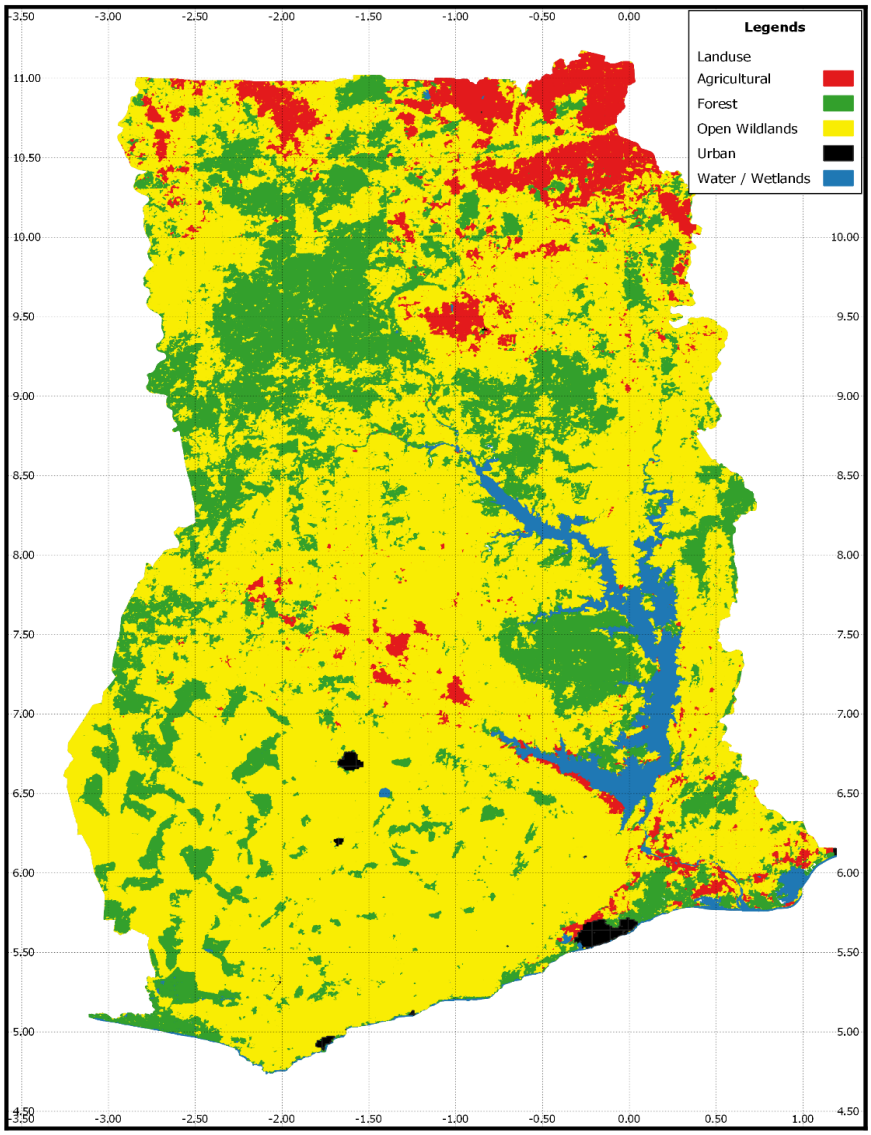


**Fig. 3.2** (a) Land-use (data extracted from Ref [47])

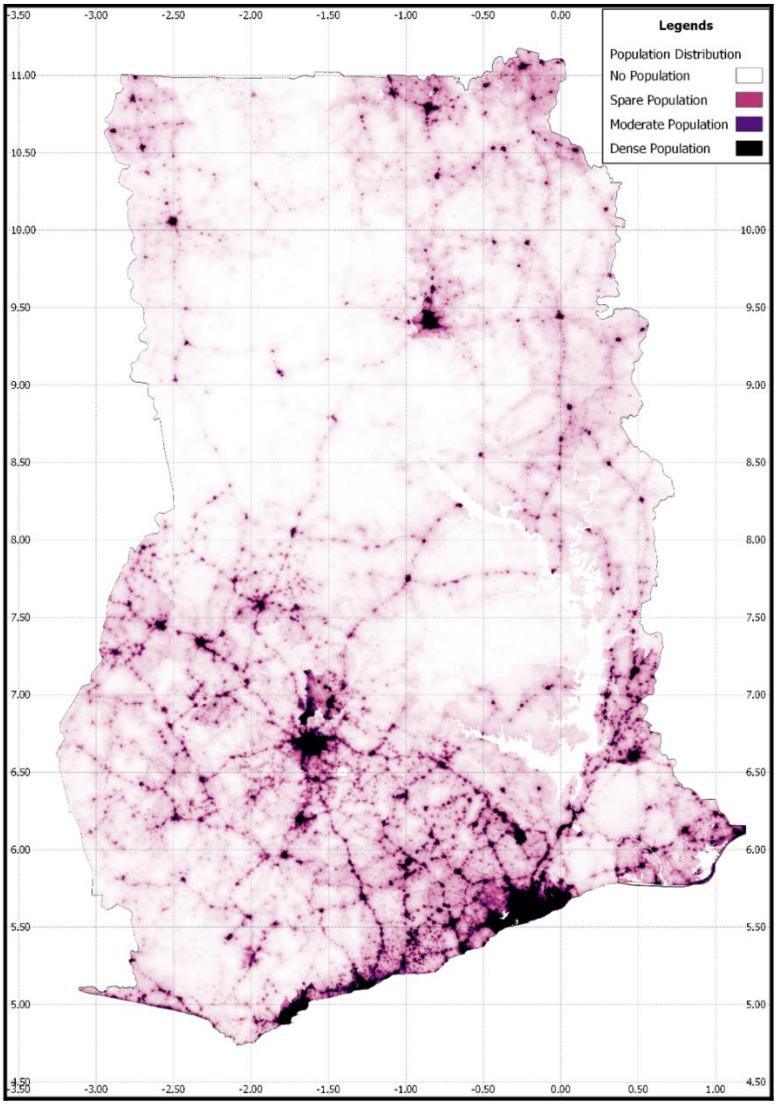


**Fig. 3.3** Population distribution (data extracted from Ref [43]) of Ghana

**(e) Protected areas** are reserved areas by the state because of either national or international agreements. These areas are all excluded from the potential sites for the construction of large-scale PV plants. An up to date data on the country's protected areas is provided by the protected planet [41]. Such areas include forest reserves, national parks, strict national reserves, wildlife sanctuaries, UNESCO biosphere reserves, and resource reserves. The other set of areas that are excluded from the location decision of the SPP are river bodies, and lakes, the data for these attributes are taken from [40], Fig. 3.1.

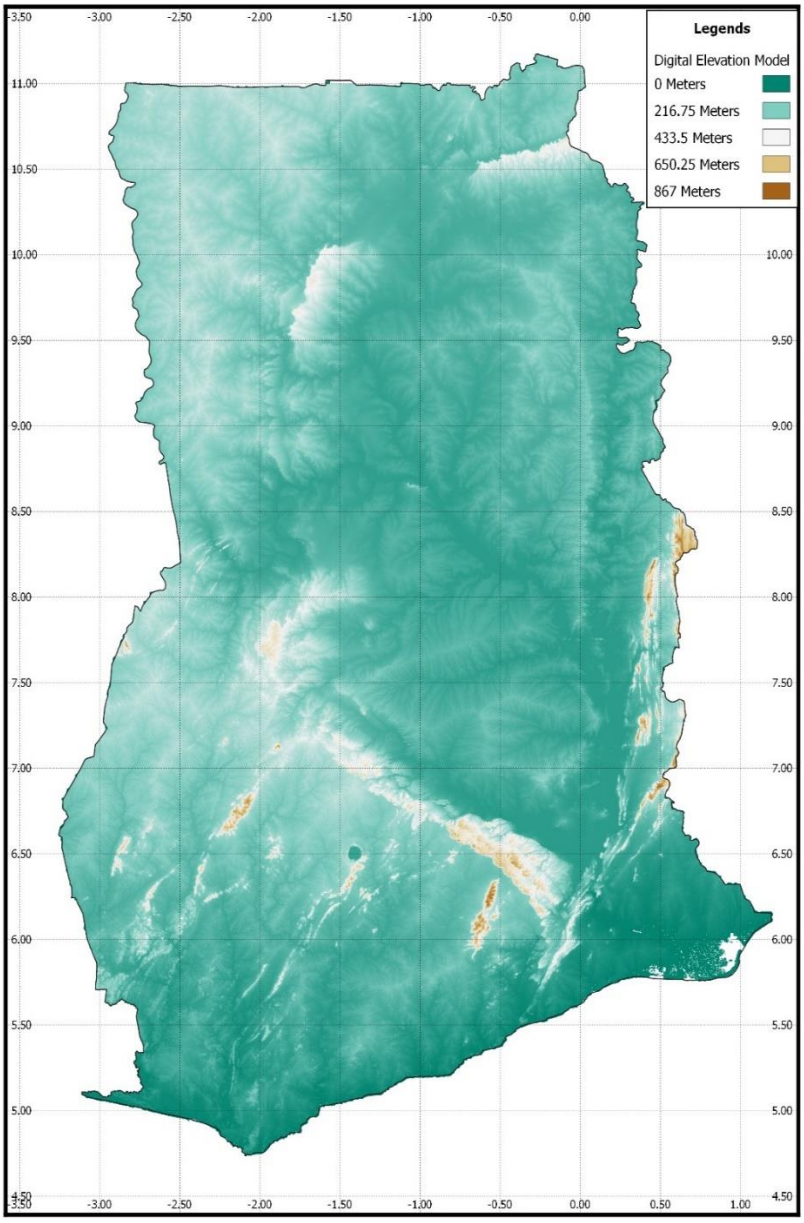


**Fig. 3.4** Elevation Model (data extracted from Ref [40])

**(f) Economic sustainability factors:** As Ghana is a developing nation dependent on its mines and mineral resources. Minerals constitute a major portion of the Ghana export, siting a large solar power plant in the near vicinity of a known mineral resource will have a negative impact the power plant as well as the mineral reserves future exploitation. For this reason, we incorporated a minimum buffer of 8 km from known mineral resources, the corresponding data on mineral resources was taken from [87].

A similar buffer is introduced when considering the gas pipeline network. National Pipelines are at risk of explosions and safeguarding large power plants from such explosion is necessary. In our analysis we did not only consider the current pipeline network but also the future expansion plans for Ghana's national pipelines [88].

**(g) Infrastructure proximity:** Siting a solar power plant in the proximity of transportation, and transmission networks can limit the normal operations and the future expansion of these infrastructures, for this reason, a minimal buffer of 0,5 km must be introduced between the road, rail, and transmission network. The transportation and transmission infrastructure are shown in Fig. 3.5.

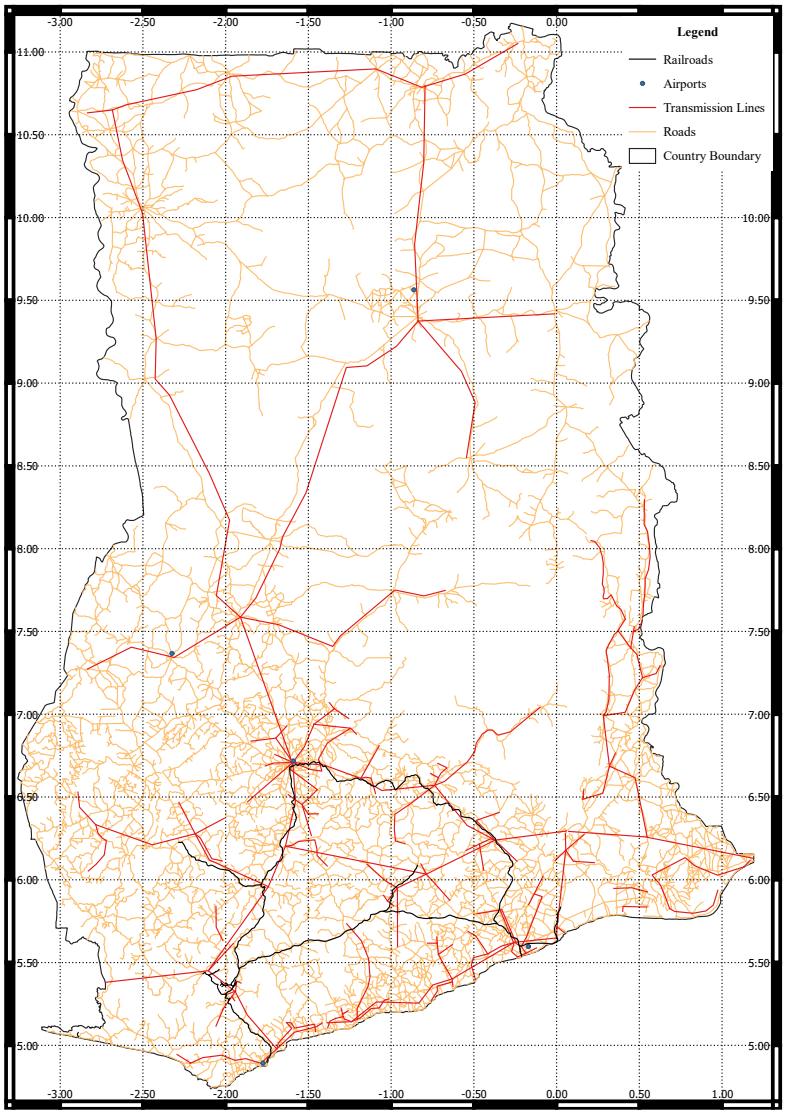


**Fig. 3.5** Infrastructure of Ghana (data extracted from Ref [40])

**Table 3.2** Criteria for the selection of solar farms location [47]

| Criteria | Suitability Ranking | | | |
|---|---|---|---|---|
| | Highly Suitable | Moderately Suitable | Low suitability | Not suitable |
| | 3 | 2 | 1 | 0 |
| Solar irradiance, (GHI) (kWh/m$^2$/day) | > 5,5 | 5 < x ≤ 5,5 | 4,7 < x ≤ 5 | ≤ 4,7 |
| Protected areas | Non protected areas | - | - | Protected areas, lakes, rivers |
| Slope, % | 0 ≤ x < 1 | 1 ≤ x < 3 | 3 ≤ x < 5 | ≥ 5 |
| Proximity to transportation in km | 0,5 ≤ x < 2 | 2 ≤ x < 5 | 5 ≤ x < 10 | ≥ 10 |
| Distance to urban settlements in km | > 1,5 | - | - | ≤ 1,5 |
| Proximity to transmission lines in km | 0 < x < 2 | 2 ≤ x < 5 | 5 ≤ x < 10 | ≥ 10 |
| Land use | Arid land | Open wildlands | - | Forests, Agriculture land |

## 3.4. Results and discussions

### 3.4.1. Application of the methodology

After applying the evaluation criteria, the suitable sites are subjected to density-based clustering to identify the energy-rich clusters suitable for installing SPP of variable capacities. The output for the PV SPP depends on the irradiance values and the energy conversion efficiency of the PV cell used in the SPP. However, for policy implications, such detailed analysis is beyond the scope of this paper. The primary objective of this analysis is to provide policy guidance regarding energy-dense regions that can be tapped for energy generation and, simultaneously, identify the relevant transmission expansion projects that can tap these renewable energy resource clusters.

Furthermore, we only considered those PV SPP sites, which receive yearly global horizontal irradiance more than or equal to 1983,308 kWh/m$^2$/year, as per the minimum economic viable limit of 1700 kWh/m$^2$/year. These sites represent Ghana's top 20 percent sites in terms of solar irradiance. These sites combined represent 6742 km$^2$ of Ghana's territory, and these sites fulfill all the evaluation criteria discussed in the previous section. The solar irradiance of these sites varies from 1983,308 to 2016,106 kWh/m$^2$/year.

The results were validated using traditional GIS-based MCDM analysis, which verified our findings but did not include the exact contours of the sites. As already indicated supra, the traditional approach also suffers from infrastructure bias and does not provide any road map for the future expansion planning of the transmission network. Here the density-based clustering has an advantage over the traditional GIS-based MCDM analysis because it provides an unsupervised identification of the energy-dense regions for future PV SPP siting, as shown in Fig. 3.6.

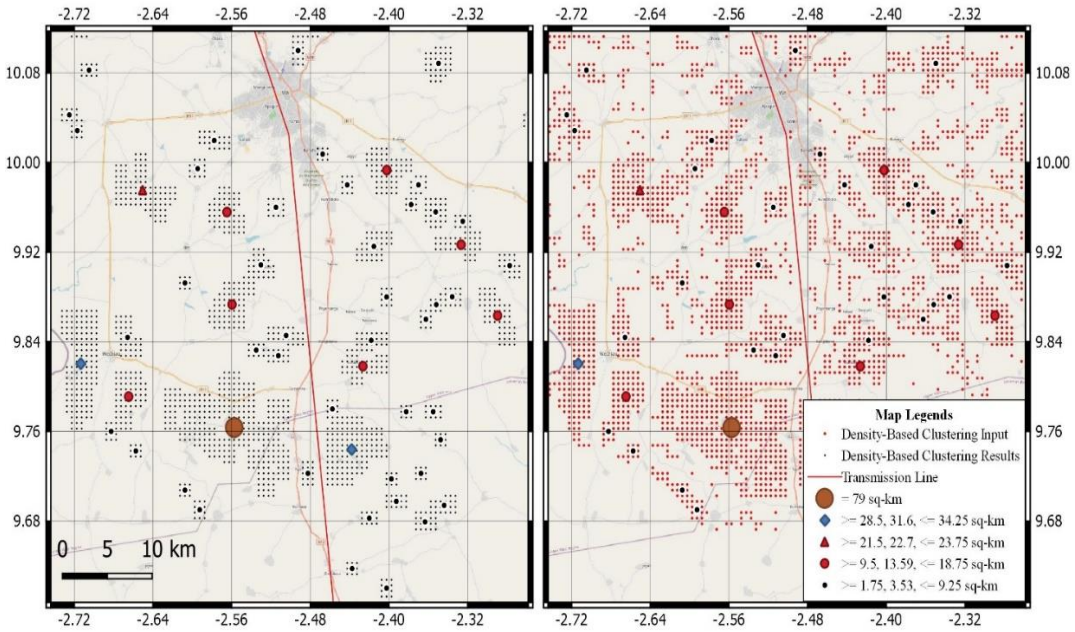


(a) (b)

**Fig. 3.6** Application of the density-based clustering

Fig. 3.6 demonstrates the advantages of applying density-based clustering on a sub-region of Ghana. This clustering technique provides dense clusters along with their sizes

and their contours. Fig. 3.6 (b) shows all the suitable sites for the siting of the SPP, but the final site contour selection for Fig. 3.6 (b) is left for human intervention. The application of the density-based clustering mitigates the human intervention and identifies clusters of the required minimum sizes Fig. 3.6 (a). This identification of the cluster provides better decision support for the decision-maker for the future expansion planning of the transmission network. The clustering identified 38 clusters suitable for large-scale PV SPP siting with a combined area of 784 $km^2$.

The smallest clusters ranged in size from 9,5 $km^2$ to 18,75 $km^2$ with a combined total area of 25 clusters equal to 340 $km^2$. The average size of these clusters is about 13,5 $km^2$ with a mean solar irradiance of 2014,45 $kWh/m^2$/year and a maximum and minimum irradiance of 2061,17 and 1985,30 $kWh/m^2$/year, respectively.

The second cluster ranged in size from 21,5 $km^2$ to 23,75 $km^2$ with a combined total area of 5 clusters totaling 113 $km^2$. The average size of these clusters is about 22,7 $km^2$ with a mean solar irradiance of 2027,55 $kWh/m^2$/year, and a maximum and minimum solar irradiance of 2052,61 $kWh/m^2$/year and 2004,75 $kWh/m^2$/year, respectively.

The third cluster ranged in size from 28,5 $km^2$ to 34,25 $km^2$ with a combined total area of 5 clusters equals 158 $km^2$. The average size of the cluster is about 31,5 $km^2$ with a mean solar irradiance of 2009,24 $kWh/m^2$/year, and a maximum and minimum solar irradiance of 2062,88 $kWh/m^2$/year and 1987,32 $kWh/m^2$/year, respectively.

The fourth cluster has a size of 44,25 $km^2$. The mean solar irradiance of this cluster is around 1998,04 $kWh/m^2$/year with the maximum and minimum solar irradiance of 1998,332 and 1997,76 $kWh/m^2$/year, respectively. The fifth cluster also has a size of 49 $km^2$. The mean solar irradiance of this cluster is 1985,62 $kWh/m^2$/year, with the maximum and minimum solar irradiance of 1985,72 and 1985,50 $kWh/m^2$/year, respectively.

The largest cluster is in the proximity of the city of Wa in the upper west region in the north of Ghana. This cluster area is 79 $km^2$ with mean, maximum, and minimum solar irradiance of 1992,49, 1992,64, and 1992,35 $kWh/m^2$/year. This cluster is also in the proximity of the national transmission network.

The above-discussed clusters are shown in Fig. 3.7. These clusters should be prioritized for development by the government of Ghana. It is reiterated that these 38 clusters of the combined area of 784 km$^2$ only represent the most significant clusters of unified areas meeting the minimum requirements of the evaluation criteria discussed previously. If the nation wants to integrate renewables into its energy mix, future transmission network extension planning should focus on these areas.

Fig. 3.7 (a) represents the 38 clusters along with their optimal site contours. From this representation, three macro clusters near the existing national transmission network are identifiable. One of the three macro clusters is in the proximity of the city of Wa. Transmission expansion projects to tap this macro cluster will have immediate gains in the national energy production using solar power. Detailed visualization of this cluster pre- and post-density-based clustering is in Fig. 3.6. The second macro cluster is near the northern border of Ghana, near the town of Pina. This macro cluster is also in the national transmission network proximity and should be given priority in national development planning, representation of this cluster is shown in Fig. 3.7 (b). The third macro cluster, also in the proximity of the transmission network and has a high potential for installing large-scale SPP, is shown in Fig. 3.7 (c).

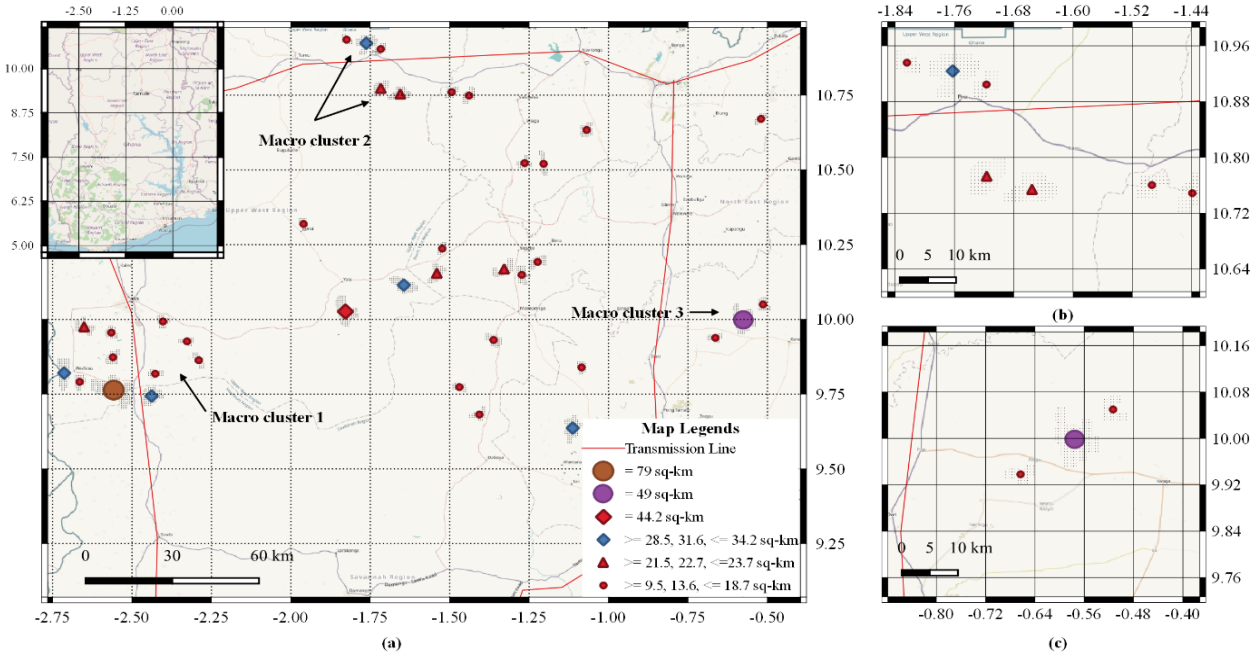


**Fig. 3.7** Identified dense clusters for SPP site locations

So far, the large clusters of land on a regional level suitable for installing the PV SPP have been identified. The last step of the analysis is ranking the above discussed macro cluster for national developmental planning. We propose AHP for the ranking of these macro clusters using four variables. These variables are the terrain ruggedness index, proxy for land development requirement, transmission network expansion requirements, transportation network expansion requirement, and the energy availability of the macro cluster sites. Using AHP we have identified their relative importance from officials of the Energy Commission of Ghana. The discussion on the relative importance of these variables are presented in section 3.7, along with the site ranking.

### 3.5. Analytical hierarchical process

This section of the work discusses the ranking of the available macro clusters for developing and integrating into the national grid of Ghana. The three macro clusters identified in the previous section were evaluated and ranked based on four variables discussed supra. Apparently, from Fig. 3.6, other large clusters do exit but farther from the national grid. These clusters can be developed with increasing energy requirements in the country in the future, but we are only considering the three macro clusters for the current analysis.

A CR and GCI of 25,0% and 0,08, respectively, were obtained from the computations. Therefore, it suggests that the experts' judgments are consistent and can be used for further analysis.

From the AHP results, it is clear that the experts prioritize the availability of solar resources at a specific site first for the siting decision of a PV facility. The availability of the required solar resource plays a vital role in the sustenance of reliable power supply in solar power plants. As part of the funding requirement of such systems, an assurance of the technologies' capacity to deliver the needed energy is necessary. The experts consulted assigned a weightage of 57% to the availability of the required energy and is also confirmed by Doorga et al. [30] who assigned 40,1% to global solar radiation, Doljak

and Stanojevic [29] assigned 47,1% to global solar radiation under climatic conditions. Furthermore, Zoghi et al. [89] assigned 25% to solar radiation in their analysis to select the optimum site for constructing solar farms in Iran, indicating the importance experts place on these criteria during site selection considerations.

Terrain ruggedness recorded a weight of 25,4% based on the judgments of the consulted experts. A terrain roughness represents irregularity or variability in a terrain unit [90]. Extracted from DEM [91], it is an intrinsic property of topography that measures the land-surface parameters. Considering the need to site solar PV on flat terrains to increase accessibility and minimize construction cost, the experts considered this an essential factor for constructing large-scale solar farms. Also, because high slopes make it difficult for engineers to achieve the required slope for maximum power generation from the solar panels, getting the proper slope during the construction of SPPs could result in higher energy generation for each unit area [29]. Similarly, [29,48,92] assigned high criteria weights to the orography mainly because of the importance of these criteria for both the economic and technical performance of the power plant.

Transmission and transportation network expansion followed with 11% and 6.5%, respectively, as indicated in Table A2. These are basically for economic and accessibility reasons. Studies such as [89,92–94] all placed transmission network expansion above transportation network expansion. Confirming the judgments of the consulted experts of the current study.

### 3.6. Macro Cluster Ranking

The results of AHP on the three macro clusters indicate that macro cluster 1 has the maximum priority for development because of the energy availability, the availability of smoother terrain, and the fewer requirements in expanding the current road and transmission network. A detailed representation of macro cluster 1 is in Fig. 3.6. Macro cluster 1 is near the town of Wa and contains the largest suitable sites for installing the PV SPP. This macro cluster is also near the existing transmission network. Additional transmission network expansion of 100 km is required to connect all the individual

clusters within this macro cluster. The total area available in this macro cluster for installing the PV SPP is 264 $km^2$ with mean annual GHI of 1998,55 $kWh/m^2$/year. An additional road network expansion of approximately 24 km is required to connect all the individual clusters to the existing national road network.

The second priority for development is for the macro cluster 3 Fig. 3.7 (c). Although this macro cluster, in comparison to the other two, has the least energy availability, it is nearest to both the road network and the transmission network with additional expansion requirements of 20 km and 40 km, respectively. The mean annual GHI of this macro cluster is 1985,69 $kWh/m^2$/year, with the total areas suitable for installing PV SPP of 73,75 $km^2$.

The third priority for development of PV SPP is at the macro cluster 2 Fig. 3.7 (b). This macro cluster has the most solar irradiance available of mean annual GHI 2054,86 $kWh/m^2$/year and an area of 123,25 $km^2$. However, an additional transmission network expansion of 58 km and the additional road network expansion of 47 km is required. Also, the terrain is rugged in comparison to the other macro clusters. Using information provided in Table 3.1, stakeholders can have a fair idea of the various power generation capacities of the identified areas.

### 3.7. Conclusions and policy implications for chapter 3

The current research provides a policy road map for developing the solar energy infrastructure in a developing country, Ghana. It informs the decision-maker of the available suitable clusters for renewable energy generation; additionally, it also supports the transmission and transportation network expansion planning. This research is innovative because it provides a more practical decision approach to incorporate renewable resources. The results indicate that Wa in the Upper West region, macro cluster 1, has the largest suitable sites for installing PV SPP, with approximately 264 $km^2$ and a mean annual GHI of 1998,55 $kWh/m^2$/year. Macro cluster 3 has second priority; the mean annual GHI of this macro cluster is 1985,69 $kWh/m^2$/year with a total area suitable for installing PV SPP of 73,75 $km^2$. Macro cluster 2 comes as the third priority, but it has the

most available mean annual solar irradiance of GHI 2054,86 kWh/$m^2$/year and an area of 123,25 $km^2$. Policymakers can use the obtained results during policy formulation for the country's energy sector. It can also serve as reference material for other stakeholders and investors, both foreign and domestic.

Based on our analysis, we have also identified relatively smaller clusters capable of providing sustainable energy availability to less-developed small communities in Ghana. Particularly the communities in the northwest of Ghana around the town of Nandom can utilize domestic solar PV cells for improving their energy availability.

Findings from this study will support decision-making for both government and stakeholders interested in developing Ghana's solar energy. It will reduce the time and funds needed to otherwise conduct such studies by stakeholders who want to invest in the country.

# CHAPTER 4. TECHNO-ECONOMIC ANALYSIS OF RENEWABLE ENERGY POTENTIAL IN GHANA

## 4.1. Optimization and Techno-Economic Assessment of Concentrated Solar Power (CSP) in South-Western Africa: A Case Study on Ghana

Concentrating solar power (CSP) technologies are part of renewable energy technologies that are viable and promising, hence can be developed to generate electricity to scale up renewable energy use around the world [95]. The innovative part of the CSP technology is its ability to covert sun energy to generate heat as an alternative to the burning of fossil fuels. Another, potential advantage associated with the CSP technology is the possibility to integrate it with a thermal energy storage (TES), and other power plants to provide dispatchable power which leads to enhanced economics [96,97]. The LCOE for Solar Tower CSP is projected to average around 9 ¢/kWh and that of Parabolic Trough CSP is also projected to average around 11 ¢/kWh by 2025 [98].

A number of studies have been conducted by several scholars around the world to ascertain their techno-economic potential in certain parts of the world. Islam et al. [99] performed a techno-economic evaluation on different CSP technologies in Malaysia. The study concluded that the parabolic trough collector (PTC), and the solar tower power plant (STPP) plants were the best for the selected sites in Malaysia. Abaza et al. [100] evaluated the techno-economic potential of a 10 MW CSP plant operated using 100% solar energy. It was identified in their study that a concentrated solar tower with packed rock bed TES and Steam Rankine Cycle would be the suitable choice for a stand-alone power plant in a 10 MW capacity range. Aly et al. [98] assessed the potential to integrate CSP technology in Tanzania's energy generation mix. Their study concluded that the viability or otherwise of such a project in Tanzania depends on the type of financing. Andika et al. [101] conducted a study on the techno-economic impact of design changes in TES of CSP systems. Their assessment indicated that the cost of the system changes with the type of storage tank used. Belgasim et al. [102] also evaluated the potential of CSP technology for electricity generation in Libya, the outcome of their study shows that CSP is techno-economically suitable in Libya. Purohit and Purohit [103] analyzed the techno-economic

potential of CSP in India. Preliminary results from their study shows that the CSP technology is feasible in India and that it makes financial sense to develop it in the north-western part of the country specifically in Rajasthan and Gujarat states. Fritsch et al. [104] also studied the techno-economics of a solar thermal power plant using liquid sodium as a fluid for heat transfer. This section of the work assesses the viability of two different CSP technologies in two separate locations in Ghana.

### 4.2. Principle of operation of CSP

Solar thermal technology uses the principle of concentrating solar radiation to generate steam or hot air which is used to produce electricity using conventional power cycles. Collecting solar energy that has relatively low density is a key challenge in engineering in the development of thermal power plant. Glass mirrors are used in most systems for the concentration because of their high reflectivity. Despite its uncomplicated nature, it involves numerous steps which can be executed in different ways [105]. The implementation procedure at every level in solar thermal power (STP) production must be optimally harmonized to various economic, technical, and environmental factors which may favor one approach over the other [106]. There are various considerations that are done in the selection of sites for the installation of CSP however, the availability of a suitable solar resource is key to the implementation of such a project. Table 4.1 gives an overview of the various technologies use in CSP and their performance.

**Table 4.1** Performance data for various CSP technologies [105]

| | Capacity, MW | Concentration | Peak Solar η (%) | Annual Solar η (%) | Thermal Cycle η (%) | CF (Solar) (%) | Land use $m^2$ MW/h/y |
|---|---|---|---|---|---|---|---|
| Trough | 10–200 | 70–80 | 21 (d) | 10–15 (d) 17–18 (p) | 30–40 ST | 24 (d) 25–70 (p) | 6–8 |
| Fresnel | 10–200 | 25–100 | 20 (p) | 9–11 (d) | 30–40 ST | 25–70 (p) | 4–6 |
| Power tower | 10–150 | 300–1000 | 20 (d) 35 (p) | 8–10 (d) 15–25 (p) | 30–40 ST 45–55 CC | 25–70 (p) | 8–12 |
| Dish-Stirling | 0.01–0.4 | 1000–3000 | 29 (d) | 16–18 (d) 18–23 (p) | 30–40 Stirl 20–30 GT | 25 (p) | 8–12 |

Where (d) – demonstrated; (P) – projected; GT – gas turbine; ST – steam turbine; CC – combined cycle.

Fig. 4.1 shows the DNI resource for the studied areas in Ghana, data from the figures shows that the dry season (harmattan) which starts from October to April experiences the highest level of beam irradiance, whereas the other months experience a relatively low irradiance as a result of the rain season within that period. The most important parameter for the energy yield calculation is the DNI, this is because, it has an effect on the performance of CSP technologies [107,108].

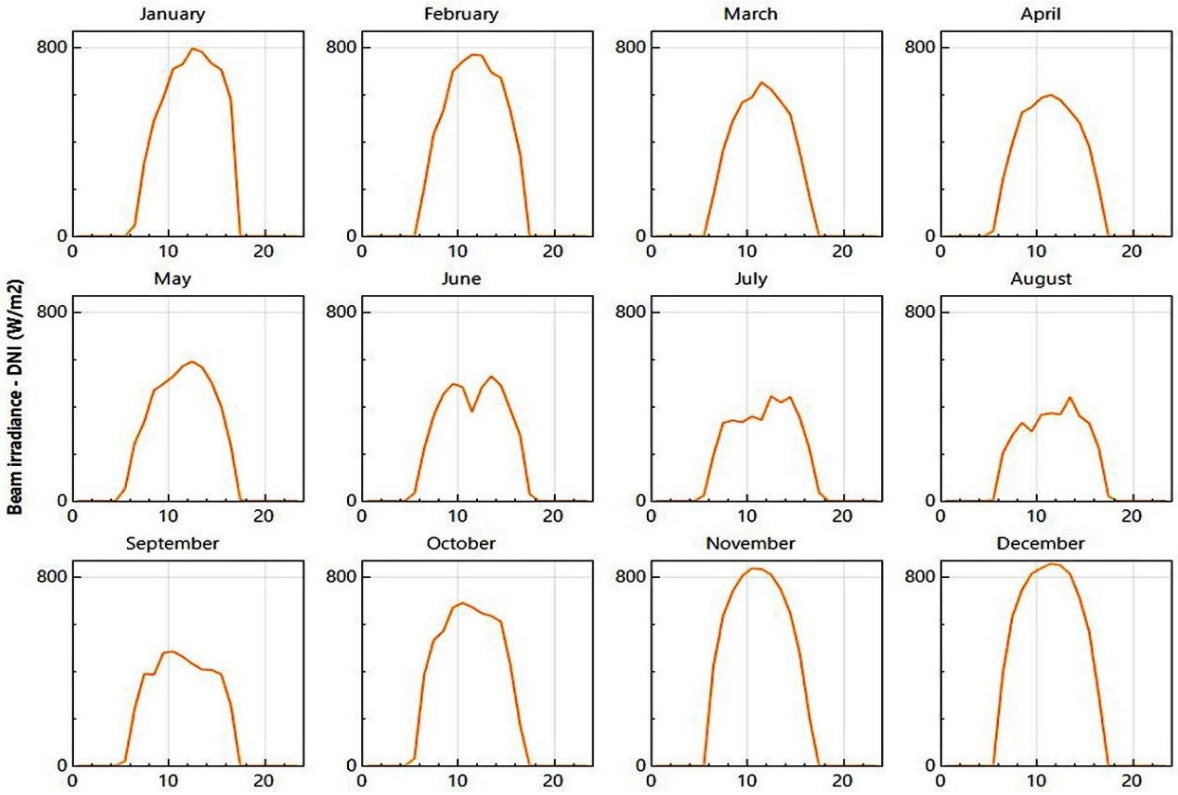


(a)

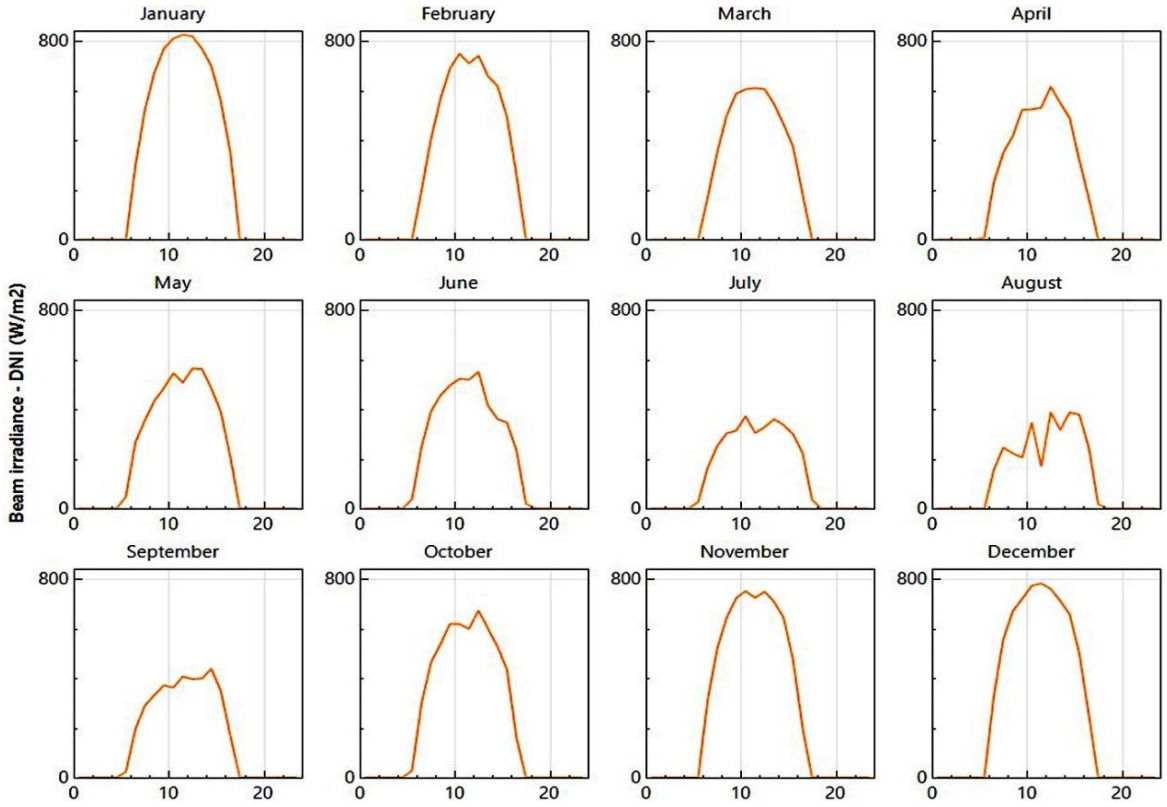


(b)

**Fig. 4.1** DNI for (a) Navrongo (b) Tamale

Areas situated in middle to high latitudes on earth are usually favorable for the installation of PV, whiles CSP systems with thermal storage incorporated, perform best in arid areas situated at relatively low latitudes [109,110]. In order to achieve high economic performance, the annual DNI at a site for CSP installation must be at least between 1900 kWh/m$^2$ and 2000 kWh/m$^2$ [111]. Africa has a huge solar energy potential with most parts having effective radiation between a period of 6 and 8 hours daily, making it a valuable resource for the continent [112]. The World Bank group published Africa's and for that matter Ghana's solar resource map which is aimed at supporting the countries on the continent to scale up the development and utilization of solar power. It was funded by the Energy Sector Management Assistance Program (ESMAP). The DNI map for Africa and Ghana developed by the World Bank Group are presented in Fig. 4.2.

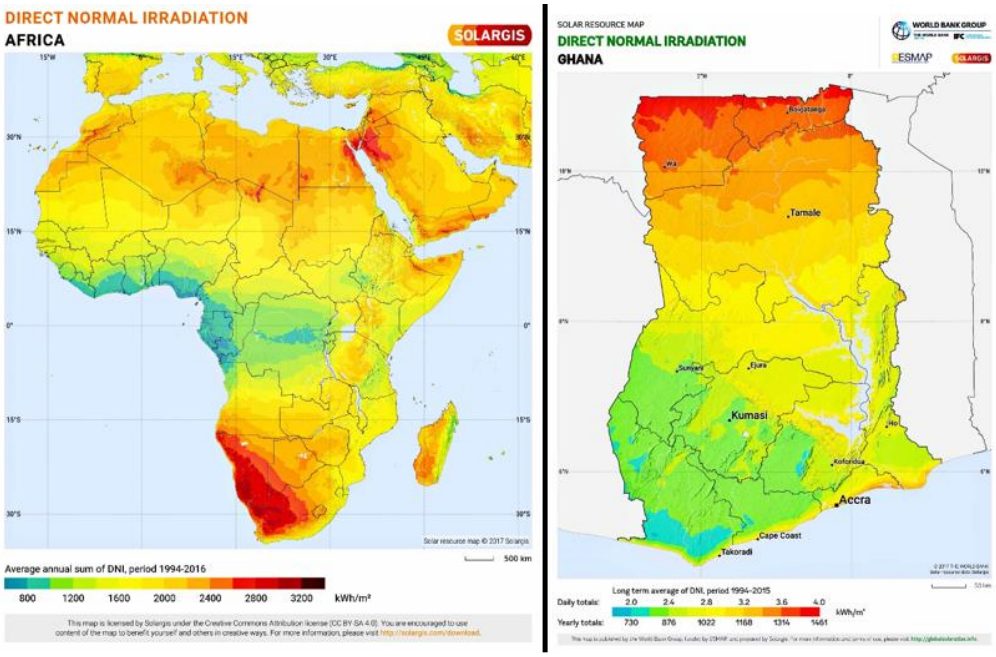


**Fig. 4.2** DNI Map of Africa (Left) and Ghana (Right) [113]

### 4.2.1. Parabolic Trough (PT)

PTC is the most advanced CSP technology, it consists of several linear interconnected PTs, steam turbines and a generator for the generation of electrical power. It also has a vacuum glass tube with an absorption tube for the flowing working fluid placed in the

focus of the cylindric-parabolic reflectors located in the solar field. To attain an efficient heating for the working fluid, there is the need to ensure a high absorption coefficient for the sun irradiation, absorption tube and its location in the focus of the troughs. The energy from the sun heats the oil (e.g., synthetic oil, mineral oil, molten salt etc.) which transfers the energy to the water in the boiler heat exchanger, which can reach a temperature of about 400 ℃. This heat is carried to the water which produces steam to turn the turbine [99].

### 4.2.2. Solar Tower Plant (STP)

An STP is made up of a tall tower supporting a heat receiver with a surrounded field of heliostats which concentrates the sun's rays onto a receiver. STP is often suitable with an integrated thermal storage system through the use of molten salts, normally nitrates serves as the heat transfer fluid, this helps to generate energy around the clock. Some also use the direct system. The receiver, heliostat, thermal storage, heat transfer and the control system are key parts of the STP system. The heat transfer fluid absorbs the concentrated heat to create steam which turns the turbines connected to a generator to produce electricity [99,114].

## 4.3. Methodology

The SAM software version 2018.11.11 was used to simulate Solar Tower and Parabolic Trough power plants at two sites in the Northern part of Ghana where solar irradiation is high. The communities considered for this study are Navrongo, located on latitude 10.90$^{o}$ N and longitude -1.10$^{o}$ E and Tamale, located on latitude 9.50$^{o}$ N and longitude -0.85$^{o}$ E. The SAM software is the most commonly used program by engineers and researchers to simulate CSP systems, it consists of components which interacts with each other [98]. SAM is an all-inclusive software which is use in designing and evaluating the techno-economic potential of various power plants for specific sites. The components are denoted by numerous parameters as well as time-dependent inputs that generate time-dependent

results. The generated output of a particular system can also be used as an input into itself or other systems [115].

### 4.3.1. Mathematical Description

This section presents brief mathematical descriptions for the two different CSP systems. Each information for the mathematical description of the PTC was obtained from [115,116]. The thermal performance of a parabolic trough collector is dependent on the modified loss coefficient known as $F'U_L$ as seen in Eq. (4.1), it is dependent on F$U_L$ which is the collector loss coefficient. Fig 4.3 is the schematic diagram of a PTC power plant.

$$F'U_L = \begin{cases} F_R\,U_L, & if\ \dfrac{F_R\,U_L}{g_{test}\,C_{p\,fluid}ConRat} \geq 1 \\ g_{test}C_{p\,fluid}\left(1 - e^{\left(\frac{F_R\,U_L}{g_{test}\,C_{p\,fluid}ConRat}\right)}\right), & if\ \dfrac{F_R\,U_L}{g_{test}\,C_{p\,fluid}ConRat} < 1 \end{cases} \quad (4.1)$$

Where, $ConRat$ is the concentration ratio, which is the ratio of the aperture area to the receiver area. The collector thermal power output is calculated using Eq (4.2).

$$Q_u = A_c[F_R(\tau\alpha)_n I_t - F_R L_L \Delta T] \quad (4.2)$$

Where, $Q_u$ is the thermal power output of the solar field (kJ/h), $\Delta T$ represents the temperature difference (°C), $A_c$ is the collector area (m$^2$), is the $F_R(\tau\alpha)_n$ represents the efficiency at which solar radiation is absorbed by the plates and removed by the fluid flowing through the collectors.

A big temperature difference in Eq. (4.2) can be used as the basis in the calculation of the useful energy gain. The usual standards are the inlet of the collector fluid temperature minus the ambient temperature. In the case of parabolic troughs, two modifiers ($R_1\ and\ R_2$) are usually applied to Eq. (4.2) to account for several other collectors in a series string and also account for other flow rates that are under test situations. In this case, the modifiers are defined Eq. (4.3) – (4.5) [115]:

$$R_1 = \frac{N_{series} C_{Pfliud} \dot{m}}{A_{aperture}} \left( \frac{1 - e^{\left((-F' U_L A_{aperture})/(N_{series} C_{Pfliud} \dot{m})\right)}}{R_{test}} \right) \tag{4.3}$$

$$R_{test} = g_{test} C_{Pfluid} \left(1 - e^{\left(-F' U_L/(g_{test} C_{Pfluid})\right)}\right) \tag{4.4}$$

$$R_2 = \frac{1 - \left(1 - \frac{R_1 A_{aperture} F_R U_L}{N_{series} C_{Pfliud} \dot{m} ConcRat}\right)^{N_{series}}}{N_{series} \left(\frac{R_1 A_{aperture} F_R U_L}{C_{Pfliud} \dot{m} ConcRat N_{series}}\right)} \tag{4.5}$$

Where, $N_{series}$ represents the number of collectors in a series, $\dot{m}$ is the mass flow rate of the fluid (kg/h), and $A_{aperture}$ is the net aperture area (m$^2$).

The output for the thermal power from the collector is dependent on Eq. (4.2) which is modified by the addition of incidence angle modifier effects as in Eq. (4.6).

$$Q_u = R_1 R_2 A_{aperture} N_{parallel} \left[ F_R (\alpha\tau)_n IAMI_{beam} - \frac{F_R U_L}{ConcRat} (T_{in} - T_{amb}) \right] \tag{4.6}$$

Where, $N_{parallel}$ represents the number of series collector strings in parallel, $IAM$ is the incidence angle modifier, $I_{beam}$ is the amount of beam solar radiation incident on the surface of the collector (kJ/hm$^2$), $T_{in}$ denotes the temperature of the fluid entering the collector array (°C) and $T_{amb}$ is the ambient temperature (°C).

The yearly mean collector efficiency $\eta_{col}$ under design situations can be calculated using Eq. (4.7) [117].

$$\eta_{col} = \frac{Q_u}{DNI \times A_{aperture}} \tag{4.7}$$

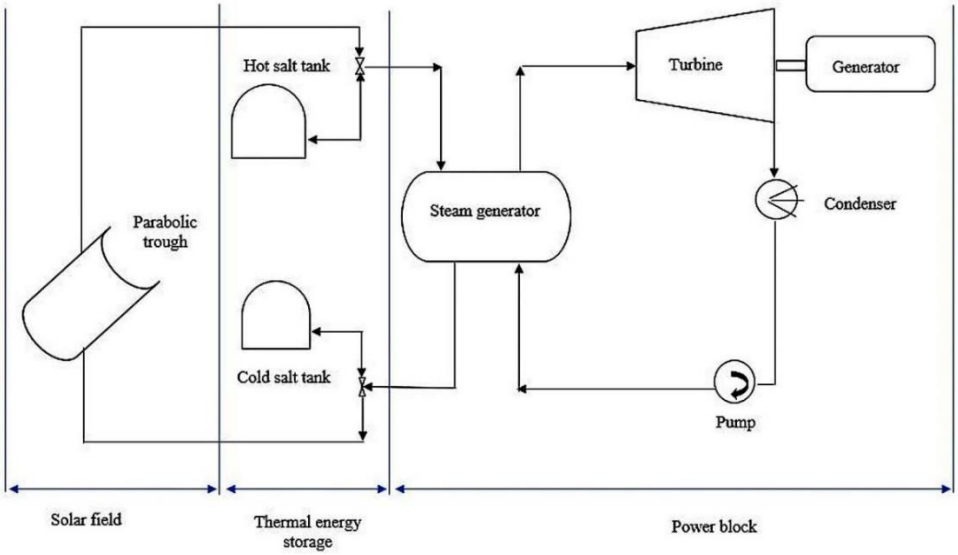


**Fig. 4.3** Schematic of a PTC power plant

One characteristic associated with the STPP compared to other solar thermal power technologies is the receiver's ability to operate at higher thermal efficiency as a result of the high incident flux concentration on the surface of the receiver [118]. The technology for the central receiver tower can be represented as a point focus type of solar thermal electrical energy generation system. The technology has a number of heliostats which is made up of dual axis control as well as an arrangement which is done in an order of focus radiation on the fixed receiver. The fixed receiver is used to absorb the solar radiation concentrated by the heliostats. The receivers then transfer the heat to the heat transfer fluid (HTF), the HTF also transfers the heat to the fluid used in the power cycle. The power cycle for thermal power plants is generally based on a Rankine cycle [119]. Excess heat during the day is diverted to the TES system to be use later when there is a shortfall in the night or during cloudy periods. A TES system makes the power plant more reliable in terms of meeting peak load demands [120]. The concentrating ratio (CR) can be calculated using Eq. (4.8) [119]. Fig. 4.4 shows the layout of the heliostat field used for the simulation.

$$CR = \frac{Area\ of\ receiver\ (m^2)}{Total\ area\ of\ heliostats\ (m^2)} \tag{4.8}$$

In order to calculate the thermal power reflected to the receiver, Eq. (4.9) [119] can be used.

$$Q_{hel} = Q_{fal}.\eta_{hel} \tag{4.9}$$

Where $Q_{hel}$ represents the reflected solar power by the heliostats, $\eta_{hel}$ denotes the efficiency of the heliostat, which consists of the cosine factor, mirror reflectivity, shading and blocking factor, attenuation factor and the interception factor. $Q_{fal}$ represent the maximum solar power incident on the total area of the heliostat which can be calculated using Eq. (4.10).

$$Q_{fal} = A_{hel} \cdot DNI/10^3 \tag{4.10}$$

Where, $A_{hel}$ is the entire area of the heliostat mirrors.

The receiver's power balance can be calculated using the following equations obtained from [121].

$$Q_{rec} = Q_{hel} - Q_{rec,\ loss} \tag{4.11}$$

$$Q_{rec,\ loss} = Q_{ref} + Q_{rad} + Q_{con} \tag{4.12}$$

Where $Q_{rec}$ denotes the absorbed power by the molten salt in the receiver; $Q_{rec,\ loss}$ signifies the power loss in the receiver; $Q_{ref}$ denotes the power loss reflected from the surface of the tube; $Q_{con}$ represents the convection loss of the receiver and $Q_{rad}$ represents the radiation loss from the receiver. The following parameters can also be computed using the following equations obtained from [121,122].

$$Q_{ref} = (1 - \delta)Q_{hel} \tag{4.13}$$

$$Q_{rad} = \sum \varepsilon\sigma_0 A\left(T_{wall,i}^4 - T_{amb}^4\right) \tag{4.14}$$

$$Q_{con} = \sum f_{mix,i} A\left(T_{wall,i} - T_{amb}\right) \tag{4.15}$$

Where $\delta$ denotes the solar absorptance of the tube panels, $\sigma_0$ represents the Stefan Boltzmann constant, $\varepsilon$ denotes the hemispherical emittance, $A$ signifies the lateral surface of the tube, $f_{mix,i}$ represents the mixed convection coefficient, $T_{amb}$ denotes the ambient temperature and $T_{wall,i}$ is the temperature of the wall.

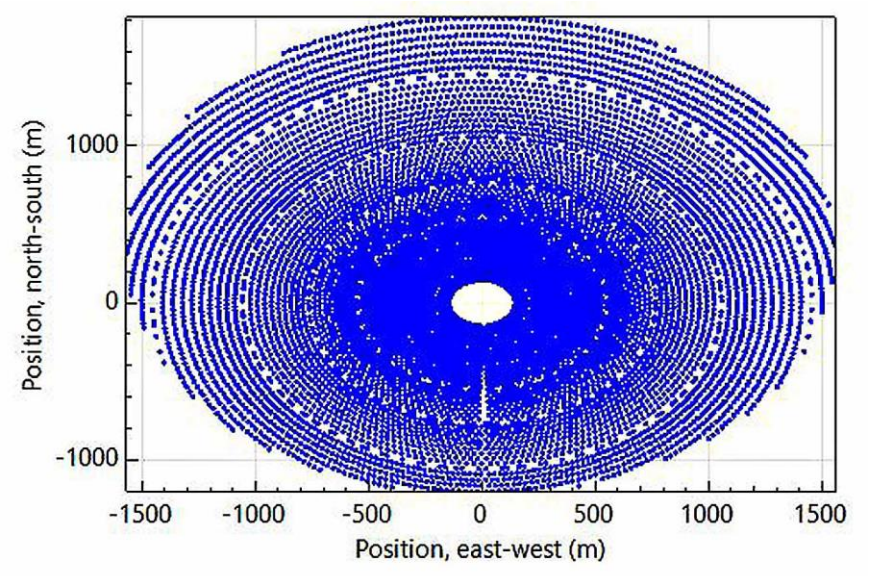


**Fig. 4.4** Layout of the heliostat field (Obtained from SAM software)

### 4.3.2. Economic Analysis

The real and nominal LCOE is calculated by the SAM software, but the nominal LCOE is the current dollar value whiles the real LCOE is the constant dollar value. This work considered the real LCOE value since it accounts for the long years of inflation over the project lifetime, hence it is good for long-term analysis whiles the nominal LCOE is good for short term evaluations. Unlike conventional fossil fuel power plants, renewable energy has high upfront investment cost, virtually no fuel cost, and relatively lower operation and maintenance cost [123]. The LCOE is usually dominated by the initial investment cost which constitutes about four-fifths of the entire cost of the project [124].

Weight Average Cost of Capital (WACC) is usually used as a discount rate to evaluate the net present value of the power generation cost, it however, varies depending on the type of project owner, the stability of regulatory regimes and regional differences in the cost of capital. Much information on WACC for African countries can be obtained from [125]. The LCOE has superiority over NPV since the latter has no restrictions on the project scale, the NPV is not a suitable metric for comparing feasibilities of projects with large differences in terms of scale. This is because large scale projects usually have larger NPV compared to small scale ones, it is for this reason that the NPV cannot be used to satisfactorily relate the pros and cons of such projects [126]. This work therefore used the LCOE more in its economic analysis although the NPV was also evaluated. The following financial parameters in Table 4.2 were used for the modelling of the CSP power plants.

**Table 4.2** Financial Parameters for the Simulation of CSP

| *Main Financial Parameters* | Value | References |
|---|---|---|
| Inflation rate | 2,2% per year | [127] |
| Analysis period | 25 years | |
| Real discount rate | 10% | [109] |
| Nominal discount rate | 12,42% per year | Calculated |
| *Project Term Debt* | | |
| Moratorium | 5 years | [128] |
| Annual interest rate | 10% | [109] |
| Up-front fee | 2,75% of the total debt | Information from experts in the field |
| *Tax and Insurance Rates* | | |
| Sales tax | 12% | [129] |
| The corporate income tax rate | 25% | |
| Annual Insurance rate | 0,5% of the installed cost | [109] |
| *Construction Period Debt* | | |
| Up-front fee | 2,75% of the principal | Default value from SAM |
| Months prior to operation | 24 months | |

The technical parameters adopted for the simulation are presented in Table 4.3. All data for the analysis were obtained from the SAM software unless otherwise indicated. A

system performance degradation rate of 0,2 % per annum was used in the simulation [109].

**Table 4.3** Parameters used for the design of the power plants

| Solar Tower plant | | | Parabolic Trough | | |
|---|---|---|---|---|---|
| Description | Parameter | Value | Description | Parameter | Value |
| Plant capacity | Nameplate | 100 MW | Plant capacity | Nameplate | 100 MW |
| Heliostat field | heliostats | 8790 | Solar field | Solar multiple | 2 |
| | Heliostat height | 12,2 m [130] | | Stow angle | 170$^{o}$ [131] |
| | Heliostat width | 12,2 m [130] | | HTF pump efficiency | 0,85 |
| | Ratio of reflective area to profile | 0,97 [132] | | Field HTF fluid | Hitec solar salt |
| | Base land area | 1847,04 acres | | Mirror reflectance | 0,935 |
| Tower and Receiver | Solar multiple | 2 | | Number of modules per assembly | 8 |
| | Coating emittance | 0,88 [133] | | Turbine inlet pressure control | Fixed pressure |
| | Coating absorptance | 0,94 [133] | | Condenser type | Air cooled |
| | HTF type | Molten Salt (60% $NaNO_3$ 40%$KNO_3$) | Thermal storage | Full load of TES | 12 hours |
| Power cycle | Estimated net output (nameplate) | 100 MWe | | Storage volume | 16697,7 $m^3$ |
| | Estimated gross to net conversion factor | 0,9 | | TES thermal capacity | 3291,34 MWht |

### 4.4. Results and Discussion

This section presents the results and discussions for the 100 MW CSP plants. The section is divided into sub-sections to cover the two different power plants at the two selected sites. It also presents a sensitivity analysis for the various systems.

#### 4.4.1. Electricity generation analysis for STPP for both sites

The maximum electricity generation for the various power plants as indicated in Fig. 4.5 and Fig. 4.6 were recorded during the first and last quarters of the year which are the harmattan periods within the year. Electricity export to grid from the STPP at both sites reached about 100 MWe during the harmattan season. The rainy season which is usually cloudy affects the generation of electricity hence, the relative drop in electric power to grid for the remaining months of the year.

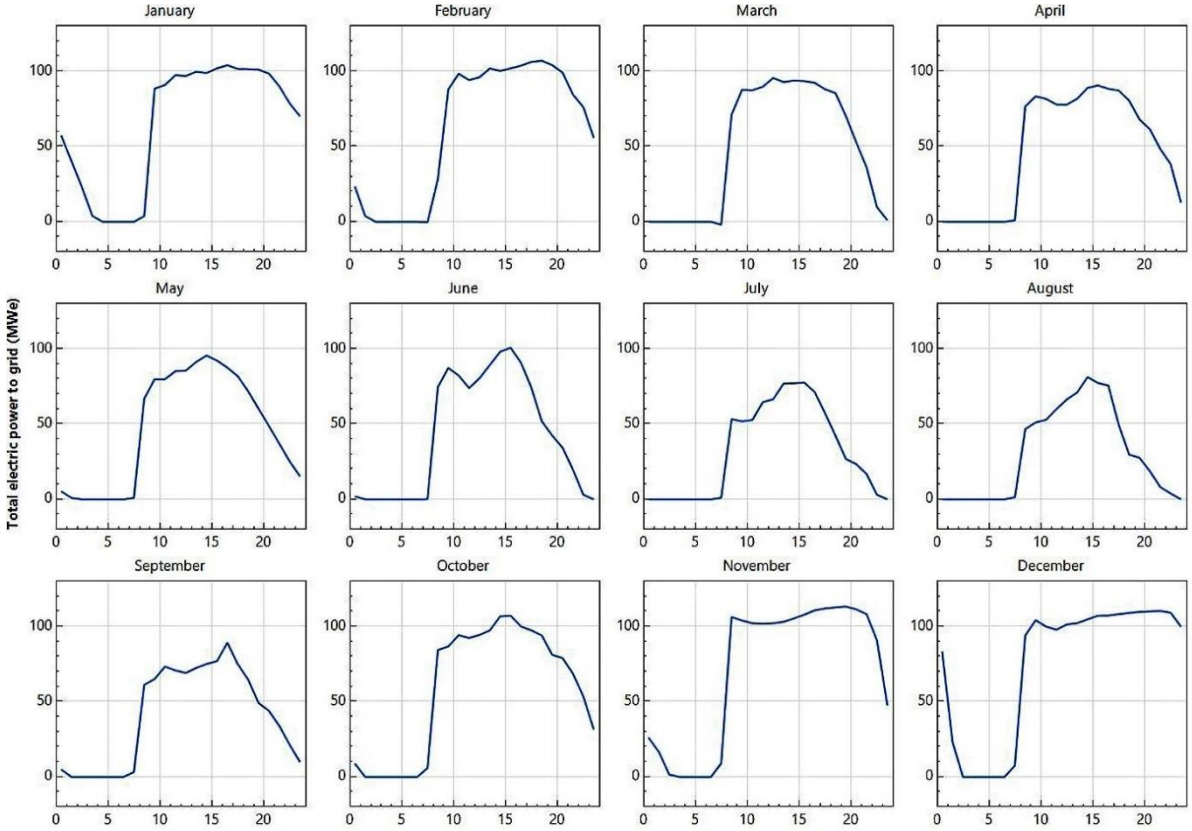


**Fig. 4.5** Total electric power to grid STP power plant at Navrongo

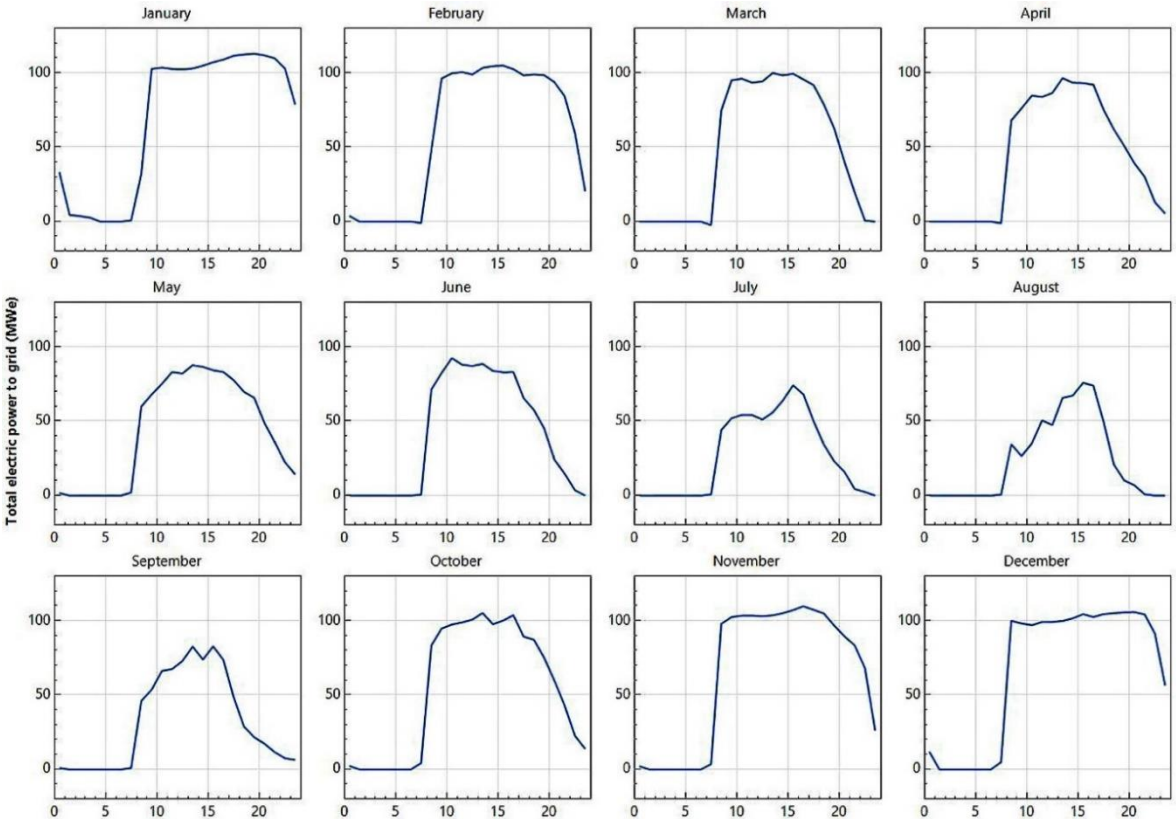


**Fig. 4.6** Total electric power to grid STP plant at Tamale

A total of 424 GWh and 393 GWh of electricity were generated in the first year of the project for the Navrongo and Tamale STPP plants at capacity factors (CF) of 48,5 % and 44,9%, respectively. A capacity factor is said to be the ratio of the actual yield or output of a plant in a certain time frame to the potential output power of the plant in that same period. Higher CF enhance grid support, particularly considering the availability of power during peak hours [134]. The obtained CF for the STPP plants in this study are all within the CF for CSP technologies published by IRENA [123].

### 4.4.2. Economic Analysis for STPP for both sites

The economic results from the simulation for the STPP are presented in Table 4.4 Data from the two modelled projects suggests that the STPP at Navrongo is the optimum option although the difference between the values obtained for the two sites is not much. Comparing the obtained real LCOEs at both sites to the current cost of electricity which ranges between 15 – 19 ¢/kWh for energy generated from other conventional power plants

in Ghana [63], the LCOEs for both projects will fall within the range of cost of energy to consumers. The global weighted average LCOE for CSP technologies continue to fall, although the CSP technologies are still at their infant stages in terms of deployment and utilization around the world [123]. According to IRENA's 2019 report, about 0,5 GW of new CSP technologies were commissioned around the world in 2018, mostly in China, Morocco, and South Africa [135]. The obtained LCOEs in this study for the STPPs are lower than the IRENA global weighted average of 0,185 $/kWh for CSP technologies in 2018 [135]. The plants at both sites have also proven to be economically viable, this is because the obtained NPVs were all positive.

**Table 4.4** Economic results from the simulation of the STPP

| | Tamale | Navrongo |
|---|---|---|
| Metric | Value | |
| Annual water usage, $m^3$ | 84949 | 87283 |
| PPA price (year 1), ¢/kWh | 13,72 | 12,82 |
| Levelized PPA price (nominal), ¢/kWh | 17,64 | 16,37 |
| Levelized PPA price (real), ¢/kWh | 14,83 | 13,77 |
| LCOE (nominal), ¢/kWh | 17,52 | 16,26 |
| LCOE (real), ¢/kWh | 14,73 | 13,67 |
| Year investor IRR achieved | 20 | 20 |
| NPV, $ | 3 526973 | 3 526383 |

A proper solar field size is key to the design parameters of CSP plants, an extremely large field size is partially not needed under a high solar irradiance, however, a small field size may also primarily reduce the work output and lead to poor utilization of invested capital. The degree of oversize is referred as the solar multiple (SM) which is the ratio of the thermal power produced by the solar field to that needed by the power block at design stage. The SM is a critical parameter needed at the design stage since it has a huge impact on not just the economics but also the work output of the system [136]. Also, CSP with a storage system can be a profitable and flexible choice for different project sites, particularly in the background of increasing shares of variable renewable electricity [137,138]. For these reasons, this study assessed the effect of both SM and TES on the

LCOE of the STPP for both sites. Results from the analysis as indicated in Fig. 4.7 and Fig. 4.8, shows that the optimum SM falls in the region of 1,4 – 1,9 depending on the TES period. This is because the least LCOE for the different TES periods converge around 1,4 – 1,9. So, for instance, the optimum SM for a 12-hour TES as used in the simulation will be 1.9 where the least LCOE of 13,62 ¢/kWh was obtained. Furthermore, results from same figures shows that the LCOE decreases with increasing TES period, however, the difference between the LCOEs beyond 8 hours of TES is relatively minimal.

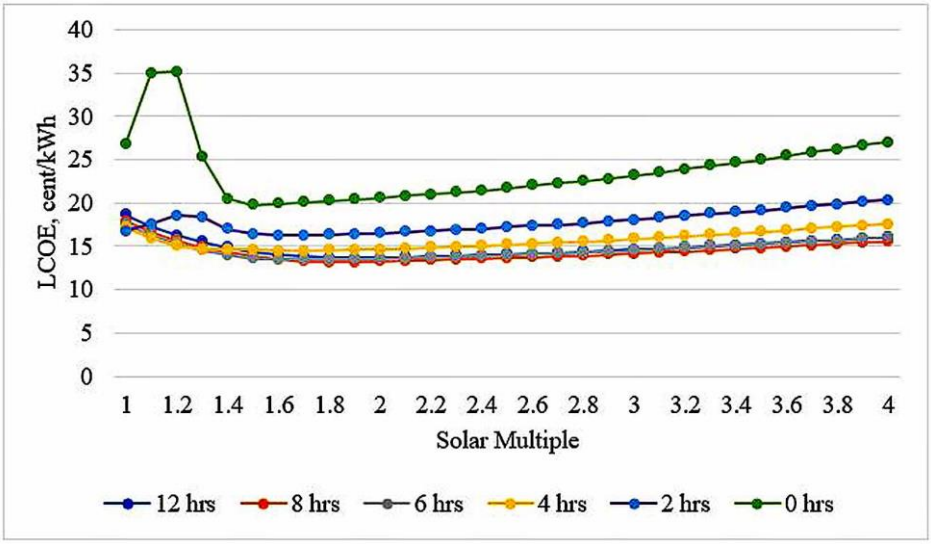


**Fig. 4.7** LCOE for Solar Tower at Navrongo under for TES period

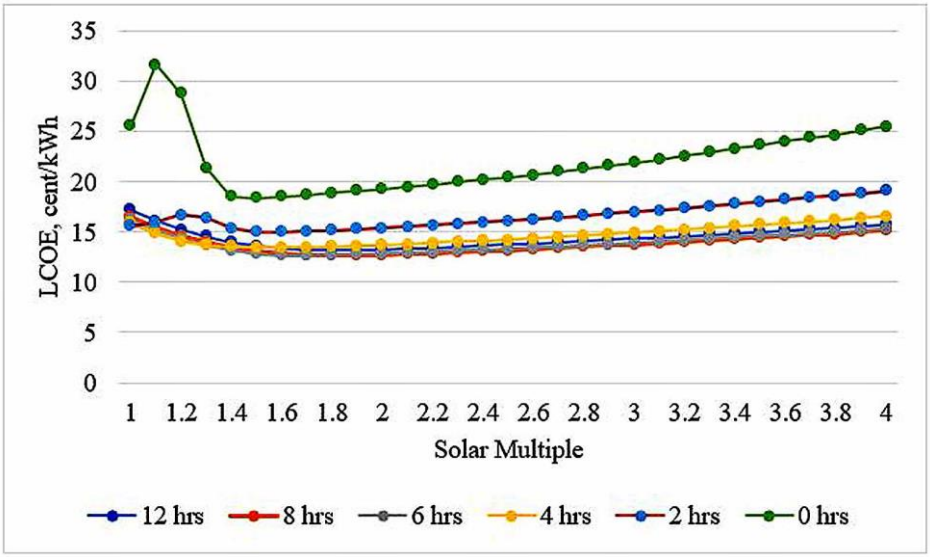


**Fig. 4.8** LCOE for Solar Tower at Tamale for varying TES period

### 4.4.3. Electricity generation analysis for PTC for both sites

The monthly cycle electrical power output (gross) from the PTC as indicated in Fig. 4.9 and Fig. 4.10 shows that just like the STPP, the output electricity from the PTC would be high during the harmattan period and low in the rainy season. Electricity export to grid monthly could be as high as 100 MWe and as low as 60 MWe during the harmattan and rainy seasons, respectively. The Navrongo PTC power plant generated a total of 211 GWh of electricity whiles that of Tamale produced 190 GWh electricity, in year one. A gross-to-net conversion rate of 74% and 75,8% were recorded for the Tamale and Navrongo power plants, respectively. The CF for the PTC power plant at Navrongo was 24,1%, whiles that of Tamale recorded a CF of 21,7%.

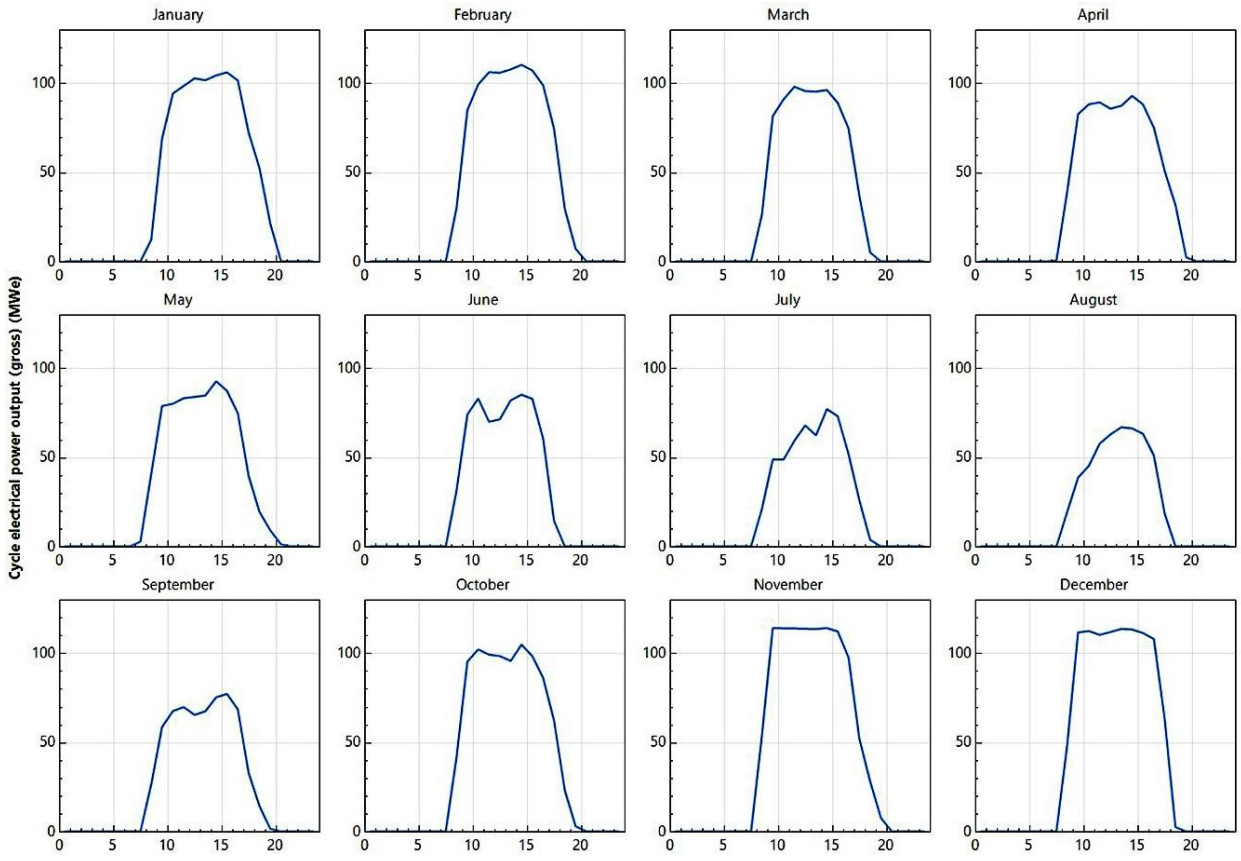


**Fig. 4.9** Cycle electrical power output (gross) for the PTC at Navrongo

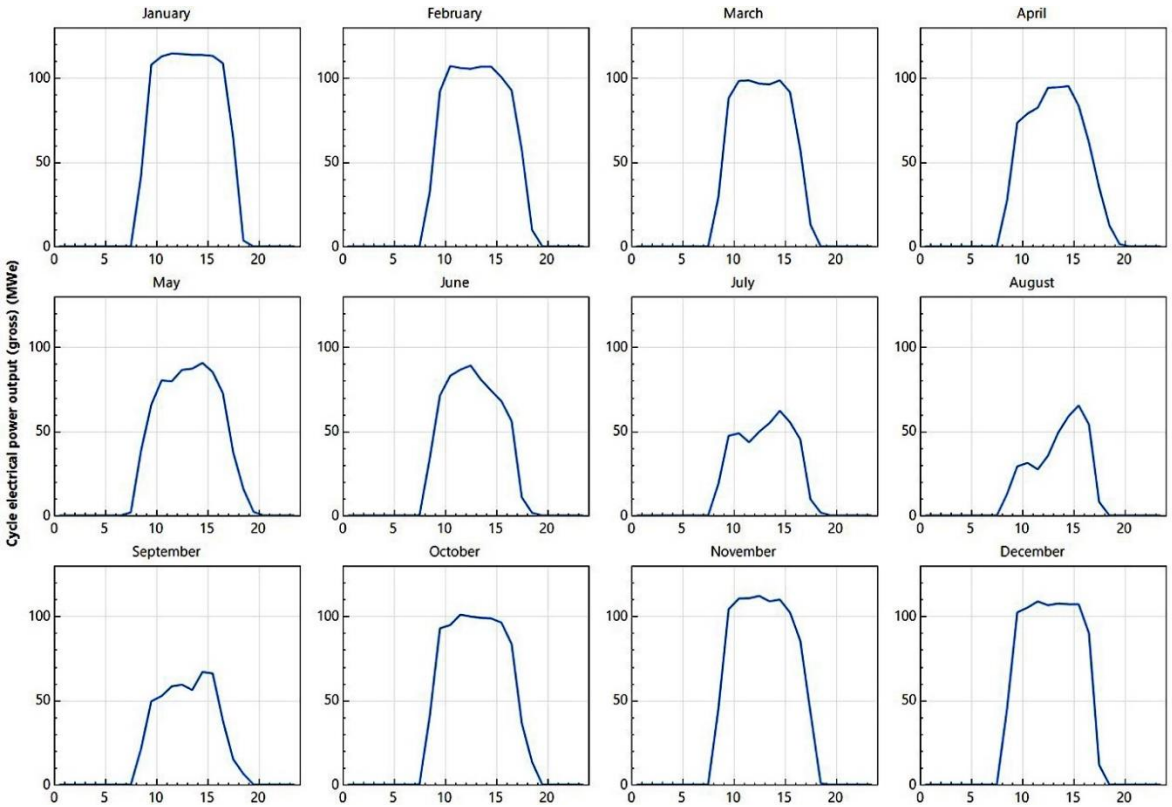


**Fig. 4.10** Cycle electrical power output (gross) for the PTC at Tamale

### 4.4.4. Economic Analysis for the PTC power plant

The economic results for the PTC are presented in Table 4.5, the results suggest real LCOEs of 25,83 ¢/kWh and 28,60 ¢/kWh for the Navrongo and Tamale power plants, respectively. The obtained LCOEs are higher than the IRENA global weighted average as indicated in Ref [135].

**Table 4.5** Economic results from the simulation of the PTC

| | Navrongo | Tamale |
|---|---|---|
| Metric | Value | |
| Annual water usage, $m^3$ | 58548 | 56977 |
| PPA price (year 1), ¢/kWh | 21,70 | 24,25 |
| Levelized PPA price (nominal), ¢/kWh | 30,95 | 34,27 |
| Levelized PPA price (real), ¢/kWh | 26,03 | 28,81 |
| LCOE (nominal), ¢/kWh | 30,72 | 34,01 |
| LCOE (real), ¢/kWh | 25,83 | 28,60 |
| Year investor IRR achieved | 20 | 20 |
| NPV, $ | 3 633594 | 3 633971 |

In addition to the energy from the sun, the relative sizing of the following components: power block, storage tank, and solar field determines the CF of the power plant. A smaller solar field leads to a reduction in the thermal energy delivered to the power block which also affect the CF [138]. An increase in the SM, combined with TES, can increase the utilization of the power block which results in the reduction of LCOE of the entire plant. However, an increase in the SM also increases the capital cost of the plant. Hence in order to resolve this contradicting effect from these parameters, there is the need to optimize to ascertain the SM which gives the least LCOE when TES is integrated. Fig. 4.11 and Fig. 4.12 shows the LCOEs of PTC power plants at Tamale and Navrongo, respectively, under different TES periods, it shows a rather stimulating behavior unlike what happened under STPP system.

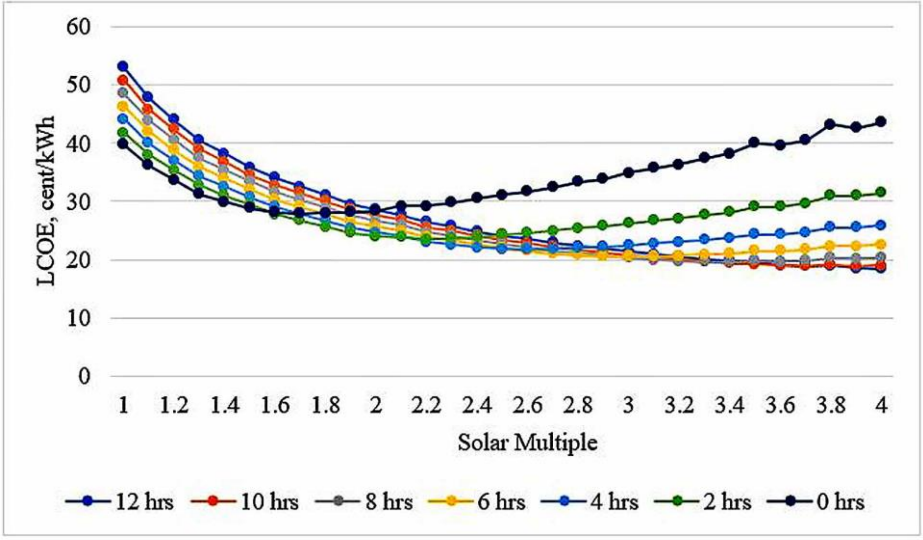


**Fig. 4.11** LCOE for PTC at Tamale for different TES period

In the case of the PTC in this study, the usual decrease in the cost of energy with increasing TES period did not appear so, within the initial SM range. It therefore suggests that the SM used in simulating the PTC power plant in this study is lower than required for the selected TES period. The results suggest that, for a system without TES, an SM of 1,5 is the optimal, however, for a system with an integrated TES system, the optimal SM depends on the TES period. For instance, the optimum SM for a system with 4 hours TES will be 2,6, whereas one with a 2-hour TES period will be 2,2 for both sites. A system

with a 12-hour TES period will experience the least LCOE of 17,24 ¢/kWh at an SM of 4, whiles that for the 10-hour TES period occurs at an SM of 3,6 at an LCOE of 17,73 ¢/kWh.

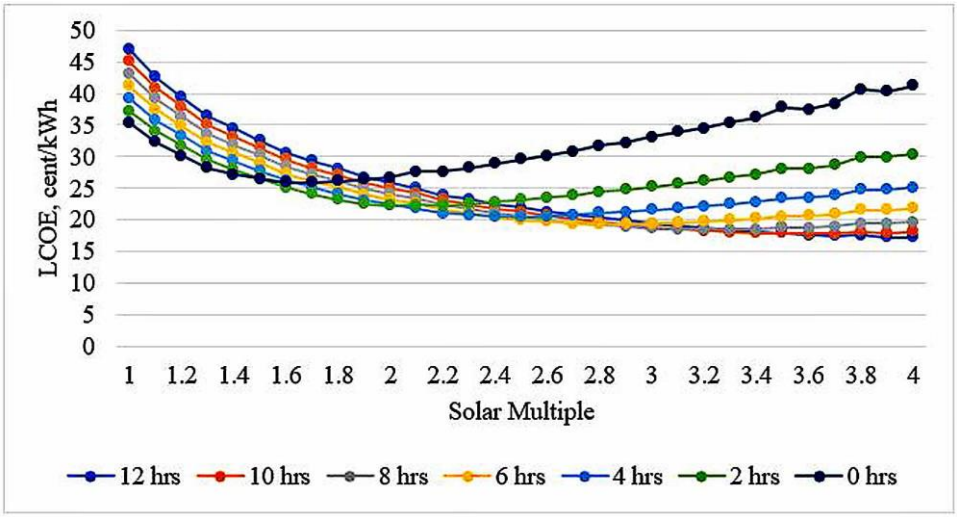


**Fig. 4.12** LCOE for PTC at Navrongo for different TES period

### 4.4.5. Sensitivity Analysis

It is clear that LCOE is prone to the influence of economic and environmental vicissitudes, a sensitivity analysis was therefore conducted to ascertain the impact of such factors on the economic indicators of the project. Factors such as discount rate, debt interest rate, TES period and cash incentives may affect the LCOEs and NPVs of power plants. Results from Fig. 4.13 shows that, the annual interest rate has a significant effect on both STPP and PTC for both sites.

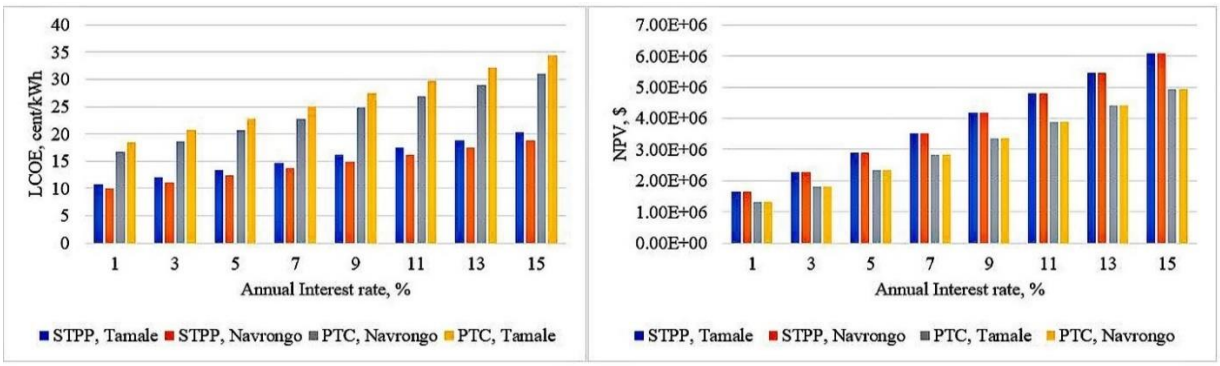


**Fig. 4.13** Effect of annual interest rate on LCOE and NPV on both scenarios at 12 hours TES

Given grid parity, the power generated from CSP particularly the STPP can compete with traditional sources of power, for instance, annual interest rate between 1% and 11% for a system with a 12-hour TES period could bring the LCOE of the STPP at par with current cost of energy to consumers in Ghana especially the one at Navrongo. Increasing the annual interest rate have an increasing effect on the NPV.

From the sensitivity analysis, the NPV is hugely dependent on the real discount rate, it decreases with increasing real discount rate, however, its impact on LCOE is fairly minimal. A real discount rate above 10% renders the NPV for both technologies at both sites negative. It therefore suggests that such projects will be economically non-competitive should the discount rate for their construction be above 10%. A higher discount rate means a high-end user tariff; therefore, the government could offer some tax relieves and incentives to investors in order to drive down the LCOE. The effect of real discount rate on the LCOE and NPV for both technologies are illustrated in Fig. 4.14.

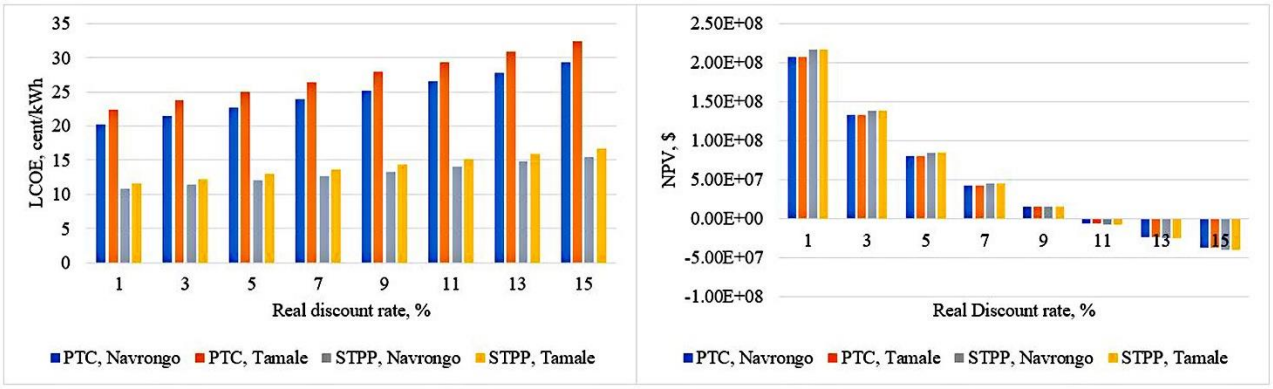


**Fig. 4.14** Effect of real discount rate on LCOE and NPV on both scenarios at 12 hours TES

Fig. 4.15 shows the effect of TES period on the CF of the various power plants, it can be seen from the figure that the TES period have a relatively minor effect on the CF of the PTC power plant for both sites. The capacity factor for PTC remains fairly constant at 21% and 24% for the Tamale and Navrongo plants with increasing TES hours, respectively, its CF flattens at 3 hours of TES and beyond, it does not change significantly after that period. However, the CF for the STPP increased with increasing TES period until 8 hours of TES before flattening the curve and reaching its maximum of about 48%

and 44% for the Navrongo and Tamale power plants, respectively. These are very important information during the project design stages.

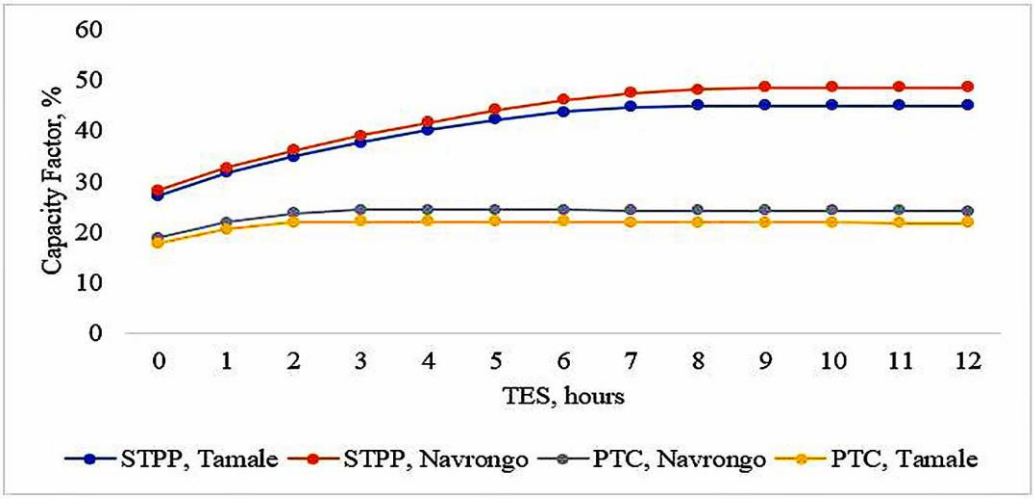


**Fig. 4.15** Influence of TES on the capacity factor

Investment in the RE sector is capital intensive and as a result, it needs corresponding funding sources to serve as a guarantee due to issues such as high cost, high risk and vulnerability to financing discrimination. Due to some of these issues, RE investments are highly reliant on policy; therefore, subsidies and incentives from governments inevitably affect investments in the sector [139]. The provision of incentives has been an effective way of promoting RE by making a viable investment case and making such technologies competitive with conventional sources of energy generation [140]. This study assessed the effect of government incentives on the cost-effectiveness of both systems at the Tamale site. Results from the analysis as shown in Fig. 4.16 suggests that incentives from government will have a significant effect on the PTC power plant more than the STPP. The LCOE for the PTC system declined from 40,52 ¢/kWh for an SM of 1,2 to 22,78 ¢/kWh for an SM of 2,4 all at a 15% cash incentive. That of the STPP decreased slightly from 16,08 ¢/kWh to 14,41 ¢/kWh under same conditions.

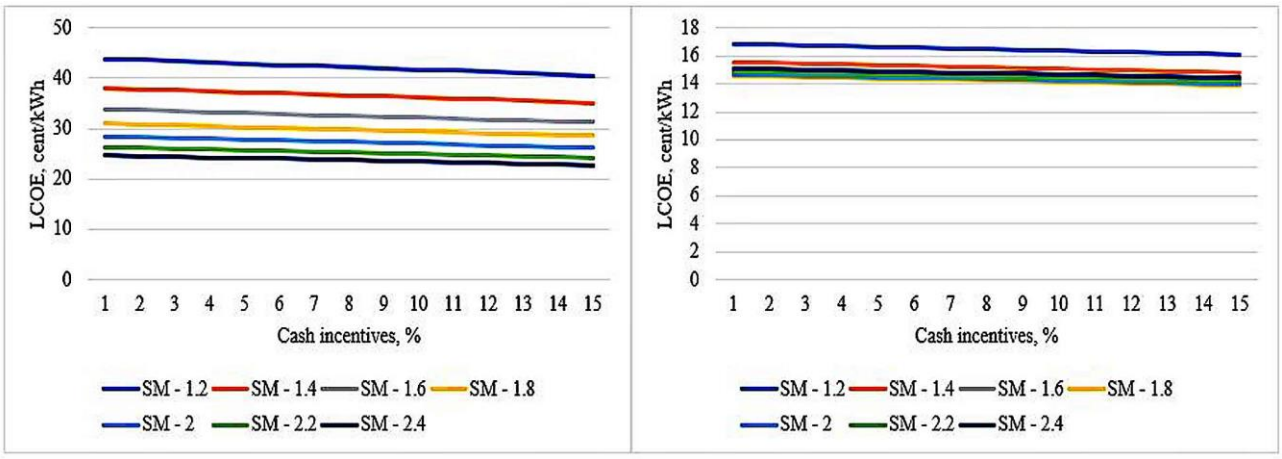


**Fig. 4.16** Effect of cash incentives on the LCOE of PTC (left) and STPP (right) at Tamale site for 12 hours TES

### 4.4.6. Comparative analysis between the STPP and PTC and other literatures

The huge differences in the LCOEs of the two technologies can be associated with the working principle of the STPP, more energy per unit mass of the molten salt is stored as a result of its higher temperature difference across the TES system. The lower temperature of operation relative to the Parabolic CSP results in less conversion efficiencies in the power block. Performance of the central receivers in STPP is better as a result of its thermo-hydraulic design which enables higher solar flux as well as higher outlet temperature of the HTF [98]. Results from the simulation shows that the STPP is the best technology for Ghana's weather conditions. The LCOEs for the PTC power plants at Navrongo and Tamale are about 47,08% and 48,49% more than that of the STPP modelled at both sites, respectively. The annual electricity export to grid for the STPP at Navrongo was about 50,33% more than that of the PTC power plant at same site. Clearly, the result from both sites shows that Navrongo will be the best site for the development of both technologies.

The study was also compared with other literatures to validate the obtained results. Fallouts from those literatures confirms the results in this study, the differences in the LCOE can be attributed to the relatively higher DNI in those areas. For instance, in the case of Ref [141], the plants were modelled at three different locations with solar insolation ranging between 2000- and 2400 kW h/m$^2$ /yr. The intensity of DNI is key to

**Table 4.6** Similar literatures on these technologies

| Location | Title of literature | System description | LCOE | TES | Reference |
|---|---|---|---|---|---|
| Tanzania | Is Concentrated Solar Power (CSP) a feasible option for Sub-Saharan Africa?: Investigating the techno-economic feasibility of CSP in Tanzania | STPP and PTC | STP ranges from 11,6 – 12,5 ¢/kWh PTP 13,0 – 14,4 ¢/kWh | 4 hours | [98] |
| India | An analysis of costs of parabolic trough technology in India | PTC | 0,14 $/kWh | 7 hours | [141] |
| Tunisia | Potential of concentrating solar power (CSP) technology in Tunisia and the possibility of interconnection with Europe | PTC | 0,23 €/kWh | 7,5 hours | [142] |
| Bangladesh | Performance optimization of parabolic trough solar thermal power plants – a case study in Bangladesh | PTC | 9,86 ¢/kWh | | [143] |
| Sevilla | Impacts of solar multiple on the performance of direct steam generation solar power tower plant with integrated thermal storage | STPP | 21,77 ¢/kWh | 3 hours | [144] |
| IRENA | Renewable Power Generation Costs in 2018 | CSP | 0,185 $/kWh | | [135] |
| Ghana, Navrongo and Tamale | Current study | PTC | 25,83 – 28,60 ¢/kWh | 12 hours | |
| Ghana, Navrongo and Tamale | Current study | STPP | 13,67 – 14,73 ¢/kWh | 12 hours | |

the techno-economic output of the studied systems in this paper, data from Fig. 4.2 shows that DNI for south-western Africa is generally low and therefore, the high LCOE values obtained in this study can be associated with it. Notwithstanding, the relatively high LCOEs for the STPP and PTC power plants in this study, they still fall within obtained values in other literatures. Table 4.6 shows a comparison of other studies.

## 4.5. Comparative assessment of PV power plants with and without storage systems in Ghana

### 4.5.1. Geographical and Solar resource data for Ghana

This study divided the country into three main sections: southern, middle, and northern belts in this study. A site each was selected from these sectors to analyze their capability to support large-scale solar PV power plant development by assessing their techno-economic potentials. Wa in the Upper West region was selected for the northern sector, it can be located on latitude 10,06$^{o}$ N and longitude -2,51$^{o}$ E, weather data from NASA indicate that Wa records an annual average of solar radiation horizontal of 5,57 kWh/m$^{2}$/day. The middle section for this study is Sunyani, which is also is located on latitude 7,34$^{o}$ N and longitude -2,35$^{o}$ E, it has an annual average solar radiation horizontal of 4,80 kWh/m$^{2}$/day. The final site is the Southern belt whose site is Nsawam in the Eastern region, it is found on latitude 5,81$^{o}$ N and longitude -0,34$^{o}$ E also with an annual average of 4,49 kWh/m$^{2}$/day of solar radiation horizontal. Fig. 4.17 displays the hourly weather data for the studied areas obtained from NASA.

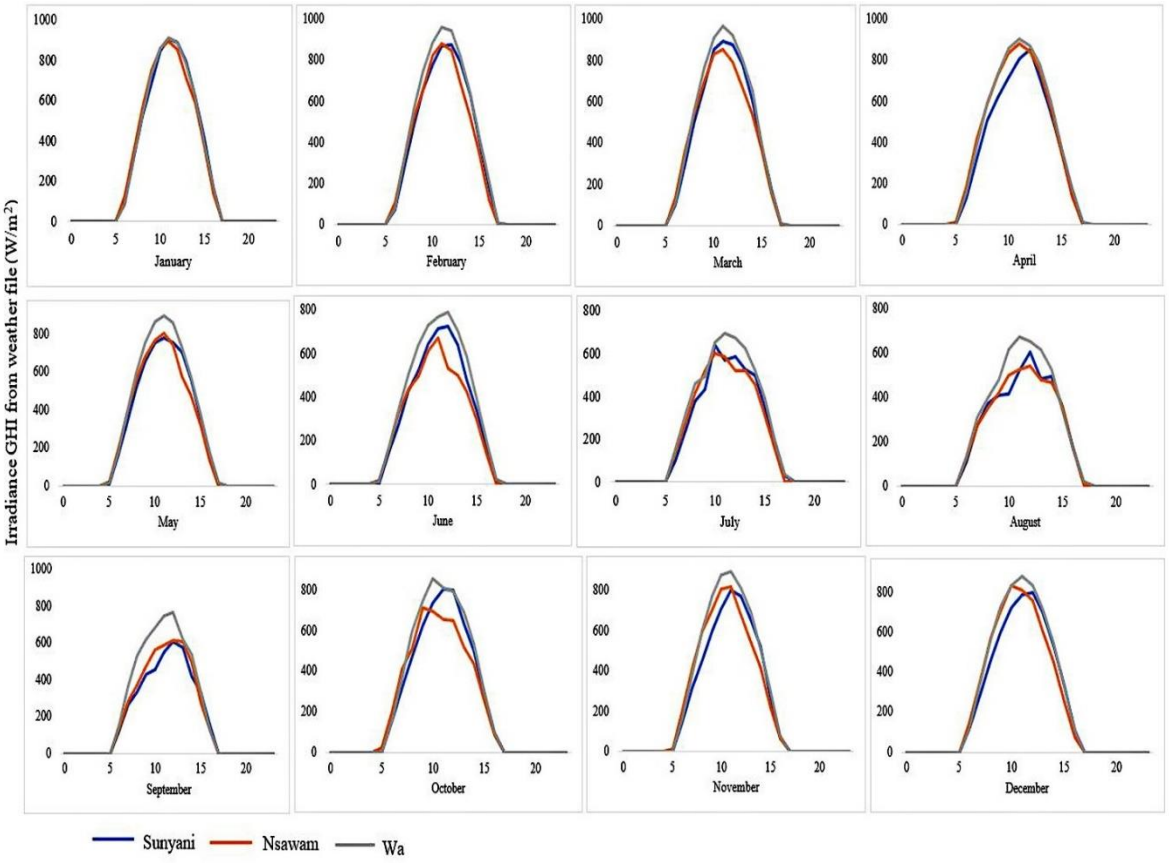


**Fig. 4.17** Hourly weather data for the selected sites (Data obtained from NASA)

Solar radiation has a significant impact on the economics of a PV power plant. According to the data presented in Fig. 4.17, it is evident that the highest solar irradiation in Ghana is experienced in the northern belt, the middle belt (Sunyani) follows and lastly the southern belt (Nsawam). The availability of solar radiation at a site has a substantial influence on the LCOE [145]. The highest solar irradiation are experience in the months of January, February, November, and December for all three sectors, as a result of the dry season during those months. The smallest amount solar irradiation was recorded in July; nevertheless, August and September also record low values because they are high rainfall months in the country. A heat map for the hourly solar radiation for the various sites are presented in Fig. 4.18 – 4.20.

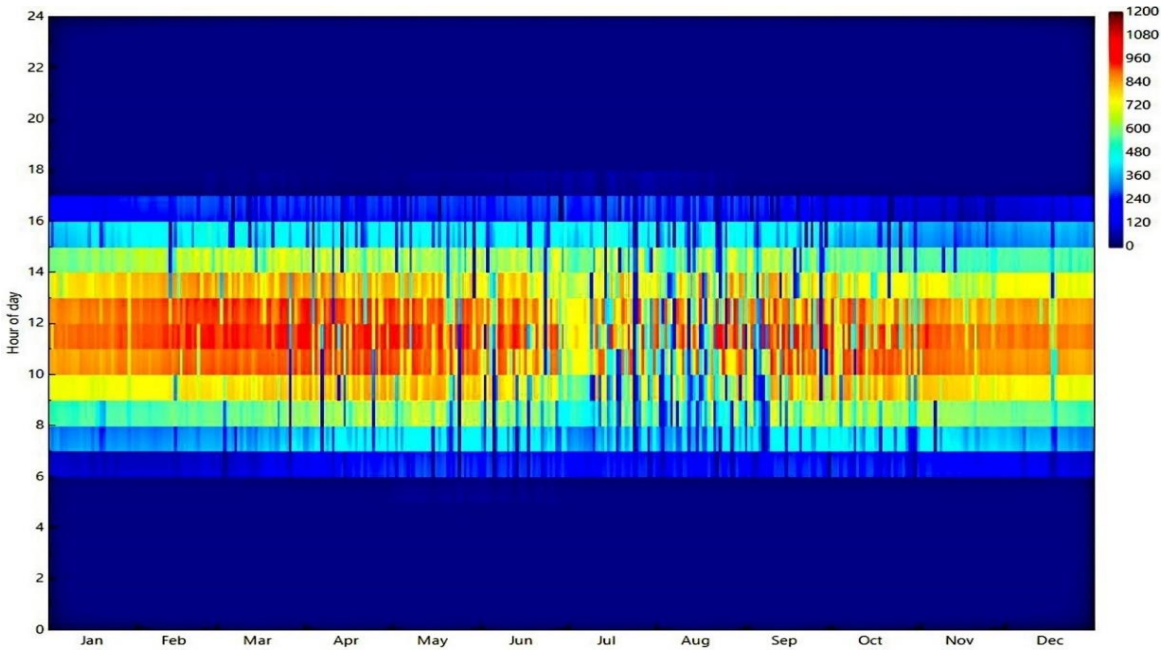


**Fig. 4.18** Wa hourly solar radiation heatmap

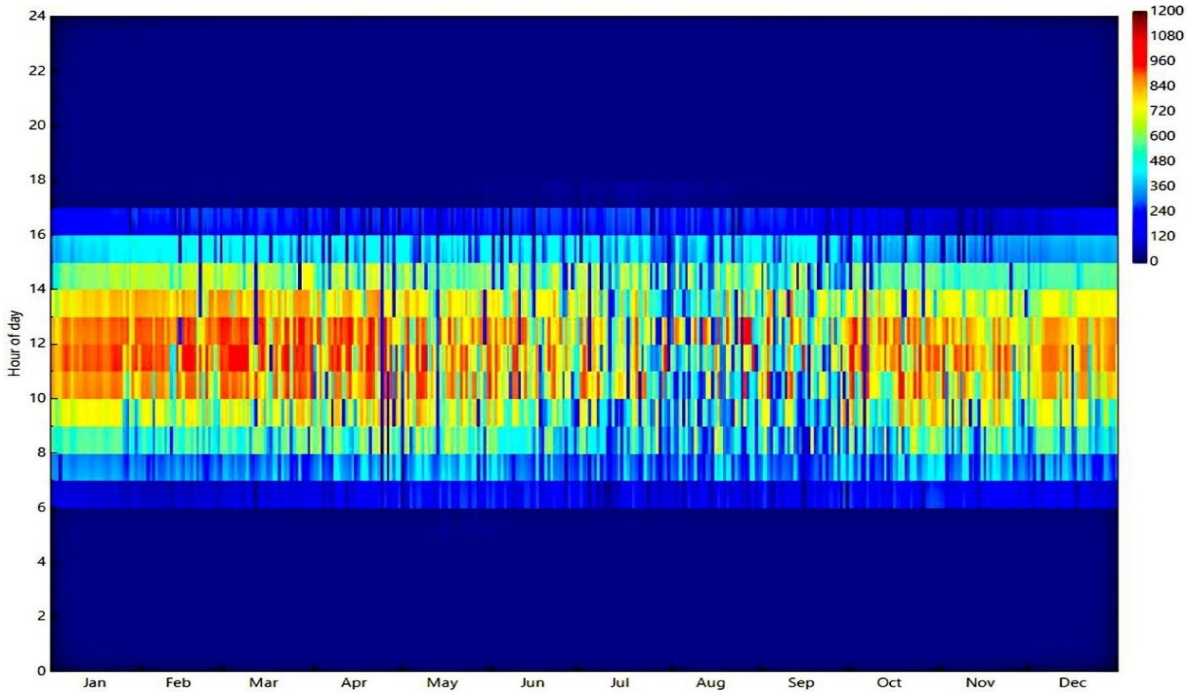


**Fig. 4.19** Heat map for hourly solar radiation for Sunyani

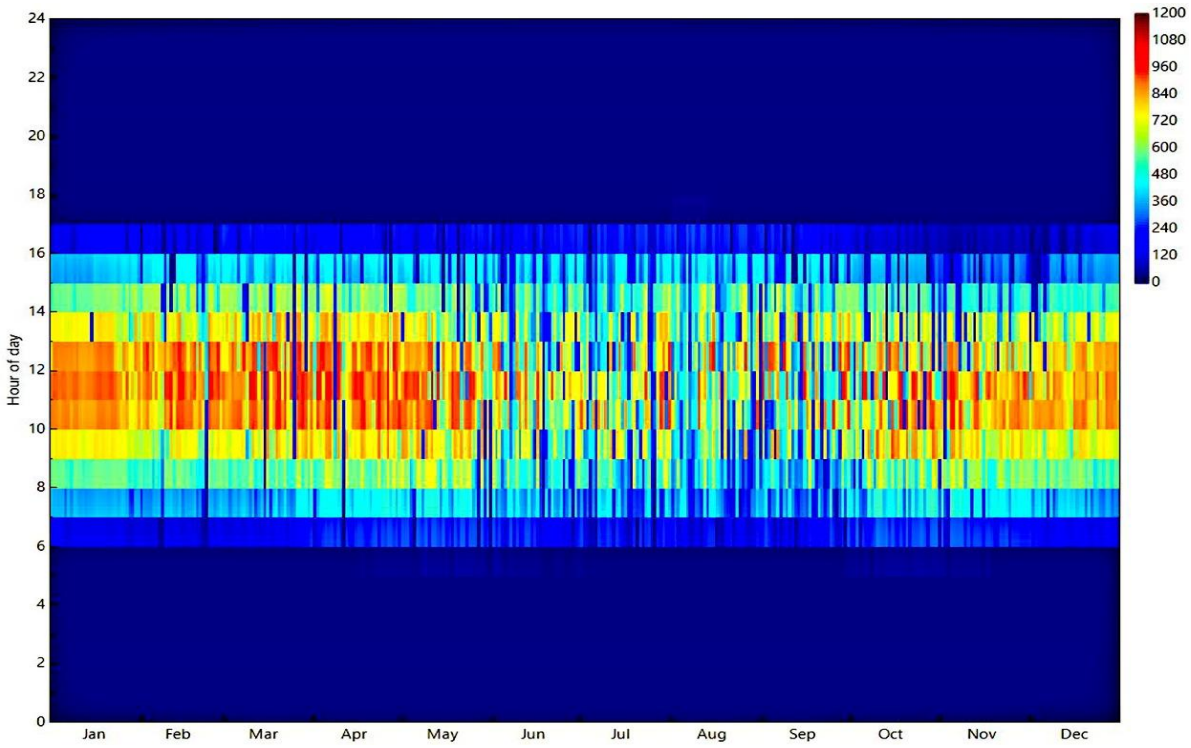


**Fig. 4.20** Heat map for hourly solar radiation for Nsawam

### 4.5.2.1. Principle of Operation of PV Cells

The photovoltaic technology produces electrical power using sunlight by an electronic process using materials called semiconductors. The semi-conductor's electrons are freed by the solar energy, the electrons can be induced to move through an electrical circuit, which then generate electricity. The semiconductor materials in the PV modules become ionized when they are strike by photons, this causes the outer electrons to break loose from their atomic bonds. The electrons are forced to move in single direction which creates a flow of electric current due to the structure of semiconductors. However, the efficiency of a solar cell is less than 100% in crystalline silicon cells because only a percentage of light within the spectrum is absorbed whiles others are too weak (infra-red) to generate electricity. Some (i.e., ultraviolet) results in heat generation rather than electrical energy [146].

### 4.5.3. Methodology

The methodology adopted for the study is presented in this section. An assessment of a solar PV power plant with and without storage system are simulated in three different areas in Ghana and the outcome presented in this section.

#### 4.5.3.1. Technical parameters

The technical parameters for the simulation are as indicated in Table 4.7. The performance of a PV module generally depends on environmental conditions such as temperature and solar irradiance, this can be estimated using Eq. (4.16) and (4.17) [147–149]:

$$P_{PV} = Y_{PV} f_{PV} \left( \frac{\bar{G}_T}{\bar{G}_{T,STC}} \right) \left[ 1 + \alpha_p \left( T_c - T_{c,STC} \right) \right] \tag{4.16}$$

Where, the rated capacity for the PV under STC is denoted by $Y_{PV}$ (kW), $f_{PV}$ denotes the derating factor (%), $\alpha_p$ represent the temperature coefficient of power (%°C), $\bar{G}_T$ is the incident solar radiation on the PV array (kW/m$^2$), $\bar{G}_{T,STC}$ represents the incident radiation at standard test conditions (kW/m$^2$), the temperature of the PV cell is denoted by $T_c$ (°C) and $T_{c,STC}$ indicates the PV cell temperature under STC (°C).

$$T_c = T_a + \bar{G}_T \left( \frac{T_{c,NOCT} - T_{a,NOCT}}{G_{T,NOCT}} \right) \left( 1 - \frac{\eta_c}{\tau \alpha} \right) \tag{4.17}$$

Where, the ambient temperature is denoted by $T_a$ (°C), the nominal operating temperature of the cell is represented by $T_{c,NOCT}$ (°C), $T_{a,NOCT}$ indicates the ambient temperature at which NOCT is 20 °C, $G_{T,NOCT}$ signifies the solar radiation at which NOCT is defined i.e., 0,8 kW/m$^2$, $\eta_c$ is the PV array's electrical conversion efficiency (%), $\alpha$ denotes the PV array's solar absorptance (%) and $\tau$ represent the solar transmittance over the PV panel (%).

The actual AC power which is attained after the DC/AC converter conversion from a module can be computed using Eq. (4.18) [147].

$$P_{ac} = P_{dc,STC}.\eta \tag{4.18}$$

Where, actual AC power output is denoted with $P_{ac}$ (kW), the converter's efficiency i.e., DC/AC is represented by $\eta$ (%), $P_{dc,STC}$ signifies the rated DC power under STC (kW).

The performance ratio (PR) can be defined as the ratio of the final yield ($Y_{final}$) to the reference yield ($Y_{ref}$) [147,150]. The PR gives information on the losses in the system which include inverter losses, losses across the bypass diodes, inverter losses, and thermal losses etc. in the course of changing from DC to AC power. The PR is stated mathematically as shown in Eq. (4.19) –(4.21) [147].

$$PR = \frac{Y_{final}}{Y_{ref}} \tag{4.19}$$

Where,

$$Y_{final} = \frac{E_{AC}}{P_{PV,rated}} \tag{4.20}$$

The final yield depends on the mounting and location of the PV modules.

$$Y_{ref} = \frac{H_{t,daily}\ (kWh/m^2)}{1\ (kW/m^2)} \tag{4.21}$$

Where the generated AC energy is denoted by $E_{AC}$ (kWh), the global in plane horizontal insolation is represented by $H_{t,daily}$ (kWh/m$^2$) and the rated power of the PV panel is also represented by $P_{PV,rated}$ (kW).

The $Y_{ref}$ is a function of the in-plane irradiation which is estimated as the ratio of the total irradiation per year or day to the reference irradiance [151]. Eq. (4.22) is use to estimate the daily $Y_{ref}$ [152].

$$Y_{ref} = \frac{\int_{t=1}^{24} G_I dt}{G_{I,ref}} \tag{4.22}$$

Where $G_I$ represents the total irradiation (kWh/m$^2$) and $G_{I,ref}$ denotes the reference irradiance (kW/m$^2$).

The capacity factor (CF) can be defined as the ratio of the actual output power of the power plant within a period to the potential power output if the power plant were to work at full nameplate capacity. It allows utilities and engineers to assess the total energy that can be added to an energy mix from a specific power plant [145]. The CF can be mathematically expressed as shown in Eq. (4.23) [153].

$$CF = \frac{E_{AC}}{P_{PV,rated} \times 8760} \tag{4.23}$$

A 0,5% annual degradation rate of the PV power plant was used in the study [154]. Fig. 4.21 shows the characteristics of the selected solar module for the analysis. A cost of 0,38 \$/W$_{dc}$ for the PV module obtained from NREL was used for the analysis [155].

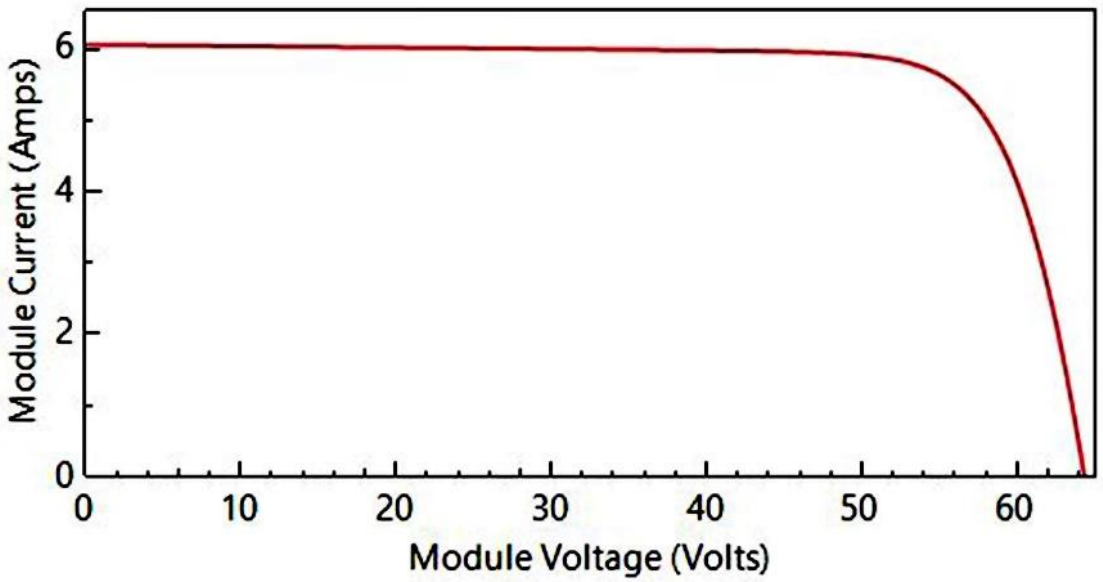


**Fig. 4.21** SunPower SPR-E19-310-COM behavior (source: SAM)

#### 4.5.3.2. Converter

There are two forms of energy conversions that occurs, AC to DC and DC to AC power. There is, therefore, the need to include an inverter to the system. Inverters connected to PV systems are devices that convert DC power from the modules to AC which is then sent to the grid. There are specific characteristics associated with inverters which are adapted for use in PV power plants, these include high conversion efficiency, MPPT, automatic harmonization and anti-islanding protection with grids. The selected inverter have be able to withstand the projected monitoring of the modeled AC loads. The inverter's efficiency is the ratio of the output power (i.e., AC) to the produced power (DC) from the PV modules as presented in Eq. (4.24) [148,152,156]. Fig. 4.22 shows the efficiency curve of the selected inverter. This study used an inverter cost of 0.06 \$/$W_{dc}$ [157].

$$\eta_{inv} = \frac{P_{inv,out}}{P_{inv,in}} \tag{4.24}$$

Where, the output power of the inverter is represented by $P_{inv,out}$ (kW) and the input power of the inverter is denoted by $P_{inv,in}$ (kW).

The manufacturer usually provide the efficiency curve of the inverters under standard optimal operating conditions under three different voltage levels, i.e., lowest, nominal, and highest. The efficiency curve makes it easy to identify the actual operating point for real operating conditions (ROC) [158]. Several literatures have reported the consideration of the dependency of inverter efficiency to the inverter's input voltage under ROC. For example, a second-order polynomial expression is proposed as presented in Eq. (4.25) – (4.27) [158,159].

$$\boldsymbol{P_{inv,n} = k_0 + k_1 P_{pv,n} + k_2 P_{pv,n}^2} \tag{4.25}$$

Where, $k_0$, $k_1$ and $k_2$ are the correlation coefficients.

$$P_{pv,n} = \frac{P_{pv}}{P_{inv,rated}} \tag{4.26}$$

$$P_{inv,n} = \frac{P_{inv}}{P_{inv,rated}} \tag{4.27}$$

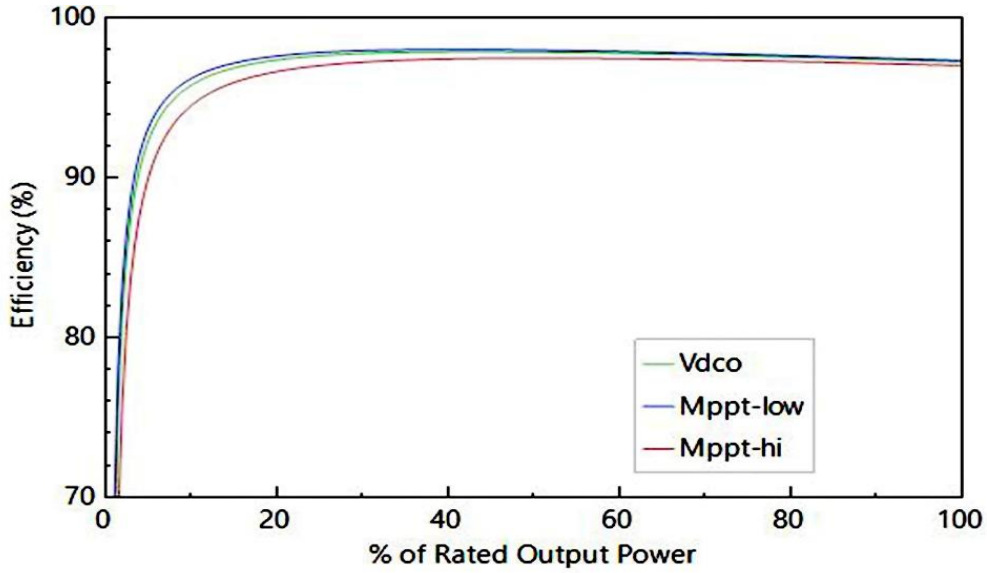


**Fig. 4.22** Efficiency curve of the selected inverter (Obtained from SAM)

#### 4.5.3.3. Battery system

This system is added to serve as a back-up when there is a drop in the power generation from the PV power plant. Table 4.7 has the technical parameters of the storage system. The battery's state of charge (SOC) can be calculated using Eq. (4.28). A cost of 200 $/kWh for the battery is used for the investigation [63].

$$SOC(t) = \frac{C_{bat}(t)}{C_{bat\ max}(t)} \tag{4.28}$$

Where, $(0 \leq SOC \leq 1)$, $C_{bat}$ signifies the battery's capacity at time (t), $C_{bat\ max}$ represents the battery's maximum capacity. The battery is considered as fully charged if SOC = 1, when the SOC = 0, it shows that the battery is empty.

**Table 4.7** Technical Parameters for the simulations obtained from SAM software

| Description | Value | Unit |
|---|---|---|
| *Module Characteristics* | | |
| Manufacturer | Sunpower SPR-E19-310-COM | |
| Cell temperature | 25 | ℃ |
| Max Power, $P_{mp}$ | 310,15 | $W_{dc}$ |
| Maximum power voltage, $V_{mp}$ | 54,70 | $V_{dc}$ |
| Module aspect ratio | 1,7 | |
| Module length | 1,67 | m |
| Module width | 0,98 | m |
| *System Design* | | |
| Modules per string in subarray | 12 | |
| Strings in parallel in subarray | 5374 | |
| Number of modules in subarray | 64488 | |
| Nameplate DC capacity | 20 | MW |
| *Inverters* | | |
| Number of inverters | 22 | |
| Type | SMA America SC750CP - US | |
| DC to AC ratio | 1,18 | |
| Total inverter capacity | 17417,541 | $kW_{dc}$ |
| Maximum AC power | 770000 | $W_{ac}$ |
| Maximum DC power | 791706 | $W_{dc}$ |
| Minimum MPPT DC voltage | 545 | $V_{dc}$ |
| Maximum MPPT DC voltage | 820 | $V_{dc}$ |
| *Battery* | | |
| Battery type | Lithium Ion: Nickel Manganese Cobalt Oxide (NMC) | |
| Nominal bank capacity | 4,000 | kWh (DC) |
| Nominal bank voltage | 500,4 | V (DC) |
| Cells in series | 139 | |
| Strings in parallel | 3,553 | |

### 4.5.4. Results and Discussion

The techno-economics of a 20 MW modelled in three sections of Ghana are presented in this section. The outcomes presented in this segment are obtained from the SAM software.

#### 4.5.4.1. Technical analysis

The technical outcome of the various systems are discussed in this section. The highest annual energy was recorded at Wa due to the high solar radiation at that territory. PV power plants have an exclusive characteristic from other RES, it goes off during sunset, this affect its CF values compared to other conventional power plants. Results as presented in Table 4.8 shows that the northern belt will record the highest CF of 18,2% whiles the other locations will record 16,3% and 16,1% for the Middle and Southern belts, respectively. The CF for each site falls within the range of acceptable CFs of SPP's globally. A study by [160], shows that CF for fixed mounted PVs around the world ranges between 15% - 21%, as recorded by all simulated PV at each site.

The exported electricity to grid for the two systems as well as the total charge of the battery for the three sites are illustrated in Fig. 4.23, Fig. 4.24, and Fig. 4.25. Results from the figures indicates that, the highest electricity export to grid from the system occurs in the first two and last two months of the year, which is also the period with high solar radiation at the selected sites. The least electricity export to grid is expected to occur in June, July, and August due to the lower solar radiation recorded during that period. Similar characteristics apply to the battery total charge during the period.

The various SPP's annual PR varied slightly, i.e., from 0,75 – 0,77 depending on the location of the plant. These outcomes can be compared to the International Energy Agency (IEA) PV power systems program (Task 2), in that program, the PR for PVs are reported to range from 0,6 – 0,8 [152].

**Table 4.8** Technical performance of both systems at all three sites

| Metric | Wa | | Sunyani | | Nsawam | |
|---|---|---|---|---|---|---|
| | With Battery | Without Battery | With Battery | Without Battery | With Battery | Without Battery |
| Annual energy (year 1), GWh | 31 | 31 | 28 | 28 | 28 | 28 |
| Capacity factor, % | 18.0 | 18.2 | 16.3 | 16.3 | 16.0 | 16.1 |
| Energy yield (year 1), kWh/kW | 1,579 | 1,591 | 1,427 | 1,425 | 1,404 | 1,409 |
| Performance ratio (year 1) | 0.75 | 0.75 | 0.76 | 0.76 | 0.77 | 0.77 |

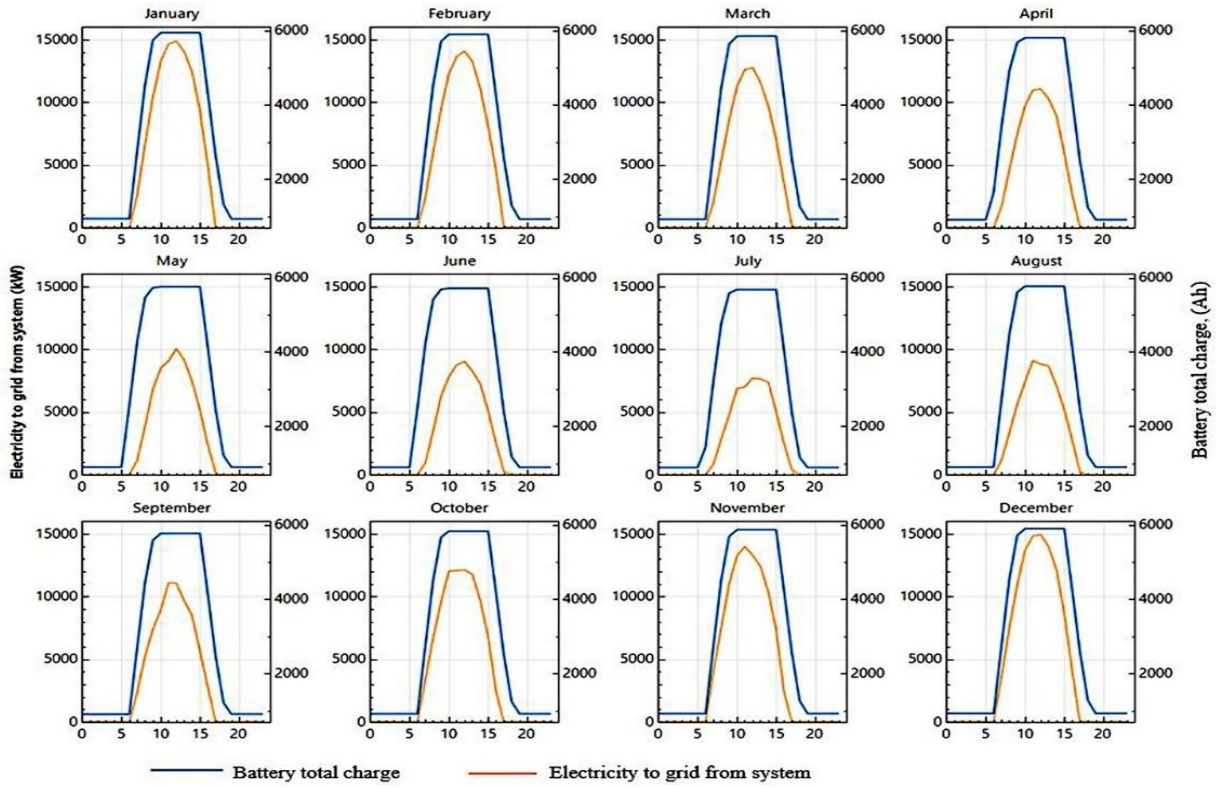


**Fig. 4.23** Monthly characteristics of electricity export to grid and battery total charge for the plant at Wa for FT system

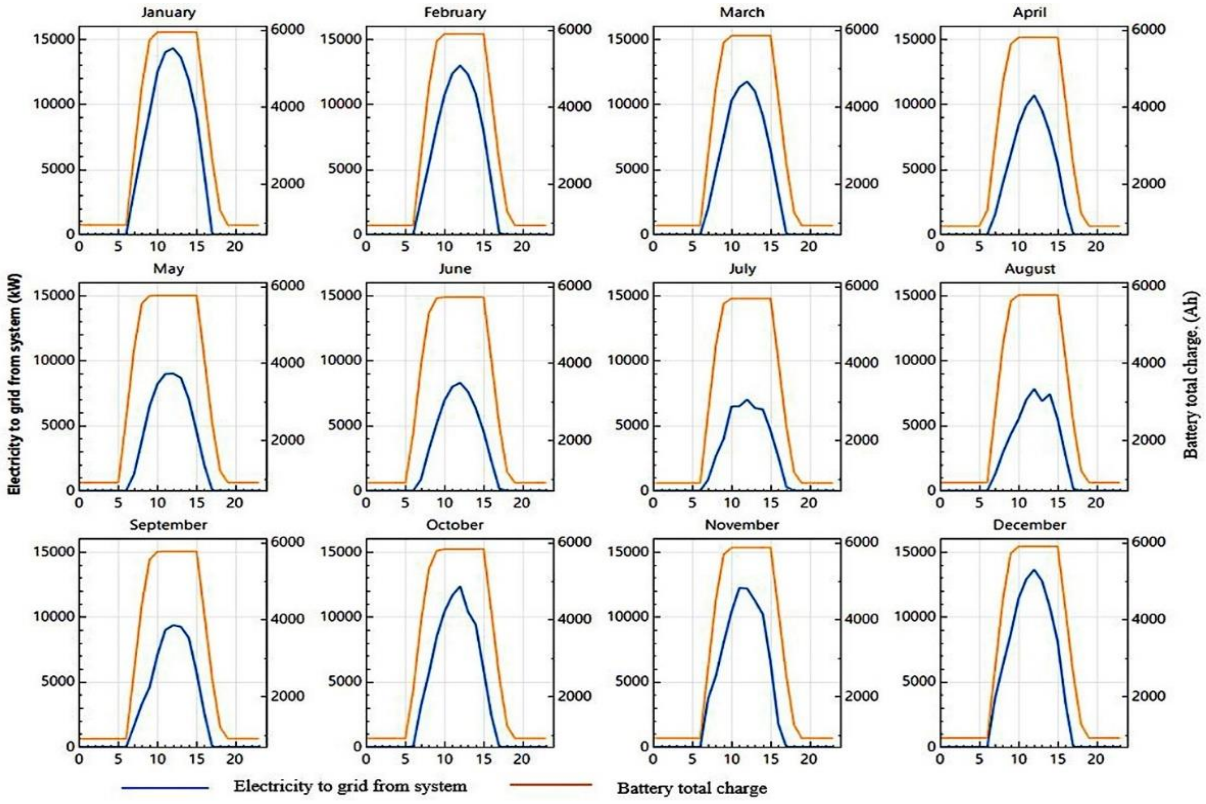


**Fig. 4.24** Monthly characteristics of electricity export to grid and battery total charge for the plant at Sunyani for FT system

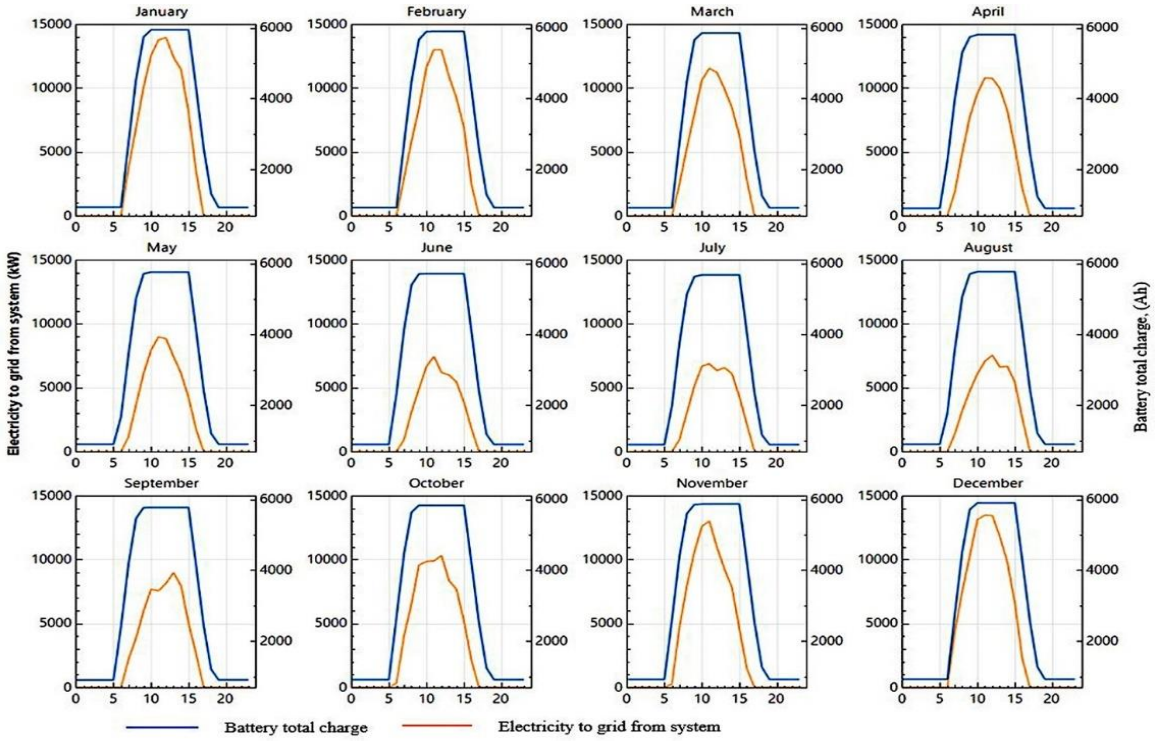


**Fig. 4.25** Monthly characteristics of electricity export to grid and battery total charge for the plant at Nsawam for FT system

#### 4.5.4.2. Sensitivity analysis on the technical performance

The impact of changing some parameters i.e., technical on the technical performance of the two systems at the various sites are assessed in this segment. This comprises of the effect of sun tracking on the techno-economics of PV systems at the selected sites. Tracing system in solar PV is a technology employed to adjust the solar panels or reflective surfaces to align with the sun's movement [161]. The fixed axis was set as a base case scenario, the PV panels in this mode are not movable but fixed at a tilt angle. Two additional tracking modes, i.e., single, and double axis tracking were also evaluated to assess their effect on the PV power plant's performance. Single axis tracking (SAT) approach is a state whereby the PV panels rotate from East to West (E-W) to align with the sun's movement. The polar aligned SAT, horizontal SAT, and the tilted SAT are some of the ways the SAT technology can be implemented [162]. The double axis tracking (DAT) is the second mode of tracking, the PV modules rotate from E-W to align with the day-to-day movement of the sun as well as south or north to track the sun's seasonal movement during the year. There are two axis of rotation for the DAT technology, it also has two common implementation options i.e., tip-tilt DAT and azimuth-altitude DAT [162].

The outcome of the simulation for the impact of tracking on the SPPs performance are presented in Table 4.9. It is clear from the results that the tracking system has a substantial effect on the system's performance at all sites. The real LCOE recorded by the SAT technology, for the PV-only system reduced to 6,12 ¢/kWh, 6,02 ¢/kWh and 5,42 ¢/kWh for the Sunyani, Nsawam and Wa sites, respectively. It recorded a minimal impact on the NPV for all sites. In the case of the PV-Battery system, the SAT had a substantial effect on the NPV, whereas the fixed tracker whose results will be presented in the subsequent section recorded negative NPV for all three sites, the SAT recorded positive values, NPVs of $5 million, $1 million, and $2 million were recorded for Wa, Sunyani and Nsawam, respectively. There was also a reduction in the real LCOE, Wa recorded 6,71 ¢/kWh, Nsawam 7,49 ¢/kWh, and Sunyani 7,60 ¢/kWh. This reduction can be connected to the rise in the annual electricity production caused by the tracking system.

**Table 4.9** Comparison of technical performances for two different trackers

| Metric | Northern belt (Wa) | | Middle belt (Sunyani) | | Southern belt (Nsawam) | |
|---|---|---|---|---|---|---|
| | SAT | DAT | SAT | DAT | SAT | DAT |
| PV only system | | | | | | |
| Annual energy (year 1), GWh | 40 | 43 | 36 | 38 | 37 | 39 |
| Capacity factor, % | 23,3 | 24,9 | 20,6 | 21,8 | 21,0 | 22,1 |
| Energy yield (year 1), kWh/kW | 2042 | 2177 | 1808 | 1908 | 1838 | 1939 |
| Performance ratio (year 1) | 0,77 | 0,76 | 0,77 | 0,77 | 0,78 | 0,77 |
| PV-Battery system | | | | | | |
| Annual energy, (year 1), GWh | 40 | 43 | 36 | 38 | 37 | 39 |
| Capacity factor, % | 23,1 | 24,6 | 20,6 | 21,8 | 20,9 | 22,1 |
| Energy yield (year 1), kWh/kW | 2021 | 2155 | 1808 | 1907 | 1832 | 1934 |
| Performance ratio | 0,76 | 0,76 | 0,77 | 0,76 | 0,77 | 0,77 |

The DAT technology had a positive impact on the performance of the various power plants at all sites. The CF and produced energy from the PV-Battery system saw significant improvement. The influence of the DAT technology on the PV-only power plant's economics was however negligible particularly the NPV, there was a slight reduction in the LCOE. For instance, the cost of energy for Wa would be 5,08 ¢/kWh against 5,80 ¢/kWh for Sunyani and 5,70 ¢/kWh at Nsawam. The NPV for all sites remained around $160000. For the PV-Battery power plant, its economic viability improved under the DAT technology compared to the SAT technology. The NPV for the DAT system under the PV-Battery system for Wa was over $7 million, Sunyani and

Nsawam also recorded over $3 million. The reduction in the LCOE in relation to the tracking system remained same for the DAT in the PV-Battery system. There was a 14-21% increase in the energy output and the CF for the PV-Battery power plant at all sites with the integration of either DAT or SAT technology.

Even though the tracking system has several advantages in relation its technical and economic performance, it also has some disadvantages. Some of these disadvantages includes the extra cost associated with O&M for the tracking systems, it also needs a larger land space compared to the FT technology since it must be spaced in order to prevent shading [162].

A project's lifetime is one of the determinant factors during the estimation of an LCOE for solar power plants, thus, it can affect the economic viability of the project if the real lifetime does not correspond with the estimated one. In PV power plants, its main components are usually given a warrantee of 25-30 years by most manufacturers [163], as a result a 25-year period was used for the analysis. A cumulative NPV and project return investigation the three project sites at a discount rate of 10% was conducted to determine the practicability tracking systems within the period of the analysis. Fig. 4.26, Fig. 4.27, and Fig 4.28 shows the after tax cumulative NPV and project returns for all three sites for both PV-only and PV-Battery systems.

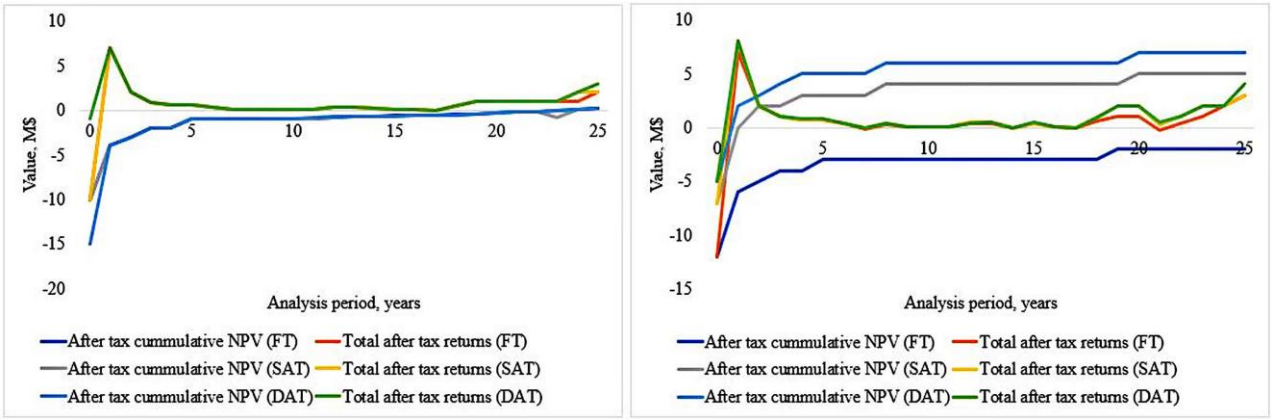


(a) (b)

**Fig. 4.26** Effect of tracking on the after tax cumulative NPV and total after tax returns for PV-only (a) and PV-Battery (b) for Wa

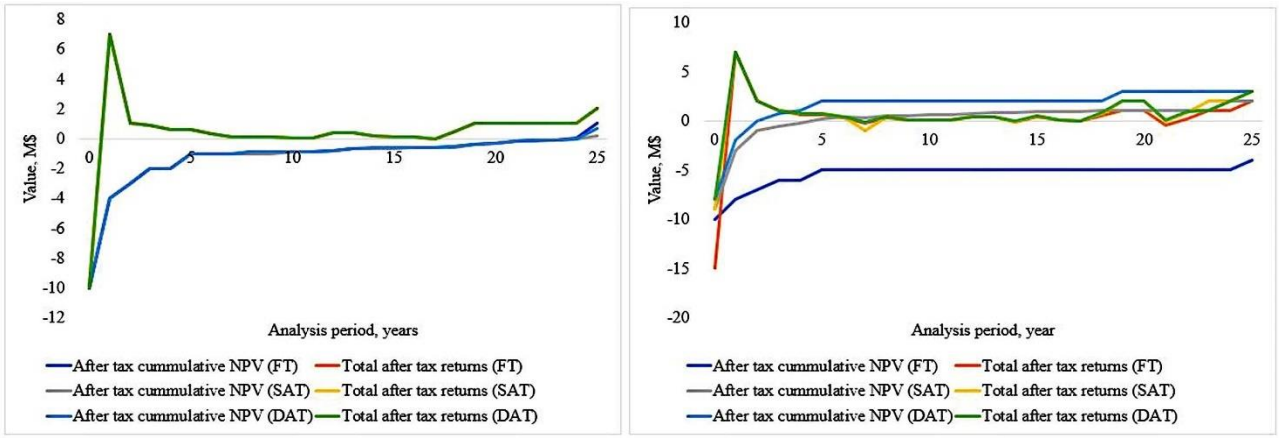


(a) (b)

**Fig. 4.27** Effect of tracking on the after tax cumulative NPV and total after tax returns for PV-only (a) and PV-Battery (b) for Sunyani

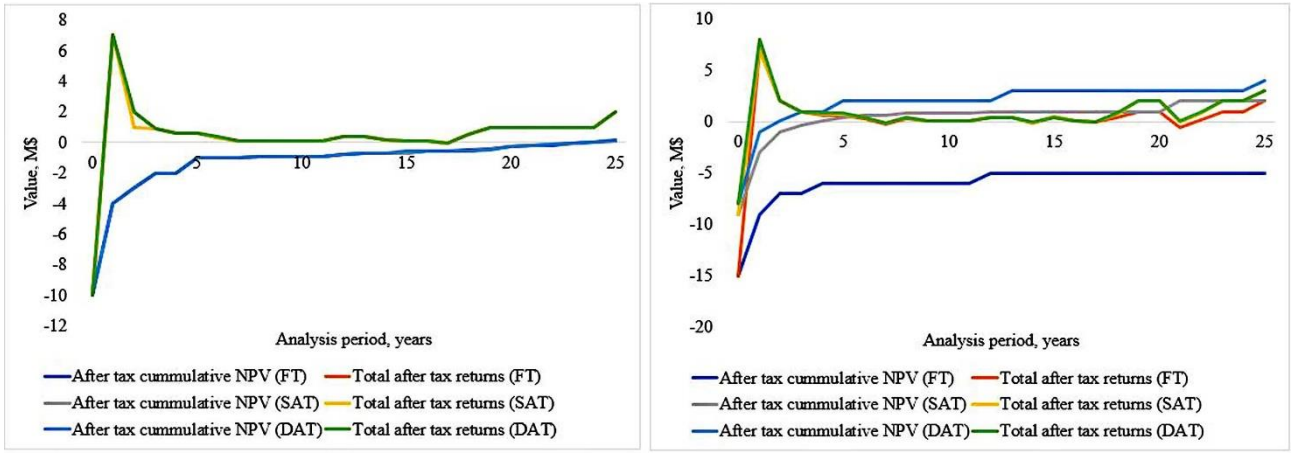


(a) (b)

**Fig. 4.28** Effect of tracking on the after tax cumulative NPV and total after tax returns for PV-only (a) and PV-Battery (b) for Nsawam

The outcome of the PV-only system will not generate the needed revenues required to pay-off the cost of the project within the study period (i.e., 25 years) for the fixed tracker technology. Nevertheless, the addition of a tracking system (both DAT and SAT) can help the PV system to produce extra electricity within the lifetime of the project to pay-off the initial investment. The PV-Battery system increased significantly in relation to electricity generation with the inclusion tracking systems which affected its NPV. It's cumulative after tax NPV generally stayed above the zero-mark different from that of the

PV-only system. The PV-Battery technology showed to be the optimal system for the economic and weather conditions in Ghana.

#### 4.5.4.3. Economic Analysis for PV-only system

The outcome of the NPV and the LCOE from the simulations for the FT system are discussed in this section. The northern section (Wa) is expected to record the least real LCOE of 6,95 ¢/kWh against 7,76 ¢/kWh and 7,85 ¢/kWh for the Middle (Sunyani) and Southern (Nsawam) sections, respectively. Positive NPV were at all sites which indicate that such a project will be a viable investment, however, there were some slight variations in NPV amongst the three sites**.** Fig. 4.29 shows the performance of the LCOE and NPV for the period of the analysis for the base case scenario. A positive NPV value was only recorded in the last year of the project.

In order to know the economic competitiveness of a project, its IRR must be more than or equal to the applied discount rate [164], this study used a discount rate of 10% for the estimations, and the results, an IRR of 12,9% was realized for the lifetime of the project. This is 2,9% more than the applied discount rate which is an indication that the project is economically viable. Table 4.10 is an illustration of the results for the economic indicators for the base-case scenario (i.e., fixed-axis tracker) for the PV-only power plant.

**Table 4.10** Results for the PV-only system with FT technology

| Description | Location | | |
|---|---|---|---|
| | Northern Belt (Wa) | Middle Belt (Sunyani) | Southern Belt (Nsawam) |
| PPA price (year 1), ¢/kWh | 7,79 | 8,69 | 8,79 |
| Levelized PPA price (nominal), ¢/kWh | 8,32 | 9,29 | 9,39 |
| Levelized PPA price (real), ¢/kWh | 7,01 | 7,83 | 7,91 |
| LCOE (nominal), ¢/kWh | 8,25 | 9,21 | 9,31 |
| LCOE (real), ¢/kWh | 6,95 | 7,76 | 7,85 |
| NPV, $ | 160395 | 160310 | 160301 |
| IRR, % | 11 | 11 | 11 |
| Year IRR is Achieved | 20 | 20 | 20 |
| IRR at end of project, % | 12,91 | 12,91 | 12,91 |
| Net capital cost, $ | 23889386 | 23889456 | 23889462 |

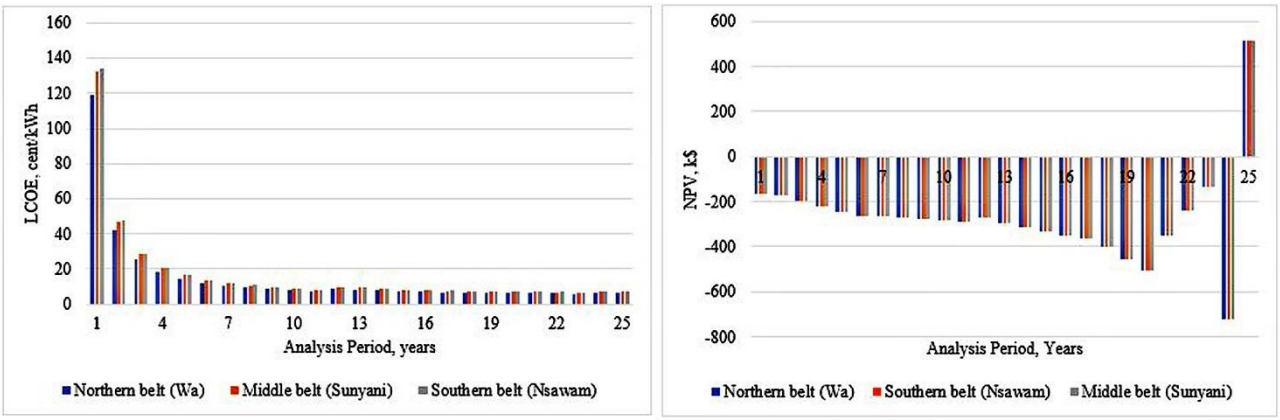


(a) (b)

**Fig. 4.29.** Behavior of LCOE (a) and NPV (b) after tax for the analysis period

#### 4.5.4.4. Sensitivity Analysis for PV-only system with FT technology

To be able to assess the economic viability of such projects it is always important to subject the project to further scrutiny through a sensitivity analysis. The sensitivity analysis is a tool used to measure the degree of uncertainties in projects. To that effect, this study analyzed the effect of certain parameters on the cost-effectiveness on the PV-only system at each site. The annual, discount, and inflation rates were assessed using different rates.

A discount rate is the opportunity cost of capital taken as a proportion of the capital value. Opportunity costs are important in economics, it is used to estimate the cost benefit analysis of a project. That type of cost are mostly not logged into the account books; it however affect decision making by estimating cash outlays as well as its accompanying losses or gains [165]. During investment, the cut-off rate below which an investment is not bankable is known as the opportunity cost of a capital. The nominal discount rate is a function of three factors: inflation, risk-free real return, and the degree of the project risk [165]. The outcome in Fig. 4.30 shows that the bankability of the project is affected by the discount rate. Increasing the discount rate increases the LCOE, whiles the NPV is inversely proportional to the discount rate. Increasing the discount rate has a diminishing effect on the NPV. In fact, any discount rate above 10% according to Fig. 4.30b renders the project economically ineffective at all three sites.

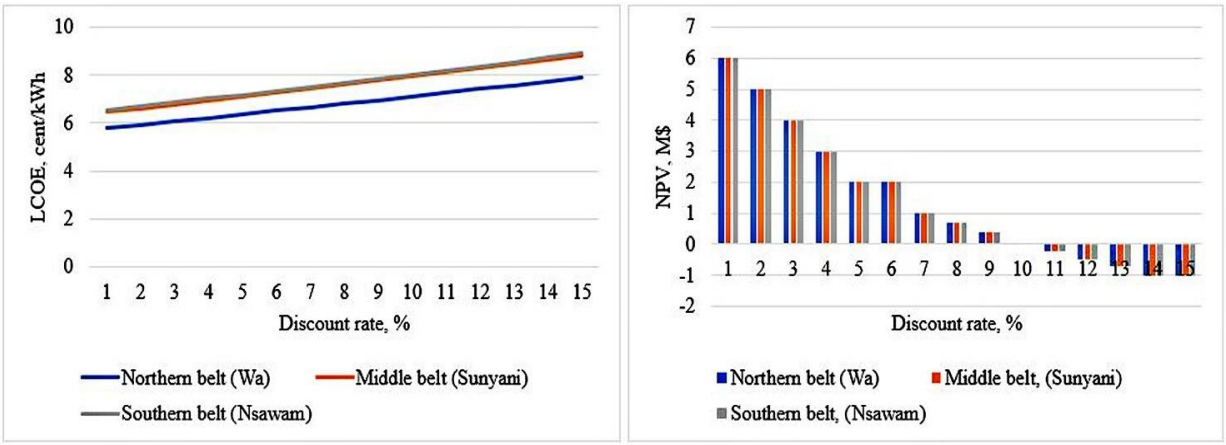


(a) (b)

**Fig. 4.30** Effect of Discount rate on (a) LCOE and (b) NPV

Financiers of projects charge interest, this maybe in the form of variable rate which is typically dependent on the lending rate of the financial institution i.e., bank, or inter bank borrowing rate with a margin, floating or fixed rate [166]. Project finance debt tends to have a fixed rate, which provides a predictable or stable reimbursement profile overtime to decrease variations in the infrastructure services cost. Volatilities between foreign and local currency debt is generally an issue of harmonizing the fixed debt rate with foreign exchange rate risk or the local currency debt, relative to interest rate risk [166]. This study assessed the impact of annual interest rate on the various projects and presented the results in Fig. 4.31, it is clear from the outcome that both the NPV and LCOE depend on the annual interest rate. Both metrics increases with increasing annual interest rates.

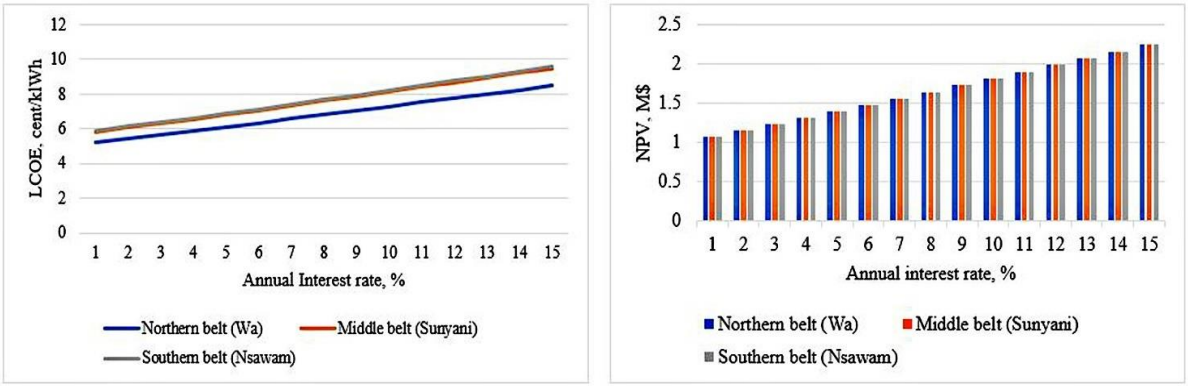


(a) (b)

**Fig. 4.31** Impact of Annual interest rate on (a) LCOE and (b) NPV

Inflation is said to be the surge in prices of goods and services over time. It indicates a loss in the value of money over time because it decreases the purchasing power of a currency. Fig 4.32a shows that, an increase in the rate of inflation has a direct impact on the LCOE, it remains quite stable between 1% and 7% inflation rate it however begins to rise steadily for inflation rate beyond 8%. Inflation above 6% also results in negative NPV as illustrated in Fig. 4.32b.

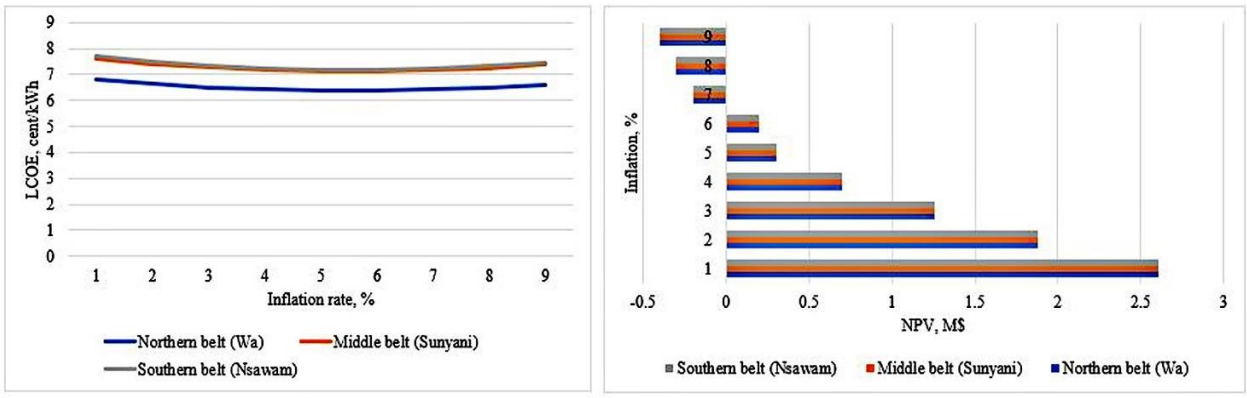


(a) (b)

**Fig. 4.32** Effect of Inflation rate on LCOE (a) and NPV (b)

### 4.5.4.5. Economic analysis for PV-Battery system

The impact of a storage system of the economics of the PV power plant is analyzed on this section. The battery is added to the system to firstly store excess power and also manage the flow of power in the plant. It comes in when the PV power plant is an unable to generate the required power to meet demand, thus, it supports in improving the reliability of power as well as the system's stability [167]. Table 4.11 presents the outcome of the real LCOE for a PV-Battery system. The results are comparatively higher than that recorded by the PV-only system shown above. This rise can be ascribed to the increased operations and installation cost due to the inclusion of the battery system. The outcome of the PV-Battery system with FT also shows it will not be financially profitable for all considered sites, taking into the negative NPV it records for all three sites.

**Table 4.11** Results for the FT PV-Battery system

| Description | Location | | |
|---|---|---|---|
| | Northern Belt (Wa) | Middle Belt (Sunyani) | Southern Belt (Nsawam) |
| PPA price (year 1), ¢/kWh | 9,00 | 9,00 | 9,00 |
| Levelized PPA price (nominal), ¢/kWh | 9,63 | 9,64 | 9,61 |
| Levelized PPA price (real), ¢/kWh | 8,11 | 8,12 | 8,10 |
| LCOE (nominal), ¢/kWh | 10,48 | 11,72 | 11,93 |
| LCOE (real), ¢/kWh | 8,84 | 9,88 | 10,05 |
| NPV, $ | -1 993375 | -4375722 | -4803070 |
| IRR, % | 5,56 | 1,13 | 0,46 |
| Year IRR is Achieved | 20 | 20 | 20 |
| IRR at end of project, % | 7,76 | 3,97 | 3,40 |
| Net capital cost, $ | 26445698 | 26277398 | 26247176 |
| Equity, $ | 12714862 | 14727164 | 15088138 |
| Size of debt, $ | 13730837 | 11550234 | 11159039 |

#### 4.5.4.6. Sensitivity analysis for PV-Battery system

There was a significant influence of discount rate on the feasibility of the PV-Battery system for all considered sites. According to the simulation results presented in Fig. 4.33, the Wa power plant will be the only project that can endure a discount rate up to 5% to remain bankable.

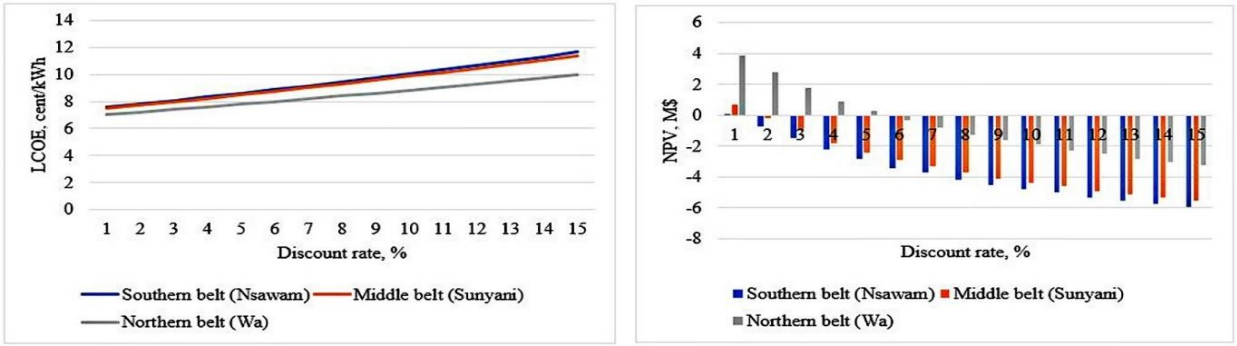


(a) (b)

**Fig. 4.33** Impact of discount rate on the LCOE (a) and NPV (b) for the PV-Battery system

The two other power plants at the other sites will be economically unviable using the adopted financial parameters used for the assessment, a discount rate more than 1% makes the other two sites unrealistic

The impact of annual interest rate on the NPV and LCOE for the PV-Battery (i.e., fixed axis tracker) is illustrated in Fig. 4.34. The outcome indicate that annual interest rate would have a significant impact on the profitability of all power plants. A 4% annual interest rate and above will make the project at Wa financially unprofitable, whiles the other sites can withstand an interest rate of 1% only. This suggests that such projects requires serious interventions from the state in order to be successful.

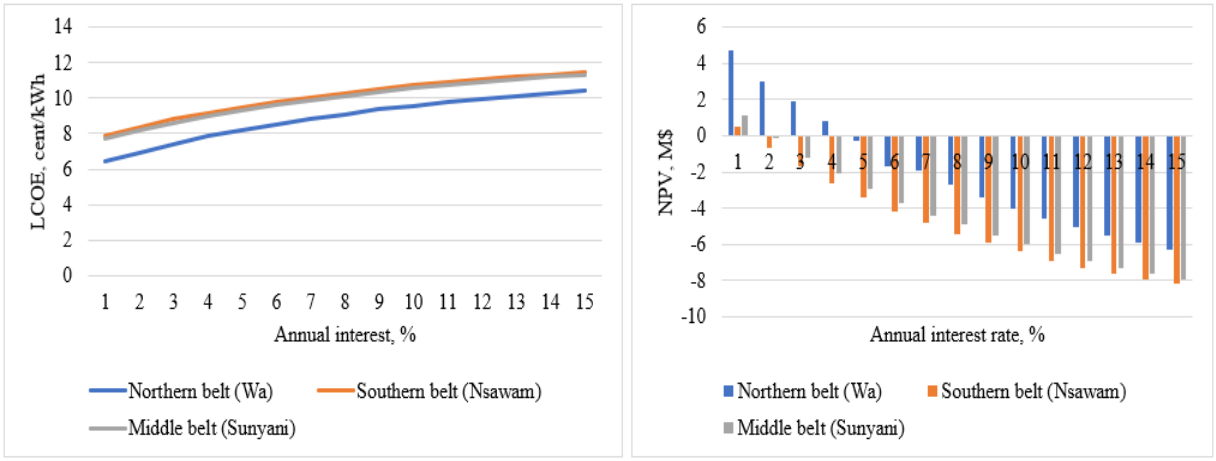


(a) (b)

**Fig. 4.34** Annual interest rate impact on the LCOE (a) and NPV (b) of PV-Battery system

### 4.5.4.7. Comparative analysis and validation of the obtained results

According to [63,145,168], electricity tariff in Ghana ranges between 15 – 19 ¢/kWh for domestic users. Tariffs for the commercial sector is however comparatively higher as a result of the cross subsidy given to the residential sector. Industries on the high voltage (HV) consumption class such as those in the mining sector are charged about 23 ¢/kWh. The non-residential sector (i.e., commercial users less than 100 kVA) pay between 15 – 26 ¢/kWh [1]. Based on these tariffs, the country is ranked among the highest countries in middle-income countries with expensive tariffs in relation to the cost of energy. For

example, the average cost of grid electricity in Ghana is virtually two times more than that of India, China and South Africa [1]. The reliance on thermal power plants which use fossil fuels for the country's energy demands account for the high cost of electricity.

Ghana can cut its electricity consumer tariff by not less than 50% using any of the scenarios presented in this study (i.e., PV- only or PV-Battery) systems be deployed at all three selected sites. The inclusion of a tracking system makes it even much better for all three sites particularly the PV-Battery system even with the current financial arrangements in the country used for the analysis. The FT system for the PV-Battery system will need suitable economic measures in its favor in order to be financially feasible since all three sites recorded negative NPV figures. This means that, the addition of a storage system is the ideal economic feasibility option, since it reduces the period required to obtain a positive NPV considerably.

The results from this study are compared with other published works in other jurisdiction to determine their validity. Cost of electricity for PV systems has in recent times reduced considerably globally [169]. International agencies used the learning curves approach to project the cost of solar power for the period between 2020 and 2030, and those predictions are indicated in Table 4.12. LCOE for PV systems in certain areas in Europe ranges between 0,074- 0,088 $/kWh [62]. Moreover, Lazard's [169], recent annual LCOE study (LCOE 12.0) has shown a decreasing cost in the LCOE of PV power plants. In some instances, the LCOE from these alternate sources of electricity generation have reduced to the point that they are presently at or less than the marginal cost of conventional energy generation. All results from all scenarios in this study are within the projected LCOE values. Even at inflation, interest, and discount, rates as high as 15%, the cost of energy across the whole country for PV power plant development still falls within the estimated LCOEs for the next decade. The high NPV especially for the PV-Battery system with the tracking technology should be reassuring for large-scale PV investments in Ghana.

**Table 4.12** Forecast value of the LCOE for PV power generation in 2020 [168,170]

| Country | Bloomberg New Energy Finance (cent/kWh) | IEA (cent/kWh) | Japan NEDO (yen/kWh) | Europe EPIA (cent euro/kWh) | NERL (cent/kWh) | China Renewable Energy Committee (yuan/kWh) |
|---|---|---|---|---|---|---|
| China | 7,36 | 9 | - | - | - | 0,6-0,8 |
| India | 6,83 | | - | - | - | - |
| Japan | 11,47 | | 14 | - | - | - |
| Germany | 9,36 | - | - | 12 | - | - |
| USA | 7,06 | 10 | - | - | 10 | - |

## 4.6. Feasibility study and economic analysis of stand-alone hybrid energy system for Southern Ghana

### 4.6.1. HOMER software as a hybrid power system simulation tool

The HOMER software is an optimization tool use to simulate several renewable energy technologies. It evaluates the techno-economic potential of a particular renewable energy by accessing whether the electrical and thermal loads can be met by the proposed technology. It also evaluates the economic viability and sensitivity analysis of the project [171]. This optimization software is used widely in several preceding hybrid energy systems in several countries. The input data for HOMER comprises renewable resources (wind speed and solar radiation), electrical load (energy demand), technical details/costs among others. The software conducts hundreds or thousands of hourly simulations to enable optimal probable matching between demand and supply to allow design the best system [172,173].

### 4.6.2. Composition of the Hybrid System

The hybrid power plant (HPP) will consist of five key components, that is, PV panels, Wind turbine, diesel generator, inverters, and battery to store excess energy for use when there is a shortfall of energy from the power plants. The inverter is to convert electrical

power from either AC or DC depending on the direction of the power. The load needs a current in the form of AC whiles the battery needs a DC to charge. The inverter is added to optimize power control and conversion. The diesel generator is to serve as a back-up when there is short-fall from all other components and is also expected to recharge the battery through a bi-directional inverter [174]. Fig. 4.35 depicts the constituents of the hybrid system.

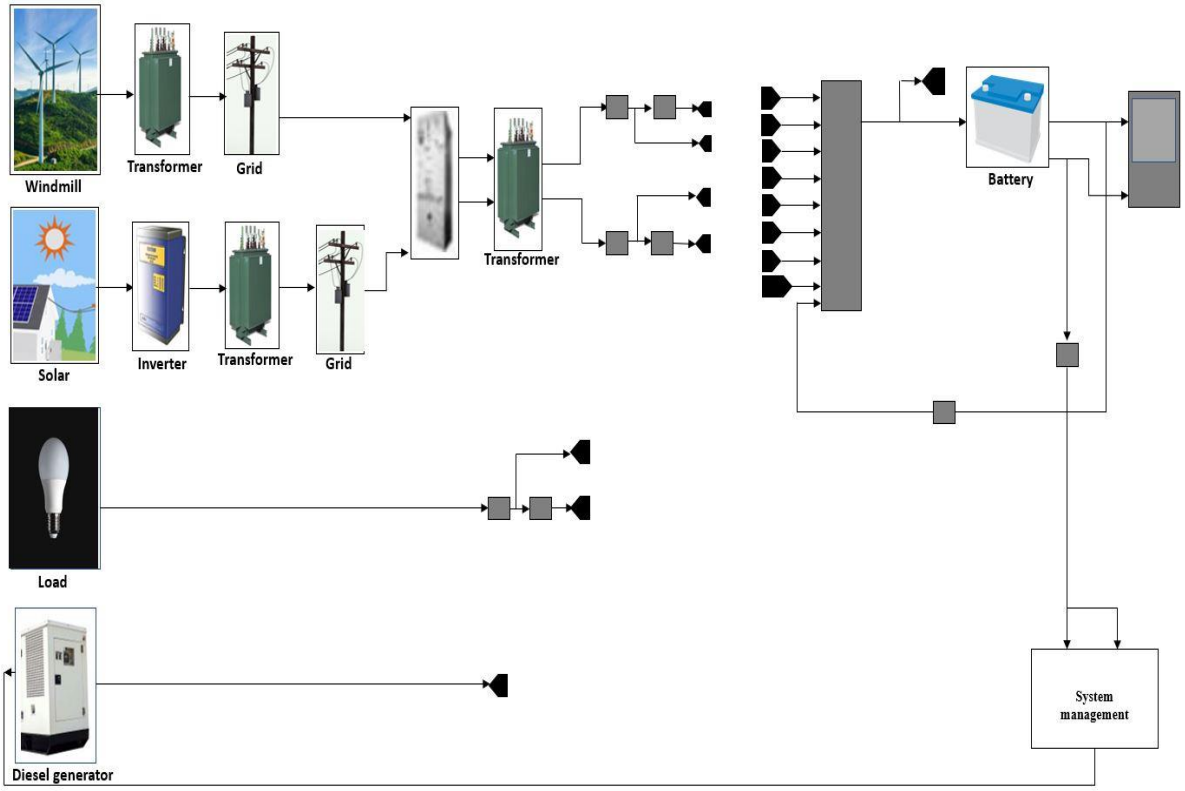


**Fig. 4.35** Block schematic for the hybrid system

The PV module consists of photovoltaic cells which convert the radiations from the sun into electrical power. The output power can be computed using equations and specifications of the module by the manufacturer. The array's output power can be assumed to be linearly proportional to the incident solar radiation on the panel. This assumption can be correct when the arrays are equipped with a Maximum Power Point Tracking (MPPT) [174]. The MPPT is an electronic DC to DC converter which is used to enhance the match between the PV modules, and the battery storage or the utility grid.

In short, they are responsible for the conversion of higher voltage DC output from PV modules or wind generators down to a lower voltage required for charging batteries. The Schneider Conext CL25000 E kW with generic PV was used for the evaluation, and the properties of the selected module is indicated in Table 4.13.

**Table 4.13** Technical parameters for the PV module

| Description | Value | Reference |
|---|---|---|
| Panel type | Flat plate | |
| Abbreviation | Conext CL25000 E | |
| Rated capacity (kW) | 25 | |
| Temperature coefficient | -0,4100 | |
| Operating temperature (°C) | 45 | |
| Efficiency (%) | 17,30 | |
| Capital cost ($/kW) | 2000 | [175] |
| Replacement cost ($/kW) | 2000 | [175] |
| O&M cost ($/year) | 40 | [175] |
| Lifetime (years) | 25 | |

The power curve denotes the amount of power generated by the turbine as a function of the speed of wind at hub height. The output power of wind turbine depends on the speed of wind. The output power of the wind turbine can be calculated using the quadratic model shown in Eq. (2.6) in chapter 2. The WES 30 [250 kW] wind turbine was selected for this study; its properties are indicated in Table 4.14. The power curve of the turbine is presented in Fig. 4.36.

**Table 4.14** Technical parameters of the wind turbine

| Description | Value | Reference |
|---|---|---|
| Manufacturer | Wind Energy Solutions | |
| Rated capacity (kW) | 250 | |
| Rotor diameter (m) | 30 | |
| Hub height (m) | 48 | |
| Capital cost ($/kW) | 1500 | [69] |
| Replacement cost ($/kW) | 1500 | [69] |
| O&M ($/year) | 0,03 | [69] |

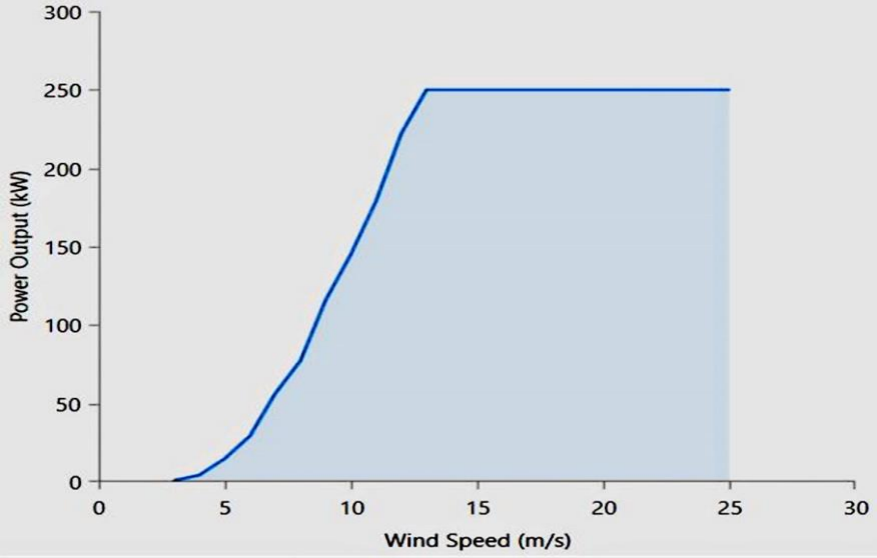


**Fig. 4.36** Power curve for the WES 30 [250kW] wind turbine

The purpose of the battery is to provide electrical power when there is a shortfall from the power plants (Wind turbine, PV, or the generator). The Surrett 4KS25P with capacity 7,546 kWh and 4V was used battery in the study and the properties for the selected battery are indicated in Table 4.15. The following parameters and equations can be used in describing the state of the battery [174]: The state of charge is as presented in Eq. (4.28).

$$SOC(t) = {}^{C_{bat}(t)}/_{C_{bat\,max}}(t) \tag{4.28}$$

Where, ($0 \leq SOC \leq 1$)

Where the capacity of the battery at time (t) is denoted by $C_{bat}(t)$, the maximum capacity of the battery is represented by $C_{bat\,max}$.

Nominal capacity Batman.

The battery's charging and discharging processes can be calculated using Eq. (4.29) and (4.30), respectively [174].

$$C_{bat}(t) = C_{bat}(t-1) + \Big((P_{tot}(t) - P_{cha}(t)) + P_{ge}(t)\Big)\eta_{ac/dc}\eta_{cha}\Delta t \tag{4.29}$$

$$C_{bat}(t) = C_{bat}(t-1) + (P_{tot}(t) - P_{cha}(t))\,{}^{\Delta t}/_{\eta_{dc/ac}\,\eta_{decha}} \tag{4.30}$$

Where, $P_{cha}$ represents the power demand, $P_{ge}$ is the produced power by the diesel generator, $\eta_{decha}$ is the efficiency of the discharging battery.

The state of charge is given according to Eq. (4.31) [174].

$$C_{bat\ min}(t) \leq C_{bat}(t) \leq C_{bat\ max}(t) \tag{4.31}$$

$$C_{bat\ min} = DOD \cdot C_{bat\ n} \tag{4.32}$$

Where, $C_{bat\ min}$ is the minimum capacity, $DOD$ is the deep discharge which is usually equal to 0,5.

The battery life is calculated by HOMER using Eq. (4.33) [176].

$$R_{batt} = MIN\left(\frac{N_{batt} \cdot Q_{lifetime}}{Q_{thrpt}} R_{batt,f}\right) \tag{4.33}$$

Where, $R_{batt}$ is the battery life (years), $Q_{lifetime}$ is the lifetime throughput for one battery (kWh), $N_{batt}$ represents the total number of batteries in the battery bank, $Q_{thrpt}$ is the annual battery throughput (kWh/year) and $R_{batt,f}$ is the battery float life (years).

**Table 4.15** Technical parameters of the battery

| Description | Value | Reference |
|---|---|---|
| Nominal voltage (V) | 4 | |
| Nominal capacity (kWh | 7,55 | |
| Maximum capacity (Ah) | 1,89E+03 | |
| Capacity ratio | 0,254 | |
| Rate constant | 0,528 | |
| Round trip efficiency | 80 | |
| Maximum charge current (A) | 459 | |
| Quantity | 12 | |
| Lifetime (years) | 20 | |
| Throughput (kWh) | 10551,70 | |
| Capital cost ($/kWh) | 200 | [176] |

Generators can be classified into two types, i.e., electric and engine generators. The electric generators convert mechanical energy into electrical energy whiles the engine generators are an amalgamation of an engine and electric generator. The engine generator can operate with the use of diesel, gasoline, propane, natural gas, water, sewage gas etc. This study uses the diesel generators. A diesel generator's fuel consumption per hour varies according to the different output power attained from the fuel supplier. The quantity of fuel consumed by the generator is described by the fuel curve [173]. The fuel consumption for the generator can be calculated using Eq. (4.34) [177]. The CAT-180kW-60Hz-PP Genset was used for the analysis. The proprieties of the selected generator are as indicated in Table 4.16. Fig. 4.37 and Fig. 4.38 denote the fuel and efficiency curve of the selected generator, respectively.

$$\boldsymbol{F = F_0 Y_{gen} + F_1 P_{gen}} \tag{4.34}$$

Where, $F$ is the fuel consumption (L), $F_0$ represents the generator's fuel curve intercept coefficient (L/h/kW), $Y_{gen}$ is the generator's rated capacity (kW), $F_1$ the fuel curve slope for the generator (L/h/kW) and $P_{gen}$ the generator's output (kW).

**Table 4.16** Technical parameters for the generator

| Description | Value | Reference |
|---|---|---|
| Fuel | Diesel | |
| Capacity (kW) | 180 | |
| Fuel curve intercept (L/hr) | 8,97 | |
| Fuel curve slope (L/hr/kW) | 0,222 | |
| CO (g/L/fuel) | 1,86 | |
| Unburned HC (g/L fuel) | 0,14 | |
| Particulates (g/L fuel) | 0,16 | |
| Fuel sulfur to PM | 0 | |
| $NO_X$ (g/L fuel) | 26,60 | |
| Initial capital ($/kW) | 1000 | [176] |
| O&M cost ($/h) | 0,010 | [176] |
| Fuel price ($/L) | 0,993 | |

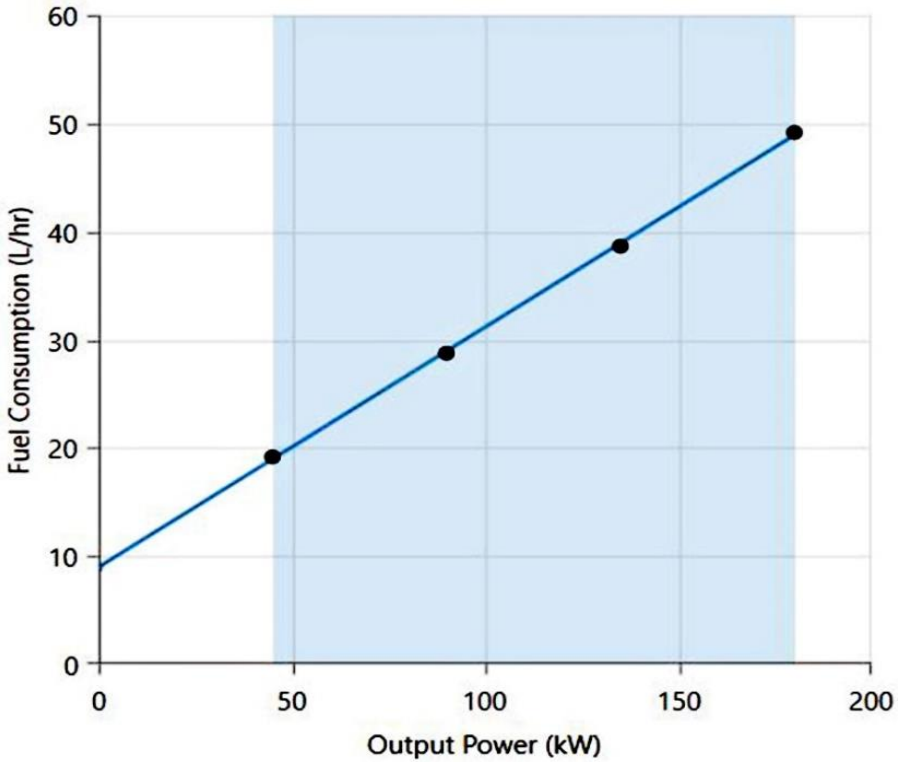


**Fig. 4.37** Fuel curve for the generator

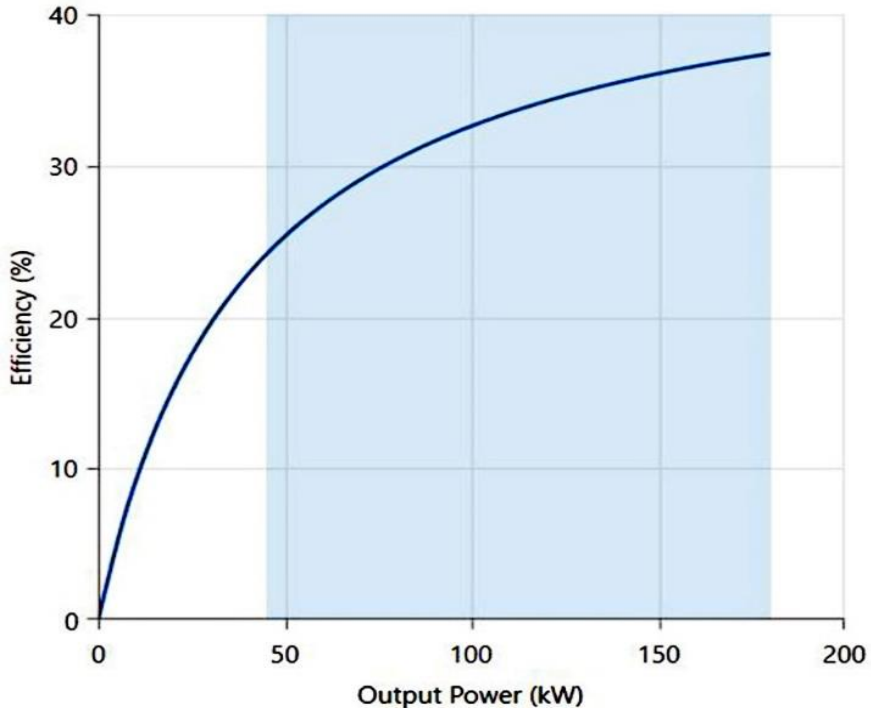


**Fig. 4.38** Efficiency curve for the generator

The Schneider Conext SW4024 converter with capacity of 1 kW was selected for this analysis. A capital cost of $ 1000, replacement cost of $1000 and O&M cost of 20 $/year was used [175]. It has a lifetime of 25 years.

### 4.6.3 Results and Discussion

This section presents the results and discussions for the simulation based on the above input data for a 25-year analysis period. The optimal system is selected by the HOMER program among the other sizes. Two different hybrid systems consisting of PV-Wind-Generator-Battery and Wind-Generator-Battery systems are compared in this segment. The hybrid system is optimized in order to meet demand for electrical energy for a particular locality. A sensitivity analysis was also conducted on certain financial parameters to ascertain their effect on the economic viability of the project. The optimization is grouped into three main parts that is: cost, architecture and some system variables based on the technical and financial parameters provided in the above section.

The daily commercial load for the area is estimated by the software to be around 2422,06 kWh/day with an average load and peak load of 100,92 kW and 407,71 kW, respectively. Fig. 4.39 shows the daily profile for the community, demand for power peaks in during the periods of 8 hours and 16 hours when commercial activities are high.

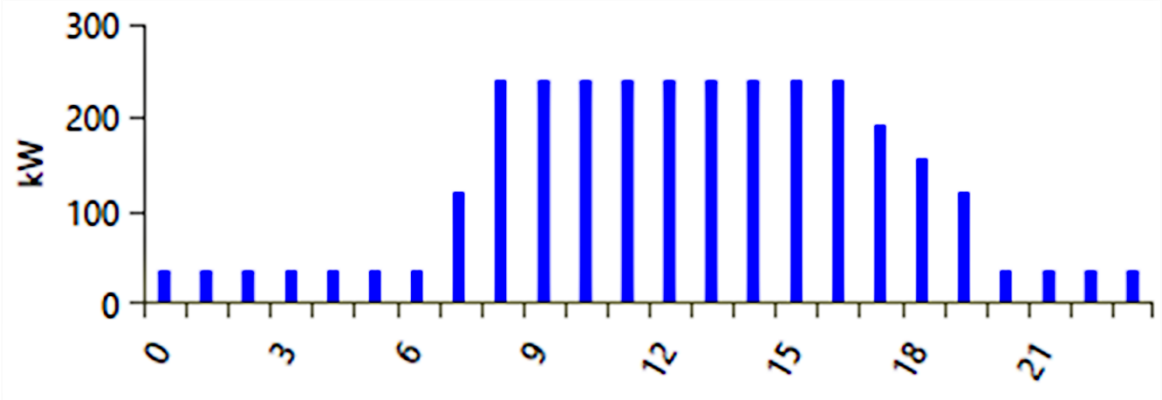


**Fig. 4.39** Commercial daily load profile for Mankwadze

### 4.6.4. Economic and Technical Analysis

#### 4.6.4.1. PV/Wind/DG/ Battery system

The obtained results for the LCOE, NPC and operating cost (OC) for the PV-Wind-Generator-Battery system are 0,382 $/kWh, $8 649054 and $303 345,90, respectively. According to the cost summary for the entire system as indicated in Table 4.17, the CAT -180 kW generator accounted for 72,05% of the entire cost of the system, taking a chunk of the cost, whiles the battery accounted for 15,98% of the capital cost. The PV array system accounted for only 0.84% of the initial cost whiles the wind energy converter (WEC) accounted for 5,43% of the initial cost. The converter represented 5,67% of the capital cost of the system. It is clear from the composition of the cost summary that, the renewable energy conversion system (RECS) constitutes just 6,27 % of the entire cost of the hybrid system whiles the generator, converter and battery system represents about 93,7% of the entire capital as shown in Fig. 4.40. The storage and converter systems have a relatively less impact on the cost of the system. The generator operated most in the afternoons when most commercial activities take place, and in the months of January to March, also in the last three months of the year when wind energy is relatively low as indicated in Fig. 4.41, when wind speed is at its lowest due to the harmattan season.

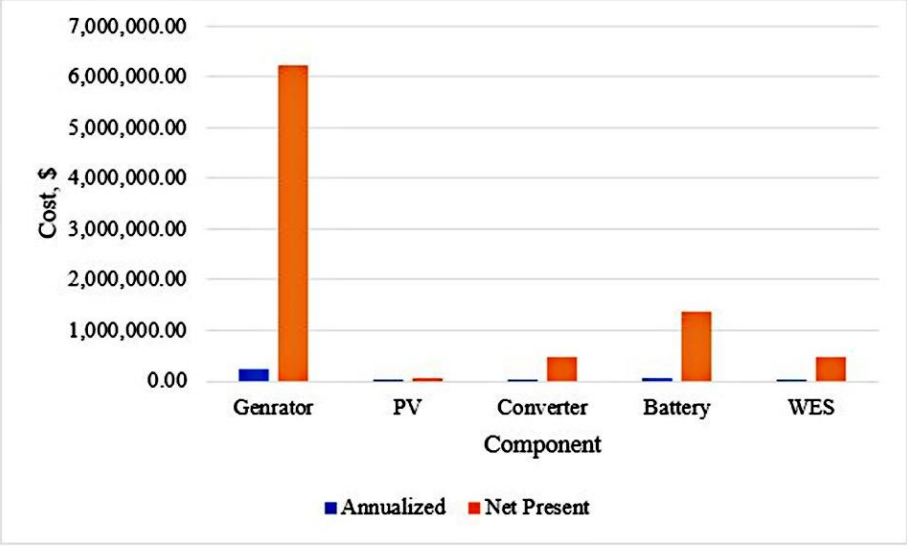


**Fig. 4.40** Cost summary of the components

**Table 4.17** Net present cost summary for the components

| Component | Capital, $ | Replacement, $ | O&M, $ | Fuel, $ | Salvage, $ | Total, $ |
|---|---|---|---|---|---|---|
| CAT–180 kW | 180 000 | 184 285,38 | 1208,32 | 5872498,89 | 6441,14 | 6231551,45 |
| PV | 50000 | 0,00 | 25611 | 0,000 | 0,00 | 75610,86 |
| Converter | 223763,0 | 230059,35 | 114615 | 0,000 | 78118,46 | 490318,40 |
| Battery | 51340,0 | 53193 | 1314862 | 0,000 | 37394,18 | 1382000,50 |
| WES | 375000,0 | 389136 | 0,768 | 0,000 | 294564,34 | 469572,40 |
| System | 880103,0 | 856674 | 1456296 | 5872498,89 | 416518,11 | 8649053,62 |

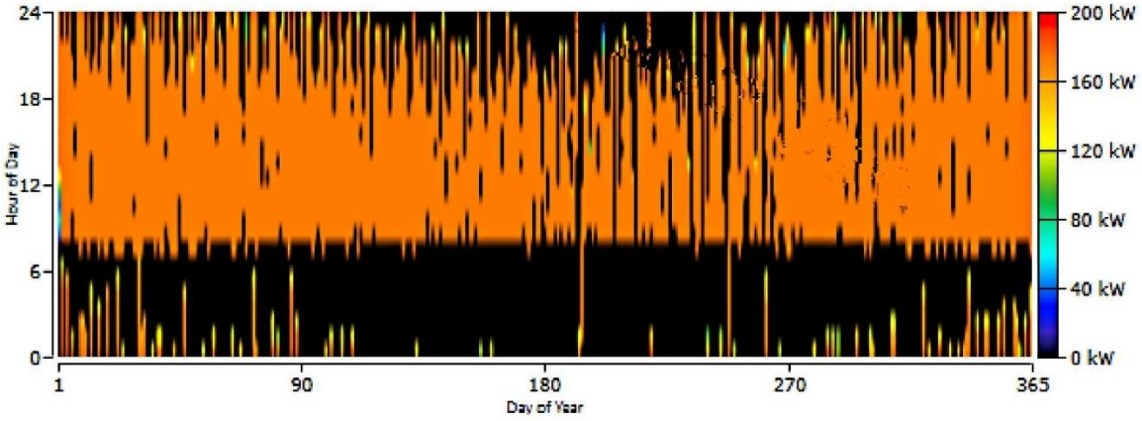


**Fig. 4.41** Generators output for PV/Wind/DG/Battery system

Electricity production from the PV/Wind/DG/Battery power plant has been mainly from the diesel generator (DG), the DG generated 842712 kWh of electricity annually representing 85,9%. The wind power plant also produced 103154 kWh of electricity per year representing 10,5% of the total electricity produced by the hybrid power plant. The solar power plant however generated the least electricity, it produced 35293 kWh of electricity per year, which represents 3,60% of the entire produced electricity. Fig. 4.42 shows the monthly electricity production from the various power plants.


**Fig. 4.42** Electricity production for the PV/Wind/DG/Battery system

The payback period is the number of years it takes to recoup the investment made for the project. In order to obtain the payback period for the hybrid system, there is the need to get a reference system usually a conventional base case system. For the purposes of this study, a generator was selected as a base case, for the PV-Wind-Generator-Battery hybrid system because the Ghana currently relies on mainly thermal power plants as source of electricity. Data from the simulation indicates that the hybrid system has a 9,62-year simple payback period and a discounted payback period of 9,53 years. The simple payback period obtained are very positive for investors, this is a short period to recover the investment.

A key metric in capital budgeting is the internal rate of return (IRR) which is used to assess the cost-effectiveness of a potential investment. It is the discount rate at which both the base case and the current systems have the same NPC. From the modelling, the IRR for the PV-Wind-Generator-Battery hybrid system is 8,9%. The present worth which is the difference between the NPCs of the current and base case system for this hybrid system is $666513 with an annual worth of 26025 $/year. The positive present worth obtained for the project indicates that the hybrid system saves money during operation compared to the base case (generator) system.  Fig. 4.43 and Fig. 4.44 are the seasonal and yearly profile for the system, respectively.

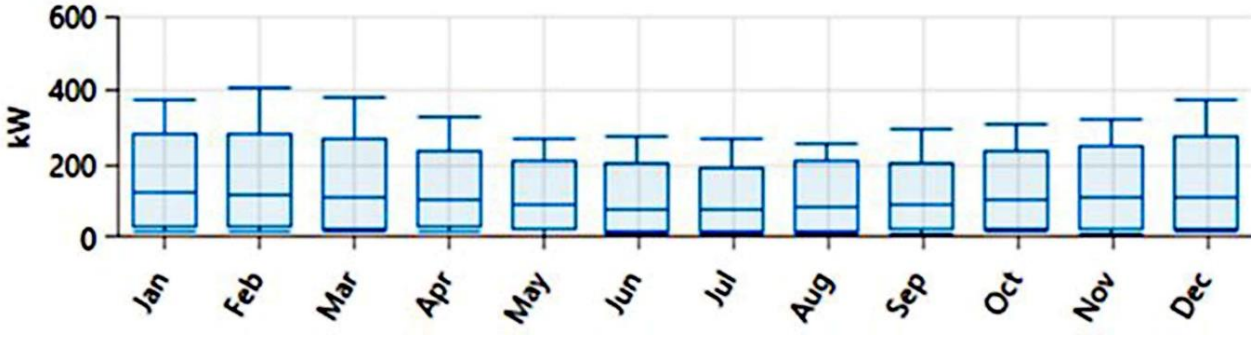


**Fig. 4.43** Seasonal profile

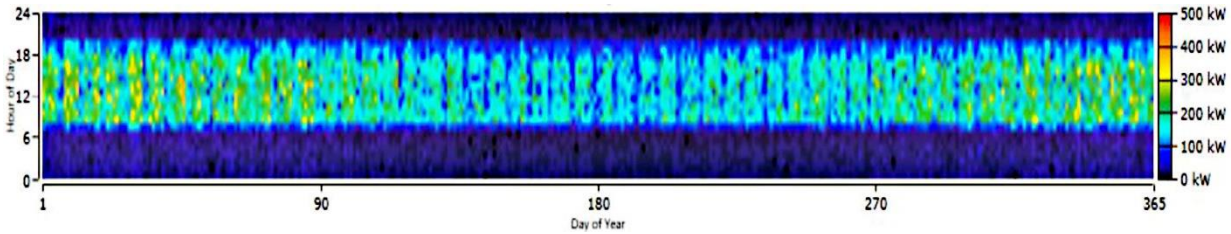


**Fig. 4.44** Yearly profile

The battery discharges most during afternoons obviously because of the huge load during that period and also because wind energy which is the second highest of electricity production is low during that period, it however, it gets between 76% and 88% charged in the evenings when wind speed is high as can be found in Fig. 4.45. The months of June and October records the least battery charge as shown in Fig. 4.46 which can be associated to two main reasons: either there is not enough power to charge them or there is a lot of discharge during the period as a result of low power generation from the power plants due to unfavorable weather conditions during that period. The intensity of solar radiation falls in the month of June, therefore energy generation from the PV power plant will also fall. Wind speed also falls in October, this means power from the wind power plant will also decrease. The services of the batteries will therefore be required to compensate the short fall.

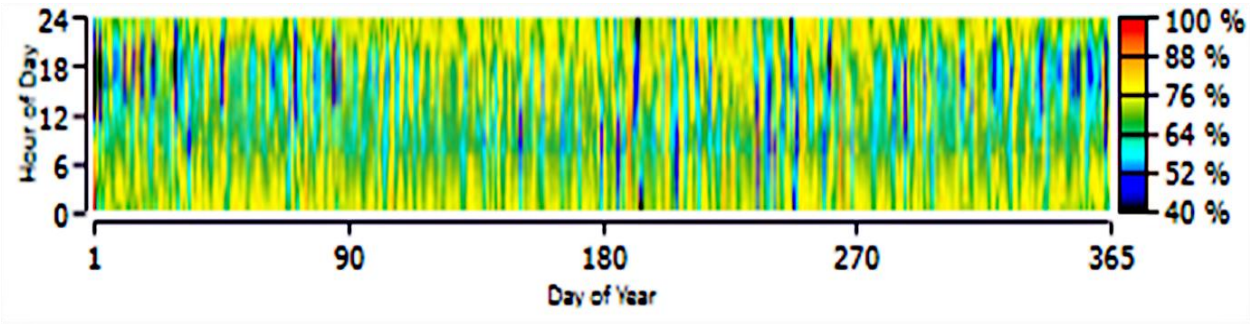


**Fig. 4.45** Yearly state of charge of battery for the PV/Wind/DG/Battery system

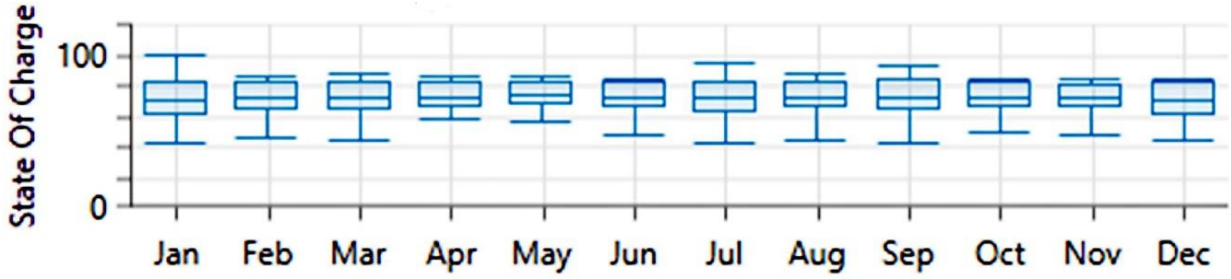


**Fig. 4.46** Monthly state of charge of battery for the PV/Wind/DG/Battery system

#### 4.6.4.2. Wind/DG/Battery system

The Wind/DG/Battery hybrid system had an LCOE, NPC and OC of 0,3962 $/kWh, $8966700 and $318690,90, respectively. The Wind/DG/Battery system had a payback simple and discounted payback of 10,31 and 10,29 years, respectively. It also recorded a present worth of $348867 and an annual worth of 13622 $/year. An ROI of 3,8% was obtained with an IRR of 6,0%. The generator alone took 72,5% of the entire annualized cost of the system obviously because of the high operation cost as a result of fuel. The rest was shared among the remaining components as follows: 4,7% for the converters, 17,6% for the batteries and 5,2% for the wind power plant.

Electricity production was mainly from the diesel generator, it contributed 880032 kWh/year representing 89,5% of the total electricity produced whiles the wind power plant generated 103154 kWh which is 10,5% of the generated electricity. Electricity production from the wind power plant was high in the months of July, August, and September when wind speed is highest as indicated in Fig 4.47.

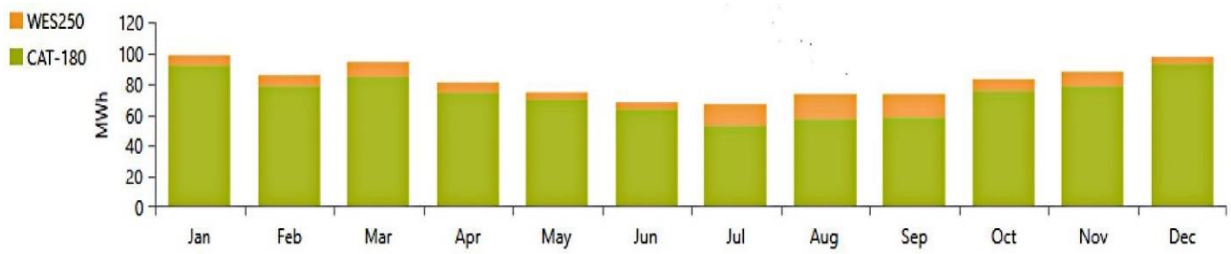


**Fig. 4.47** Electricity production Wind/DG/Battery system

### 4.6.5. Sensitivity Analysis

A sensitivity analysis enables us to track the effect of certain parameters on the bankability of the project. We varied parameters such as cost of fuel, inflation, and discount rates to ascertain their effect on the optimized system.

The discount rate can be described as the opportunity cost of capital taken as a percentage of the capital value. The opportunity cost of capital is also defined as the return on investments inevitable elsewhere by committing capital into the investment under consideration. During investment, the opportunity cost of a capital is the cut-off rate, below which the investment is not cost-effective [165]. The sensitivity analysis as indicated in Fig. 4.48 suggests that the discount rate varies directly proportional to the LCOEs of both hybrid systems. Increasing the discount rate increases the LCOE, which means, the effect of the discount rate cannot be underestimated if the cost-effectiveness and the affordability of the project are to be considered. The effect of inflation on the NPC is also significant, increasing inflationary rate decreases the NPC, this presupposes that the inflation rate is a key parameter in the viability of the project.

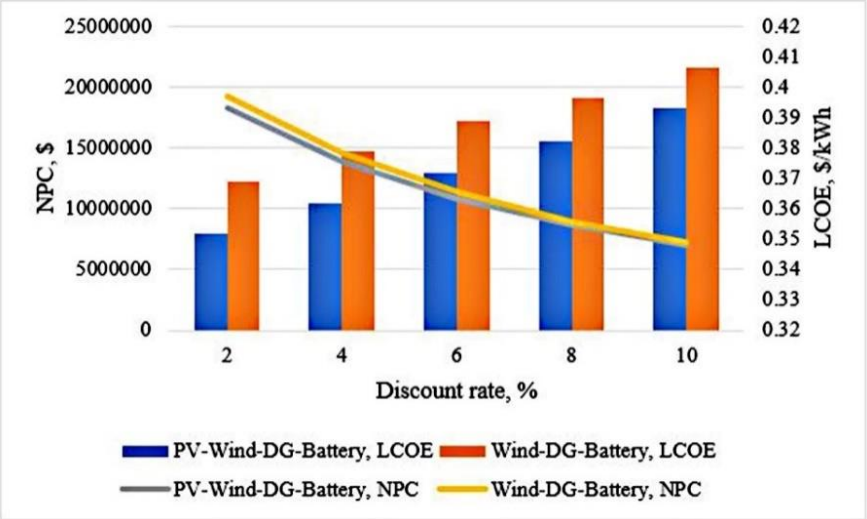


**Fig. 4.48** Sensitivity of discount rate on LCOE and NPC

Inflation is said to be the surge in prices for goods and services over time. It indicates a loss in the value of money over time. Different inflation rates between 2% and 10% were used to evaluate their effect on the NPC and the LCOE of both projects. From Fig. 4.49, the inflation rates have some substantial effect on the LCOE, as increasing inflation rate decreases the cost of energy for both technologies.

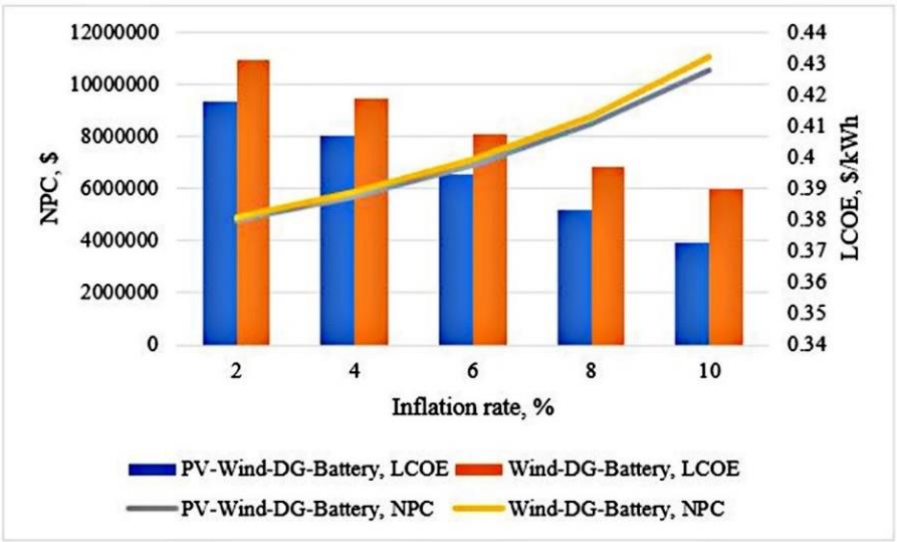


**Fig. 4.49** Sensitivity of inflation rate on the LCOE and NPC

Ghana's fuel market has seen a lot of volatilities over the years. Prices of oil in the country are subject to several factors such as exchange rate, international oil prices and

inflation. For this reason, there is the need to forecast the possible effect of such fluctuations on the economic viability of a project which will rely on fuel for its operation. Cost of diesel in Ghana as at the time of conducting this research ranges between 5,31 GHS and 5,44 GHS [178]. This study used an average price of 5,37 GHS which is equivalent to 0,9925 $ per liter at the current exchange rate of $1 =5,4214 GHS for the analysis. For convenience, we ran the cost to the nearest amount to obtain 1$/liter. An analysis of the cost of fuel for the diesel generator (DG), indicates that cost of fuel has an increasing effect on both the NPC and LCOE of both systems. This is because the generator operated virtually all year round, the percentage of electricity generation from the renewables were relatively low. The LCOE for both technologies could decrease to an average of 0,25 $/kWh if the cost of fuel is decreased to 0,5 $/liters as indicated in Fig. 4.50. It could even decrease further to become more competitive if cost of fuel could be decreased further. This invites the government of Ghana to create the enabling environment to drive down the cost of fuel if these technologies are to be deployed.

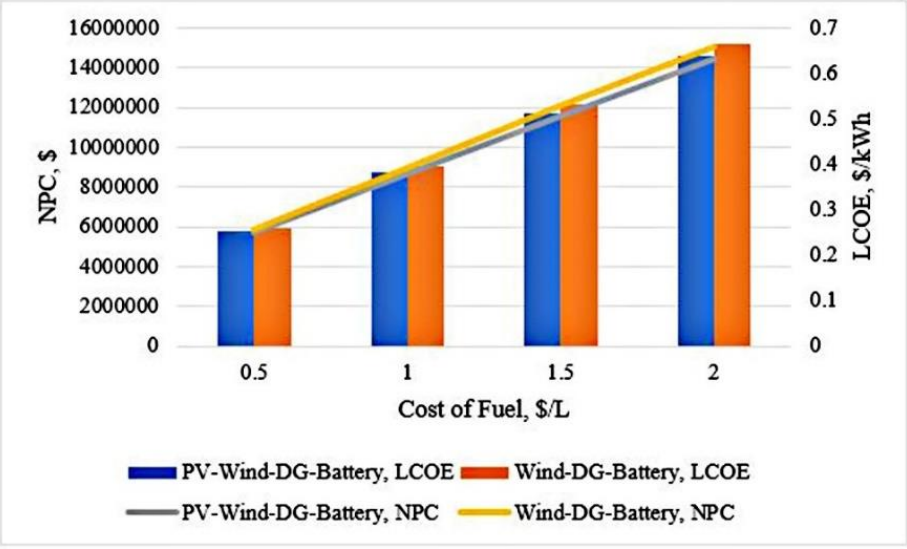


**Fig. 4.50** Sensitivity of fuel price on LCOE and NPC

The speed of wind also has a significant effect on the LCOE as demonstrated in Fig. 4.51, an increase in wind speed to 8 m/s with a fuel price of 0,60 $/L for instance can reduce the cost of energy to 0,164 $/kWh which can be compared to the current cost of

electricity to household consumers in the country. It even becomes more cheaper when the cost of fuel decreases.

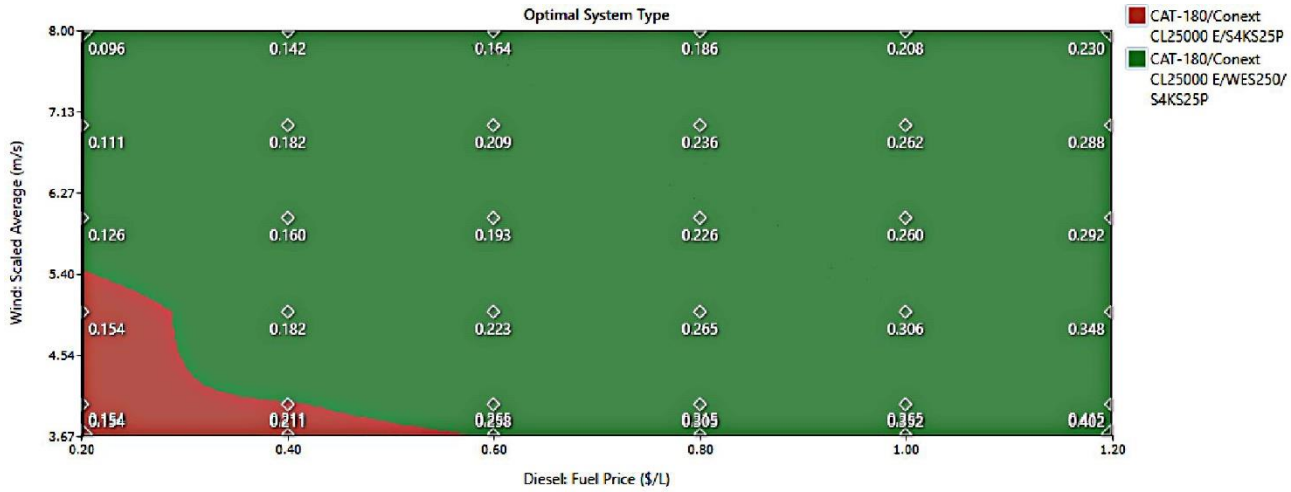


**Fig. 4.51** Sensitivity analysis on wind speed and diesel price

### 4.6.6. Comparative Analysis

Table 4.18 shows the comparative cost summary for the base case and the current system (hybrid) for the two different systems. The base case (generator) recorded an LCOE of 0,412 $/kWh and an OC of $345998 with an initial cost of $454256. Notwithstanding the high initial cost associated with the hybrid system as compared to the base case scenario, its (base case) cost of energy and operating cost are much higher than the two modelled hybrid systems. This could be attributed to the cost of fuel. The optimal system is the PV/Wind/DG/Battery, it recorded a relatively lower LCOE, even though still higher for the end-user in Ghana. End-user tariff for the Ghanaian consumer ranges between 15-19 cents/kWh [1], meaning the obtained LCOE for the PV/Wind/DG/Battery system is 0,23 $/kWh and 0,19 $/kWh for the higher and lower limits of the current tariff regime, respectively. The Wind/DG/Battery system, if implemented will have its LCOE higher than the current cost of electricity in Ghana by 0,25 $/kWh for the lower limit and 0,21 $/kWh for the upper limit.

The mining industries are charged about 0,296 $/kWh (exclusive a maximum demand charge of 1,54 $/kVA/month, 17,5% VAT and monthly service charge of $1,54) for electricity consumed from the national grid [13]. The obtained LCOEs for both modelled

power plants will, however, be lower and better for the mining industries should all the excluded parameters be included.

**Table 4.18** Comparative economic summary for the two-hybrid systems

| Parameter | PV/Wind/DG/Battery system | | Wind/DG/Battery system | |
|---|---|---|---|---|
| | Base case | Current case | Base case | Current case |
| Initial capital, $ | 454256 | 880103 | 454256 | 804750 |
| NPC, $ | 9,32 million | 8,65 million | 9,32 million | 8,97 million |

We compared our study with other studies that has been conducted both in Ghana and elsewhere, even though the economics of such projects are site dependent, comparing them gives an idea on the performance of the modelled systems relative to what exist elsewhere. This gives investors and decision makers the opportunity to compare and draw conclusions with respect to what exists in other jurisdictions.

According to the information presented in Table 4.19, the obtained LCOEs for both PV-Wind-DG-Battery and Wind-DG-Battery falls within the obtained results of other authors. For instance, Adaramola et al. [176], obtained an LCOE of 0,760 $/kWh for PV-DG-Converter hybrid power plant for a remote community in the northern part of Ghana, which is high, because the research was conducted in an area where load is relatively low due to low consumption. Ansong et al. [179], also obtained an LCOE of 0,212 for a hybrid power plant for mining in off-grid locations in Ghana.

The present study had a relatively high LCOE due to the longer periods of operation of the diesel generator. The diesel generator produced over 75% of the generated power in all two scenarios which means the operation cost i.e., cost of fuel will affect the cost of electricity. It therefore suggests that if power generation from the renewables increase, the LCOE will be brought down. Investors may have to look at options such as the use of solar and wind trackers to help maximize the use of those resources for electricity production.

**Table 4.19** Comparison with other literature

| Author(s) | Title of paper | Hybrid Composition | LCOE, $/kWh |
|---|---|---|---|
| Adaramola et al. (2017) [176] | Multipurpose renewable energy resources-based hybrid energy system for remote community in northern Ghana | PV-DG-Battery-Converter | 0,760 |
| Ansong et al. (2017) [179] | Techno-economic analysis of a hybrid system to power a mine in an off-grid area in Ghana | PV-DG-Fuel Cell-Converter | 0,212 |
| Azimoh et al. (2016) [69] | Electricity for development: mini-grid solution for rural electrification in South Africa | PV-Wind-Diesel-Battery | 0,400 |
| Shezan et al. (2017) [180] | Techno-economic analysis of a smart-grid hybrid renewable energy system for Brisbane of Australia | PV-wind-diesel-battery | 0,209 |
| Salisu et al. (2019) [181] | Assessment of technical and economic feasibility for a hybrid PV-wind-diesel-battery energy system in a remote community of north central Nigeria | PV-wind-diesel-battery | 0,110 |
| Current work | Feasibility study and economic analysis of stand-alone hybrid Photovoltaic-Wind-Diesel-Battery energy system for Southern Ghana | PV-Wind-DG-Battery | 0,382 |
| Current work | Feasibility study and economic analysis of stand-alone hybrid Photovoltaic-Wind-Diesel-Battery energy system for Southern Ghana | Wind-DG-Battery | 0,396 |

### 4.6.7. Effect of Ghana's RE agenda and it's possible impact on the economy

The world's attention towards sustainable development has resulted in the development and promotion of renewable energy in recent years. Bhattacharya et al. [182] used heterogeneous panel estimation technique to assess the effect of renewable energy on 38 renewable energy consuming countries and established renewable energy sources as a significant driver in economic growth. According to information from the World Bank, Ghana lost about 1,8% of its GDP in the 2007 electricity crisis. Research also shows that, the country lost about US$2,1 million each day, equivalent to US$670.8 million in a year in the 2014 national electric power crisis representing 2% of GDP [183].

Energy policy goals can be categorized into three main points, that is: access, economic growth, and protection of the environment [184]. Access to energy simply implies the provision of reliable, affordable, and sustainable energy to majority of the people. Economic growth also looks at the role energy plays in economic development whiles environmental protection looks at measures that mitigate the release of harmful substances into the environment during the process of generating energy. It is the view of experts that all these three issues cannot be met simultaneously, as a result, there must be a trade-off which is dependent on the short and long-term goals of the country involved. That is, developing countries such as Ghana could give credence to accessibility and consumption to promote economic development whiles issues relating to environmental protection are considered in the long-term. In the same way, developed economies are to fashion out measures that cuts down the emission of greenhouse gases since they have already achieved economic stability [45]. As indicated earlier, there is a direct nexus between access to energy and economic development of a country, hence the need to conscientiously create the enabling environment to help develop the sector. The effect of renewable energy in the exception of hydropower in Ghana's economy has been infinitesimal, solar energy according to the Energy Commission's 2018 report constitute only 0,5% of the country's total installed electricity generating capacity [1]. The country's current major source of electricity is from thermal power plants which depend on fossil

fuels, this has often plunged the country into energy crisis as a result of huge debt in the sector due to the high cost of running such facilities.

According to the modelled results in the previous sections of this paper, Ghana has the potential to develop its renewable energy sector if the right investment climate is created. Creating a conducive climate for investment in the sector, removing of both political and financial barriers are critical steps towards the promotion and development of renewable energy. Development of renewable energy have not seen the needed investment in Ghana despite the huge potential due to hinderances such as corruption, inappropriate policies as well as lack of knowledge about the cost-effectiveness of the various RETs. By corruption, we mean, corruption scares away investment, it increases cost of projects and in power generation projects, it affects the cost of energy generation. Corruption has been a canker in most developing countries and Ghana is no exception [185]. In the case of inappropriate policies, even though the government of Ghana passed the renewable energy Act (Act 832) in 2011 [186], there has not been enough conscious effect to promote the use of renewables, the government of Ghana still implement some level of fossil fuel subsidizes for consumers, this keeps the conventional energy sources afloat over the renewables. Lastly, the lack of knowledge about the huge economic potential and benefits in the renewable energy sector by most Ghanaians is partly to blame for the low patronage in the sector. The inertia to venture into new areas of electricity generation particularly in the direction of renewable energy is as a result of lack of conviction for the renewable energy sector.

### 4.7. Performance, degradation, and energy loss for solar PV module under Ghana's weather conditions

A 345 $W_p$ is modelled at Lawra in the Upper West region of Ghana to assess the performance, energy loss and rate of degradation of the PV module. The performance of the PV module is presented below:

The total energy produced from the power plant is 10845 MWh/year with a performance ratio of 79,74 %. The specific production for the power plant is 1668

Wh/kW$_p$/year. Fig. 4.52 shows the monthly performance ratio (PR) and the normalized productions (per installed kW$_p$). The negative effect of temperature on the output of the PV module is seen in the months with high ambient temperature. This is shown in the monthly PR. The effect of temperature alone led to 12,46% loss in the PV performance as shown in the loss diagram illustrated in Fig. 4.53.

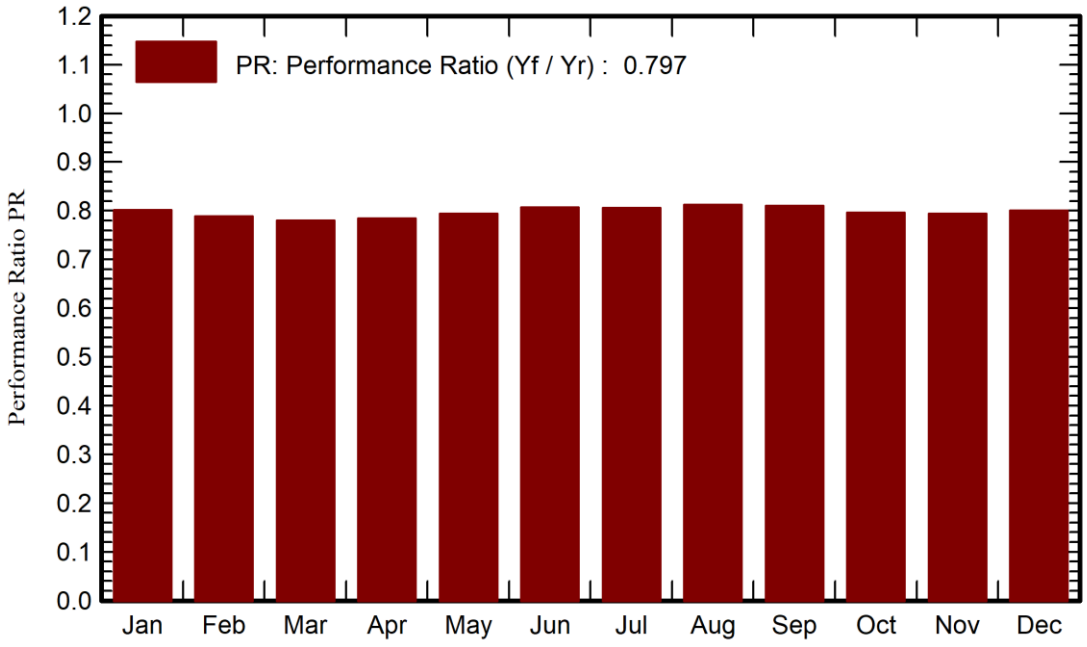


**Fig. 4.52** Monthly performance ratio of the SPP

The probability distribution (PD) for the total annual produced energy by the PV module which can be transferred to grid is shown in Fig. 4.54. The PD variance for power plant's production forecast is dependent on a number of factors, some of these are, meteo data, PV module modeling/parameters, inverter efficiency uncertainty, and soiling and mismatch uncertainties, and degradation uncertainty [187]. The P50 – P90 shows the different levels of yield, for which the probability that a specific year's yield is over 50%, or 90%. The results for the annual production PD shows that the PV module could generate 10845 MWh, 10585 MWh and 10512 MWh for the P50, P90 and P95, respectively. The annual production variability is 203 MWh.

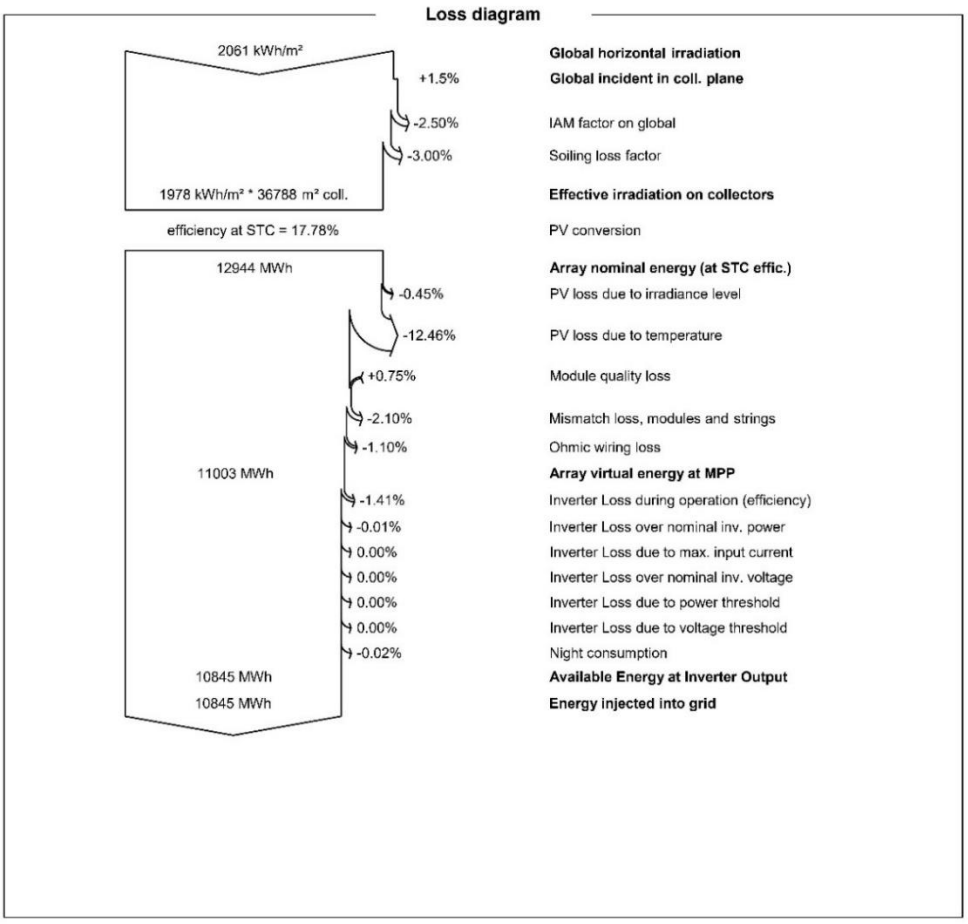


**Fig. 4.53** Loss diagram

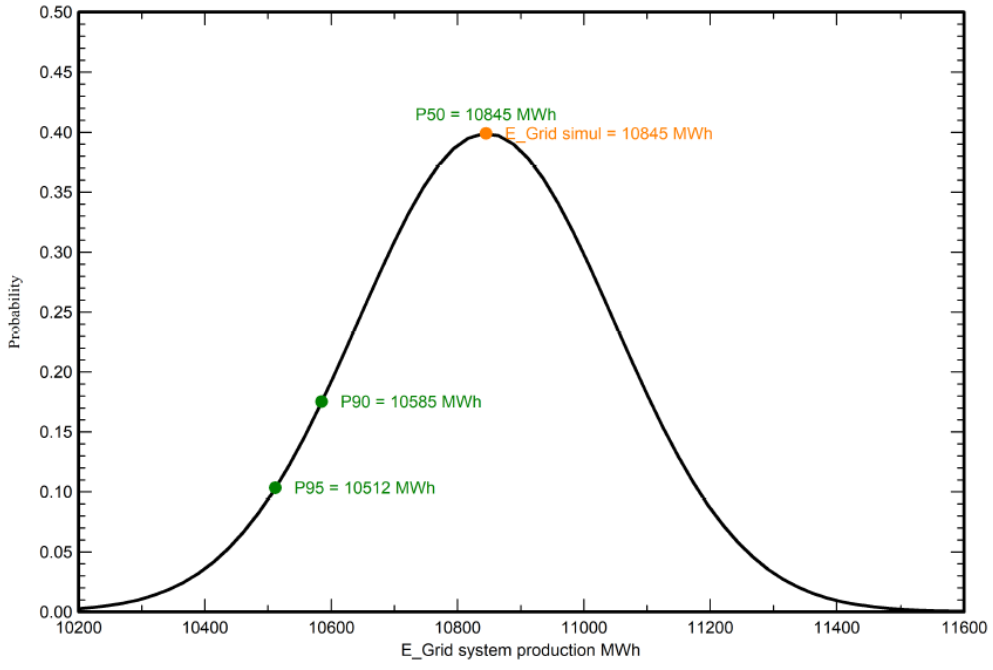


**Fig. 4.54** Probability distribution

### 4.8. Conclusion for chapter 4

This chapter assessed the techno-economic potential of solar photovoltaic, concentrated solar power plants and hybrid systems in Ghana. The following conclusions are made for this chapter:

1. From the simulated outcomes for the CSP, LCOE of 13,67 ¢/kWh and 14,73 ¢/kWh were recorded for the STPP modelled at Navrongo and Tamale, respectively. The PTC power plants modelled at Tamale and Navrongo sites also recorded LCOEs of 28,83 ¢/kWh and 25,83 ¢/kWh, respectively. Based on the outcome of the study, the STPP technology has been identified as the best option for the Ghanaian weather conditions.
2. Results from the simulation of the PV module also indicate that the PV-only and PV-Battery systems with FT technology would produce an annual energy of 31 GWh at Wa and 28 GWh at Sunyani and Nsawam in the first year. CF ranging from 16% to 18% were obtained for both systems with FT technology for all sites.
3. LCOE of 0,382 $/kWh and NPC of $8649054 were recorded for the PV/WPP/DG/Battery system, whiles the WPP/DG/Battery system had an LCOE of 0,396 $/kWh with NPC of $8 966700.
4. The negative effect of temperature on the output of the PV module is seen in the months with high ambient temperature. This is shown in the monthly PR. The effect of temperature alone led to 12,46% loss in the PV performance.

# CHAPTER 5. EXPERIMENTAL ANALYSIS OF DIFFERENT MECHANISMS TO ENHANCE THE EFFICIENCY OF PV MODULES

## 5.1. The impact of dual surface cooling on the efficiency of a solar PV module: an experimental examination

Power generated from solar PV is one of the most widely used around the world, the PV technology is probably the most common technology in the solar energy industry [188–190]. The continuous improvement of solar technologies in terms of its efficiency and cost has led to its increased use [191,192]. Even though the solar PV technology is widely used across the world, it has some disadvantages, this include a reduction in its efficiency with an increase in its operating temperature [193], and relatively low energy conversion etc. [194]. An increase in the PV cell's temperature principally affect its operating parameters which in the end decrease its output efficiency [195,196]. It has been estimated that every 1℃ increase in the ambient temperature decreases the performance efficiency of the PV by 0,4 – 0,5% [194]. The lifetime of a PV module can also be increased, this is because it slows down its degradation rate. A study by Royo et al. [197], suggest that the lifetime of a PV module which is generally 25-30 years can be increased to about 48 years when cooled. It is for these reasons that scientists are researching into different ways to reduce the PV module's operating temperature.

A number of researchers have adopted different techniques in the cooling of solar PV panels, this include active and passive methods. Hernández et al. [198] used forced air stream to enhance the PV module's output performance. Their study indicates that the temperature of the PV module can be reduced by 15 °C which led to a 15% increase in its energy yield. Chavan and Devaprakasam [199] employed phase change material (PCM) to improve a solar PV thermal system's performance. The outcome of their study suggest that the PVT-PCM had an 8,10% reduction in its temperature compared to the referenced panel. Nada et al. [200] by experimentation examined the impact of a mixture of PCM and nano materials on a PV panel's thermal characteristics. The study showed that the combination of PCM and nano-particles could enhance the PV module's

efficiency by 13,2%. Furthermore, a study by [201] indicates that flowing a water film on the surface of a PV module can reduce its temperature considerably which can lead to a 10% enhancement in its efficiency.

According to the reviewed literature above, it is clear that several researchers have used different approaches to cool a PV module. This section of the work also seeks to enhance the current literature by proposing other cooling method. The study employed water and cotton wick mesh to cool the panel's rear surface using capillary action techniques, in this case the water is absorbed by the cotton wick from the perforated pipe and spread it down the back surface of the panel. One issue that this study minimizes is the loss of water through evaporation through the covering of the back surface of the panel with aluminum sheet which is also strategically perforated to allow the flow of air into the inner section of the enclosed area. This method of cooling does not completely avert water loss but rather minimize its loss especially at the back section of the panel. This is very important because water is not abundant in every part of this world and so appropriate mechanisms have to be instituted to minimize the loss of water for reuse by the system. This cooling process is also simple to construct and less bulky. This cooling method is also different in the sense that, it needs only a single polyvinyl chloride (PVC) pipe to spread the water at the back and front surface of the panel simultaneously, this cuts down cost.

### 5.1.1. The impact of temperature on PV cell's efficiency

As indicated earlier, the output performance of PV cell decreases with increasing temperature, mainly because of increase in the rate of internal carrier recombination, which is triggered by increased carrier concentrations. The temperature of the PV cell has a vital role in the conversion process of the photovoltaic. The electrical efficiency and the power output of the PV panel relate linearly with its operating temperature (OT) [202]. A temperature above the 25 ℃ OT of a panel results in a reduction in the band gap of the semi-conductor material in the solar cell leading to a reduction in the open circuit voltage [203]. The correlations which shows the temperature $T_c$ of a PV cell as a function of weather variables such as solar radiation $(I(t))$, local wind speed $V_w$, and ambient

temperature $T_a$ are presented below. Eq. (5.1) shows the effect of temperature on the PV cell's electrical efficiency [193,202].

$$P_m = I_m V_m = (FF) I_{sc} V_{oc} \tag{5.1}$$

Where the $FF$ denotes the fill factor, the open circuit voltage is denoted by $V_{oc}$, $I_{sc}$ signifies the short circuit current, and the maximum power point in the module's I–V curve is denoted by the subscript $m$.

The open circuit voltage and the fill factor decrease considerably with rise in temperature (this is due to the domination of thermally excited electrons over the electrical properties of the semi-conductor), the short circuit current increase but very slightly [193,204]. This results in a linear relation as shown in Eq. (5.2).

$$\eta_c = \eta_{T_{ref}} \left[1 - \beta_{ref} \left(T_c - T_{ref}\right) + \gamma log_{10} I(t)\right] \tag{5.2}$$

Where the electrical efficiency of the module at the reference temperature $T_{ref}$ is denoted by $\eta_{T_{ref}}$ and at a solar radiation flux of 1000 W/m$^2$. The solar radiation coefficient $\gamma$ and the temperature coefficient $\beta_{ref}$ are primarily dependent on the properties of the material with values around 0,12 and 0,004 K$^{-1}$, respectively, for crystalline silicon modules [205]. Taking that of the solar radiation coefficient as zero yields Eq. (5.3) which is the traditional linear relation for electrical efficiency of a PV system [193].

$$\eta_c = \eta_{T_{ref}} [1 - \beta_{ref} (T_c - T_{ref})] \tag{5.3}$$

The manufacturer usually give the values of $\eta_{T_{ref}}$ and $\beta_{ref}$. However, they can be found from flash tests, for that, at a given solar radiation flux, the electrical output of the PV panel is measured at two different temperatures. The temperature coefficient's actual

value does not only depend on the material of the PV material but also on the $T_{ref}$ [191]. It is given by the ratio as indicated in Eq. (5.4).

$$\beta_{ref} = \frac{1}{T_0 - T_{ref}} \tag{5.4}$$

Where the high temperature at which the electrical efficiency of the module drops to zero is denoted by $T_0$ [206]. This temperature is 270 ℃ for crystalline silicon solar cells. The PV cell temperature that cannot be easily obtained can be substituted with the $T_{NOCT}$, which is the nominal operating cell temperature. The expression for it is indicated in Eq. (5.5) [193].

$$\eta = \eta_{ref}\left\{1 - \beta_{ref}\left[T_a - T_{ref} + (T_{NOCT} - T_a)\frac{G_T}{G_{NOCT}}\right]\right\} \tag{5.5}$$

The effect of wind on the temperature of the cell $T_c$ is suggested by Skoplaki et al. [207] as indicated in Eq. (6).

$$T_c = T_a + \frac{I}{I_{NOCT}} \cdot \left(T_{NOCT} - T_{a,NOCT}\right) \cdot \frac{h_{w,NOCT}}{h_{w(v)}} \cdot \left[1 - \frac{\eta_{STC}}{\tau \cdot \alpha}(1 - \beta_{STC}T_{STC})\right] \tag{5.6}$$

Where temperature coefficient and efficiency of the maximal power under standard test conditions (STC) are denoted by $\eta_{STC}$ and $\beta_{STC}$, respectively. The absorption coefficient for the cells is denoted by $\alpha$, I signify the in-plane irradiance, the transmittance of the cover system is also denoted by $\tau$ and the wind convection coefficient (WCC) is denoted by $h_w = 5{,}7 + 2{,}8V_w$ which is normally a linear function of the wind speed v. $h_{w,NOCT}$ represent the WCC for wind speed under NOCT conditions, i.e., $V_w = 1\ m/s$.

The effect of temperature on the current, voltage and power of a generic 30 W PV module are presented in Fig. 5.1 to Fig. 5.3, these are figures obtained using the PVsyst software.

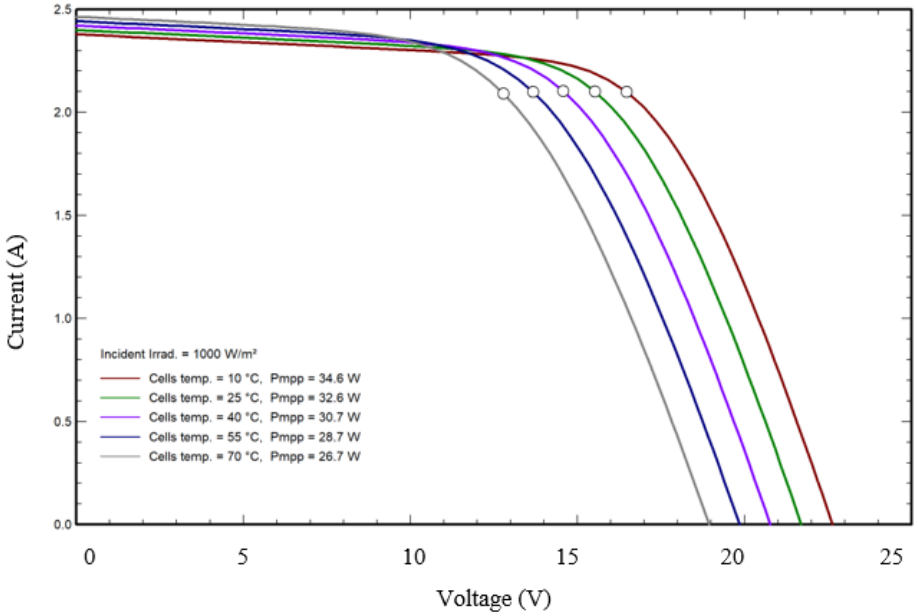


**Fig. 5.1** Effect of temperature on I-V characteristics of PV

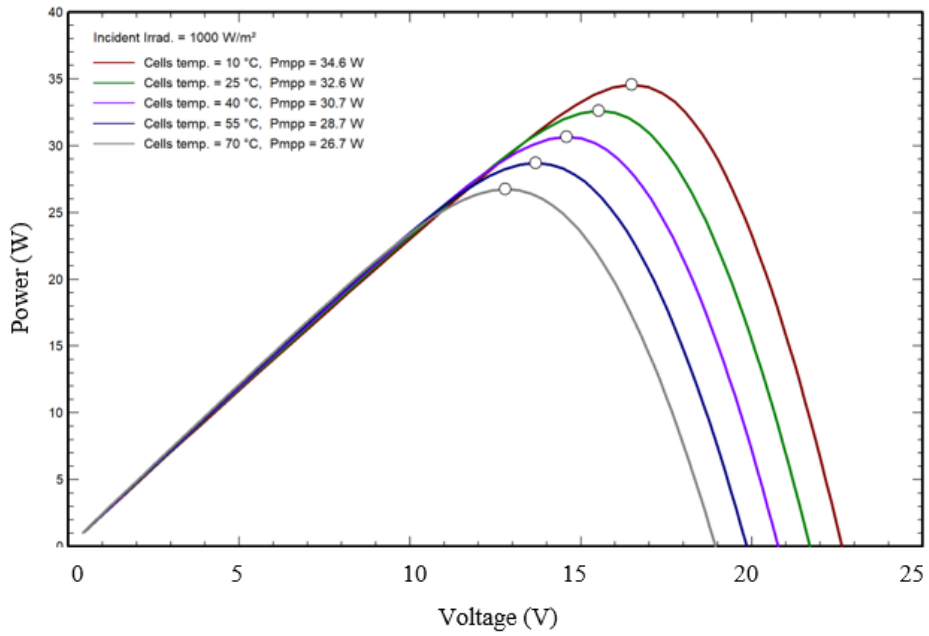


**Fig. 5.2** Effect of temperature on the P-V characteristics of the PV

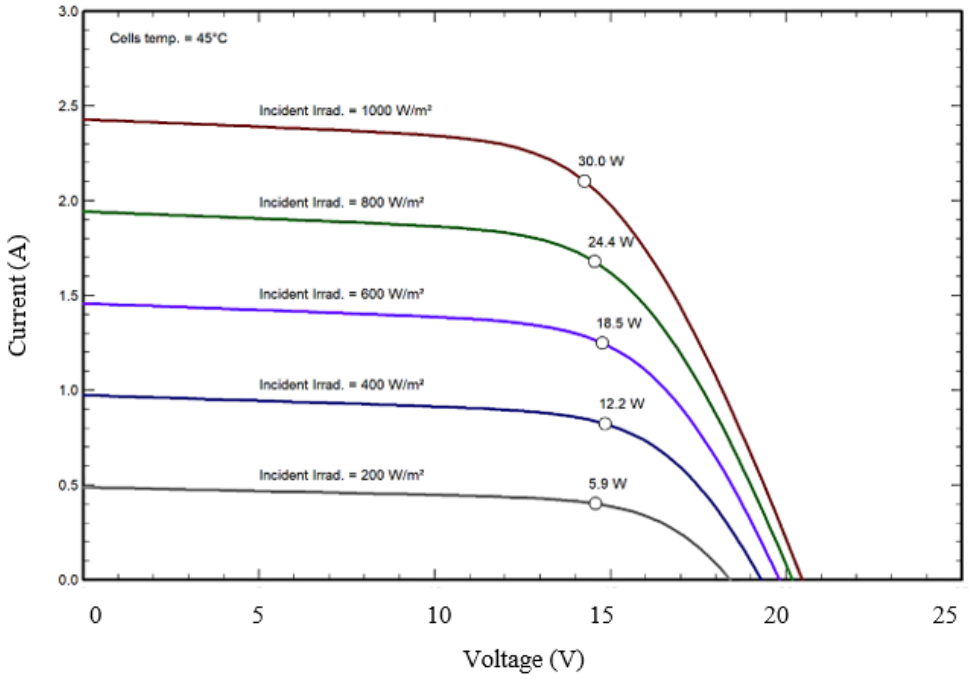


**Fig. 5.3** Effect of temperature on the I-V characteristics of the PV

### 5.1.2. Materials and Methods

This section contains a description of the materials used in the investigation as well as the experimental apparatus. The experiment's arrangement was created with the goal of minimizing water loss. The experiment took place at the Ural Federal University in Yekaterinburg, Russia, during the summer of 2021.

### 5.1.3. Experimental setup and components

The experimental setup consists of a cooled panel that is cooled with water via capillary action by a cotton wick mesh fixed to the back side of the panel. A 16 mm PVC pipe tube was connected to a water source in a tank higher than the PV panel. This allows for the free flow of water using gravity without the need for additional energy to pump the water to the module; however, a pump is required to pump the water back into the storage tank. The PVC pipe was perforated with a 1 mm driller tooth several times along its length to allow water to flow simultaneously into the cotton mesh and onto the front surface of the panel. A section of the cotton mesh that extends down the PV panel’s back surface is

wrapped around the pipe at the top of the PV panel to absorb water from the perforated pipe.

A total of 14 K-type thermocouples with temperature range -200 ℃ – 1370 ℃ and a resolution of 0,1 ℃ were used to measure the temperatures of the two PV panels with the help of SD logger 88598. The two panels had 7 K-type thermocouples each strategically installed at their rear side, this is to enable us to measure the average temperature of each module. They were attached to the rear side of each of the panels as shown in Fig. 5.4a before the cotton mesh was laid over them as shown in Fig. 5.4b. The cotton mesh and the thermocouples were tightly held to the back surface of the PV module using universal sealant moment silicone gel (white). To be able solve one major issue that is linked to the evaporative cooling technique as stated in [208], an aluminum metal sheet was attached to the rear side of the PV module. This metal sheet with ridges was selected in order to enable the creation of holes on the crest section of the sheet. The essence of these holes on the metal sheet is to enhance the flow of air into the enclosed area, this is as shown in Fig. 5.4c. The evaporating water is captured by the galvanized sheet and returns it into the basin that is fixed underneath the PV module, which is then pumped back into the storage tank for reuse. The GM 1362-EN-01 temperature thermometer with temperature range of -30℃ - 70℃ was also used to measure the ambient temperature. The solar irradiation was measured with the Tenmars TM-207 pyranometer, it has a typical accuracy of ±10 W/m$^2$ and an additional temperature induced error of ±0,38 W/m$^2$. The clamp meter used to measure the current and voltage has uncertainty that range from ±1,5 – 2,0%.

The two panels used for the experiment have capacities of 30 W each with dimensions 95 × 45 cm. Testo 875 camera thermal imager is used to capture the infra-red thermal images for both panels at mid-day. These images are to act as additional information for the results obtained in the experiment.

(a)

(b)

(c)

**Fig. 5.4** PV panel with (a) installed K-type thermocouples (b) installed cotton mesh (c) rear side of the cooled panel with aluminum sheet and perforated holes

(a) (b)

**Fig. 5.5** (a) Front view (b) rear view of the experimental setup

### 5.1.4. Experimental procedure

The panels were placed on adjustable stand and were positioned at a tilt angle of 45$^{o}$ towards the southern section of the country in order to receive the maximum total solar radiation as shown in Fig. 5.6. The voltage, temperature and current of the two PV panels were measured at regular interval during the experiment. A digital clamp multimeter was employed for the measurement of the current and voltage for the two panels.


(a)

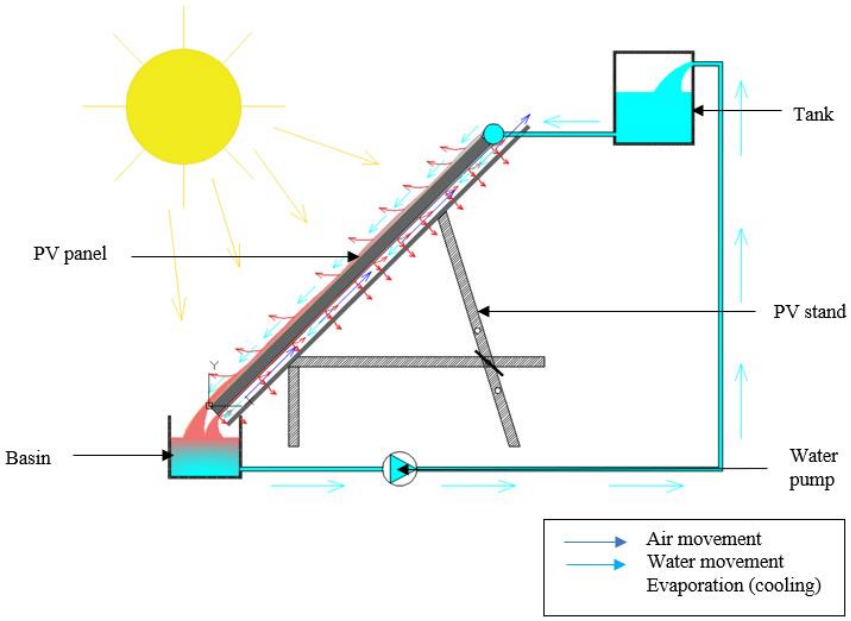


(b)

**Fig. 5.6** (a) Experimental setup (b) Schematic diagram of the experiment

### 5.1.5. Experimental uncertainty assessment

In any experimental works, there is the potential to encounter some level of errors that may arise from the measurand or the measurements [209]. In mathematics if there are $N$ number of observations and $x_i$ denotes any of the observations (where $i$ can have any integer value beginning from 1 to $N$), the mean which in this case is denoted by $\bar{x}$ can be calculated using Eq. (5.7).

$$\bar{x} = \frac{x_1 + x_2 + \cdots + x_N}{N} = \frac{1}{N}\sum_{i=1}^{N} x_i \tag{5.7}$$

In experimental works, it is important to quantitatively assess how much each measurement scatter about the mean. The level of scatter about the mean value helps in identifying the level of precision of the experimental results, and as a result assist in the quantification of the random uncertainty. The standard deviation (SD) is the most recognized quantitative measure of scatter. The SD can be estimated with the help of Eq. (8) for situations with data points that have equal weights [210].

$$SD = \sqrt{\frac{\sum_{i=1}^{N}(x_i - \bar{x})^2}{N-1}} \tag{5.8}$$

The SD provides the estimate for the random uncertainty for any one of the values used in calculating the SD. The SD of the mean value for a number of measurements $\sigma_m$ with equal statistical weights can be calculated using Eq. (5.9), the $\sigma_m$ is the uncertainty [210].

$$\sigma_m = \sqrt{\frac{\sum_{i=1}^{N}(x_i - \bar{x})^2}{N(N-1)}} = \frac{SD}{\sqrt{N}} \tag{5.9}$$

### 5.1.6. Results and Discussion

This section present two analysis, i.e., the thermal characteristics of the PV panels and the electrical output performance for the proposed dual surface cooling of the panel.

#### 5.1.6.1. Thermal characteristics of the panel and weather conditions

The solar radiation and the ambient temperature was recorded from 10:00 am to 4:00 pm within a 30-minute interval and the results are presented in Fig. 5.7.

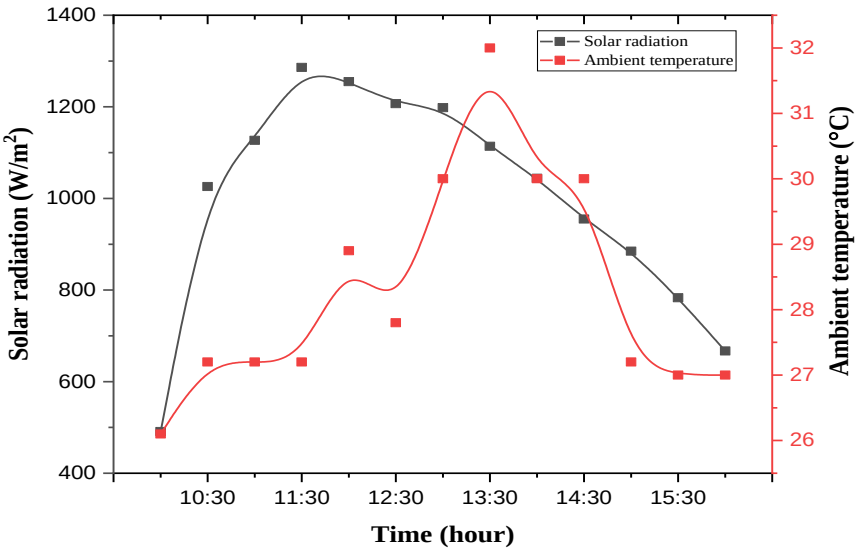


**Fig. 5.7** Weather characteristics

As indicated in that figure, the highest solar radiation on the day of the experiment was recorded around 11:30 am. The day recorded an average solar irradiation of 1002 W/m$^2$. The average ambient temperature for the day is also around 28,28 ℃ with the highest temperature of about 32 ℃ occurring at about 1:30 pm.

The temperature of both panels were attained by computing the average of the temperatures recorded by each of the seven thermocouples fitted at the back of the two modules for each 30 minutes interval. The results for the temperature distribution for the period within which the experiment was conducted is as shown in Fig. 5.8. It can be detected from the figure that the uncooled panel's temperature reached its peak between 1:00 pm and 1:30 pm. This can be attributed to the high ambient temperature recorded between that period of the experiment as indicated in Fig. 5.7. However, the cooled panel was able to sustain a level of stability in relation to its temperature as a result of the effectiveness of the cooling system. Both panel's temperatures however started plummeting after 1:30 pm a result of a sharp drop in the ambient temperature induced by the formation of clouds which also affected the intensity of the solar radiation and humidity. According to the results the cooled system recorded an average temperature of 35,72 ℃ whiles the uncooled system recorded an average temperature of 59,27 ℃. The difference in temperature between the two panels averagely is 23,55 ℃. It can be observed from the figure that, the temperature of the cooled panel was slightly higher than the uncooled panel at the beginning of the experiment, obviously due to the fact that, the cooled panel was deficient of natural air at the rear side of the panel, because of both the cotton wick mesh and the aluminum sheet at its back. As a result, the referenced panel was cooled by the ambient air during the start of the experiment since it was relatively colder. The SD for the referenced module was relatively high compared to the cooled system, the uncooled panel recorded 11,57 against 2,47 for the cooled system. Similarly, the uncertainty for the uncooled system was 3,21 against 0,69 for the cooled system. These large uncertainties can be associated with the sharp rise in the ambient temperature after mid-day and the subsequent drop in the ambient temperature after about 2:30 pm. This triggered sharp increase in the modules temperature particularly the uncooled panel,

hence the high SD for the referenced module. However, the SD in the cooled panel was significantly consistent, this is obviously due to the positive effect of the cooling system on the PV panel.

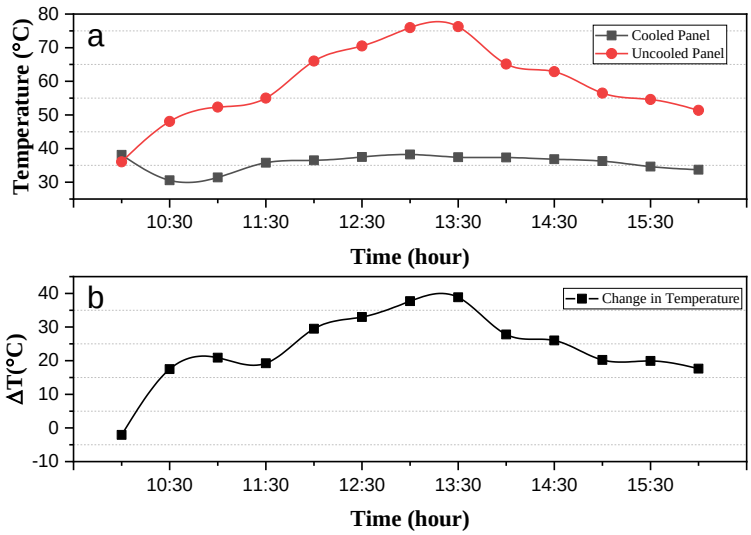


**Fig. 5.8** (a) Temperature of both panels (b) change in temperature between both panels

The temperature of the two modules were recorded around 11:30 am, using the thermal imager camera, the results of which are illustrated in Fig. 5.9. The thermal imager camera is contactless and fast, it therefore allow users to evaluate facility's temperature even under operation conditions. It is generally advisable to conduct such assessment under sunny weather conditions with sun irradiance of at least 600 W/m$^2$ [191]. The PV module's temperature is visualized to show the temperature distribution across the module's surface. The thermal image results suggest that the temperature distribution does not differ much from that obtained from the thermocouples. The average temperature for the uncooled panel using the thermal imager is 51,9 ℃ compared to the 53 ℃ recorded using the thermocouples during the same period. In the case of the cooled panel the average temperature recorded using the thermal imager is 37,8 ℃ compared to 35,78 ℃ recorded using the thermocouples. These differences could be because the thermocouples are closer in terms of contact than the thermal imager and therefore can record more accurately than the thermal imager, also, time differences, i.e., the figures for that of the

thermocouples and the thermal imager were not simultaneously recorded. Therefore, time differences could cause the temperature to either increase or decrease slightly based on the ambient temperature at the time. It is discovered from the thermal image for the cooled module that the distribution of temperature for the panel is highly uniform manifestly because of the cotton wick that was positioned homogeneously at the back of the module with uniform water absorption. The figures on the y-axis within the histogram signify the share of temperature distribution on the PV module's surface. This indicate that the temperature of the panel is not equal at every section, certain parts of the module are hotter than others.

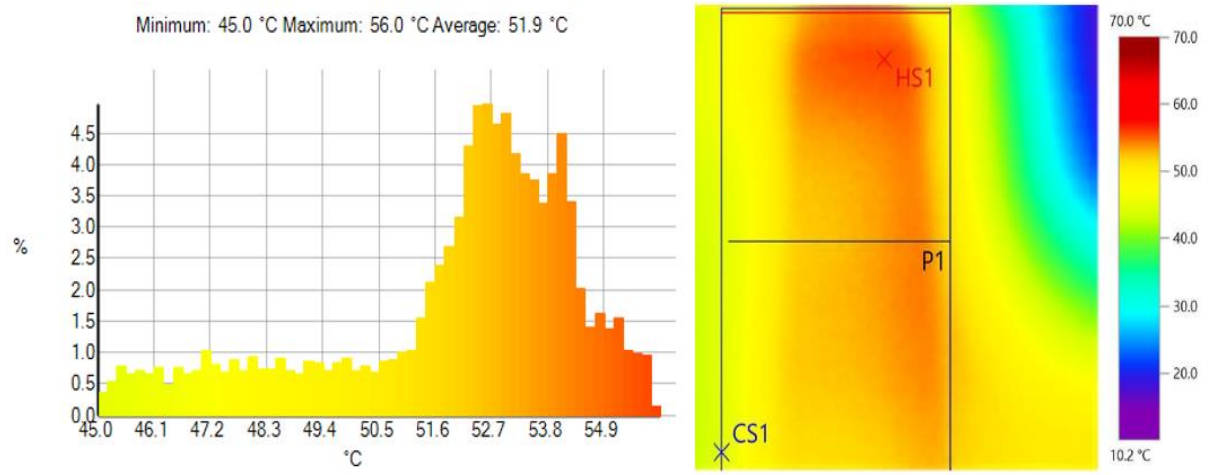


(a)

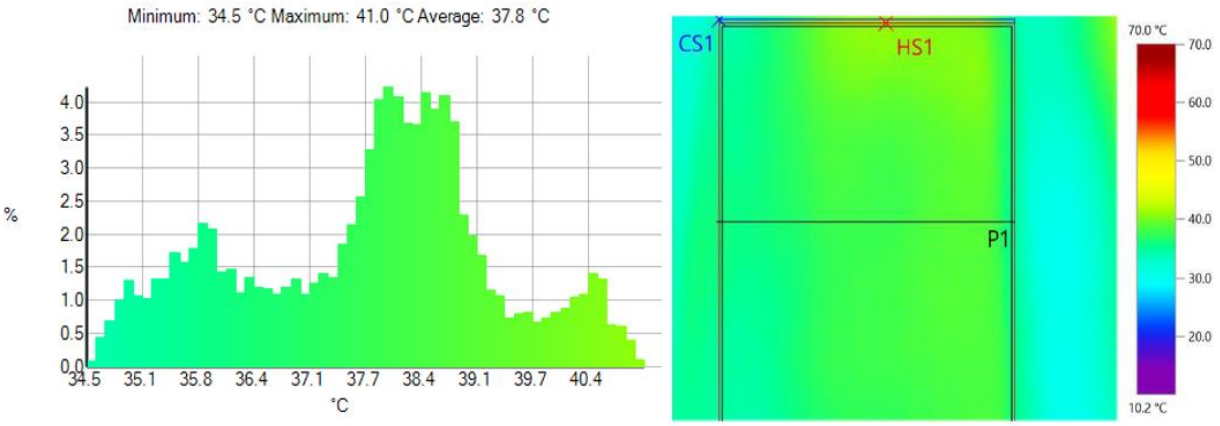


(b)

**Fig. 5.9** Temperature distribution histogram and thermal images for the (a) uncooled panel (b) cooled panel

### 5.1.6.2. Effect on the electrical characteristics of the panel

The comparison of the output power for the two PV modules is presented in Fig. 5.10. The uncooled panel's power at the start of the experiment was comparatively higher than the cooled panel. It however changed in favor of the cooled panel as the temperature of the uncooled panel increased. The maximum power output of 15,04 W was measured at about 11:30 am which is also the period for the highest solar irradiation during the experiment for the cooled PV panel, the uncooled panel however recorded 11,60 W at that same period. This represent approximately 29,66% improvement in the cooled PV's energy yield due to the implementation of the cooling system. The cooled PV module during the entire experimental period recorded an average power of 13,03 W compared to 10,00 W for the referenced PV module. It can be said that the 23,55 ℃ reduction of the temperature as presented earlier in this research led to an overall increment of 30,3% in the output power.

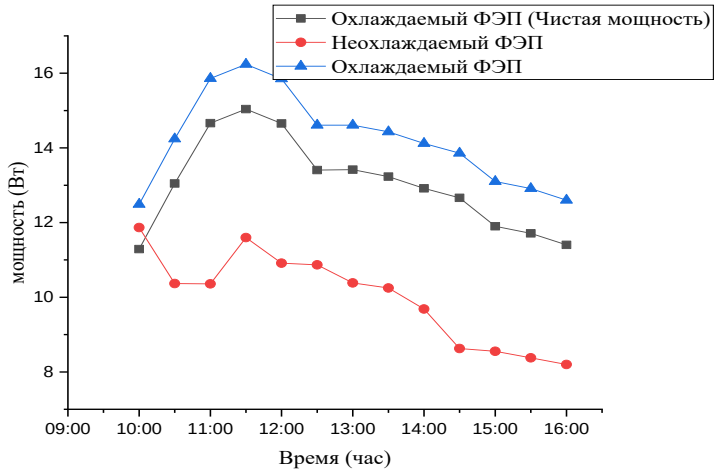


**Fig. 5.10 Comparison of the power output for the two modules**

The influence of the cooling process on the PV panel's efficiency and improvement in efficiency are presented in Fig. 5.11. The results shows that the proposed cooling method had a substantial impact on the cooled PV module's efficiency. The cooled PV module recorded 14,36% average efficiency whiles that of the referenced PV module recorded 12,83%. This characterize a 1,53% difference which is 11,9% enhancement in the cooled panel's efficiency. It is seen that the efficiency of the panel decreased with increasing

temperature. It decreased sharply after mid-day when the temperature of the panel was highest. The impact of the cooling process was felt most during mid-day, the cooled panel's efficiency remained comparatively constant during the high temperature periods. The negative improvement at the start of the experiment shows that, the referenced module was more efficient at start of the experiment. This is because, the uncooled panel was relatively colder than the cooled panel at the beginning of the experiment. However, the cool panel recorded a sharp improvement in its efficiency when the cooling process started. This confirms the effectiveness of the cooling method. Earlier studies such as [211] got 6,5 – 7,0% electrical efficiency enhancement using a combination of pure water, activated alumina, and circular perforation for the cooling.

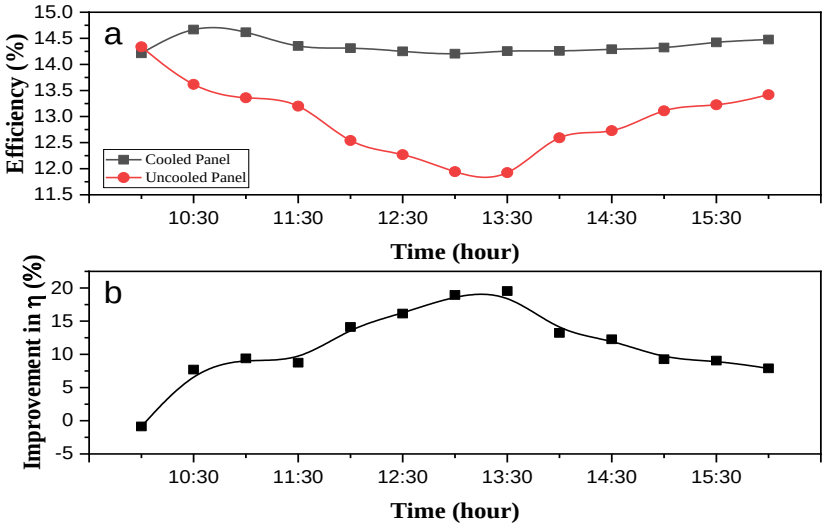


**Fig. 5.11** (a) Efficiency for both panels (b) improvement in panel efficiency

Elbreki et al. [212] obtained an electrical efficiency of 10.68% using passive cooling, i.e. fins and planar reflector to cool PV panels. Chandrasekar et al. [213] also used a combination of water and cotton wicks to cool a PV panel, their results indicate that, the maximum efficiency is 10,4% for the cooled module. Sun et al. [214] employed the optics based approach: selective-spectral and radiative cooling to manage the temperature of a PV module. They obtained an efficiency increment of 0,5–1,8%. Equally, [215] was able to enhance the PV module's efficiency by some 1,3%. In other studies, [216] evaluated the feasibility of photovoltaic evaporative chimney as cooling mechanism of PV modules.

Their results shows that the PV system could improve in its electrical efficiency by some 4,9%-7,9% during mid-day under Mediterranean summer weather conditions. Finally, Dida et al. [217] used the passive cooling approach to manage the temperature of PV systems under hot climatic conditions. An electrical efficiency of enhancement of 9–14,75% was obtained in their study. Comparing the outcome of the current study to the previous studies indicate that the proposed technique in this study can enhance the performance of a PV panel better than most of the proposed methods reviewed above. The enhancement in the electrical efficiency of the PV panel in this study either falls above the efficiencies reported by earlier works or falls within the range recounted by such studies.

## 5.2. Experimental Study on Performance Enhancement of a Photovoltaic Module Using a Combination of Phase Change Material and Aluminum Fins—Exergy, Energy and Economic (3E) Analysis

This section proposed a mechanism that uses independent containers to house the PCM which are then fixed behind the PV module. It is combined with aluminum fins which also depends on natural ventilation for the cooling of the PV module. Unlike the orthodox single block application style of PV panel cooling using PCM as demonstrated in literature, this study uses PCM filled cylindrical cans to cool a PV module. One benefit if the proposed cooling method is the potential to cool portions of the rear surface with ambient air. This is because the PV panel’s rear surface is not fully covered with the paraffin wax, this enables the natural air to cool its back.

### 5.2.1. Materials and Methods

The experiment was carried out by comparing modified photovoltaic module, which is integrated with horizontal aluminum fins and PCM, i.e., paraffin in an aluminum container attached to the back of the panel. Most studies apply the PCM at the bac of the panel in a single compartment. In this study, the PCM are placed in separate capsule-like aluminum containers and fixed at the back side of the PV panel. This approach is unique

and simple to construct. A key problem this technique is expected to resolve is the leakage of melted PCM. The proposed cooling method in this study is able to store the melted PCM without leakage, thereby reducing maintenance and replacement cost. This approach also allows natural air to cool the back of the panel since the cylindrical containers do not fully cover the whole surface.

Twelve (12) PCM filled cylindrical aluminum containers were fixed at the back of a PV module (here recognized as the cooled PV module). A thermal glue was used to provide appropriate contact between the containers of the paraffin wax and the PV module's back surface. This is a very important step since it increases the contact surface area between the PV module back surface and the containers for the paraffin wax. Therefore, adequate thermal glue have to be applied to realize the maximum contact. The experimental setup is as presented in Fig. 5.12.


**Fig. 5.12.** Experimental setup

During the experiment, the two modules were placed 45° to the south to acquire the maximum solar radiation. Fig. 5.13 is an illustrations of the back side of the two modules (i.e., referenced, and cooled PV modules).

**Fig. 5.13** Rear side of the PV panels: referenced (left) cooled (right)

Fig. 5.14 is the schematic diagram of the experimental set-up. The temperature of the two panels were recorded using 7 thermocouples manufactured by Weewooday and supplied by Amazon, for each module. Seven thermocouples for each PV module were attached at different locations to help in finding the mean temperature distribution. The clamp meter (RS Components Ltd, China) was employed to measure the current and voltage. The wind speed was also recorded with the help of an anemometer, the solar radiation intensity was measured using pyranometer provided by Amazon, the humidity and the ambient temperature were measured by means of the GM 1362-EN-01 thermometer manufactured by Shenzhen Jumaoyuan Science And Technology Co., Ltd, Shenzhen, China.

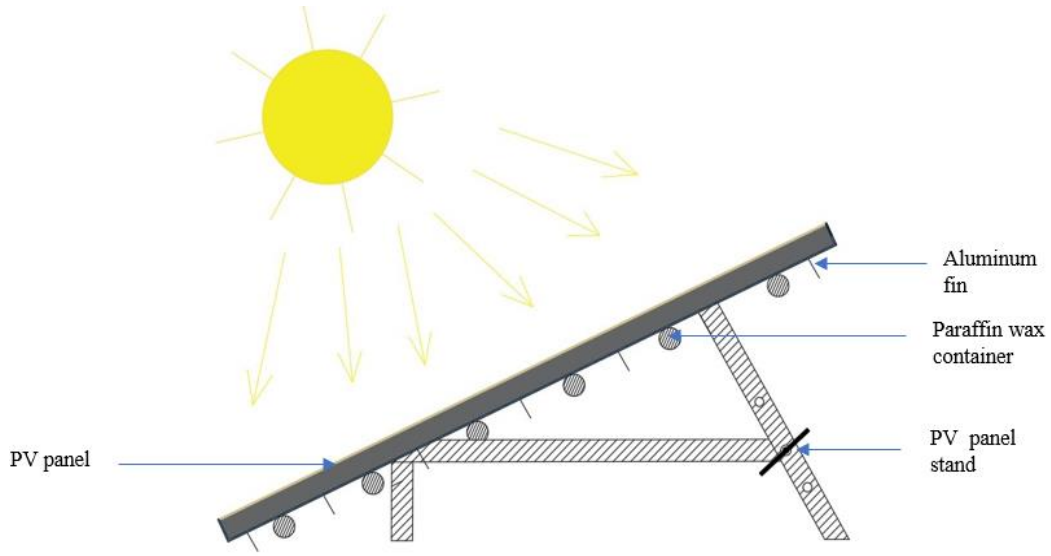


**Fig. 5.14.** Schematic diagram of the experimental set-up

### 5.2.2. Phase Change Material

This is a material that capable of storing energy in the form of latent heat (LH). Latent heat storage is about phase transition of a material, i.e., energy is released or stored as a result of the variation in the enthalpy of the phase change. As a result of the contribution of the phase change, at the phase change temperature of the material, thermal energy storage operate virtually isothermally [218]. The LH thermal energy storage with respect to energy density is higher than sensible heat thermal energy storage. The melting temperature of a PCM must be as low as possible in order to get the highest enhancement in electrical performance [219]. To find the phase change of a PCM (i.e., solid or liquid), with specific heat capacity for every phase, the temperature field is given as shown in [220] as presented in Eq. (5.10). A PCM's behavior under varying temperature is presented in Fig. 5.15**.**

$$T = \begin{cases} E/c_s \;\; T < T_m \; (solid\ phase) \\ T_m \;\; 0 < E < H, \;\; T > T_m \; (melt\ zone) \\ T_m + (E - H)/c_L \;\; E \geq H, \;\; T > T_m \; (liquid\ phase) \end{cases} \tag{5.10}$$

where the thermal energy is denoted with $E$ (J/kg), c is the specific heat capacity for every phase, and the latent heat is represented by $H$ (J/kg).

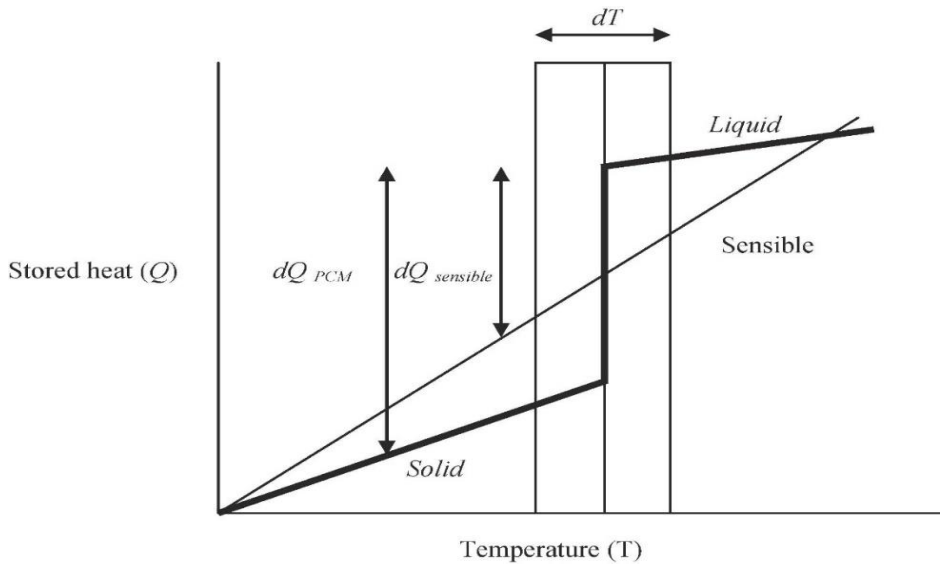


**Fig. 5.15.** Performance of PCM for different temperatures [221]

Paraffin wax was used in this study as a PCM to cool the panel, the characteristics paraffin wax are as follows: the thermal conductivity is 0,2 W $m^{-1}$ $K^{-1}$, melting point is 28 °C, and heat of fusion 222 kJ/kg.

### 5.2.3. Exergy Analysis

Exergy is defined as the maximum useful work done by a system enclosed in an environment in a constant temperature and pressure in a reversible process. Therefore, the following assumptions are made during the calculation of the exergy efficiency of a system [222]:

There is no irreversibility for the environment.

Uniformity in the environment relative to intensive properties.

The PV system's electrical exergy is projected to utilize the present energy as a useful energy. An analysis of exergy takes into account energy capability and quality. The overall exergy balance for a PV system can be mathematically expressed as follows:

$$\sum \dot{E}_{in} = \sum \dot{E}_{out} \tag{5.11a}$$

$$\sum \dot{E}_{in} = \sum \dot{E}_{out} + \sum \dot{E}_{loss} + \sum \dot{E}_{irreversibility} \tag{5.11b}$$

The exergy efficiency for a PV system can be defined as the ratio of the total output exergy to the total input exergy, this is expressed mathematically as indicated in Eq. (5.12) [223].

$$\psi_{system} = \frac{Ex_{out}}{Ex_{in}} \tag{5.12}$$

where the input exergy for the PV module include the solar radiation intensity exergy on as expressed in Eq (5.13) [223,224].

$$\dot{Ex}_{in} = \left(1 - \frac{T_a}{T_s}\right) I_s A \tag{5.13}$$

The output exergy can also be calculated using Eq (5.14) [223].

$$\dot{Ex}_{out} = V_m I_m - \left(1 - \frac{T_a}{T_{cell}}\right) h_c A (T_{cell} - T_a) \tag{5.14}$$

The exergy efficiency of the PV module can therefore be calculated using Eq (5.15) [225].

$$\psi_{system} = \frac{V_m I_m - \left[\left(1 - \frac{T_a}{T_{cell}}\right) \cdot \left(h_c A \cdot (T_{cell} - T_a)\right)\right]}{\left(1 - \frac{T_a}{T_s}\right) \cdot I_s \cdot A} \tag{5.15}$$

where the maximum power voltage and current of the system are represented by $V_m$ and $I_m$, respectively. $T_s$ signify the surface temperature of the sun assumed to be 5762 K, the ambient temperature is represented by $T_a$ (K), the module surface temperature is denoted $T_{cell}$ (K). The area of the panel is represented by $A$ ($m^2$), which is 0,4275 $m^2$. The convective heat transfer is represented by $h_c$, it is contingent on the wind velocity $v$, it can be estimated using Eq. (5.16) [222].

$$h_c = 5{,}7 + 3{,}8v \tag{5.16}$$

### 5.2.4. Error Analysis

Errors associated with experiment are calculated using uncertainty analysis. There are two basic types of errors, namely constant error and variable error during measurements [194]. The various instruments' accuracies are presented in Table 5.1. Experimental errors as a result of various data measurements are estimated using the methods provided in [226]. The resultant $N$ in this method is a function of the independent variables as presented in Eq (5.17).

$$N = N(Y_1, Y_2, Y_3, \ldots\ Y_n) \tag{5.17}$$

The percentage of uncertainty in the resultant '$N$' can be computed using Eq (5.18).

$$U_N = \sqrt{\left(\frac{\partial N}{\partial Y_1}\Delta Y_1\right)^2 + \left(\frac{\partial N}{\partial Y_2}\Delta Y_2\right)^2 + \cdots + \left(\frac{\partial N}{\partial Y_n}\Delta Y_n\right)^2} \tag{5.18}$$

where uncertainties in the independent variables are represented by $\Delta Y_1$, $\Delta Y_2$ …. $\Delta Y_n$.

**Table 5.1.** Accuracies and uncertainties of various instruments

| Instrument | Accuracy | Range | Uncertainty, % |
|---|---|---|---|
| GM 1362-EN-01 thermometer, °C | ±2% | −30–70 | 1,15 |
| Clamp meter, V | ±1.5 | | 0,87 |
| Pyranometer, W/m$^2$ | ±5 % | 0–2000 | 2,89 |
| Anemometer, m/s | 0,2 | 0–25 | 0,12 |
| Thermocouple, °C | ±0.1 | −200–1370 | 0,06 |

The proportion of entire uncertainty of the entire system in this experiment is equal to 3,2%.

### 5.2.5. Economic Analysis

The electricity generation cost of the two panels, namely the reference module and the cooling module, were analyzed using the LCOE method. It is a method that is mostly employed to evaluate the economics of RE power plants. It is a measure of cost that compares varying approaches of electricity generation on comparable basis [227,228]. The levelized cost of electricity is the assessment of the average total cost of building and operating a power plant over its lifetime divided by the total power output generated over the lifetime of the power plant. It can also be defined as the minimum cost at which the produced electrical energy from the power plant have to be sold to be able to achieve a break-even over the project's lifetime [229,230]. The LCOE can be mathematically expressed as [231]:

$$LCOE = \frac{LC_{inv} + LC_{O\&M} + LC_{fuel}}{E_{annual}} \tag{5.19}$$

$$LC_{inv} = CRF \times C_{inv} \tag{5.20}$$

$$CRF = \frac{i_{eff} \cdot (1+i_{eff})^n}{\left((1+i_{eff})^n\right)-1} \tag{5.21}$$

$$LC_{O\&M} = C_{O\&M} \times CELF \tag{5.22}$$

$$CELF = \left(K_{O\&M} \times \frac{1-K_{O\&M}^n}{1-K_{O\&M}}\right) CRF \tag{5.23}$$

$$K_{O\&M} = \frac{1+r_n}{1+i_{eff}} \tag{5.24}$$

where the investment cost is denoted by $C_{inv}$, $n$ is the plant's lifetime, the capital recovery factor (%) is represented by $CRF$, $C_{O\&M}$ is the annual cost of operations and maintenance, $CELF$ is the constant-escalation levelization factor, $i_{eff}$ is the effective discount rate and $r_n$ is the nominal escalation rate (%).

### 5.2.6. Results and Discussion

The results for the PV panel's temperature, exergy, and electric efficiencies of the two panels due to the integration of the PCM and aluminum fins.

### 5.2.6.1. Weather Characteristics

Fig. 5.16 presents the weather data on the period of the experiment. The day's highest solar irradiation was recorded at 12:30 pm which is 1391 W/m$^2$, the least solar radiation of 543 W/m$^2$ was however recorded at 17:00 pm. A mean solar of 994,59 W/m$^2$ was recorded for the experimental period. The highest ambient temperature of 37,6 °C was recorded at 2:30 pm and the lowest in the morning around 9:00 am at the beginning of the experiment. The mean ambient temperature for the experimental period is 33,7 °C. Also, daily humidity dropped with increasing ambient temperature. On the experimental day, the average humidity and wind speed were recorded at 43,45% and 5,35 m/s, respectively.

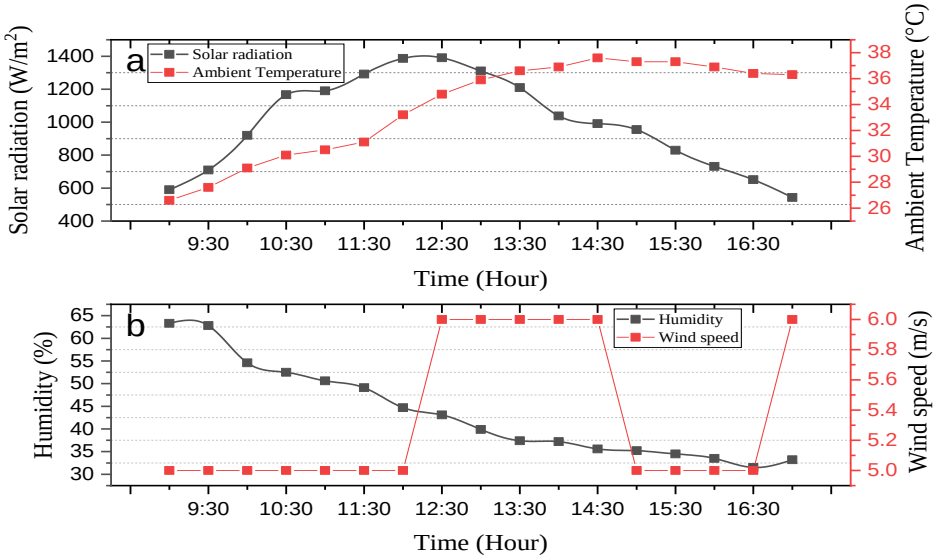


**Fig. 5.16** (a) Solar radiation and ambient temperature (b) humidity and wind speed characteristics for the experimental day

### 5.2.6.2. Impact of Cooling Method on the Panel's Temperature

The modified module's temperature results, i.e., a cooled module being compared to a reference module without any modification. The temperature results for both panels are shown in Fig. 5.17. The results showed that the proposed mechanism in this research has a positive effect on the heat management of the cooled panel. The cooled panel had a comparatively lower temperatures during the experimental process. The difference in

temperature between the cooled and referenced panels in the beginning of the experiment was relatively inconsequential, due to the fact that the PCM was still in the solid phase. However, when the temperature of the panel rose as the ambient temperature rose, the temperature of the PCM inside the container also rose, and the PCM melts. According to the results obtained, the cooled panel recorded a maximum temperature of 46.52 °C at 14:30 versus 62.6 °C for the reference module in the same period. This shows that the combination of paraffin wax and aluminum fins works great even at very high temperatures. The cooled PV module had an average temperature of 36,62 °C whiles that of the uncooled module was 48,75 °C. This represents a mean drop of 12,13 °C for the cooled panel. After noon, when the ambient temperature was at its highest, the highest temperatures for both modules were recorded.

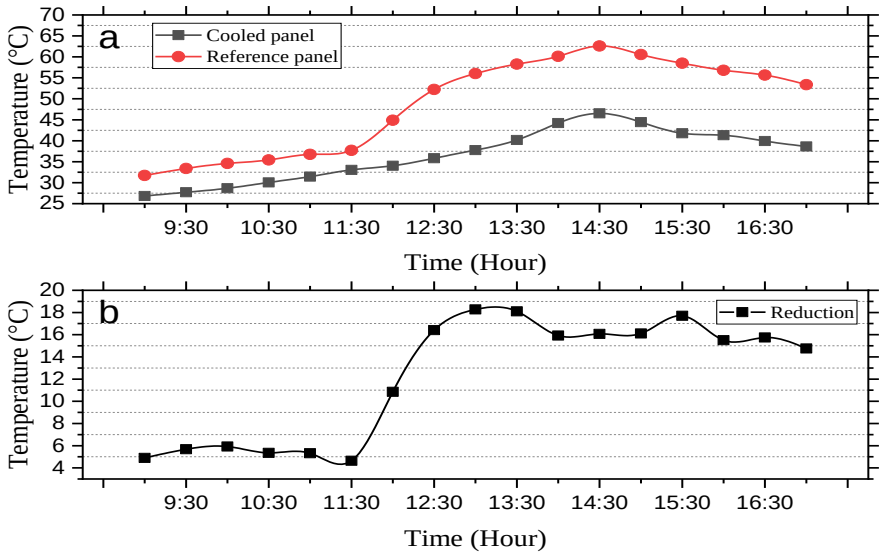


**Fig. 5.17** (a) Temperature (b) change in temperature for the cooled and referenced module.

One of the positive effects of the aluminum fins and the PCM on the cooled module's temperature distribution is the steadiness that the cooling approach has on the PV module temperature. The SD for the cooled panel was 6,06 °C whiles that of the uncooled panel recorded 11,27 °C. The cooled panel recorded an uncertainty of 1,46 against 2,73 for the uncooled module. This shows that the cooling method was able to not only enhance the

rate of heat loss but also assisted in bringing homogeneity in the temperature variation of the power plant.

The temperature distribution of the two panels were recorded using the testo infrared camera (manufactured by Testo in Germany). The picture was taken at 12:00 pm when the paraffin wax had almost fully melted. The maximum temperature for the cooled PV module was 43,9°C, it also recorded a minimum temperature of 34,9 °C and an average temperature of 34,9 °C. However, the maximum temperature for the uncooled PV was 43,9 °C with a minimum temperature of 38,1 °C, and an average temperature of 42,1 °C. There are slight variations between the values from the thermocouples as presented supra and that recorded by the thermal camera. The thermocouples however measured an average temperature of 34,04 °C and 44,9 °C for the modified and referenced panels, respectively, during that same period. The temperature distribution for both modules are presented in Fig. 5.18. Fig. 5.19 illustrate the thermal image for both panels.

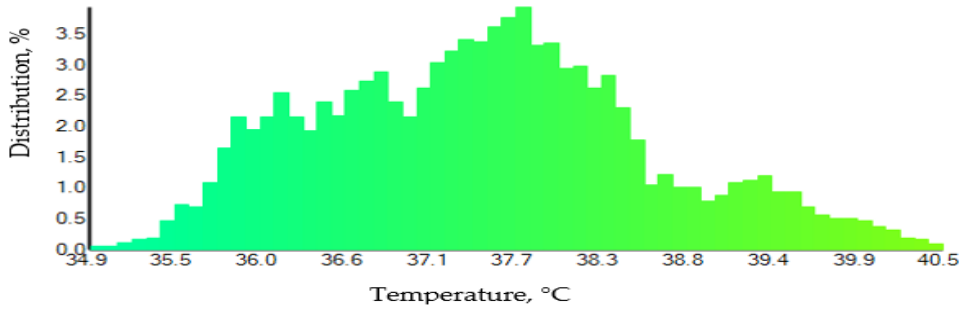


(a)

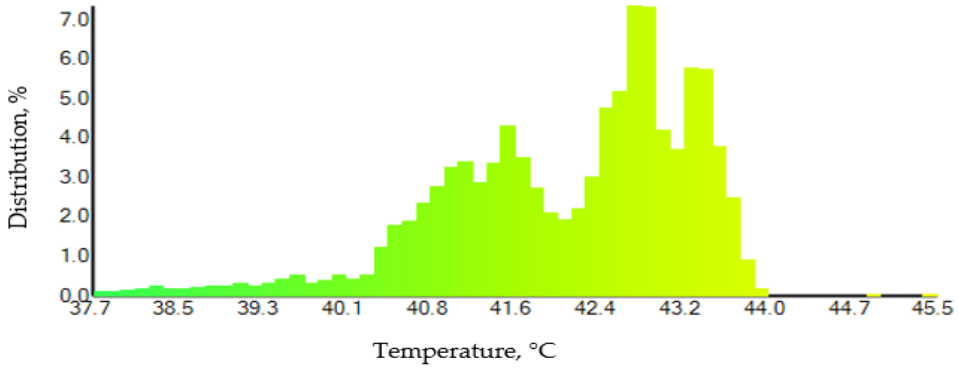


(b)

**Fig. 5.18** Histogram for the temperature distribution of (a) cooled panel (b) referenced panel

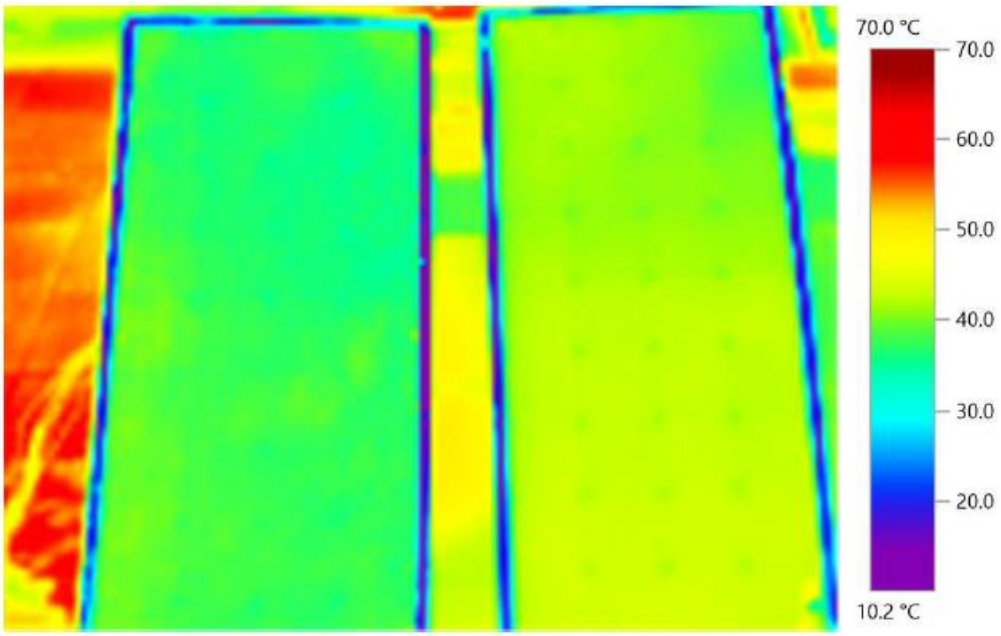


**Fig. 5.19** Thermal image for the cooled panel (left) referenced panel (right).

### 5.2.6.3. Electrical Performance of the Module

The influence of the cooling process on the PV module's electrical performance are presented in this section. The results for the voltage and current recorded during the experimental period are illustrated in Fig. 5.20. The effect of temperature on the PV cell's voltage is seen in the obtained results. The voltage saw a significant reduction due to the high temperature of the PV cell for the uncooled panel. The cooled panel recorded an average voltage of 18,85 V against 17,33 V for the referenced module. This is a 1,52 V reduction in the voltage of the referenced module.

The cooled panel's current was also relatively higher than the uncooled panel but only slightly, this was however predictable since temperature affect the short circuit current but only slightly.

The cooled module had an average current of 0,65 A, while the reference module had a current average of 0,63 A. The difference is minor because the current in both panels was nearly identical until about midday, when the ambient temperature rose dramatically, affecting the temperature of the PV cell.

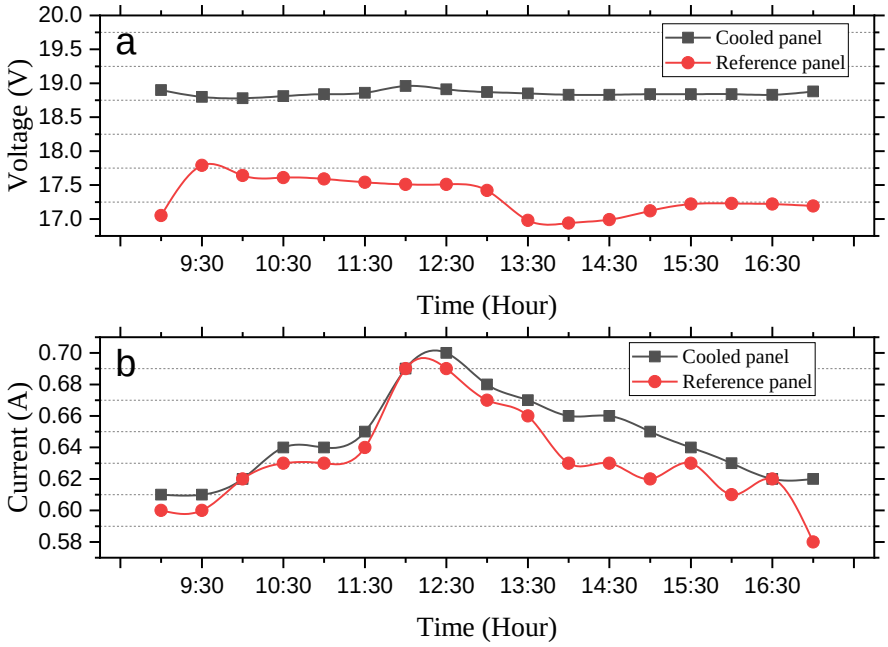


**Fig. 5.20** (a) voltage (b) current for the cooled and referenced panel.

The power output for both panels are represented in Fig. 5.21. Throughout the trial, the output power of the cooled panel was determined to be the highest. With rising solar radiation throughout the day, the power of both modules rose. After midday, both modules recorded their peak solar radiation, which occurred at 12:30 p.m. However, after midday, as the temperature of the cell climbed and the intensity of the solar radiation decreased, the power began to decline. An average power of 12,19 W and 10,95 W were recorded by the modified and referenced PV panels, respectively. Therefore, an improvement of 11,33% in power output was recorded as a result of the cooling mechanism. In the study of Luo et al. [232] they got a maximum power of 18,30 W for the PV-PCM panel vs 17,85 W for the referenced module using the standard method of using paraffin PCM for temperature regulation of a PV module. The difference between the two modules is only 0.45 W.

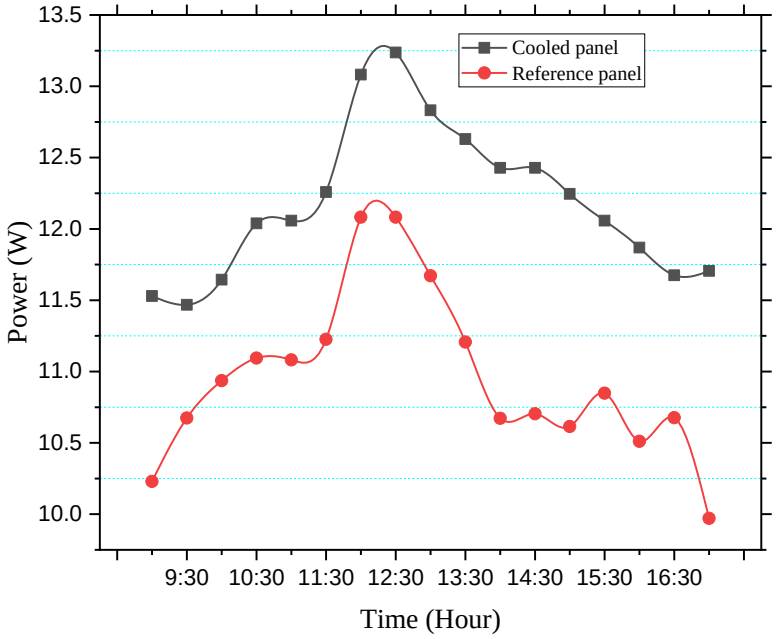


**Fig. 5.21** Power output for the cooled and referenced modules

### 5.2.6.4. Electrical and Exergy Efficiency

The results for the efficiency computations are presented in Fig. 5.22. The reference module recorded the least efficiency during the period of the experiment as a result of its high temperature. The average electrical efficiency of the cooled module is 14,30% against 13,60% for the reference panel. This is a 5,15% improvement in the efficiency occasioned by the cooling process. The highest improvement in the electrical efficiency of 8,35% was recorded at 1:30 pm. This is a substantial enhancement bearing in mind that this proposed method does not use any form of active approach or water for the cooling. This is also an approach that employs a comparatively small quantity of PCM compared to the other styles of smearing the PCM at the back of the panel. A comparison of the obtained results with other literature are presented in Table 5.2, it is observed that the proposed method in this study is effective. It produced outcomes that are either better than or competitive to other cooling methods in other published studies.

**Table 5.2.** Comparison with other studies

| Ref | Cooling Mechanism | $T_{PV}$ without Cooling, °C | $T_{PV}$ with Cooling, °C | Temp Reduction, °C | Eff Improvement, % |
|---|---|---|---|---|---|
| [233] | PCM RT27 | 32,6 | 22,4 | 10,2 | 5,90 |
| [234] | RT35, 35 °C/240 kJ/kg | 60 | 54,9 | 5,1 | 5,00 |
| [235] | Organic PCM | 54,88 | 47,58 | 7,30 | 4,22% |
| [236] | PCM | 53,7 | 49,2 | 4,2 | 1,49% |
| [237] | Organic PCM | 36 | 31 | 5 | 3,10 |
| [238] | RT42 | 53 | 42,5 | 10,5 | 5,9% |
| [239] | RT42, 38–43 °C/174 kJ/kg, (0.5 wt% CuO added) | 72 | 62 | 10 | 5,35% |
| [240] | Organic PCM | 56,1 | 50,5 | 5,6 | - |
| [241] | Paraffin wax | 58 | 47 | 11 | - |
| [242] | PV with Praffin | 71 | 64 | 7 | - |
| Current study | PCM (paraffin wax) and aluminum fins | 48,75 | 36,62 | 12,13 | 5,15 |

Exergy assessment is a thermodynamic analysis of processes and systems which combines the first and second thermodynamic laws to find a system's available energy values and the amount of energy loss [243]. Eq. (5.15) was employed to estimate the exergy efficiency of both PV modules. The variations of the exergy efficiency for the two modules is presented in Fig. 5.23. The outcome of the calculations indicate that an increase the ambient temperature of the PV panel leads to a decrease in the exergy efficiency. The PV module's exergy efficiency are however higher when the solar irradiation is low. This is illustrated in Fig. 5.23, the exergy efficiency decreased from the beginning of the experiment till mid-day for the cooled PV module, however, it began to increase again with a reduction in solar radiation. The exergy efficiency of the referenced PV panel however saw a decrease up till 15:00 before it started to climb up again. This is attributable to the high temperature of the referenced module after mid-day. This is because the degree of increase for input exergy is comparatively more than the degree of

increase of the output exergy with increasing solar irradiation at constant ambient temperature. The cooled and uncooled PV panels recorded average exergy efficiency of 7,99% and 5,61%, respectively.

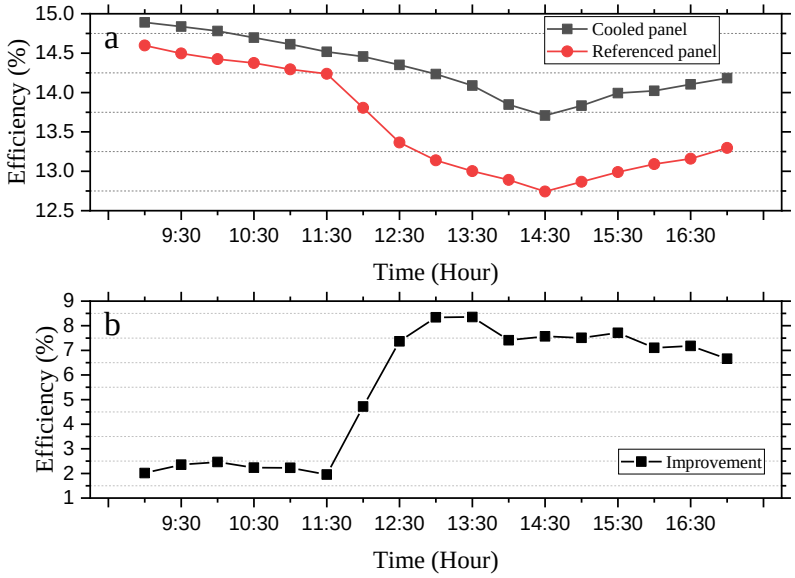


**Fig. 5.22.** (a) Efficiency (b) improvement of the two modules with time

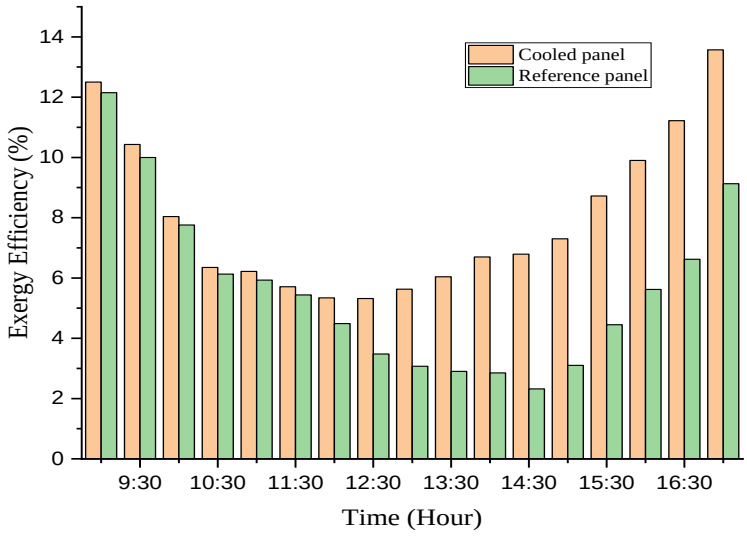


**Fig 5.23.** Exergy efficiency of both modules with time

### 5.2.6.5. Economic results

The cooling was done using aluminum fins paraffin wax and an aluminum container. A 25 kg paraffin wax was purchased at the cost of 5000 rubles equivalent to $ 68,16 at

an exchange rate of 1 ruble = $ 0,0136. The weight of paraffin used for the cooling is however 2,4 kg, which is equivalent to 0,2 kg for each of the 12 cylindrical containers used. This means the cost of the 2,4 kg paraffin wax used for the experiment is $ 6,54. The aluminum sheet used for the experiment is $ 2,91, the thermal glue also cost $ 4,10. The total cost for the cooling system in effect cost $63,55, this include an assumed $50 cost of the 30 W PV module.

Two scenarios were considered in relation to the energy generated by the power plant, the initial scenario considers a situation whereby the power plant operate all year round (i.e., 365 days). The second scenarios considers a situation whereby the power plant works only in the summer period, i.e., 120 days which is four months of sunshine as happens in Russia. It is assumed that same power will be generated by the power plant all year round under same solar radiation intensity. It is also assumed that the SPP received effective solar radiation for a period of 9 hours each day. In effect, a total of 40,04 kWh and 13,17 kWh will be produced by the cooled SPP for the first and second scenarios, respectively. The uncooled panel would also produce a total of 35,97 kWh and 11,83 kWh for the first and second scenarios, respectively. The cost associated with each panel is therefore computed by means of the parameters provided in Table 5.3.

The outcome of the calculations indicate that the cooled panel would have an LCOE of 0,198 $/kWh against 0,221 $/kWh for the first scenario. In the case of the second scenario, the cooled module would record 0,603 $/kWh whiles that of the reference module will be 0,671 $/kWh. The results show that despite the additional cost incurred for the cooling of the PV module (i.e., the integration of the aluminum fins and paraffin wax), the cooled module still performed better in relation to the cost of energy under both scenarios. It thus means the proposed cooling system would not only improve the electrical and exergy efficiencies but also reduce its cost.

**Table 5.3.** Parameters used for the LCOE calculation

| Parameter | Cooled PV | Referenced PV |
|---|---|---|
| Investment cost ($C_{inv}$), $ | 63,55 | 60,00 |
| Annual operation and maintenance cost ($C_{O\&M}$), $ | 3,50 | 3,50 |
| Effective discount rate ($i_{eff}$), % [231] | 5,00 | 5,00 |
| Lifetime of the plant ($n$), years | 30,00 | 30,00 |
| Nominal escalation rate ($r_n$), % [231] | 1,00 | 1,00 |
| Capital recover factor (CRF), (%) | 6,50 | 6,50 |
| $K_{O\&M}$ | 096 | 0,96 |
| Levelized cost of fuel ($LC_{fuel}$), $/kWh | 0 | 0 |
| Constant-escalation levelization factor O&M, (CELF) | 1,10 | 1,10 |

## 5.3. Experimental investigation of the effect of a combination of active and passive cooling mechanism on the thermal characteristics and efficiency of solar PV module

This section combines aluminum fins, water, and ultrasonic humidifier to cool PV panel under real weather conditions

### 5.3.1. Materials and Methods

The rate of transfer of heat from the back surface of a PV panel is governed by Newton's law of cooling as indicated in Eq (5.25) [244].

$$\dot{Q}_{conv} = hA_s(T_s - T_a) \tag{5.25}$$

Where the area and temperature of the heat transfer surface are denoted by $A_s$ and $T_s$, and $h$ represent the coefficient of convection heat transfer. As can be seen from Eq. (5.25), it is clear that the heat transfer rate can be increased in two ways, i.e., either to increase the convection heat transfer coefficient $h$ in the form of active cooling or to increase the area of the heat transfer surface $A_s$, which is passive cooling. It is for this reason that the

aluminum fins were used in this study to enhance the heat transfer rate. Eq (5.26) governs the total heat transfer from fins, this includes the transfer of heat from both the finned and un-finned surface areas, which needs cooling [244].

$$\dot{Q}_{total,fin} = n\dot{Q}_{unfin} + n\eta_{fin}\dot{Q}_{fin}$$

$$\dot{Q}_{total,fin} = nh_{unfin}A_{unfin}\left(T_{s,unfin} - T_a\right) + nh_{fin}A_{fin}\eta_{fin}\left(T_{s,fin} - T_a\right) \quad (5.26)$$

The number of fins attached to the back of the panel is denoted by $n$, surface temperatures for the finned and un-finned area are also represented with $T_{s,fin}$ and $T_{s,unfin}$, respectively, the coefficient of the convection heat transfer for the finned and un-finned areas, i.e., $h_{fin}$ and $h_{unfin}$, respectively, will be different as a result of the differences in geometry. $A_{unfin}$ and $A_{fin}$ are the area of one of the fins and un-finned portion of the surface area, respectively. The efficiency of the fin is defined as the ratio of the actual rate of heat transfer from fin to the rate of heat transfer from the fin ideally if the whole fin was to be at the back surface temperature of the module.

### 5.3.2. Construction of the cooling system

The use of fins to cool PV panels is an old method that has been studied by several researchers as reviewed supra. However, one disadvantage with this mechanism of cooling is the low temperature reduction that is usually associated with it. As a result, the use of fins alone especially in very hot climate areas turn to have very low effect on the efficiency of the panel compared to other mechanisms that uses water or other PCMs as cooling agent. According to [245] when the ambient temperature exceeds 35 °C, heat dissipation from a PV module that relies on only heat sink cooling system becomes limited and unable to maintain acceptable PV module temperature. In effect, active cooling is usually preferred in harsher environments. In order to increase the efficiency of the temperature reduction process using fins, this study proposed the addition of

ultrasonic humidifier to create a humid environment at the back surface of the panel to enhance the cooling process. The construction of the setup was done with minimal water loss in mind.

The cooling mechanism consist of discontinuous aluminum sheets which were attached at the rear side of the PV module as shown in Fig. 5.24a. A thermal grease was used in order to increase thermal conductivity between the rear side of the panel and the aluminum sheet fins. The universal sealant moment silicone gel (white) was also used to hold the various sheets firmly at the back of the panel. An aluminum basin with length and width (95 cm × 40 cm) similar to the solar PV panel was used as a basin to host the water and the ultrasonic humidifier. In order to prevent the transfer of heat from the surrounding environment into the water through the aluminum basin, we used an insulator to rap around the basin.

A 30 W solar polycrystalline PV panel used for the experiment. In order to assess the effect of the cooling mechanism on the efficiency of the PV module, a reference module without any modifications as shown in Fig. 5.24b was also assessed simultaneously with the modified panel. Seven k-type thermocouples were attached at the rear side of each panel to take temperature readings from seven spots in order to find the average temperature of the panel. The temperature range of the thermocouple is -200 ℃ – 1370 ℃ and a resolution of 0,1 ℃. The specifications for the two ultrasonic humidifiers are presented in Table 5.4. The ultrasonic humidifier is presented in Fig. 5.25

**Fig. 5.24** (left) Modified panel with aluminum fins (right) referenced module

**Fig. 5.25** Ultrasonic humidifier

**Table 5.4** Specifications for the ultrasonic humidifier

| Parameter | Value |
|---|---|
| Diameter | 45 mm |
| Atomization amount | 400 cc/har |
| Capacity | 160 ml |
| Voltage | 24 V |
| Power | 14 W |
| Humidification method | Mist discharge |

Heat is transferred from the rear side of the panel to the heat sink which is dissipated into the environment. Heat dissipation from the fins in most studies is facilitated through the help of natural or forced air, however, in this study, the humid environment created by the ultrasonic humidifier in the basin cools the aluminum fins. The vapor that is generated by the ultrasonic also cools the exposed rear surface of the panel which are not covered by the aluminum fins. The experimental test rig is presented in Fig. 5.26.


(a)

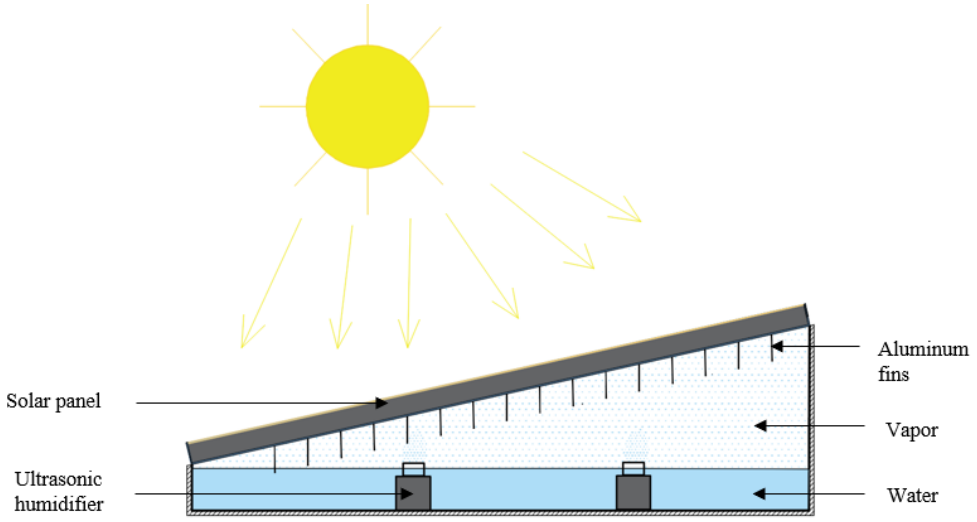


(b)

**Fig. 5.26** (a) Experimental test rig (b) schematic diagram of the proposed system

**Table 5.5.** Accuracies and uncertainties of various instruments

| Instrument | Range | Accuracy | Uncertainty | Error |
|---|---|---|---|---|
| GM 1362-EN-01 thermometer | -30 – 70 °C | ±2% | 1,15% | 2,8% |
| Clamp meter | | ±1.5 | 0,87% | 0,2% |
| Thermocouple | -200 – 1370 °C | ±0.1°C | 0,58% | 3,0% |
| Pyranometer | 0 – 2000 W/m$^2$ | ±0.1 % | 0,058% | 0,1% |

### 5.3.3. Results and Discussion

The whole experimental test was conducted under real environmental conditions from 8:30 to 17:00 on July 8, 2021, in Ekaterinburg. The experimental results were taken in a 30-minute interval. The progression of the ambient temperature, humidity, and the solar irradiation on the day of the experiment is shown in Fig. 5.27. As can be seen from the weather characteristics for the day, the intensity of the solar radiation is highest at 12:30 pm with an intensity of 1235 W/m$^2$. The highest ambient temperature of 31,8 ℃ was also recorded during that same time. The average temperature for the day is 27.79 ℃ with an average humidity of 28,51%. An average solar irradiation of 991,44 W/m$^2$ was also recorded for the day.

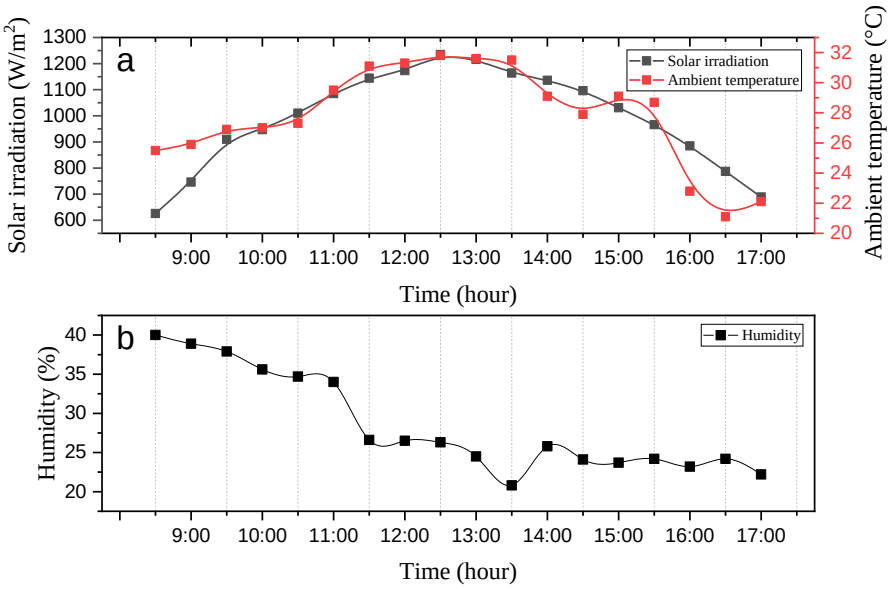


**Fig. 5.27.** (a) solar irradiation and ambient temperature (b) humidity

#### 5.3.3.1. Impact of the cooling mechanism on temperature of panel

The difference between the temperature of the cooled and uncooled modules are illustrated in Fig. 5.28**.** Clearly, the effect of the cooling mechanism on the temperature of the cooled panel is visible from that figure. The cooling mechanism proposed in this study was able to stabilize the temperature of the panel even under very hot temperatures within the day. The maximum temperature 62,1 ℃ for the referenced panel occurred at 13:30 whiles the cooled panel recorded a temperature of 41,59 ℃. This shows the positive

impact of the cooling process on the temperature regulation of the PV module. The cooling mechanism developed in this study was able to reduce the temperature of the module at its highest peak on the day of the experiment by 20,51 ℃. The average temperature of the cooled panel during the entire experimental period is 35,74 ℃ against 50,35 ℃ for the referenced module. On the average, the cooling mechanism was able to reduce the temperature of the panel by 14,61 ℃.

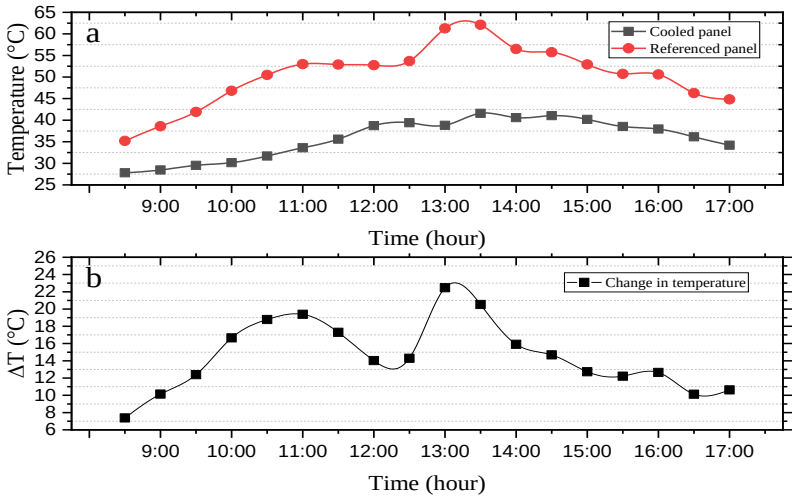


**Fig. 5.28** Variation of temperature for the two panels

An infrared thermal image of the front surface for the two panels is presented in Fig. 5.29, this was taken at mid-day, i.e., 12:00 pm. The maximum temperature of the cooled panel is 39,6 ℃ whiles the referenced panel had a maximum temperature of 50,7 ℃. The cooled panel recorded a minimum value of 31,1 ℃ against 40 ℃ for the referenced module. In effect, it is clear about the positive effect of the cooling mechanism on the cooled panel, it was able to significantly reduce the temperature of the module.

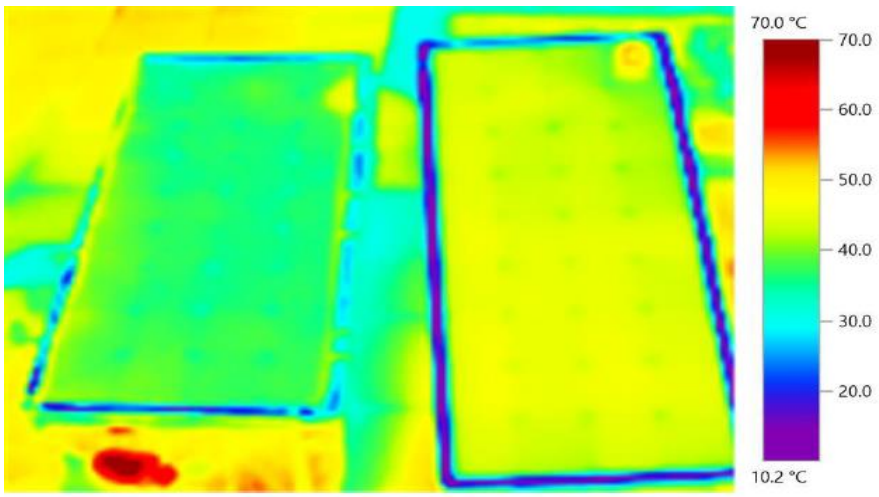


**Fig. 5.29** Thermal image for both panels, cooled (left) referenced (right)

### 5.3.3.2. Electrical analysis of both panels

The effect of the cooling mechanism on the electrical output is discussed in this section. The voltages of both panels are presented in Fig. 5.30a. The effect of the cooling process on the output voltage of the cooled panel is very significant. According to the results from the study, the voltage of the uncooled panel, i.e., the referenced panel decreased considerably with increasing temperature. This confirms what is already known in literature about the negative effect of temperature on PV cells. The maximum voltage of the cooled panel was 18,89 V was recorded around 12:30 pm when the intensity of the solar radiation was highest, the referenced module also recorded its maximum voltage of 17,48 V around that same period. It was around this same period that the highest ambient temperature for the day was also recorded. This implies that the effect of the cooling mechanism on the PV module was positive. The average voltage of the cooled panel for the entire experimental period is 18,69 V against 17,27 V for the referenced module. In effect it can be said that the lack of cooling on the referenced module led to a drop of 1,42 V in its output voltage.

The effect of the cooling process on the current of the panel was however minimal, this is expected because the change in current with increasing temperature is not as significant as that of voltage. The current for both panels remained almost same from the beginning of the experiment until mid-day when the ambient temperature and the temperature of the panels increased sharply. The current of the cooled panel remained relatively stable even

under high temperatures, this is not same for the uncooled panel. In general, the cooled panel recorded an average current of 0,65 A against 0,63 A for the referenced panel. The change in current is not significant, the result for the current is illustrated in Fig. 5.30b.

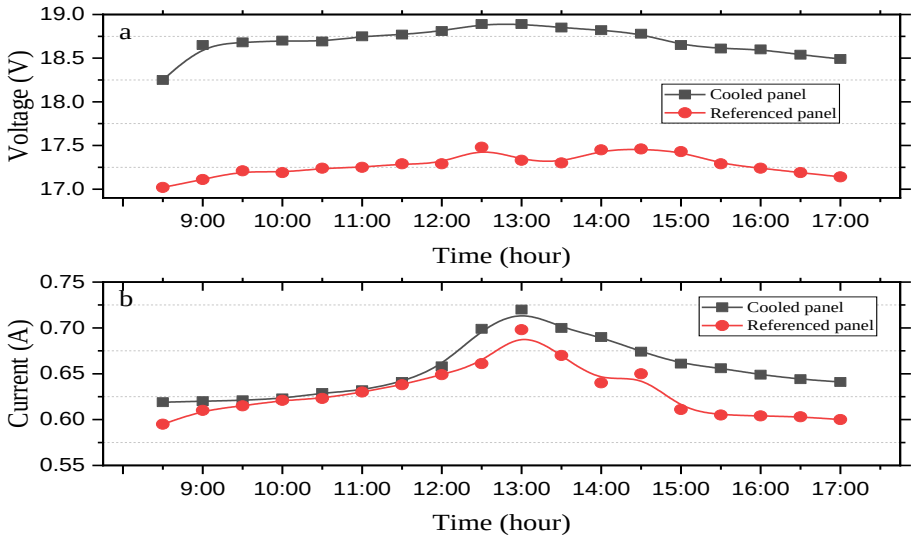


**Fig. 5.30** (a) Voltage (b) current

The power output of the two panels is illustrated in Fig. 5.31. An average power of 12,23 W was recorded for the cooled panel against 10,87 W for the referenced module.

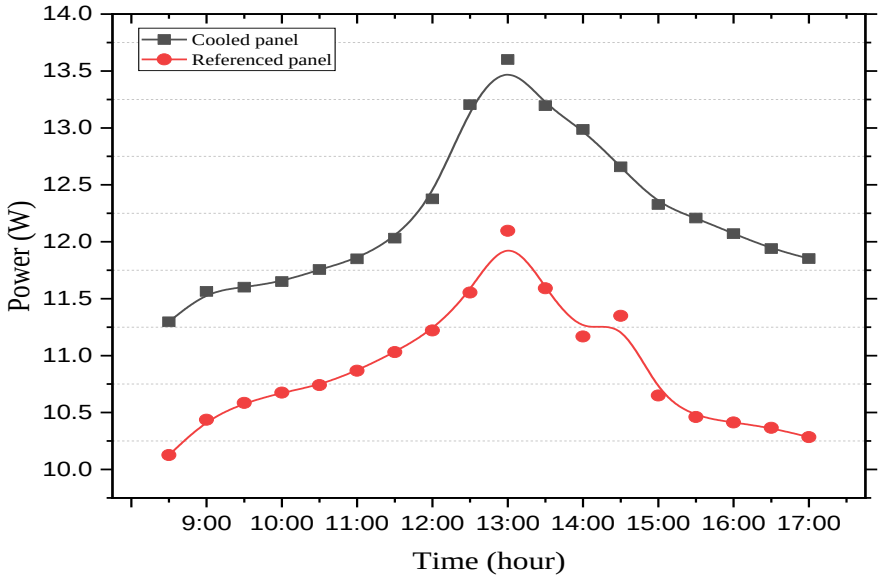


**Fig. 5.31** Output power for both panels

This represent an improvement of 12,51% in the power output of the module due to the integration of the proposed cooling mechanism. As expected, the highest output power for both panels was recorded when the solar irradiation was highest after mid-day.

Efficiency for both panels is as shown in Fig. 5.32 The average efficiency of the cooled panel is 14,4% whiles the referenced module recorded 13,48%, this represent an improvement of 6,8% in the electrical efficiency of the module due to the cooling system.

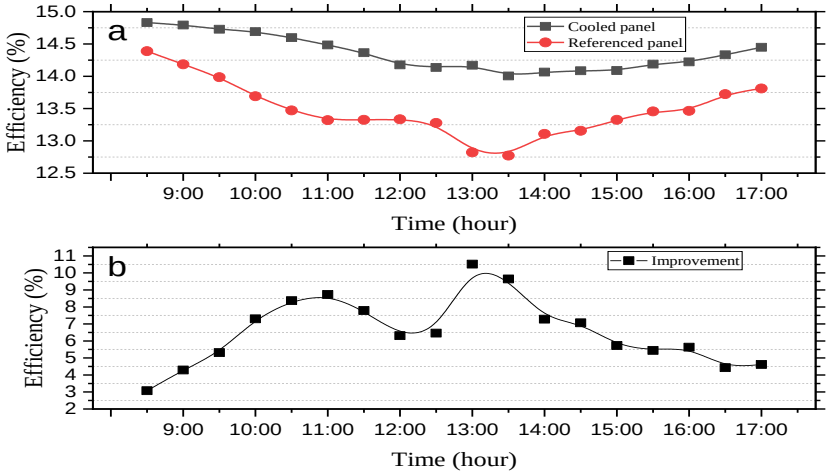


**Fig. 5.32** (a) Efficiency (b) improvement in efficiency

### 5.3.3.3. Water consumption

A total of 15 liters of water was poured into the basin in the beginning of the experiment. At the end of the experiment a total of 13,5 liters was left, which means about 1,5 liters of water was approximately consumed in the course of the experiment, and this is due to evaporation. This translates into a total of 0,015 L/hour water consumption during the experiment.

### 5.3.3.4. Economic analysis

In assessing the economics of the PV system, it is important to evaluate it at least with a one-year period, however, the poor weather conditions in greater part of the year in Russia does not allow such an assessment. To that effect, we assumed that the effective period for the period of operations of the PV system is only during the summer period, i.e., May, June, July, and August, this is equal to 120 days per year. For the purposes of

the economic analysis, we also assumed that the power generation from the PV module is equal throughout this period as recorded in this experiment for the cooled module. We also assumed that the panel generated energy for 12 hours per day. Then the 12,23 W generated by the cooled panel translate to 17,611 kWh per year. However, if all 12 months in a year are taken into consideration, then a total of 40,175 kWh will be the annual energy yield. The aluminum sheet cost 640 rubles which translates to $8,64, however, only a third of it was used for which also translate to $ 2,88. The cost of the used panel and its operations and maintenance cost $C_{O\&M}$ were also assumed to be $50 and $3,00, respectively. The ultrasonic humidifier cost 560 rubles each on Amazon which translate to $7,62. The cost of the basin for storing is also 400 rubles equivalent to $5,45 at an exchange rate of 1 rub = $0,0136. Other installation cost of $5 was assigned (this include the cost of thermal glue, silicone gel and insulation). This translates into a total of $ 78,57 invest cost $C_{inv}$. Fuel is not required in PV power plants so cost of fuel is zero under this circumstance. An effective discount rate and nominal escalation rate of 5% and 1% were applied in this calculations. By the calculations, an LCE of 0,478 $/kWh will be the cost of the PV system for the 120 days and 0,210 $/kWh for a 365-day period for a total of 9 hours of energy generation each day. These figures are less than the 1,57 €/kW h obtained by [231] for their cooled panel.

### 5.4. Conclusion for chapter 5

This section evaluated three methods of cooling a PV module. This include:

- the use of cotton wick, water, aluminum to simultaneously cool the front and rear surface of the PV module. This mechanism led to a temperature drop of 23,55 ℃ for the cooled panel.
- the second experiment combined both aluminum fins and paraffin wax to cool the PV module. The cooled panel's average temperature for the entire experimentation period is 36,62 ℃ against 48,75 ℃ for the referenced PV module, this represents an average reduction of 12,13 ℃.
- a combination of ultrasonic humidifier and aluminum fins, which led to a temperature reduction of 12,13℃.

**General Conclusion**

The paper considers the possibility of strengthening the position of the Republic of Ghana in the field of renewable energy.

Based on modeling, theoretical calculations and experimental studies, the following conclusions can be drawn:

1. The results of the technical and economic assessment of the potential of solar and wind energy are as follows:

- The results for 100 MW CSP, i.e., STPP and PTC, modeled in Navrongo and Tamale show that if they are implemented, Ghana can reduce the current cost of electricity, which is currently is 15-25 cents/kWh, up to 13,67 cents/kWh using the SPP tower type. However, the parabolic type of solar power plant will be too expensive and impracticable. The city of Navrongo has been identified as the best location for the construction of thermodynamic solar power plants in Ghana. The STPP modelled in the two study areas would be able to generate a total of 393 GWh to 424 GWh, while PTC can generate from 190 GWh to 211 GWh per year.
- The northern part of the country has been identified as the location with the greatest potential for a solar photovoltaic power plant. A simulated photovoltaic power plant with a capacity of 20 MW in three parts of the country will be able to produce in the three regions of Ghana 31 GWh, 28 GWh and 28 GWh of energy in the first year for the northern, middle, and southern sectors, respectively.
- The WPP/DG/Battery system in 14 sites of the country recorded LCOE in the range of $0,21–0,22/kWh. However, LCOE can be reduced to 0,10 – 0,13 $/kWh if separate WPPs are built on 14 territorial WPP clusters.

2. A map of Ghana has been developed showing effective locations for large-scale solar and wind farms. Below are the results of the evaluation using the combination of DBSCAN and AHP implemented in QGIS:

- A total of 3 clusters have been identified for the installation of large-scale photovoltaic power plants in Ghana, with the largest potential in the northern part. The AHP results show that Wa located in the Upper West region, i.e., macro-cluster

1 has the largest suitable area for the installation of a large-scale solar photovoltaic power plant (about 264 $km^2$). Macro-cluster 3 is the second largest in the AHP with a total area of 73.75 $km^2$. Macro-cluster 2 ranks third in terms of AHP priority with an area of 123.25 $km^2$.

- A total of 14 territorial clusters of wind turbines were identified for the installation of large-scale wind farms in Ghana. Together these 14 territorial clusters make up approximately 280 $km^2$. The average size of territorial clusters is about 19 $km^2$, the maximum size is up to 32 $km^2$. All found clusters are in relative proximity to the transport networks and the transmission network.

3. It has been experimentally proven that the temperature of the solar cell in hot weather can be reduced by an average of 23,5℃ using the proposed dual-surface cooling mechanism at a lower cost. A decrease in the temperature of the solar cell led to an overall increase in electrical efficiency by 11,9%.
4. Modified PV panel, combined with paraffin stored in cylindrical containers and aluminum plates on its back surface, resulted in a temperature decrease of 12,13 ℃. This resulted in an efficiency increase of 5,15% for the modified PV panel. It has been experimentally proven that the integration of a combination of paraffin wax and aluminum fins on the back surface of the PV panel can reduce the LCOE of the PV panel by 10,5%.
5. The integration of brush-like aluminum fins at the back of the PV panel, cooled by an ultrasonic humidifier, reduced the temperature of the panel by 14,61℃. This led to an increase in the output power of the modified solar cell by 12,51%.

**Recommendations for the use of research materials:**

In order for the state to reach 10% of renewable energy in the country's electricity generation mix by 2030, the following is recommended:

- Creation of an investment climate to support the private sector in the transition to the development and use of renewable energy sources, including, but not limited to investment subsidies, competitive feed-in tariffs and tax exemptions on sales of renewable energy equipment.

- The identified territorial clusters for both wind and PV power plant should be promoted for the country's leadership, local and foreign investors.
- In the study, for the first time, suitable sites for the installation of wind turbines and PV power plants were identified with their contours and sizes, taking into account the existing roads and power lines. This gives the government and investor an idea of the potential costs of developing Ghana's various renewable energy sectors.
- Finally, the method used for the identification of the various suitable sites can be implemented especially in developing countries where infrastructural development is not advanced.

**Abbreviation**

| | |
|---|---|
| AHP | Analytical Hierarchy Process |
| CF | Capacity Factor |
| CI | Consistency index |
| COPRAS | Complex Proportional Assessment |
| CR | Consistency Ratio |
| CW | Criteria Weight |
| CSP | Concentrating Solar Power |
| DBC | Density-Based Clustering |
| DBCA | Density-Based Clustering Approach |
| DG | Diesel Generator |
| DNI | Direct Normal Irradiation |
| ESMAP | Energy Sector Management Assistance Program |
| ¢/kWh | Cent per kilowatt hour |
| LCOE | Levelized Cost of Energy |
| TES | Thermal Energy Storage |
| FANP | Fuzzy Analytic Hierarchy Process |
| FTOPSIS | Fuzzy Technique for Order of Preference by Similarity to Ideal Solution |
| GIS | Geographical Information System |
| GW | Gigawatt |
| GHG | Greenhouse Gases |
| GM | Geometric Mean |
| NPV | Net Present Value |
| SAM | System Advisor Model |
| STP | Solar Thermal Power |
| MW | Megawatt |
| HTF | Heat Transfer Fluid |
| GWh | Gigawatt hour |

| | |
|---|---|
| c€/kWh | Euro cent |
| RE | Renewable Energy |
| PCM | Phase Change Material |
| PTC | Parabolic Trough Collector |
| R&D | Research and Development |
| MCDM | Multi-Criteria Decision Making |
| MPPT | Maximum Power Point Tracking |
| SMCA | Spatial Multi-Criteria Analysis |
| TRI | Terrain Ruggedness Index |
| WACC | Weight Average Cost of Capital |
| WGS | World Geodetic System |
| WPP | Wind Power Plant |

## Appendix

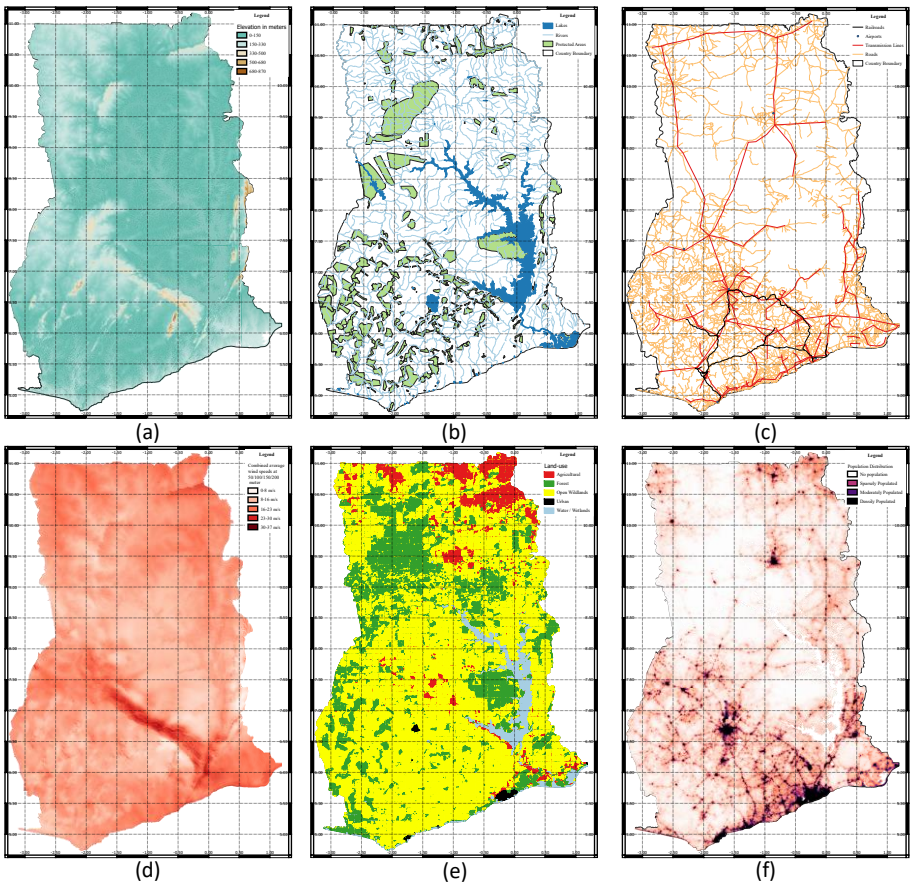


**Fig. A1** Elevation (A), Protected Areas, Lakes, and Rivers (B), Road, Rail, Airports, Transmission network (C), Wind Speeds (D), Land use (E), Population Distribution (F) maps of Ghana

**Table A1** Pairwise comparison matrix

| | Energy availability | Transmission network expansion | Terrain ruggedness | Transportation network expansion |
|---|---|---|---|---|
| Energy availability | 1.00 | 5.00 | 3.00 | 7.00 |
| Transmission network expansion | 0.20 | 1.00 | 0.33 | 2.00 |
| Terrain ruggedness | 0.33 | 3.00 | 1.00 | 4.00 |
| Transportation network expansion | 0.14 | 0.50 | 0.25 | 1.00 |
| Total | 1.67 | 9.50 | 4.58 | 14.00 |

**Table A2** Normalization of matrix

| | Energy availability | Transmission network proximity | Terrain ruggedness | Transportation network proximity | CW |
|---|---|---|---|---|---|
| Energy availability | 0.599 | 0.526 | 0.655 | 0.500 | 0.570 |
| Transmission network proximity | 0.120 | 0.105 | 0.072 | 0.143 | 0.110 |
| Terrain ruggedness | 0.200 | 0.316 | 0.218 | 0.286 | 0.254 |
| Transportation network proximity | 0.084 | 0.053 | 0.055 | 0.071 | 0.065 |
| Total | 1.000 | 1.000 | 1.000 | 1.000 | 1.000 |

**Table A3** Normalized GM

| Criteria | Priority | Rank | Error (+/-) |
|---|---|---|---|
| Energy availability | 0.570 | 1 | 12.7% |
| Transmission network expansion | 0.108 | 3 | 1.9% |
| Terrain ruggedness | 0.253 | 2 | 5.3% |
| Transportation network expansion | 0.066 | 4 | 1.2% |

A CR of 0.02 and a GCI of 0.08 were obtained which indicate that the consistency of the judgements from the experts is acceptable.

References

1. Energy Commission, Ghana [Electronic resource]. 2018. URL: http://www.energycom.gov.gh/ (accessed: 02.11.2020).
2. Gyamfi S., Modjinou M., Djordjevic S. Improving electricity supply security in Ghana—The potential of renewable energy // Renewable and Sustainable Energy Reviews. 2015. Vol. 43. P. 1035–1045.
3. GhanaWeb. The state of the Akosombo Dam [Electronic resource] // GhanaWeb. URL: http://www.ghanaweb.com/GhanaHomePage/NewsArchive/The-state-of-the-Akosombo-Dam-794454?gallery=1 (accessed: 08.03.2022).
4. Afful M.C. Ghana: President Akufo-Addo To Commission Solar Park Project In Lawra [Electronic resource] // Energy News Africa. 2020. URL: https://energynewsafrica.com/index.php/2020/10/09/ghana-president-akufo-addo-to-commission-solar-park-project-in-lawra/ (accessed: 08.03.2022).
5. Pueyo A. What constrains renewable energy investment in Sub-Saharan Africa? A comparison of Kenya and Ghana // World Development. 2018. Vol. 109. P. 85–100.
6. REMP. Ghana Renewable Energy Master Plan. 2019.
7. UNFCC. Ghana's intended nationally determined contribution (INDC) and accompanying explanatory note. 2015. P. 16.
8. Asumadu-Sarkodie S., Asantewaa Owusu P., Sustainable Environment and Energy Systems, Middle East Technical University—Northern Cyprus Campus, Kalkanli, Guzelyurt, TRNC 99738/Mersin 10, Turkey. A review of Ghana's solar energy potential // AIMS Energy. 2016. Vol. 4, № 5. P. 675–696.
9. IRENA. Ghana Renewables Readiness Assessment. 2015. P. 60.
10. Essandoh E.O., Osei E.Y., Adam F.W. Prospects of Wind Power Generation in Ghana // International Journal of Mechanical Engineering and Technology. 2014. Vol. 5, № 10. P. 156–179.
11. UNDP. Renewable Energy Policy Review, Identification of Gaps and Solutions in Ghana. 2015.

12. Eshun M.E., Amoako-Tuffour J. A review of the trends in Ghana's power sector // Energ Sustain Soc. 2016. Vol. 6, № 1. P. 9.
13. Agyekum E.B. Energy poverty in energy rich Ghana: A SWOT analytical approach for the development of Ghana's renewable energy // Sustainable Energy Technologies and Assessments. 2020. Vol. 40. P. 100760.
14. Hossain I. et al. Structural Design Development of a Float Type Wave Micro Power Plant // IOP Conf. Ser.: Mater. Sci. Eng. 2019. Vol. 481. P. 012007.
15. Xorse T.M. Impact of Wave Dynamics on the Coast Of Ghana: Thesis. University of Ghana, 2013.
16. Duku M.H., Gu S., Hagan E.B. Biochar production potential in Ghana—A review // Renewable and Sustainable Energy Reviews. 2011. Vol. 15, № 8. P. 3539–3551.
17. Costa A. et al. Assessment of Renewable Energy Sources Using a Geographical Information System // New and Renewable Technologies for Sustainable Development / ed. Afgan N.H., da Graça Carvalho M. Boston, MA: Springer US, 2002. P. 211–220.
18. ESRI. GIS for Renewables | Spatial Analysis Improves Energy Production & Delivery [Electronic resource]. URL: https://www.esri.com/en-us/industries/natural-resources/segments/renewables (accessed: 06.03.2021).
19. Calvert K., Pearce J.M., Mabee W.E. Toward renewable energy geo-information infrastructures: Applications of GIScience and remote sensing that build institutional capacity // Renewable and Sustainable Energy Reviews. Elsevier, 2013. Vol. 18. P. 416–429.
20. Angelis-Dimakis A. et al. Methods and tools to evaluate the availability of renewable energy sources // Renewable and Sustainable Energy Reviews. 2011. Vol. 15, № 2. P. 1182–1200.
21. Melnikova A. Assessment of renewable energy potentials based on GIS. A case study in southwest region of Russia: PhD. University Koblenz-Landau, 2018.
22. Tahri M., Hakdaoui M., Maanan M. The evaluation of solar farm locations applying Geographic Information System and Multi-Criteria Decision-Making methods: Case

study in southern Morocco // Renewable and Sustainable Energy Reviews. 2015. Vol. 51. P. 1354–1362.

23. Amjad F., Shah L.A. Identification and assessment of sites for solar farms development using GIS and density based clustering technique- A case of Pakistan // Renewable Energy. 2020. Vol. 155. P. 761–769.
24. Fluri T.P. The potential of concentrating solar power in South Africa // Energy Policy. 2009. Vol. 37, № 12. P. 5075–5080.
25. Marques-Perez I. et al. Territorial planning for photovoltaic power plants using an outranking approach and GIS // Journal of Cleaner Production. 2020. Vol. 257. P. 120602.
26. Alami Merrouni A. et al. A GIS-AHP combination for the sites assessment of large-scale CSP plants with dry and wet cooling systems. Case study: Eastern Morocco // Solar Energy. 2018. Vol. 166. P. 2–12.
27. Sindhu S., Nehra V., Luthra S. Investigation of feasibility study of solar farms deployment using hybrid AHP-TOPSIS analysis: Case study of India // Renewable and Sustainable Energy Reviews. 2017. Vol. 73. P. 496–511.
28. Mensour O.N. et al. A geographical information system-based multi-criteria method for the evaluation of solar farms locations: A case study in Souss-Massa area, southern Morocco // Energy. 2019. Vol. 182. P. 900–919.
29. Doljak D., Stanojević G. Evaluation of natural conditions for site selection of ground-mounted photovoltaic power plants in Serbia // Energy. 2017. Vol. 127. P. 291–300.
30. Doorga J.R.S., Rughooputh S.D.D.V., Boojhawon R. Multi-criteria GIS-based modelling technique for identifying potential solar farm sites: A case study in Mauritius // Renewable Energy. 2019. Vol. 133. P. 1201–1219.
31. Martin D. Geographic Information Systems: Socioeconomic Applications. Psychology Press, 1996. 230 p.
32. Olaofe Z.O. Review of energy systems deployment and development of offshore wind energy resource map at the coastal regions of Africa // Energy. 2018. Vol. 161. P. 1096–1114.

33. He J. et al. Spatiotemporal analysis of offshore wind field characteristics and energy potential in Hong Kong // Energy. 2020. Vol. 201. P. 117622.
34. Jangid J. et al. Potential zones identification for harvesting wind energy resources in desert region of India – A multi criteria evaluation approach using remote sensing and GIS // Renewable and Sustainable Energy Reviews. 2016. Vol. 65. P. 1–10.
35. Quantum G.I.S. Development Team.(2013). Quantum GIS geographic information system. Open Source Geospatial Foundation Project. 2013.
36. Team C.R. Team RDC. R: A language and environment for statistical computing. R Foundation for statistical computing: Vienna, Austria // Computing. 2013. Vol. 1. P. 12–21.
37. Hennig C. fpc: Flexible procedures for clustering. R package version 2.1-5. 2013.
38. Kassambara A., Mundt F. Factoextra: Extract and visualize the results of multivariate data analyses. R package version 1.04. 999 // Available ao hoop://www. sohda. com/english/rpkgs/facooexora. 2017.
39. Kahle D., Wickham H. ggmap: Spatial Visualization with ggplot2 // The R journal. 2013. Vol. 5, № 1. P. 144–161.
40. NREL. RED-E Ghana [Electronic resource]. URL: https://maps.nrel.gov/rede-ghana/?aL=33LD6x%255Bv%255D%3Dt&bL=clight&cE=0&lR=0&mC=7.98851761453913%2C0.5548095703125&zL=7 (accessed: 05.11.2020).
41. Protected Planet | Ghana [Electronic resource] // Protected Planet. URL: https://www.protectedplanet.net/country/GH (accessed: 17.11.2020).
42. Linard C. et al. Population Distribution, Settlement Patterns and Accessibility across Africa in 2010 // PLoS ONE / ed. Schumann G.J.-P. 2012. Vol. 7, № 2. P. e31743.
43. Tatem A.J. WorldPop, open data for spatial demography: 1 // Scientific Data. Nature Publishing Group, 2017. Vol. 4, № 1. P. 170004.
44. Global Wind Atlas [Electronic resource]. URL: https://globalwindatlas.info/ (accessed: 17.11.2020).

45. Tegou L.-I., Polatidis H., Haralambopoulos D.A. Environmental management framework for wind farm siting: Methodology and case study // Journal of Environmental Management. 2010. Vol. 91, № 11. P. 2134–2147.
46. Höfer T. et al. Wind farm siting using a spatial Analytic Hierarchy Process approach: A case study of the Städteregion Aachen // Applied Energy. 2016. Vol. 163. P. 222–243.
47. Ali S. et al. GIS based site suitability assessment for wind and solar farms in Songkhla, Thailand // Renewable Energy. 2019. Vol. 132. P. 1360–1372.
48. Uyan M. GIS-based solar farms site selection using analytic hierarchy process (AHP) in Karapinar region, Konya/Turkey // Renewable and Sustainable Energy Reviews. 2013. Vol. 28. P. 11–17.
49. Amankwah E. Environmental Impact Assessment (EIA); A Useful Tool to Address Climate Change in Ghana // IJEPP. 2013. Vol. 1, № 4. P. 94.
50. Baseer M.A. et al. GIS-based site suitability analysis for wind farm development in Saudi Arabia // Energy. 2017. Vol. 141. P. 1166–1176.
51. MacQueen J. Some methods for classification and analysis of multivariate observations. University of California Press, 1967. Vol. 1.
52. Kaufman L., Rousseeuw P.J. Partitioning around medoids (program pam) // Finding groups in data: an introduction to cluster analysis. Wiley New York, 1990. Vol. 344. P. 68–125.
53. Kassambara A. Practical Guide to Cluster Analysis in R. Unsupervised Machine Learning. STHDA, 2017.
54. Ester M. et al. A density-based algorithm for discovering clusters in large spatial databases with noise. // Kdd. 1996. Vol. 96, № 34. P. 226–231.
55. Sander J. et al. Density-based clustering in spatial databases: The algorithm gdbscan and its applications // Data mining and knowledge discovery. Springer, 1998. Vol. 2, № 2. P. 169–194.
56. Saaty T. L. 1980 // The analytic hierarchy process. 1990.

57. Saaty T.L. What is the Analytic Hierarchy Process? // Mathematical Models for Decision Support / ed. Mitra G. et al. Berlin, Heidelberg: Springer, 1988. P. 109–121.
58. Agyekum E.B. et al. A bird's eye view of Ghana's renewable energy sector environment: A Multi-Criteria Decision-Making approach // Utilities Policy. 2021. Vol. 70. P. 101219.
59. Ali E.B., Agyekum E.B., Adadi P. Agriculture for Sustainable Development: A SWOT-AHP Assessment of Ghana's Planting for Food and Jobs Initiative: 2 // Sustainability. Multidisciplinary Digital Publishing Institute, 2021. Vol. 13, № 2. P. 628.
60. Goepel K.D. Implementing the Analytic Hierarchy Process as a Standard Method for Multi-Criteria Decision Making in Corporate Enterprises – a New AHP Excel Template with Multiple Inputs. 2013.
61. Goepel K.D. New AHP Excel template with multiple inputs – BPMSG [Electronic resource]. URL: https://bpmsg.com/new-ahp-excel-template-with-multiple-inputs/ (accessed: 19.07.2021).
62. Goepel K.D. Implementation of an Online Software Tool for the Analytic Hierarchy Process (AHP-OS): 3 // International Journal of the Analytic Hierarchy Process. 2018. Vol. 10, № 3.
63. Agyekum E.B., Nutakor C. Feasibility study and economic analysis of stand-alone hybrid energy system for southern Ghana // Sustainable Energy Technologies and Assessments. 2020. Vol. 39. P. 100695.
64. Suzer A., Atasoy V., Eckici S. Developing a holistic simulation approach for parametric techno-economic analysis of wind energy // Energy Policy. 2021. Vol. 149. P. 112105.
65. Bilal B. et al. Determination of wind potential characteristics and techno-economic feasibility analysis of wind turbines for Northwest Africa // Energy. 2021. Vol. 218. P. 119558.

66. Mahian O. et al. Optimal sizing and performance assessment of a hybrid combined heat and power system with energy storage for residential buildings // Energy Conversion and Management. 2020. Vol. 211. P. 112751.
67. Ali F. et al. A techno-economic assessment of hybrid energy systems in rural Pakistan // Energy. 2021. Vol. 215. P. 119103.
68. Ruegg R.T., Marshall H.E. Payback (PB) // Building Economics: Theory and Practice / ed. Ruegg R.T., Marshall H.E. Boston, MA: Springer US, 1990. P. 92–104.
69. Azimoh C.L. et al. Electricity for development: Mini-grid solution for rural electrification in South Africa // Energy Conversion and Management. 2016. Vol. 110. P. 268–277.
70. Energy Commission. 2020 Energy (Supply and Demand) Outlook for Ghana. 2020.
71. Kousky C. et al. Return on investment analysis and its applicability to community disaster preparedness activities: Calculating costs and returns // International Journal of Disaster Risk Reduction. 2019. Vol. 41. P. 101296.
72. Zamfir M., Manea M.D., Ionescu L. Return on Investment – Indicator for Measuring the Profitability of Invested Capital // Valahian Journal of Economic Studies. Sciendo, 2016. Vol. 7, № 2. P. 79–86.
73. Said Z. et al. Central versus off-grid photovoltaic system, the optimum option for the domestic sector based on techno-economic-environmental assessment for United Arab Emirates // Sustainable Energy Technologies and Assessments. 2021. Vol. 43. P. 100944.
74. Narasimhan. Area Required for Solar PV Power Plants [Electronic resource]. 2014. URL: http://www.suncyclopedia.com/en/area-required-for-solar-pv-power-plants/ (accessed: 22.10.2020).
75. Ong S. et al. Land-Use Requirements for Solar Power Plants in the United States: NREL/TP-6A20-56290, 1086349. 2013. P. NREL/TP-6A20-56290, 1086349.

76. Aly A., Jensen S.S., Pedersen A.B. Solar power potential of Tanzania: Identifying CSP and PV hot spots through a GIS multicriteria decision making analysis // Renewable Energy. 2017. Vol. 113. P. 159–175.
77. Charabi Y., Gastli A. PV site suitability analysis using GIS-based spatial fuzzy multi-criteria evaluation // Renewable Energy. 2011. Vol. 36, № 9. P. 2554–2561.
78. Al Garni H.Z., Awasthi A. Solar PV power plant site selection using a GIS-AHP based approach with application in Saudi Arabia // Applied Energy. 2017. Vol. 206. P. 1225–1240.
79. Hott R., Santini R., Brownson J. GIS-based Spatial Analysis For Large-Scale Solar Power And Transmission Line Issues: Case Study Of Wyoming, U.S. 2012.
80. Solargis. Global Solar Atlas [Electronic resource]. URL: https://globalsolaratlas.info/download/china (accessed: 01.11.2020).
81. JAXA. What is remote sensing? [Electronic resource]. URL: https://www.eorc.jaxa.jp/ (accessed: 03.12.2020).
82. Adortse P. Coastal flood hazard assessment of Ghana. Salem State University, 2019.
83. Murnane R., Simpson A., Jongman B. Understanding risk: what makes a risk assessment successful? // International Journal of Disaster Resilience in the Built Environment. Emerald Group Publishing Limited, 2016. Vol. 7, № 2. P. 186–200.
84. UNOSAT. UNOSAT Flood Portal [Electronic resource]. URL: http://floods.unosat.org/geoportal/catalog/main/home.page (accessed: 06.11.2020).
85. LaFree G., Dugan L. Introducing the Global Terrorism Database // Terrorism and Political Violence. 2007. Vol. 19, № 2. P. 181–204.
86. Colak H.E., Memisoglu T., Gercek Y. Optimal site selection for solar photovoltaic (PV) power plants using GIS and AHP: A case study of Malatya Province, Turkey // Renewable Energy. 2020. Vol. 149. P. 565–576.
87. Mason G.T., Arndt R.E. Mineral Resources Data System (MRDS): USGS Numbered Series 20 // Mineral Resources Data System (MRDS). The Survey, 1996. Vol. 20.
88. Ministry of Petroleum. Ghana gas pipeline master plan. 2016.

89. Zoghi M. et al. Optimization solar site selection by fuzzy logic model and weighted linear combination method in arid and semi-arid region: A case study Isfahan-IRAN // Renewable and Sustainable Energy Reviews. 2017. Vol. 68. P. 986–996.
90. Smith M.W. Roughness in the Earth Sciences // Earth-Science Reviews. 2014. Vol. 136. P. 202–225.
91. Lindsay J.B., Newman D.R., Francioni A. Scale-Optimized Surface Roughness for Topographic Analysis: 7 // Geosciences. Multidisciplinary Digital Publishing Institute, 2019. Vol. 9, № 7. P. 322.
92. Sánchez-Lozano J.M. et al. GIS-based photovoltaic solar farms site selection using ELECTRE-TRI: Evaluating the case for Torre Pacheco, Murcia, Southeast of Spain // Renewable Energy. 2014. Vol. 66. P. 478–494.
93. Ghose D. et al. Siting high solar potential areas using Q-GIS in West Bengal, India // Sustainable Energy Technologies and Assessments. Elsevier, 2020. Vol. 42. P. 100864.
94. Noorollahi E. et al. Land Suitability Analysis for Solar Farms Exploitation Using GIS and Fuzzy Analytic Hierarchy Process (FAHP)—A Case Study of Iran: 8 // Energies. Multidisciplinary Digital Publishing Institute, 2016. Vol. 9, № 8. P. 643.
95. Powell K.M. et al. Hybrid concentrated solar thermal power systems: A review // Renewable and Sustainable Energy Reviews. Elsevier, 2017. Vol. 80. P. 215–237.
96. Rashid K., Mohammadi K., Powell K. Dynamic simulation and techno-economic analysis of a concentrated solar power (CSP) plant hybridized with both thermal energy storage and natural gas // Journal of Cleaner Production. Elsevier, 2020. Vol. 248. P. 119193.
97. Rashid K., Sheha M.N., Powell K.M. Real-time optimization of a solar-natural gas hybrid power plant to enhance solar power utilization // 2018 Annual American Control Conference (ACC). IEEE, 2018. P. 3002–3007.
98. Aly A. et al. Is Concentrated Solar Power (CSP) a feasible option for Sub-Saharan Africa?: Investigating the techno-economic feasibility of CSP in Tanzania // Renewable Energy. 2019. Vol. 135. P. 1224–1240.

99. Islam M.T., Huda N., Saidur R. Current energy mix and techno-economic analysis of concentrating solar power (CSP) technologies in Malaysia // Renewable Energy. 2019. Vol. 140. P. 789–806.
100. Abaza M.A. et al. 10 MW concentrated solar power (CSP) plant operated by 100% solar energy: Sizing and techno-economic optimization // Alexandria Engineering Journal. Elsevier, 2020. Vol. 59, № 1. P. 39–47.
101. Andika R. et al. Techno-economic assessment of technological improvements in thermal energy storage of concentrated solar power // Solar Energy. Elsevier, 2017. Vol. 157. P. 552–558.
102. Belgasim B. et al. The potential of concentrating solar power (CSP) for electricity generation in Libya // Renewable and sustainable energy reviews. Elsevier, 2018. Vol. 90. P. 1–15.
103. Purohit I., Purohit P. Techno-economic evaluation of concentrating solar power generation in India // Energy policy. Elsevier, 2010. Vol. 38, № 6. P. 3015–3029.
104. Fritsch A., Frantz C., Uhlig R. Techno-economic analysis of solar thermal power plants using liquid sodium as heat transfer fluid // Solar Energy. Elsevier, 2019. Vol. 177. P. 155–162.
105. Steinhagen H.M., Trieb F. Concentrating solar power, a review of the technology // Ingenia. 2004. Vol. 18. P. 43–50.
106. Barlev D., Vidu R., Stroeve P. Innovation in concentrated solar power // Solar energy materials and solar cells. Elsevier, 2011. Vol. 95, № 10. P. 2703–2725.
107. Asdrubali F. et al. Life cycle assessment of electricity production from renewable energies: Review and results harmonization // Renewable and Sustainable Energy Reviews. Elsevier, 2015. Vol. 42. P. 1113–1122.
108. Soomro M.I. et al. Performance and economic analysis of concentrated solar power generation for Pakistan // Processes. Multidisciplinary Digital Publishing Institute, 2019. Vol. 7, № 9. P. 575.

109. Hernández-Moro J., Martinez-Duart J.M. Analytical model for solar PV and CSP electricity costs: Present LCOE values and their future evolution // Renewable and Sustainable Energy Reviews. Elsevier, 2013. Vol. 20. P. 119–132.
110. Purohit I., Purohit P., Shekhar S. Evaluating the potential of concentrating solar power generation in Northwestern India // Energy policy. Elsevier, 2013. Vol. 62. P. 157–175.
111. Parrado C. et al. 2050 LCOE (Levelized Cost of Energy) projection for a hybrid PV (photovoltaic)-CSP (concentrated solar power) plant in the Atacama Desert, Chile // Energy. Elsevier, 2016. Vol. 94. P. 422–430.
112. Kabir E. et al. Solar energy: Potential and future prospects // Renewable and Sustainable Energy Reviews. Elsevier, 2018. Vol. 82. P. 894–900.
113. Solargis. Global Solar Atlas, Ghana [Electronic resource]. URL: https://globalsolaratlas.info/download/ghana (accessed: 22.04.2021).
114. Kamel S. et al. Comparative Analysis of Rankine Cycle Linear Fresnel Reflector and Solar Tower Plant Technologies: Techno-Economic Analysis for Ethiopia: 3 // Sustainability. Multidisciplinary Digital Publishing Institute, 2022. Vol. 14, № 3. P. 1677.
115. Trabelsi S.E. et al. Techno-economic performance of concentrating solar power plants under the climatic conditions of the southern region of Tunisia // Energy Conversion and Management. 2016. Vol. 119. P. 203–214.
116. Duffie J.A., Beckman W.A., Blair N. Solar engineering of thermal processes, photovoltaics and wind. John Wiley & Sons, 2020.
117. Duffie J.A., Beckman W.A. Solar Engineering of Thermal Processes, 54–55 (1991). John Wiley & Sons, New York.
118. Li X. et al. Modeling and simulation of a novel combined heat and power system with absorption heat pump based on solar thermal power tower plant // Energy. 2019. Vol. 186. P. 115842.

119. Ahmadi M.H. et al. Solar power technology for electricity generation: A critical review // Energy Science & Engineering. Wiley Online Library, 2018. Vol. 6, № 5. P. 340–361.
120. Franchini G. et al. A comparative study between parabolic trough and solar tower technologies in Solar Rankine Cycle and Integrated Solar Combined Cycle plants // Solar Energy. Elsevier, 2013. Vol. 98. P. 302–314.
121. Li C. et al. Annual performance analysis and optimization of a solar tower aided coal-fired power plant // Applied Energy. Elsevier, 2019. Vol. 237. P. 440–456.
122. Wagner M.J., Klein S.A., Reindl D.T. Simulation of utility-scale central receiver system power plants // Energy Sustainability. 2009. Vol. 48906. P. 605–614.
123. IRENA. Renewable Energy Technologies: Cost Analysis Series, Concentrating Solar Power (CSP). 2012. P. 1–48.
124. Chandel M. et al. Techno-economic analysis of solar photovoltaic power plant for garment zone of Jaipur city // Case Studies in Thermal Engineering. Elsevier, 2014. Vol. 2. P. 1–7.
125. Labordena M. et al. Impact of political and economic barriers for concentrating solar power in Sub-Saharan Africa // Energy Policy. 2017. Vol. 102. P. 52–72.
126. Zhao Z.-Y., Chen Y.-L., Thomson J.D. Levelized cost of energy modeling for concentrated solar power projects: A China study // Energy. 2017. Vol. 120. P. 117–127.
127. Trading Economics. United States Inflation Rate | 2021 Data | 2022 Forecast | 1914-2020 Historical [Electronic resource]. URL: https://tradingeconomics.com/united-states/inflation-cpi (accessed: 07.11.2021).
128. Taxes for Expats. Simple Tax Guide for Americans in Ghana [Electronic resource]. URL: https://www.taxesforexpats.com/country_guides/ghana/us-tax-preparation-in-ghana.html (accessed: 07.11.2021).
129. Trading Economics. Ghana Interest Rate | 2021 Data | 2022 Forecast | 2002-2020 Historical | Calendar [Electronic resource]. URL: https://tradingeconomics.com/ghana/interest-rate (accessed: 07.11.2021).

130. Kincaid N. et al. An optical performance comparison of three concentrating solar power collector designs in linear Fresnel, parabolic trough, and central receiver // Applied energy. Elsevier, 2018. Vol. 231. P. 1109–1121.
131. Awan A.B. et al. Design and comparative analysis of photovoltaic and parabolic trough based CSP plants // Solar Energy. Elsevier, 2019. Vol. 183. P. 551–565.
132. Collado F.J., Guallar J. A review of optimized design layouts for solar power tower plants with campo code // Renewable and Sustainable Energy Reviews. Elsevier, 2013. Vol. 20. P. 142–154.
133. Collado F.J., Guallar J. Two-stages optimised design of the collector field of solar power tower plants // Solar Energy. Elsevier, 2016. Vol. 135. P. 884–896.
134. Kassem A., Al-Haddad K., Komljenovic D. Concentrated solar thermal power in Saudi Arabia: Definition and simulation of alternative scenarios // Renewable and Sustainable Energy Reviews. Elsevier, 2017. Vol. 80. P. 75–91.
135. IRENA. Renewable Power Generation Costs in 2019 [Electronic resource] // /publications/2020/Jun/Renewable-Power-Costs-in-2019. URL: /publications/2020/Jun/Renewable-Power-Costs-in-2019 (accessed: 23.11.2020).
136. Li Y., Yuan J., Yang Y. A study on solar multiple for an integrated solar combined cycle system with direct steam generation // Energy Procedia. Elsevier, 2014. Vol. 61. P. 29–32.
137. Lunz B. et al. Evaluating the value of concentrated solar power in electricity systems with fluctuating energy sources // AIP Conference Proceedings. AIP Publishing LLC, 2016. Vol. 1734, № 1. P. 160010.
138. Mehos M. et al. An assessment of the net value of CSP systems integrated with thermal energy storage // Energy Procedia. Elsevier, 2015. Vol. 69. P. 2060–2071.
139. Yang X. et al. Effect of government subsidies on renewable energy investments: The threshold effect // Energy Policy. Elsevier, 2019. Vol. 132. P. 156–166.
140. Punda L. et al. Integration of renewable energy sources in southeast Europe: A review of incentive mechanisms and feasibility of investments // Renewable and Sustainable Energy Reviews. Elsevier, 2017. Vol. 71. P. 77–88.

141. Krishnamurthy P., Mishra S., Banerjee R. An analysis of costs of parabolic trough technology in India // Energy Policy. Elsevier, 2012. Vol. 48. P. 407–419.
142. Balghouthi M. et al. Potential of concentrating solar power (CSP) technology in Tunisia and the possibility of interconnection with Europe // Renewable and Sustainable Energy Reviews. Elsevier, 2016. Vol. 56. P. 1227–1248.
143. Bhuiyan N. et al. Performance optimisation of parabolic trough solar thermal power plants–a case study in Bangladesh // International Journal of Sustainable Energy. Taylor & Francis, 2020. Vol. 39, № 2. P. 113–131.
144. Luo Y. et al. Impacts of solar multiple on the performance of direct steam generation solar power tower plant with integrated thermal storage // Frontiers in Energy. Springer, 2017. Vol. 11, № 4. P. 461–471.
145. Agyekum E.B., Velkin V.I. Optimization and techno-economic assessment of concentrated solar power (CSP) in South-Western Africa: A case study on Ghana // Sustainable Energy Technologies and Assessments. 2020. Vol. 40. P. 100763.
146. Photovoltaics [Electronic resource] // SEIA. URL: https://www.seia.org/initiatives/photovoltaics (accessed: 03.11.2020).
147. Bhakta S., Mukherjee V. Performance indices evaluation and techno economic analysis of photovoltaic power plant for the application of isolated India's island // Sustainable Energy Technologies and Assessments. 2017. Vol. 20. P. 9–24.
148. Li C., Zhou D., Zheng Y. Techno-economic comparative study of grid-connected PV power systems in five climate zones, China // Energy. 2018. Vol. 165. P. 1352–1369.
149. Pan Y. et al. Feasibility analysis on distributed energy system of Chongming County based on RETScreen software // Energy. 2017. Vol. 130. P. 298–306.
150. Kymakis E., Kalykakis S., Papazoglou T.M. Performance analysis of a grid connected photovoltaic park on the island of Crete // Energy Conversion and Management. 2009. Vol. 50, № 3. P. 433–438.
151. Dobaria B., Pandya M., Aware M. Analytical assessment of 5.05 kWp grid tied photovoltaic plant performance on the system level in a composite climate of western India // Energy. 2016. Vol. 111. P. 47–51.

152. Emmanuel M., Akinyele D., Rayudu R. Techno-economic analysis of a 10 kWp utility interactive photovoltaic system at Maungaraki school, Wellington, New Zealand // Energy. 2017. Vol. 120. P. 573–583.
153. de Lima L.C., de Araújo Ferreira L., de Lima Morais F.H.B. Performance analysis of a grid connected photovoltaic system in northeastern Brazil // Energy for Sustainable Development. 2017. Vol. 37. P. 79–85.
154. Pillai G., Naser H.A.Y. Techno-economic potential of largescale photovoltaics in Bahrain // Sustainable Energy Technologies and Assessments. 2018. Vol. 27. P. 40–45.
155. Download - System Advisor Model (SAM) [Electronic resource]. URL: https://sam.nrel.gov/download.html (accessed: 03.11.2020).
156. Singh A., Baredar P., Gupta B. Techno-economic feasibility analysis of hydrogen fuel cell and solar photovoltaic hybrid renewable energy system for academic research building // Energy Conversion and Management. 2017. Vol. 145. P. 398–414.
157. Fu R., Feldman D.J., Margolis R.M. U.S. Solar Photovoltaic System Cost Benchmark: Q1 2018: NREL/TP-6A20-72399. National Renewable Energy Lab. (NREL), Golden, CO (United States), 2018.
158. Edalati S. et al. Technical and economic assessments of grid-connected photovoltaic power plants: Iran case study // Energy. 2016. Vol. 114. P. 923–934.
159. Peippo K., Lund P.D. Optimal sizing of solar array and inverter in grid-connected photovoltaic systems // Solar Energy Materials and Solar Cells. 1994. Vol. 32, № 1. P. 95–114.
160. Martín-Martínez S. et al. Performance evaluation of large solar photovoltaic power plants in Spain // Energy Conversion and Management. 2019. Vol. 183. P. 515–528.
161. Schenkelberg F. 11 - Reliability modeling and accelerated life testing for solar power generation systems // Reliability Characterisation of Electrical and Electronic Systems / ed. Swingler J. Oxford: Woodhead Publishing, 2015. P. 215–250.

162. Said M., EL-Shimy M., Abdelraheem M.A. Photovoltaics energy: Improved modeling and analysis of the levelized cost of energy (LCOE) and grid parity – Egypt case study // Sustainable Energy Technologies and Assessments. 2015. Vol. 9. P. 37–48.
163. Hernández-Moro J., Martínez-Duart J.M. Analytical model for solar PV and CSP electricity costs: Present LCOE values and their future evolution // Renewable and Sustainable Energy Reviews. 2013. Vol. 20. P. 119–132.
164. Alonso G., Bilbao S., Valle E. del. Economic competitiveness of small modular reactors versus coal and combined cycle plants // Energy. 2016. Vol. 116. P. 867–879.
165. Khatib H. The discount rate-a tool for managing risk in energy investments // Risk. 2012. Vol. 2002, № 8.71. P. 1–65.
166. World Bank. Risk Allocation, Bankability and Mitigation in Project Financed Transactions | Public private partnership [Electronic resource]. 2019. URL: https://ppp.worldbank.org/public-private-partnership/financing/risk-allocation-mitigation (accessed: 03.11.2020).
167. Valenzuela C. et al. CSP+PV hybrid solar plants for power and water cogeneration in northern Chile // Solar Energy. 2017. Vol. 157. P. 713–726.
168. Agyekum E.B., Velkin V.I., Hossain I. Sustainable energy: Is it nuclear or solar for African Countries? Case study on Ghana // Sustainable Energy Technologies and Assessments. 2020. Vol. 37. P. 100630.
169. Lazard.com | Levelized Cost of Energy and Levelized Cost of Storage 2018 [Electronic resource]. URL: https://www.lazard.com/perspective/levelized-cost-of-energy-and-levelized-cost-of-storage-2018 (accessed: 03.11.2020).
170. Zhao L. et al. Economic analysis of solar energy development in North Africa // Global Energy Interconnection. 2018. Vol. 1, № 1. P. 53–62.
171. Rehman S., Al-Hadhrami L.M. Study of a solar PV–diesel–battery hybrid power system for a remotely located population near Rafha, Saudi Arabia // Energy. Elsevier, 2010. Vol. 35, № 12. P. 4986–4995.

172. Bhattacharjee S., Acharya S. PV–wind hybrid power option for a low wind topography // Energy Conversion and Management. Elsevier, 2015. Vol. 89. P. 942–954.
173. Mondal A.H., Denich M. Hybrid systems for decentralized power generation in Bangladesh // Energy for sustainable development. Elsevier, 2010. Vol. 14, № 1. P. 48–55.
174. Baghdadi F. et al. Feasibility study and energy conversion analysis of stand-alone hybrid renewable energy system // Energy Conversion and Management. 2015. Vol. 105. P. 471–479.
175. Odou O.D.T., Bhandari R., Adamou R. Hybrid off-grid renewable power system for sustainable rural electrification in Benin // Renewable Energy. 2020. Vol. 145. P. 1266–1279.
176. Adaramola M.S. et al. Multipurpose renewable energy resources based hybrid energy system for remote community in northern Ghana // Sustainable Energy Technologies and Assessments. Elsevier, 2017. Vol. 22. P. 161–170.
177. Lambert T., Gilman P., Lilienthal P. Micropower system modeling with HOMER // Integration of alternative sources of energy. John Wiley & Sons New York, NY, USA, 2006. Vol. 1, № 1. P. 379–385.
178. Global petrol prices. Ghana diesel prices [Electronic resource] // GlobalPetrolPrices.com. URL: https://www.globalpetrolprices.com/Ghana/diesel_prices/ (accessed: 24.09.2019).
179. Ansong M., Mensah L.D., Adaramola M.S. Techno-economic analysis of a hybrid system to power a mine in an off-grid area in Ghana // Sustainable Energy Technologies and Assessments. Elsevier, 2017. Vol. 23. P. 48–56.
180. Shezan S.K.A., Das N., Mahmudul H. Techno-economic analysis of a smart-grid hybrid renewable energy system for Brisbane of Australia // Energy Procedia. Elsevier, 2017. Vol. 110. P. 340–345.

181. Salisu S. et al. Assessment of technical and economic feasibility for a hybrid PV-wind-diesel-battery energy system in a remote community of north central Nigeria // Alexandria Engineering Journal. 2019. Vol. 58, № 4. P. 1103–1118.
182. Bhattacharya M. et al. The effect of renewable energy consumption on economic growth: Evidence from top 38 countries // Applied Energy. Elsevier, 2016. Vol. 162. P. 733–741.
183. Kumi E.N. The Electricity Situation in Ghana: Challenges and Opportunities. P. 30.
184. Lin B., Ankrah I. Renewable energy (electricity) development in Ghana: Observations, concerns, substitution possibilities, and implications for the economy. // Journal of Cleaner Production. 2019. Vol. 233. P. 1396–1409.
185. Agyekum E.B., Ansah M.N.S., Afornu K.B. Nuclear energy for sustainable development: SWOT analysis on Ghana's nuclear agenda // Energy Reports. 2020. Vol. 6. P. 107–115.
186. Atsu D., Agyemang E.O., Tsike S.A.K. Solar electricity development and policy support in Ghana // Renewable and Sustainable Energy Reviews. 2016. Vol. 53. P. 792–800.
187. Dahmoun M.E.-H. et al. Performance evaluation and analysis of grid-tied large scale PV plant in Algeria // Energy for Sustainable Development. 2021. Vol. 61. P. 181–195.
188. Homadi A., Hall T., Whitman L. Study a novel hybrid system for cooling solar panels and generate power // Applied Thermal Engineering. 2020. Vol. 179. P. 115503.
189. Alwan N.T., Shcheklein S.E., Ali O.M. Experimental investigation of modified solar still integrated with solar collector // Case Studies in Thermal Engineering. 2020. Vol. 19. P. 100614.
190. Alwan N.T., Shcheklein S.E., Ali O.M. Experimental analysis of thermal performance for flat plate solar water collector in the climate conditions of Yekaterinburg, Russia // Materials Today: Proceedings. 2021. Vol. 42. P. 2076–2083.

191. Ahmad F.F. et al. Performance enhancement and infra-red (IR) thermography of solar photovoltaic panel using back cooling from the waste air of building centralized air conditioning system // Case Studies in Thermal Engineering. 2021. Vol. 24. P. 100840.
192. Agbo Emmanuel.P. et al. Solar energy: A panacea for the electricity generation crisis in Nigeria // Heliyon. 2021. Vol. 7, № 5. P. e07016.
193. Skoplaki E., Palyvos J.A. On the temperature dependence of photovoltaic module electrical performance: A review of efficiency/power correlations // Solar Energy. 2009. Vol. 83, № 5. P. 614–624.
194. Sudhakar P. et al. Performance augmentation of solar photovoltaic panel through PCM integrated natural water circulation cooling technique // Renewable Energy. 2021. Vol. 172. P. 1433–1448.
195. Sudhakar P., Kumaresan G., Velraj R. Experimental analysis of solar photovoltaic unit integrated with free cool thermal energy storage system // Solar Energy. 2017. Vol. 158. P. 837–844.
196. Ahmad E.Z. et al. Recent advances in passive cooling methods for photovoltaic performance enhancement // IJECE. 2021. Vol. 11, № 1. P. 146.
197. Royo P. et al. Hybrid diagnosis to characterise the energy and environmental enhancement of photovoltaic modules using smart materials // Energy. 2016. Vol. 101. P. 174–189.
198. Mazón-Hernández R. et al. Improving the Electrical Parameters of a Photovoltaic Panel by Means of an Induced or Forced Air Stream // International Journal of Photoenergy. 2013. Vol. 2013. P. 1–10.
199. Chavan S.V., Devaprakasam D. Improving the performance of solar photovoltaic thermal system using phase change material // Materials Today: Proceedings. 2020.
200. Nada S.A., El-Nagar D.H., Hussein H.M.S. Improving the thermal regulation and efficiency enhancement of PCM-Integrated PV modules using nano particles // Energy Conversion and Management. 2018. Vol. 166. P. 735–743.

201. Krauter S. Increased electrical yield via water flow over the front of photovoltaic panels // Solar Energy Materials and Solar Cells. 2004. Vol. 82, № 1. P. 131–137.
202. Dubey S., Sarvaiya J.N., Seshadri B. Temperature Dependent Photovoltaic (PV) Efficiency and Its Effect on PV Production in the World – A Review // Energy Procedia. 2013. Vol. 33. P. 311–321.
203. Khan M.S., Hegde V., Shankar G. Effect of Temperature on Performance of Solar Panels- Analysis // 2017 International Conference on Current Trends in Computer, Electrical, Electronics and Communication (CTCEEC). 2017. P. 109–113.
204. Dincer F., Meral M.E. Critical Factors that Affecting Efficiency of Solar Cells // SGRE. 2010. Vol. 01, № 01. P. 47–50.
205. Notton G. et al. Modelling of a double-glass photovoltaic module using finite differences // Applied Thermal Engineering. 2005. Vol. 25, № 17. P. 2854–2877.
206. Garg H.P., Agarwal R.K. Some aspects of a PV/T collector/forced circulation flat plate solar water heater with solar cells // Energy conversion and management. Elsevier, 1995. Vol. 36, № 2. P. 87–99.
207. Skoplaki E., Boudouvis A.G., Palyvos J.A. A simple correlation for the operating temperature of photovoltaic modules of arbitrary mounting // Solar Energy Materials and Solar Cells. 2008. Vol. 92, № 11. P. 1393–1402.
208. Haidar Z.A., Orfi J., Kaneesamkandi Z. Experimental investigation of evaporative cooling for enhancing photovoltaic panels efficiency // Results in Physics. 2018. Vol. 11. P. 690–697.
209. Chandrika V.S. et al. Experimental analysis of solar concrete collector for residential buildings // International Journal of Green Energy. Taylor & Francis, 2021. Vol. 18, № 6. P. 615–623.
210. Pengra D., Dillman T. Notes on Data Analysis and Experimental Uncertainty [Electronic resource]. URL: https://courses.washington.edu/phys431/uncertainty_notes.pdf (accessed: 27.06.2021).

211. Abdallah S.R., Saidani-Scott H., Benedi J. Experimental study for thermal regulation of photovoltaic panels using saturated zeolite with water // Solar Energy. 2019. Vol. 188. P. 464–474.
212. Elbreki A.M. et al. An innovative technique of passive cooling PV module using lapping fins and planner reflector // Case Studies in Thermal Engineering. 2020. Vol. 19. P. 100607.
213. Chandrasekar M. et al. Passive cooling of standalone flat PV module with cotton wick structures // Energy Conversion and Management. 2013. Vol. 71. P. 43–50.
214. Sun X. et al. Optics-Based Approach to Thermal Management of Photovoltaics: Selective-Spectral and Radiative Cooling // IEEE Journal of Photovoltaics. 2017. Vol. 7, № 2. P. 566–574.
215. Hasan A., Alnoman H., Shah A.H. Energy Efficiency Enhancement of Photovoltaics by Phase Change Materials through Thermal Energy Recovery: 10 // Energies. Multidisciplinary Digital Publishing Institute, 2016. Vol. 9, № 10. P. 782.
216. Lucas M. et al. Photovoltaic Evaporative Chimney as a new alternative to enhance solar cooling // Renewable Energy. 2017. Vol. 111. P. 26–37.
217. Dida M. et al. Experimental investigation of a passive cooling system for photovoltaic modules efficiency improvement in hot and arid regions // Energy Conversion and Management. 2021. Vol. 243. P. 114328.
218. Raj V., Goswami T. Use of phase change material (PCM) for the improvement of thermal performance of cold storage // MOJ Current Research & Reviews. MedCrave Publishing, 2018. Vol. Volume 1, № Issue 2.
219. Choubineh N., Jannesari H., Kasaeian A. Experimental study of the effect of using phase change materials on the performance of an air-cooled photovoltaic system // Renewable and Sustainable Energy Reviews. 2019. Vol. 101. P. 103–111.
220. Jun Huang M. The effect of using two PCMs on the thermal regulation performance of BIPV systems // Solar Energy Materials and Solar Cells. 2011. Vol. 95, № 3. P. 957–963.

221. Preet S., Bhushan B., Mahajan T. Experimental investigation of water based photovoltaic/thermal (PV/T) system with and without phase change material (PCM) // Solar Energy. 2017. Vol. 155. P. 1104–1120.
222. Rezvanpour M. et al. Using CaCl2·6H2O as a phase change material for thermo-regulation and enhancing photovoltaic panels' conversion efficiency: Experimental study and TRNSYS validation // Renewable Energy. 2020. Vol. 146. P. 1907–1921.
223. Bayrak F., Oztop H.F., Selimefendigil F. Experimental study for the application of different cooling techniques in photovoltaic (PV) panels // Energy Conversion and Management. 2020. Vol. 212. P. 112789.
224. Hepbasli A. A key review on exergetic analysis and assessment of renewable energy resources for a sustainable future // Renewable and Sustainable Energy Reviews. 2008. Vol. 12, № 3. P. 593–661.
225. Akyuz E. et al. A novel approach for estimation of photovoltaic exergy efficiency // Energy. 2012. Vol. 44, № 1. P. 1059–1066.
226. Kline S.J., McClintock F.A. Describing Uncertainties in Single-Sample Experiments // Describing Uncertainties in Single Sample Experiments. 1953. P. 3–8.
227. Agyekum E.B. et al. Effect of Two Different Heat Transfer Fluids on the Performance of Solar Tower CSP by Comparing Recompression Supercritical CO2 and Rankine Power Cycles, China: 12 // Energies. Multidisciplinary Digital Publishing Institute, 2021. Vol. 14, № 12. P. 3426.
228. Boddapati V., Daniel S.A. Design and Feasibility Analysis of Hybrid Energy-Based Electric Vehicle Charging Station // Distributed Generation & Alternative Energy Journal. 2022. P. 41-72-41–72.
229. Lai C.S., McCulloch M.D. Levelized Cost of Energy for PV and Grid Scale Energy Storage Systems // arXiv preprint arXiv. 2016. P. 11.
230. Amjad F. et al. Site location and allocation decision for onshore wind farms, using spatial multi-criteria analysis and density-based clustering. A techno-economic-environmental assessment, Ghana // Sustainable Energy Technologies and Assessments. 2021. Vol. 47. P. 101503.

231. Baloch A.A.B. et al. Experimental and numerical performance analysis of a converging channel heat exchanger for PV cooling // Energy Conversion and Management. 2015. Vol. 103. P. 14–27.
232. Luo Z. et al. Numerical and experimental study on temperature control of solar panels with form-stable paraffin/expanded graphite composite PCM // Energy Conversion and Management. 2017. Vol. 149. P. 416–423.
233. Savvakis N., Tsoutsos T. Theoretical design and experimental evaluation of a PV+PCM system in the mediterranean climate // Energy. Elsevier Ltd, 2021. Vol. 220. P. 119690.
234. Kant K. et al. Heat transfer studies of photovoltaic panel coupled with phase change material // Solar Energy. 2016. Vol. 140. P. 151–161.
235. Kazemian A. et al. Experimental study of using both ethylene glycol and phase change material as coolant in photovoltaic thermal systems (PVT) from energy, exergy and entropy generation viewpoints // Energy. 2018. Vol. 162. P. 210–223.
236. B R., CK S., Sudhakar K. Sustainable passive cooling strategy for PV module: A comparative analysis // Case Studies in Thermal Engineering. Elsevier Ltd, 2021. Vol. 27, № May. P. 101317.
237. Park J., Kim T., Leigh S.B. Application of a phase-change material to improve the electrical performance of vertical-building-added photovoltaics considering the annual weather conditions // Solar Energy. 2014. Vol. 105. P. 561–574.
238. Hasan A. et al. Yearly energy performance of a photovoltaic-phase change material (PV-PCM) system in hot climate // Solar Energy. 2017. Vol. 146. P. 417–429.
239. Sharma S. et al. Nano-enhanced Phase Change Material for thermal management of BICPV // Applied Energy. 2017. Vol. 208, № September 2017. P. 719–733.
240. Hachem F. et al. Improving the performance of photovoltaic cells using pure and combined phase change materials – Experiments and transient energy balance // Renewable Energy. Elsevier Ltd, 2017. Vol. 107. P. 567–575.

241. Hasan A. et al. Energy and Cost Saving of a Photovoltaic-Phase Change Materials (PV-PCM) System through Temperature Regulation and Performance Enhancement of Photovoltaics. 2014. P. 1318–1331.
242. Klugmann-Radziemska E., Wcisło-Kucharek P. Photovoltaic module temperature stabilization with the use of phase change materials // Solar Energy. 2017. Vol. 150. P. 538–545.
243. Chahartaghi M., Nikzad A. Exergy, environmental, and performance evaluations of a solar water pump system // Sustainable Energy Technologies and Assessments. Elsevier, 2021. Vol. 43. P. 100933.
244. Khan S. et al. Thermal management of solar PV module by using hollow rectangular aluminum fins // Journal of Renewable and Sustainable Energy. AIP Publishing LLC, 2020. Vol. 12, № 6. P. 063501.
245. Al-Amri F. et al. Innovative technique for achieving uniform temperatures across solar panels using heat pipes and liquid immersion cooling in the harsh climate in the Kingdom of Saudi Arabia // Alexandria Engineering Journal. Elsevier, 2021.